On new physics in non-leptonic tree level b-quark decays and hadron-quark duality violations.

Gilberto Tetlalmatzi Xolocotzi

On new physics in non-leptonic tree level b-quark decays and hadron-quark duality violations

Gilberto Tetlalmatzi-Xolocotzi

A Thesis presented for the degree of
Doctor of Philosophy

Institute for Particle Physics and Phenomenology
Department of Physics
University of Durham
England

September 2016

Dedicated to

My parents and my brother, who made this possible.

On new physics in non-leptonic tree level b-quark decays and hadron-quark duality violations

Gilberto Tetlalmatzi-Xolocotzi

Submitted for the degree of Doctor of Philosophy
September/2016

Abstract

We review the validity of the assumption of having no new physics in tree level b quark transitions $b \to qq'd$ and $b \to qq's$ $(q, q' = u, c)$. In particular we test for possible deviations on the Wilson coefficients of the corresponding effective current-current operators with respect to their Standard Model values. The allowed new physics regions are determined using a global fit. We take into account constraints from different flavour observables calculated from the hadronic decays $B_d^0 \to \pi\pi$, $B_d^0 \to \rho\pi$, $B_d^0 \to \rho\rho$, $B \to X_s\gamma$ and $B \to X_d\gamma$. We also include observables from neutral B meson mixing such as $\Delta\Gamma_s$ and the semileptonic asymmetries $a_{sl}^{s,d}$. We show that deviations in the tree level Wilson coefficients of the order $\mathcal{O}(10\%)$ are consistent with state of the art experimental measurements. We study the implications of these deviations over the decay width $\Delta\Gamma_d$ of B_d^0 meson mixing, not measured yet by experiments, and over the precision of the CKM phase γ. Our results show that enhancements on $\Delta\Gamma_d$ by up to a factor of 3.6 with respect to the Standard Model value are allowed by data. Moreover the effects on γ can compete with the corresponding experimental precision $\mathcal{O}(6^\circ)$. Finally we explore for possible hadron-quark duality violations in the neutral B and D meson sectors. This analysis includes constraints from mixing observables and from the lifetimes of B_d^0 and B_s^0 mesons. We find that duality violations of $\mathcal{O}(20\%)$ can provide an explanation to the tension of several orders of magnitude between the Heavy Quark Expansion and experimental data in the observable $\Delta\Gamma_D$ of neutral D meson mixing.

Declaration

The work in this thesis is based on research carried out at the Institute for Particle Physics and Phenomenology, Department of Physics, Durham University, United Kingdom. No part of this thesis has been submitted elsewhere for any other degree or qualification and it is all my own work in collaboration with my supervisor Dr. A. Lenz unless referenced to the contrary within the text.

Some sections of Chapter 4 are based upon join research with Dr. J. Brod and Dr. M. Wiebusch in the publication: J. Brod, A. Lenz, G. Tetlalmatzi-Xolocotzi and M. Wiebusch. *"New physics effects in tree-level decays and the precision in the determination of the CKM angle γ"*. Phys. Rev. D **92**, 033002 (2015) [hep-ph/1412.1446].

The material presented in Chapter 5 is based on the research work done with Dr. C. Bobeth, Dr. U. Haisch and Dr. B. Pecjak in the publication: C. Bobeth, U. Haisch, A. Lenz, B. Pecjak and G. Tetlalmatzi-Xolocotzi. *"On new physics in $\Delta\Gamma_d$"* JHEP **1406** (2014) 040 [hep-ph/1404.2531].

The content of Chapter 6 is the result of the project developed with T. Jubb and M. Kirk in: T. Jubb, M. Kirk, A. Lenz, G. Tetlalmatzi-Xolocotzi. *"On the ultimate precision of meson mixing observables"* [hep-ph/1603.07770].

Acknowledgements

First of all I would like to thank my supervisor Alexander Lenz for his invaluable help, patience and support during my PhD studies. He was always available for engaging and fruitful physics discussions. Moreover his encouragement and motivation played a central role during my academic life in Durham.

Sincere thanks to Ben Pecjak for the enjoyable collaboration during the first stages of my PhD and to Martin Wiebusch for patiently answering my e-mails concerning the statistical analysis in global fits. Thanks to Michael Spannoswky and Joachim Brod for interesting physics discussions. I want to thank Celine Boehm for friendly physics and non physics conversations and to Oliver Smith for helping me to solve technical issues with the batch system at the IPPP.

I am very grateful with Alex Lenz, Ben Pecjak and Guennadi Borissov for writing reference letters for my postdoctoral applications.

I had a fantastic time at the institute thanks to the friendship of Ryan Wilkinson, Eirini Mavroudi and Thomas Morgan, they made my stay in Durham pleasant and memorable. Thank you very much to Matthew Kirk and Darren Scott for checking the grammar of different sections of my PhD dissertation. In general I have a lot of fun at lunch time and during our visits to the pub thanks to the PhD students from different generations. I want to thank to Dr. Gilberto Tavares-Velasco for his friendship and motivation in physics during my undergraduate studies.

I would like to express my infinite gratitude to my parents Rocio Xolocotzi-Romano

and Marcos Tetlalmatzi-Cuatecontzi, and to my brother Israel Tetlalmatzi-Xolocotzi for all their love and unconditional support. Without them I would have never made this far.

Finally I want to acknowledge CONACYT (Consejo Nacional de Ciencia y Tecnologia, Mexico) for providing the financial support during my PhD studies.

December 1, 2016

Contents

List of Figures

List of Tables

Preface

The Standard Model of particle physics has proven to be a theory with amazing predictive power. To date, it has passed successfully stringent experimental tests. Nevertheless, there are open problems of conceptual and observational origin that cannot be addressed within this theoretical framework, for instance it does not provide an explanation of the asymmetry between matter and antimatter observed in the universe and it does not clarify the nature of dark matter. It is well accepted that in order to solve the outstanding open problems in high energy physics, new particles and interactions need to be introduced. Until now direct searches carried out by experimental collaborations such as ATLAS and CMS have not found unambiguous evidence of new physics.

Flavour Physics in the Quark sector possess different attributes that make it special when seeking for indirect signals beyond the Standard Model. On the experimental side, precision measurements are being performed by collaborations such as LHCb and Belle, in this respect there is plenty of data available that can be compared against theoretical calculations. On the theoretical side, the mathematical formalism developed within the context of quark flavour physics allows to keep hadronic uncertainties under control. This holds, for instance, in the case of b-mesons where the Heavy Quark Expansion (HQE) allows us to express the decay amplitudes for different physical processes as series in Λ_{QCD}/m_b. The relatively large mass of the bottom quark permits to obtain reliable results from the leading terms in this systematic expansion. Moreover, the effective theory approach used is an amazing tool to disentangle perturbative and non perturbative effects within the calculations.

As is well known, higher order corrections are an essential ingredient in the search for new physics. There are currently huge efforts in this direction. However, we consider that it is necessary to critically review the validity of well accepted assumptions in the light of new data. Consider for example the determination of the CKM phase γ; in the last 11 years experimental facilities have been able to reduce the uncertainty significantly. In 2005, using $B \to DK$, the Belle Collaboration measured γ to be $(68^{+22}_{-23})^\circ$ [1]. A more recent measurement by the LHCb collaboration determined γ to be $(70.9^{+7.1}_{-8.5})^\circ$ [1]. This shows an error drop by a factor of 3 with a central value left relatively unaffected. As we will discuss in Section 1.4.2 and Section 4.8.5, the theoretical determination of γ from $B \to DK$ decays is purely tree level. As a matter of fact it is estimated that higher order electroweak corrections will produce a shift at the level of $\delta\gamma \approx \mathcal{O}(10^{-7})$. Consequently the extraction of γ can be considered extremely clean. Here however, we are making the seemingly safe assumption of no new physics at tree level b quark decays. A valid question is, what is really the precision on the theoretical tools used for the computation of tree level processes? As we will see in Chapter 4, new physics effects can cause deviations in γ that saturate the current experimental uncertainty, while being totally consistent with other experimental constraints.

The main aim of the work presented in this thesis is to revise the generalized assumption of no new physics at tree level in $b \to q\bar{q}'s$ and $b \to q\bar{q}'d$ transitions ($q, q' = u, c$) and on the validity of the hadron quark duality (essential in the HQE). In the first case, we check how constrained are the deviations of the Standard Model Wilson coefficients of the current-current operators. Our strategy uses a statistical fit and a set of physical constraints from B meson hadronic decays and observables from B meson mixing. We show that, taking into account the data available, sizeable deviations with respect to the Standard Model are possible at tree level. We then investigate how these results affect the decay width $\Delta\Gamma_d$ of neutral B^0_d mesons and the precision in the determination of the CKM phase γ.

We can speculate on potential enhancements in $\Delta\Gamma_d$ with respect to the Standard

Model, since this physical quantity has not been measured yet. Moreover an interesting connection between $\Delta\Gamma_d$ and the anomalous measurement of the like sign dimuon asymmetry was reported recently in the literature, we will review issues with this interpretation in Chapter 5. Then as a second source of enhancement in $\Delta\Gamma_d$, we investigate for the impact of the effective operators $\left(\bar{d}b\right)\left(\bar{\tau}\tau\right)$ considering different Lorentz structures.

The CKM phase γ is an obvious choice for analysing the consequences of our new physics regions because , as it has been briefly mentioned above, its theoretical determination is a purely tree level one. As a matter of fact the extraction of γ is based on the interference of the decay chains $b \to c\bar{u}s$ and $b \to u\bar{c}s$; and it is free from other weak phases introduced through penguin topologies. Here we show that new physics effects from tree level operators can compete with the most recent experimental precision in the determination of γ.

Our last investigation is centred on the possibility of having hadron quark duality violation in neutral B meson decays. We constrain duality violation effects using the B mixing observable $\Delta\Gamma_s$ and analyse their implications on the observables $a_{sl}^{s,d}$, $\Delta\Gamma_d$ and the ratio of lifetimes $\tau(B_s^0)/\tau(B_d^0)$. As a final step, we show that duality violations of $\mathcal{O}(20\%)$ can explain the experimental result for the decay width $\Delta\Gamma_D$ in neutral D meson oscillations. This is a non trivial result regarding that the HQE gives a theoretical result that disagrees with the experiment by several orders of magnitude.

The structure of this thesis is as follows, Chapters 1, 2 and 3 present the basic theoretical background for the development of the research material. Particular emphasis has been given to the description of the renormalization group evolution of the Wilson coefficients of heavy quark effective theories at next-to-leading order in QCD and Electroweak interactions. Also, we have summarized the most relevant concepts on neutral B meson mixing and on the QCD Factorization (QCDF) approach in Chapter 2 and Chapter 3 respectively. In Chapter 4, we develop our

new physics at tree level decays investigation. The results presented in this chapter will appear in a forthcoming publication, this can be considered an update of the analyses shown previously in Refs. [2, 3]; however, the strategy followed here is by far more rigorous from a statistical point of view. Moreover, it takes into account important physical effects that were previously neglected such as QCD factorization power corrections. In Chapter 5 our study on possible enhancements on the observable $\Delta\Gamma_d$ is described. We present our analysis of duality violations in Chapter 6. Finally the general conclusions and outlook appear in Chapter 7.

Chapter 1

CP Violation

1.1 CP violation in the Standard Model

Here we describe how $\mathcal{CP}$ violation arises in the quark sector of the Standard Model of Particle Physics [4] (SM). Informally speaking the transformation of charge $\mathcal{C}$ interchanges particles by their anti-particles and the transformation of parity $\mathcal{P}$ reverses the handedness of space $\vec{x} \to -\vec{x}$. The gravitational, electromagnetic and strong forces preserve $\mathcal{C}$ and $\mathcal{P}$ individually and consequently also the combination $\mathcal{CP}$. The weak interaction is different in this respect because it breaks each one of these discrete symmetries individually. Moreover, experimental evidence shows that the combination of $\mathcal{C}$ and $\mathcal{P}$ is also broken in the case of neutral Kaons and B mesons.

$\mathcal{CP}$ violation is of fundamental importance not only in particle physics but also in cosmology, where it is an essential ingredient to create the asymmetry between baryonic matter and baryonic antimatter observed in the universe. Theoretically a small baryon asymmetry may have been produced in the early universe if three conditions were satisfied: baryon number violation, $\mathcal{C}$ and $\mathcal{CP}$ violation as well as interactions out of thermal equilibrium [5]. The first condition allows an imbalance between baryons and anti-baryons to develop starting from a baryon symmetric universe. The second condition is necessary because if $\mathcal{C}$ and $\mathcal{CP}$ are exact symmetries it is possible to prove that the total production rate of baryons and antibaryons in any process is the same and then no net baryon number can be created. The

last condition is required to avoid compensation between processes increasing and decreasing the baryon number.

To start a proper discussion of $\mathcal{CP}$ violation in the SM, consider the electroweak quark sector of the full SM Lagrangian written in terms of gauge states for the "up" type quarks $p'_A = (u', c', t')$ and the "down" type quarks $n'_A = (d', s', b')$.

$$\mathcal{L}_{EW,quark} = \mathcal{L}^{kin}_{EW,quark} + \mathcal{L}^{Y}_{EW,quark}. \tag{1.1.1}$$

Here $\mathcal{L}^{kin}_{EW,quark}$ contains all the dynamics for the fermionic fields and also the interactions with the $SU(2)_L$ and $U(1)_Y$ gauge fields $\mathbf{A}_\mu = \{A^1_\mu, A^2_\mu, A^3_\mu\}$ and B_μ respectively, more explicitly

$$\begin{aligned}\mathcal{L}^{kin}_{EW,quark} = {} & i\bar{Q}_{A,L}\Big(\partial\!\!\!/ - \frac{ig}{2}\mathbf{T}\cdot\mathbf{A}\!\!\!/ - \frac{ig'}{6}B\!\!\!/\Big)Q_{A,L} + i\bar{p}'_{A,R}\Big(\partial\!\!\!/ - \frac{2ig'}{3}B\!\!\!/\Big)p'_{A,R} \\ & + i\bar{n}'_{A,R}\Big(\partial\!\!\!/ + \frac{ig'}{3}B\!\!\!/\Big)n'_{A,R},\end{aligned} \tag{1.1.2}$$

where an implicit summation over repeated flavour indices should be understood. To account for the effects of parity violation we have introduced the fermionic doublets $Q_{A,L} = \begin{pmatrix} p'_A \\ n'_A \end{pmatrix}_L$ where the subindex L stands for the left handed projection of the corresponding fermionic fields $\psi_L = \frac{1-\gamma_5}{2}\psi$. In the same way the subindex R stands for the right handed projection $\psi_R = \frac{1+\gamma_5}{2}\psi$. In addition $\vec{T} = \{T_1, T_2, T_3\}$ denotes the $SU(2)$ generators, here we use

$$\mathbf{T} = \left\{ \begin{pmatrix} 0 & 1 \\ 1 & 0 \end{pmatrix}, \begin{pmatrix} 0 & -i \\ i & 0 \end{pmatrix}, \begin{pmatrix} 1 & 0 \\ 0 & -1 \end{pmatrix} \right\}. \tag{1.1.3}$$

The quark-Yukawa sector $\mathcal{L}^{Y}_{EW,quark}$ allows us to introduce mass to the different quarks in the standard model. In the gauge basis it reads

$$\mathcal{L}^{Y}_{EW,quark} = \Big(Y^d_{AB}\bar{Q}_{A,L}\bar{\Phi}n'_{B,R} + Y^u_{AB}\bar{Q}_{A,L}\tilde{\Phi}p'_{B,R} + \text{h. c.}\Big), \tag{1.1.4}$$

where Φ is the Higgs doublet

$$\Phi = \frac{1}{\sqrt{2}}\begin{pmatrix} \phi_1 + i\phi_2 \\ \phi_0 + i\phi_3 \end{pmatrix}, \tag{1.1.5}$$

and $\tilde{\Phi} = i\mathbf{T}_2\Phi^*$.

The coefficients Y^d_{AB} and Y^u_{AB} are the components of the Yukawa matrices in flavour space for the "down" and the "up" type quarks respectively.

Next we identify

$$W^+_\mu := \frac{1}{\sqrt{2}}\Big(A'^1 - iA'^2\Big) \qquad W^-_\mu := \frac{1}{\sqrt{2}}\Big(A'^1 + iA'^2\Big), \tag{1.1.6}$$

and develop the products involving the non diagonal SU(2) generators in Eq.(1.1.2) to get

$$\begin{aligned}
\frac{g}{2}\bar{Q}_{A,L}\Big(T^1 \not{A}^1 + T^2 \not{A}^2\Big)Q_{A,L} &= \frac{g}{\sqrt{2}}\Big(\bar{p}'_{A,L}, \bar{n}'_{A,L}\Big)\begin{pmatrix} 0 & \not{W}^+ \\ \not{W}^- & 0 \end{pmatrix}\begin{pmatrix} p'_{A,L} \\ n'_{A,L} \end{pmatrix} \\
&= \frac{g}{\sqrt{2}}\Big(\bar{p}'_{A,L}\gamma^\mu n'_{A,L}W^+_\mu + \bar{n}'_{A,L}\gamma^\mu p'_{A,L}W^-_\mu\Big) \\
&= \frac{g}{\sqrt{2}}\Big(J'^{\mu+}W^+_\mu + J'^{\mu-}W^-_\mu\Big) := \mathcal{L}^{CC}_{quark}.
\end{aligned} \tag{1.1.7}$$

Here we have identified the "charged" current contributions

$$J'^+_\mu = \bar{p}'_{A,L}\gamma_\mu n'_{A,L} \qquad J'^-_\mu = \bar{n}'_{A,L}\gamma_\mu p'_{A,L}. \tag{1.1.8}$$

The contribution from the diagonal generators to Eq.(1.1.2) can be written as follows

$$\begin{aligned}
\bar{Q}_{A,L}\Big(\frac{g}{2}T^3 \not{A}'^3 + \frac{g'}{6}\not{B}\Big)Q_{A,L} + \frac{2g'}{3}\bar{p}'_{A,R}\not{B}'p'_{A,R} - \frac{g'}{3}\bar{n}'_{A,R}\not{B}'n'_{A,R} &= \\
g J'^3_\mu A'^{3\mu} + \frac{g'}{2}J'^Y_\mu B'^\mu &:= \mathcal{L}^{NC}_{quark},
\end{aligned} \tag{1.1.9}$$

where the isospin neutral current J'^3_μ and the hypercharge neutral current J'^Y_μ are given by

$$\begin{aligned}
J'^3_\mu &= \frac{1}{2}\bar{p}'_{A,L}\gamma_\mu p'_{A,L} - \frac{1}{2}\bar{n}'_{A,L}\gamma_\mu n'_{A,L}, \\
J'^Y_\mu &= \frac{1}{3}\bar{p}'_{A,L}\gamma_\mu p'_{A,L} + \frac{1}{3}\bar{n}'_{A,L}\gamma_\mu n'_{A,L} + \frac{4}{3}\bar{p}'_{A,R}\gamma_\mu p'_{A,R} - \frac{2}{3}\bar{n}'_{A,R}\gamma_\mu n'_{A,R}.
\end{aligned} \tag{1.1.10}$$

We can connect J'^3_μ and J'^Y_μ with the electromagnetic current J^{em}_μ through the Gell-Mann-Nishijima formula

$$J^{em}_\mu = J^3_\mu + 1/2 J^Y_\mu. \tag{1.1.11}$$

We write A'^μ_3 and B'^μ in terms of the photon A^μ and the Z^μ boson as follows

$$A'^3_\mu := \sin\theta_W\ A_\mu + \cos\theta_W\ Z\mu, \qquad B'^\mu := \cos\theta_W\ A_\mu - \sin\theta_W\ Z_\mu. \tag{1.1.12}$$

The rotation angle θ_W in Eq.(1.1.12) is written as the ratio of the coupling constants g and g' according to

$$\tan\,\theta_W = g'/g. \tag{1.1.13}$$

With the aid of Eq.(1.1.11) and Eq.(1.1.12) we can now rewrite the neutral sector given in Eq.(1.1.9) as a function of the fields A^μ and Z^μ as

$$\begin{aligned} gJ^3_\mu A'^{3\mu} + \frac{1}{2}g' J^Y_\mu B'^\mu &= gJ^3_\mu\Big(\cos\theta_W Z^\mu + \sin\theta_W A^\mu\Big) \\ &\quad +\tan\theta_W g\Big(J^{em}_\mu - J^3_\mu\Big)\Big(\cos\theta_W A^\mu - \sin\theta_W Z^\mu\Big) \\ &= eJ^{em}_\mu A^\mu + \frac{g}{\cos\theta_W}\Big(J^3_\mu - \sin^2\theta_W J^{em}_\mu\Big)Z^\mu \\ &= eJ^{em}_\mu A^\mu + \frac{g}{\cos\theta_W}J^0_\mu Z^\mu, \end{aligned} \tag{1.1.14}$$

where in the last two lines we have identified the charge of the electron and the neutral current J^0_μ as

$$e = g\ cos\theta_W \quad , \quad J^0_\mu = J^3_\mu - \sin^2\theta_W J^{em}_\mu. \tag{1.1.15}$$

Up to now we have focused our discussion on $\mathcal{L}^{kin}_{EW,quark}$. Let us now analyse the Yukawa sector $\mathcal{L}^{Y}_{EW,quark}$, this is crucial to understand the origin of $\mathcal{CP}$ violation in the SM. To begin with, recall that after spontaneous symmetry breaking the Higgs doublet in the unitary gauge becomes

$$\Phi \;\rightarrow\; \begin{pmatrix} 0 \\ \frac{h(x)+v}{\sqrt{2}} \end{pmatrix}, \tag{1.1.16}$$

here v is the vacuum expectation value of Φ and $h(x)$ is a real field.
Inserting Φ into Eq.(1.1.4) and after some trivial algebra we get

$$\mathcal{L}^{Y}_{EW,quark} = \frac{v+h(x)}{\sqrt{2}}\Big(Y^d_{AB}\bar{n}'_{A,L}n'_{B,R} + Y^u_{AB}\bar{p}'_{A,L}p'_{B,R}\Big) + h.c.. \tag{1.1.17}$$

The Yukawa matrices $\hat{Y}^u$ and $\hat{Y}^d$ with components Y^d_{AB} and Y^u_{AB} respectively are in general non-diagonal; to generate mass terms we turn to a diagonal basis by applying a bi unitary transformation according to

$$\hat{Y}^{u,d}_D = \hat{L}^{\dagger u,d}\hat{Y}^{u,d}\hat{R}^{u,d}, \tag{1.1.18}$$

where the matrices $\hat{L}^{u,d}$ and $\hat{R}^{u,d}$ are unitary and Y_D is diagonal.
The different terms appearing in Eq.(1.1.17) have the following generic structure $\bar{\hat{\psi}}'_L \hat{Y} \hat{\psi}'_R$, here $\hat{Y}$ represents any of the two Yukawa matrices $\{\hat{Y}^u, \hat{Y}^d\}$ and $\hat{\psi}'_L$, $\hat{\psi}'_R$ are two fermionic fields of left and right chirality respectively. We can rotate to the diagonal basis by applying the following combination of unitary transformations

$$\begin{aligned} \bar{\hat{\psi}}'_L \hat{Y} \hat{\psi}'_R &= \bar{\hat{\psi}}'_L \hat{L}\hat{L}^\dagger \hat{Y} \hat{R}\hat{R}^\dagger \hat{\psi}'_R = (\bar{\hat{\psi}}'_L \hat{L})(\hat{L}^\dagger \hat{Y} \hat{R})(\hat{R}^\dagger \hat{\psi}'_R) \\ &= \bar{\hat{\psi}}_L \hat{Y}_D \hat{\psi}_R, \end{aligned} \tag{1.1.19}$$

with

$$\psi_R := \hat{R}^\dagger \psi'_R, \quad \psi_L := \hat{L}^\dagger \psi'_L, \quad \hat{Y}_D := \hat{L}^\dagger \hat{Y} \hat{R}. \tag{1.1.20}$$

The diagonal mass matrices M_D are defined in terms of the diagonal Yukawa $Y_D^{u,d}$ matrices as follows

$$\hat{M}_D^{u,d} := \frac{v}{\sqrt{2}} \hat{Y}_D^{u,d}, \tag{1.1.21}$$

where the components of $\hat{M}_D^{u,d}$ are the physical masses of the corresponding quarks

$$\hat{M}_D^u = \text{diag}(m_u, m_c, m_t) \quad , \quad \hat{M}_D^d = \text{diag}(m_d, m_s, m_b). \tag{1.1.22}$$

Finally, if we apply the result found in Eq.(1.1.19) and substitute Eq.(1.1.21) into Eq.(1.1.17) we get the following expression for the Yukawa sector in the mass basis

$$\begin{aligned} \mathcal{L}^Y_{EW,quark} &= M^d_{D,AB} \bar{n}_{A,L} n_{B,R} + M^u_{D,AB} \bar{p}_{A,L} p_{B,R} + \\ &\quad \frac{h(x)}{v} \Big(M^d_{D,AB} \bar{n}_{A,L} n_{B,R} + M^u_{D,AB} \bar{p}_{A,L} p_{B,R} \Big) + h.c.. \end{aligned} \tag{1.1.23}$$

Considering the diagonal structure of $\hat{M}_D^{u,d}$ we have $M^{u,d}_{D,AB} \propto \delta_{AB}$. We now analyse the implcations of the diagonal basis on the neutral $\mathcal{L}^{NC}$ (1.1.9) and the charged sector $\mathcal{L}^{CC}$ (1.1.7). In the case of $\mathcal{L}^{NC}$ the basic fermionic structures in the gauge basis are $\bar{p}'_{A,L} \gamma_\mu p'_{A,L}$ and $\bar{n}'_{A,L} \gamma_\mu n'_{A,L}$ (plus the corresponding ones with the right handed chirality), then using Eq.(1.1.20) we write

$$p'_{A,L} = L^u_{AB} p_{B,L}, \qquad n'_{A,L} = L^d_{AB} n_{B,L}, \tag{1.1.24}$$

and taking into account the unitarity of $\hat{L}^{u,d}$ we get

$$\begin{aligned} \bar{p}'_{A,L} \gamma_\mu p'_{A,L} &= \bar{p}_{C,L} L^{u\dagger}_{CA} \gamma_\mu L^u_{AB} p_{B,L} = \bar{p}_{A,L} \gamma_\mu p_{A,L}, \\ \bar{n}'_{a,L} \gamma_\mu n'_{a,L} &= \bar{n}_{C,L} L^{d\dagger}_{CA} \gamma_\mu L^d_{AB} n_{B,L} = \bar{n}_{A,L} \gamma_\mu n_{A,L}. \end{aligned} \tag{1.1.25}$$

Then $\mathcal{L}^{NC}$ can be totally rewritten in the diagonal basis by just dropping the prime symbols in Eq.(1.1.9).

The effect of switching to the mass basis are more interesting in the case of the charged currents, take for example J'^{+}_{μ} in Eq.(1.1.8)

$$\begin{aligned} J'^{+}_{\mu} &= \bar{p}'_{A,L}\gamma_\mu n'_{A,L} = \bar{p}_{B,L}L^{u}_{BA}\gamma_\mu L^{d\dagger}_{AC}n_{C,L} = \bar{p}_{B,L}\Big(L^{u}L^{d\dagger}\Big)_{BC}\gamma_\mu n_{C,L} \\ &= \bar{p}_{b,L}V^{CKM}_{BC}\gamma_\mu n_{C,L}, \end{aligned} \tag{1.1.26}$$

where we have introduced the Cabibbo-Kobayashi-Maskawa (CKM) matrix [6, 7] defined as

$$\hat{V}^{CKM} := \hat{L}^{u}\hat{L}^{d\dagger} \tag{1.1.27}$$

and, in a totally analogous way for the negative currents in Eq.(1.1.8), we find

$$J'^{-}_{\mu} = \bar{n}_{B,L}V^{CKM*}_{BC}\gamma_\mu p_{C,L}\ . \tag{1.1.28}$$

Then the quark charged sector in Eq.(1.1.7) becomes

$$\mathcal{L}^{CC}_{quark} = \frac{g}{\sqrt{2}}\Big(\bar{p}_{B,L}V^{CKM}_{BC}\gamma_\mu n_{C,L}W^{+\mu} + \bar{n}_{B,L}V^{CKM*}_{BC}\gamma_\mu p_{C,L}W^{-\mu}\Big). \tag{1.1.29}$$

If a $\mathcal{CP}$ transformation is applied on (1.1.29) we arrive to

$$\mathcal{L}^{CC,CP}_{quark} = \frac{g}{\sqrt{2}}\Big(\bar{n}_{B,L}V^{CKM}_{BC}\gamma_\mu p_{C,L}W^{-\mu} + \bar{p}_{B,L}V^{CKM*}_{BC}\gamma_\mu n_{C,L}W^{+\mu}\Big). \tag{1.1.30}$$

To satisfy $\mathcal{CP}$ invariance (i.e. $\mathcal{L}^{CC}_{quark} = \mathcal{L}^{CC,CP}_{quark}$) we require $V^{CKM}_{AB} = V^{CKM*}_{AB}$, we will see in the next section that this does not hold in the SM. Moreover, the non-diagonal character of $\hat{V}_{CKM}$ leads to interactions between quarks of different families, this fact is supported by experiment. From now on we write the different components of the CKM matrix as

$$\hat{V}^{CKM} := \begin{pmatrix} V_{ud} & V_{us} & V_{ub} \\ V_{cd} & V_{cs} & V_{cb} \\ V_{td} & V_{ts} & V_{tb} \end{pmatrix}, \tag{1.1.31}$$

where the subindices label the different quark flavours undergoing mixing.

1.2 The CKM matrix

Let us now discuss in more detail the structure of the CKM matrix $\hat{V}^{CKM}$ as given by Eq.(1.1.31). We begin by counting the number of independent parameters.

1. A generic $n \times n$ complex matrix has n^2 complex elements, this implies $2n^2$ real parameters.

2. From the unitarity condition we get $\hat{V}^{CKM\dagger}\hat{V}^{CKM} = \hat{1}$ leading to n^2 constraints, consequently the number of independent parameters is reduced from $2n^2$ to $2n^2 - n^2 = n^2$.

3. It is possible to rephase each one of the CKM entries as $V_{AB}^{CKM} \to e^{-i(\phi_A - \phi_B)} V_{AB}^{CKM}$ by changing the phases of each one of the quark fields according to

$$\begin{aligned} p_{L,A} &\to e^{i\phi_A^p} p_{L,A}, \\ n_{L,B} &\to e^{i\phi_B^n} n_{L,B}. \end{aligned} \tag{1.2.32}$$

   since we have n "up" type quarks and n "down" type quarks, this in principle means that we can eliminate $2n$ phases; however, only the differences matter leaving us with the possibility of dropping only $2n-1$ unphysical phases overall. This reduces our number of independent parameters from n^2 to $n^2 - 2n + 1 = (n-1)^2$.

4. Since we are dealing with a complex matrix, we can divide the $(n-1)^2$ parameters into Euler angles and phases; the Euler angles would arise if the matrix were purely real, i.e. orthogonal. For an n^2 orthogonal matrix $\hat{M}$ we have only $1/2\ n(n-1)$ independent components, because the orthogonality condition $\hat{M}\hat{M}^T = \hat{1}$ removes $1/2\ n(n+1)$ components, leaving us with precisely $n^2 - 1/2\ n(n+1) = 1/2\ n(n-1)$ independent elements.

5. Finally the number of phases will be the $(n-1)^2$ elements calculated in #3 minus the total Euler angles estimated in #4.

   Then our total number of physical phases is

$$(n-1)^2 - \frac{n(n-1)}{2} = \frac{1}{2}(n-1)(n-2). \tag{1.2.33}$$

In a nutshell, for n generations of quarks the CKM matrix should have a total of $1/2\ n(n-1)$ Euler angles and $1/2\ (n-1)(n-2)$ real phases. In the SM we have 3

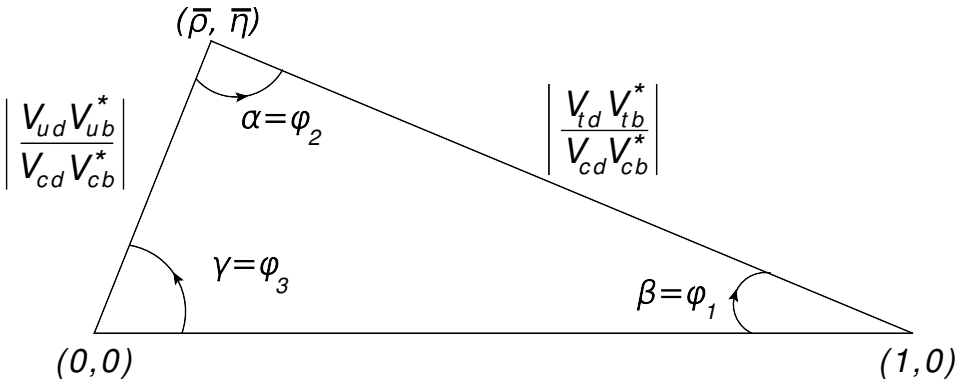

Figure 1.1: Unitarity triangle for $\sum_{A=u,c,t} V_{Ad}V_{Ab}^* = 0$

generations of quarks hence 3 Euler angles and 1 phase, this phase is the source of the $\mathcal{CP}$ violation effects in the SM.

From the unitarity product $\hat{V}^{CKM\dagger}\hat{V}^{CKM} = \hat{1}$ we obtain the following three orthogonality conditions

$$\sum_{A=u,c,t} V_{Ad}V_{As}^* = 0, \quad \sum_{A=u,c,t} V_{Ad}V_{Ab}^* = 0, \quad \sum_{A=u,c,t} V_{As}V_{Ab}^* = 0. \tag{1.2.34}$$

These equalities represent closed triangles in the complex plane, Fig.1.1 provides an explicit example for the second of the equalities in Eq.(1.2.34); as we will see in the next chapter the second and the third equations in Eq. (1.2.34) are very useful when studying mixing for B_d^0 and B_s^0 mesons, respectively.

1.2.1 Parameterizations of the CKM Matrix

The standard convention to parameterize the CKM matrix, following Chau and Keung [8], is defined in terms of three Euler angles $\theta_{12}, \theta_{13}, \theta_{23}$ and one overall phase δ

$$V^{CKM} = \begin{pmatrix} c_{12}c_{13} & s_{12}c_{13} & s_{13}e^{-i\delta} \\ -s_{12}c_{23} - c_{12}s_{23}s_{13}e^{i\delta} & c_{12}c_{23} - s_{12}s_{23}s_{13}e^{i\delta} & s_{23}c_{13} \\ s_{12}s_{23} - c_{12}c_{23}s_{13}e^{i\delta} & -c_{12}s_{23} - s_{12}c_{23}s_{13}e^{i\delta} & c_{23}c_{13} \end{pmatrix}. \tag{1.2.35}$$

Here $c_{ij} = \cos\theta_{ij}$ and $s_{ij} = \sin\theta_{ij}$ for $i < j = 1, 2, 3$, and the angles θ_{ij} are chosen to be in the first quadrant $s_{ij}, c_{ij} \geq 0$.

Based on the experimentally observed hierarchy $s_{13} \ll s_{23} \ll s_{12} \ll 1$, Wolfenstein [9] introduced the expansion parameter λ, at leading order $V_{us} \approx \lambda$; from unitarity considerations η and ρ were also included and finally in order to account for the order of magnitude difference between V_{us} and V_{cb} and extra factor A was also added. Nowadays the following parameterization [10] valid to all orders in λ is accepted in the literature

$$\begin{aligned} s_{12} &:= \lambda = \frac{|V_{us}|}{\sqrt{|V_{ud}|^2 + |V_{us}|^2}}, \\ s_{23} &:= A\lambda^2 = \lambda \Big| \frac{V_{cb}}{V_{us}} \Big|, \\ s_{13} e^{i\delta} &:= A\lambda^3(\rho + i\eta). \end{aligned} \tag{1.2.36}$$

By expanding in λ we present the CKM matrix up to order $\mathcal{O}(\lambda^5)$ in the Wolfenstein parameterization

$$\begin{aligned} V^{CKM} &= \begin{pmatrix} 1 - \lambda^2/2 - \lambda^4/8 & \lambda & A\lambda^3(\rho - i\eta) \\ -\lambda + 1/2A^2\lambda^5[1 - 2(\rho + i\eta)] & 1 - \lambda^2/2 - \lambda^4/8(1 + 4A^2) & A\lambda^2 \\ A\lambda^3[1 - (1 - \lambda^2/2)(\rho + i\eta)] & -A\lambda^2 + A\lambda^4/2[1 - 2(\rho + i\eta)] & 1 - A^2\lambda^2/2 \end{pmatrix} \\ &+ \mathcal{O}(\lambda^6). \end{aligned} \tag{1.2.37}$$

1.2.2 The Jarlskog invariant

In this subsection we describe briefly a particular invariant under different reparameterizations of the CKM matrix known as the Jarlskog invariant. We start by writing generic mass matrices in flavour space as

$$\hat{M}^{u,d} = \frac{v}{\sqrt{2}} \hat{Y}^{u,d}. \tag{1.2.38}$$

It can be seen that Eq.(1.1.21) is a special case of the generic formula above when the Yukawa matrices are diagonal. From the mass matrices we construct the following products

$$\hat{S}^u = \hat{M}^u \hat{M}^{u\dagger}, \qquad \hat{S}^d = \hat{M}^d \hat{M}^{d\dagger}. \tag{1.2.39}$$

It is found in [11] and [12] that the determinant of the commutator between $\hat{S}^u$ and $\hat{S}^d$ defines a CKM parameterization invariant that allows to quantify $\mathcal{CP}$ violation in the SM

$$\det[\hat{S}^u, \hat{S}^d] \;= 2i \cdot J \cdot v(\hat{S}_u) \cdot v(\hat{S}_d), \tag{1.2.40}$$

where

$$\begin{aligned} v(\hat{S}_u) &= (m_u^2 - m_c^2)(m_c^2 - m_t^2)(m_t^2 - m_u^2), \\ v(\hat{S}_d) &= (m_d^2 - m_s^2)(m_s^2 - m_b^2)(m_b^2 - m_d^2). \end{aligned} \tag{1.2.41}$$

The factor J in Eq.(1.2.40) is known as the Jarlskog invariant and satisfies the following condition in terms of the CKM elements [13]

$$\sum_{A,C=u,c,t} \sum_{B,D=d,s,b} \mathcal{I}m\Big(V_{AB} V_{CD} V_{AD}^* V_{CB}^*\Big) = J \sum_{M,N} \varepsilon_{ACM} \varepsilon_{BDN}. \tag{1.2.42}$$

Geometrically J corresponds to two times the area of the different unitary triangles defined by the conditions $\hat{V}^{CKM}\hat{V}^{CKM\dagger} = 0$ and $\hat{V}^{CKM\dagger}\hat{V}^{CKM} = 0$; moreover the determinant in Eq.(1.2.40) vanishes if and only if there is no $\mathcal{CP}$ violation.

In the paper where the Jarlskog invariant was first introduced [11], the commutator in Eq.(1.2.40) was replaced by the single mass matrices commutator $[\hat{M}^u, \hat{M}^d]$ and the final result was written in terms of linear quark mass differences rather than quadratic differences as in (1.2.41). However, as it is argued in [14] the products $\hat{S}^u$ and $\hat{S}^d$ are more suitable for the construction of invariants under unitarity transformations rather than single mass matrices.

1.3 Mixing and CP violation

1.3.1 Introduction to neutral meson mixing

We now develop the basic formalism used to describe the mixing for neutral meson systems $B_d^0 - \bar{B}_d^0$, $B_s^0 - \bar{B}_s^0$ and $D^0 - \bar{D}^0$. In order to simplify the notation we will denote by M^0 any of the neutral mesons $\{B_s^0, B_d^0, D^0\}$, they can be connected with their corresponding $\bar{M}^0$ states $\{\bar{B}_s^0, \bar{B}_d^0, \bar{D}^0\}$ through a $\mathcal{CP}$ transformation according to

$$\hat{\mathcal{CP}}|M^0\rangle \;= \; e^{i\xi}|\bar{M}^0\rangle, \tag{1.3.43}$$

where ξ is a constant phase.

We write the time dependent state $|M^0(t)\rangle$ as

$$|M^0(t)\rangle \;=\; c(t)|M^0\rangle + \bar{c}(t)|\bar{M}^0\rangle + c_1(t)|f_1\rangle + c_2(t)|f_2\rangle + ... \qquad (1.3.44)$$

There is also an analogous evolution equation for $|\bar{M}^0(t)\rangle$. In Eq.(1.3.44) we are considering all the possible final states $|M^0\rangle, |\bar{M}^0\rangle, |f_1\rangle, |f_2\rangle, ...$ and all the time dependence enters through the coefficients $c(t), \bar{c}(t), c_j(t)$. Since we are only interested in neutral meson mixing, i.e. in transitions $M^0 \leftrightarrow \bar{M}^0$, we consider only the time evolution into the states $|M^0\rangle, |\bar{M}^0\rangle$. Mathematically the time evolution can be written using the Wigner-Weisskopf approximation in terms of the following Schrödinger-like equation

$$i\frac{d}{dt}\begin{pmatrix} |M^0(t)\rangle \\ |\bar{M}^0(t)\rangle \end{pmatrix} \;=\; \hat{\mathcal{H}}\begin{pmatrix} |M^0(t)\rangle \\ |\bar{M}^0(t)\rangle \end{pmatrix}. \qquad (1.3.45)$$

Since we are considering only two possible final states, the probability is not conserved and $\hat{\mathcal{H}}$ is non-hermitian, we can introduce a generalized pseudo Hamiltonian considering that any matrix can be decomposed in terms of a hermitian and a skew-hermitian matrix as follows

$$\hat{\mathcal{H}} \;=\; \hat{M} - \frac{i}{2}\hat{\Gamma}, \qquad (1.3.46)$$

where

$$\hat{M} = \begin{pmatrix} M_{11} & M_{12} \\ M_{12}^* & M_{22} \end{pmatrix} \;\;,\;\; \hat{\Gamma} = \begin{pmatrix} \Gamma_{11} & \Gamma_{12} \\ \Gamma_{12}^* & \Gamma_{22} \end{pmatrix}. \qquad (1.3.47)$$

The non-diagonal elements M_{12} and Γ_{12} are complex numbers describing the transitions $M^0 \to \bar{M}^0$ and $\bar{M}^0 \to M^0$. They will be essential in Section 2.4 and 2.4.1 focused on $B_d^0 - \bar{B}_d^0$ and $B_s^0 - \bar{B}_s^0$ oscillations. Here we quote the relative phase between them

$$\phi_{12} \;=\; \arg\Big(-M_{12}\Gamma_{12}^*\Big) = \arg\Big(-\frac{M_{12}}{\Gamma_{12}}\Big). \qquad (1.3.48)$$

Notice that in Eq.(1.3.47) we have taken $M_{21} = M_{12}^*$ and $\Gamma_{21} = \Gamma_{12}^*$ in order to guarantee hermiticity in $\hat{M}$ and $\hat{\Gamma}$.

The phase ϕ_{12} is physical and is responsible for $\mathcal{CP}$ violation in mixing. From CPT invariance we get $M_{11} = M_{22}$ and $\Gamma_{11} = \Gamma_{22}$, then

$$\hat{\mathcal{H}} \;=\; \begin{pmatrix} M_{11} - \frac{i}{2}\Gamma_{11} & M_{12} - \frac{i}{2}\Gamma_{12} \\ M_{12}^* - \frac{i}{2}\Gamma_{12}^* & M_{11} - \frac{i}{2}\Gamma_{11} \end{pmatrix} := \begin{pmatrix} \alpha & \beta \\ \gamma & \alpha \end{pmatrix}, \qquad (1.3.49)$$

where we have defined

$$\alpha = M_{11} - \frac{i}{2}\Gamma_{11}, \quad \beta = M_{12} - \tfrac{i}{2}\Gamma_{12}, \quad \gamma = M_{12}^* - \frac{i}{2}\Gamma_{12}^*. \tag{1.3.50}$$

To solve the differential equation in Eq.(1.3.45) we work in a basis where $\hat{\mathcal{H}}$ is diagonal. First we calculate the eigenvalues of $\hat{\mathcal{H}}$

$$\begin{aligned} \lambda_H = \alpha + \sqrt{\beta\gamma} &:= M_H - \frac{i}{2}\Gamma_H, \\ \lambda_L = \alpha - \sqrt{\beta\gamma} &:= M_L - \frac{i}{2}\Gamma_L, \\ M_H, M_L, \Gamma_H, \Gamma_L &\in \mathbb{R}, \end{aligned} \tag{1.3.51}$$

with $M_H > M_L$; here we use the convention followed in e.g. [15] and label the diagonal basis elements according to their mass eigenvalue. We also compute the transformation between the non-diagonal basis and the diagonal one

$$|M_H\rangle = p|M^0\rangle + q|\bar{M}^0\rangle \quad , \quad |M_L\rangle = p|M^0\rangle - q|\bar{M}^0\rangle, \tag{1.3.52}$$

where $|M_H\rangle$ and $|M_L\rangle$ have eigenvalues λ_H and λ_L respectively and

$$p = \sqrt{\beta} = \sqrt{M_{12} - \frac{i}{2}\Gamma_{12}} \quad , \quad q = \sqrt{\gamma} = \sqrt{M_{12}^* - \frac{i}{2}\Gamma_{12}^*}. \tag{1.3.53}$$

The ratio q/p will be very important when studying mixing in the B_s^0 and B_d^0 systems. We now turn to the calculation of this quantity in some detail, by direct substitution of Eq.(1.3.53) we get

$$\frac{q}{p} = \sqrt{\frac{2M_{12}^* - i\Gamma_{12}^*}{2M_{12} - i\Gamma_{12}}}. \tag{1.3.54}$$

Further simplifications can be made in the case of neutral $B_{d,s}^0$ mesons taking into account that for these cases $|\Gamma_{12}| \ll |M_{12}|$

$$\frac{q}{p} = \sqrt{\frac{M_{12}^*}{M_{12}}}\sqrt{\frac{1 - i\frac{\Gamma_{12}^*}{2M_{12}^*}}{1 - i\frac{\Gamma_{12}}{2M_{12}}}} \approx \sqrt{\frac{M_{12}^*}{M_{12}}}\sqrt{1 - \mathcal{I}m\frac{\Gamma_{12}}{M_{12}}} \approx \sqrt{\frac{M_{12}^*}{M_{12}}}\Big(1 - \frac{1}{2}\frac{|\Gamma_{12}|}{|M_{12}|}\sin\phi_{12}\Big). \tag{1.3.55}$$

We identify the semileptonic asymmetry

$$a_{sl} = \frac{|\Gamma_{12}|}{|M_{12}|}\sin\phi_{12}. \tag{1.3.56}$$

It will arise again in Eq.(1.3.103) when studying $\mathcal{CP}$ violation in mixing. To finish this subsection we write Eq.(1.3.54) in terms of Eq.(1.3.56)

$$\frac{q}{p} = \frac{M_{12}^*}{|M_{12}|}\Big(1-\frac{1}{2}a_{sl}\Big). \tag{1.3.57}$$

1.3.2 Time dependent solution for neutral meson mixing

The time evolution of the system $\{|M_H\rangle, |M_L\rangle\}$ introduced in Eq.(1.3.52) can be written in terms of Eq.(1.3.51) as

$$i\frac{d}{dt}\begin{pmatrix} |M_H(t)\rangle \\ |M_L(t)\rangle \end{pmatrix} = \begin{pmatrix} \lambda_H & 0 \\ 0 & \lambda_L \end{pmatrix}\begin{pmatrix} |M_H(t)\rangle \\ |M_L(t)\rangle \end{pmatrix}. \tag{1.3.58}$$

We can immediately solve for $|M_H(t)\rangle$ and $|M_L(t)\rangle$ in terms of the initial states $|M_H(0)\rangle := |M_H\rangle$ and $|M_L(0)\rangle := |M_L\rangle$ and get

$$|M_{H,L}(t)\rangle = \exp(-i\lambda_{H,L}t)|M_{H,L}\rangle. \tag{1.3.59}$$

In order to turn to the non diagonal basis we first invert the transformations (1.3.52) to obtain

$$\begin{aligned} |M\rangle &= \frac{1}{2p}\Big(|M_L\rangle + |M_H\rangle\Big), \\ |\bar{M}\rangle &= \frac{1}{2q}\Big(|M_L\rangle - |M_H\rangle\Big), \end{aligned} \tag{1.3.60}$$

switching to the time dependent basis and substituting Eq.(1.3.59) we get

$$\begin{aligned} |M(t)\rangle &= \frac{1}{2p}\Big(|M_L(t)\rangle + |M_H(t)\rangle\Big) \\ &= \frac{1}{2p}\Big(\exp(-i\lambda_L t)\Big[p|M\rangle + q|\bar{M}\rangle\Big] + \exp(-i\lambda_H t)\Big[p|M\rangle - q|\bar{M}\rangle\Big]\Big) \\ &= g_+(t)|M\rangle + \frac{q}{p}g_-(t)|\bar{M}\rangle, \end{aligned} \tag{1.3.61}$$

with

$$g_\pm(t) = \frac{1}{2}\Big(\exp(-i\lambda_L t) \pm \exp(-i\lambda_H t)\Big). \tag{1.3.62}$$

In a similar way

$$|\bar{M}(t)\rangle = \frac{p}{q}g_-(t)|M\rangle + g_+(t)|\bar{M}\rangle. \tag{1.3.63}$$

1.3.3 ΔM and $\Delta\Gamma$

With the real components of the eigenvalues introduced in Eq.(1.3.51) we can define the following two observables

$$\begin{aligned}\Delta M &:= M_H - M_L,\\ \Delta\Gamma &:= \Gamma_L - \Gamma_H.\end{aligned} \tag{1.3.64}$$

We want to derive explicit expressions for ΔM and $\Delta\Gamma$ in terms of M_{12} and Γ_{12}. We begin by calculating the square of the difference between the two eigenvalues in Eq.(1.3.51)

$$\Big(\lambda_H - \lambda_L\Big)^2 \;=\; 4\beta\gamma = \Big(\Delta M + \frac{i}{2}\Delta\Gamma\Big)^2 = \Delta M^2 - \frac{1}{4}\Delta\Gamma^2 + i\Delta M\Delta\Gamma. \tag{1.3.65}$$

Alternatively the difference of the eigenvalues λ_H and λ_L in Eq.(1.3.65) can be written in terms of the non diagonal elements M_{12} and Γ_{12} according to Eq.(1.3.50) as

$$\begin{aligned}\Big(\lambda_H - \lambda_L\Big)^2 &= 4\Big(M_{12} - \frac{i}{2}\Gamma_{12}\Big)\Big(M^*_{12} - \frac{i}{2}\Gamma^*_{12}\Big)\\ &= 4|M|^2_{12} - |\Gamma_{12}|^2 - 2i\Big(M^*_{12}\Gamma_{12} + M_{12}\Gamma^*_{12}\Big)\\ &= 4|M|^2_{12} - |\Gamma_{12}|^2 - 4i\mathcal{R}e\Big(M_{12}\Gamma^*_{12}\Big).\end{aligned} \tag{1.3.66}$$

By comparing Eq.(1.3.65) and Eq.(1.3.66) we get

$$\begin{aligned}4|M_{12}|^2 - |\Gamma_{12}|^2 &= \Delta M^2 - \frac{1}{4}\Delta\Gamma^2\\ -4\mathcal{R}e\Big(M_{12}\Gamma^*_{12}\Big) &= 4|M_{12}||\Gamma_{12}|\cos\phi_{12} = \Delta M\Delta\Gamma.\end{aligned} \tag{1.3.67}$$

To solve for ΔM and $\Delta\Gamma$ we use the fact that for B^0_d and B^0_s the condition $|\Gamma_{12}| \ll |M_{12}|$ holds. The second equality in Eq.(1.3.67) implies

$$\Delta M = \quad \frac{4|M_{12}||\Gamma_{12}|\cos(\phi_{12})}{\Delta\Gamma}, \tag{1.3.68}$$

and we can plug this result into the first equality in Eq.(1.3.67) to obtain

$$4|M_{12}|^2 - |\Gamma_{12}|^2 \;=\; \frac{16|M_{12}|^2|\Gamma_{12}|^2\cos^2(\phi_{12})}{\Delta\Gamma^2} - \frac{1}{4}\Delta\Gamma^2. \tag{1.3.69}$$

Solving for $\Delta\Gamma^2$

$$\begin{aligned}\Delta\Gamma^2 &= \frac{-4\Big(4|M_{12}|^2-|\Gamma_{12}|^2\Big)\pm 4\sqrt{\Big(4|M_{12}|^2-|\Gamma_{12}|^2\Big)^2+16|M_{12}|^2|\Gamma_{12}|^2\cos^2(\phi_{12})}}{2}\\ &= -2\Big(4|M_{12}|^2-|\Gamma_{12}|^2\Big)\\ &\quad \pm 2\sqrt{16|M_{12}|^4-8|M_{12}|^2|\Gamma_{12}|^2+|\Gamma_{12}|^4+16|M_{12}|^2|\Gamma_{12}|^2\cos^2(\phi_{12})}\\ &= -2\Big(4|M_{12}|^2-|\Gamma_{12}|^2\Big)\\ &\quad \pm 8|M_{12}|^2\sqrt{1-\frac{|\Gamma_{12}|^2}{2|M_{12}|^2}+\frac{|\Gamma_{12}|^2\cos^2(\phi_{12})}{|M_{12}|^2}+\frac{|\Gamma_{12}|^4}{16|M_{12}|^4}}. \end{aligned} \tag{1.3.70}$$

We can now make use of the fact $|\Gamma_{12}| \ll |M_{12}|$ to simplify the square root in Eq.(1.3.70) and get

$$\Delta\Gamma^2 \approx 2|\Gamma_{12}|^2-8|M_{12}|^2\pm 8|M_{12}|^2\Big(1-\frac{1}{4}\frac{|\Gamma_{12}|^2}{|M_{12}|^2}+\frac{|\Gamma_{12}|^2\cos^2(\phi_{12})}{2|M_{12}|^2}+\frac{|\Gamma_{12}|^4}{32|M_{12}|^4}\Big). \tag{1.3.71}$$

The left hand side of the previous equation should be real and positive. This can only hold if we take the upper sign in front of the third term in Eq.(1.3.71)

$$\Delta\Gamma \approx 2|\Gamma_{12}|\cos(\phi_{12}). \tag{1.3.72}$$

We can proceed in a similar way and solve for ΔM. Using both expressions in Eq.(1.3.67) we get

$$\Delta M^4-\Delta M^2\Big(4|M_{12}|^2-|\Gamma_{12}^2|\Big)-4|M_{12}|^2|\Gamma_{12}|^2\cos^2(\phi_{12})=0. \tag{1.3.73}$$

And solving for ΔM^2

$$\begin{aligned}\Delta M^2 &= \frac{\Big(4|M_{12}|^2-|\Gamma_{12}|^2\Big)\pm\sqrt{\Big(4|M_{12}|^2-|\Gamma_{12}|^2\Big)^2+16|M_{12}|^2|\Gamma_{12}|^2\cos^2(\phi_{12})}}{2}\\ &= \frac{\Big(4|M_{12}|^2-|\Gamma_{12}|^2\Big)}{2}\\ &\quad \pm\frac{\sqrt{16|M_{12}|^4-8|M_{12}|^2|\Gamma_{12}|^2+|\Gamma_{12}|^4+16|M_{12}|^2|\Gamma_{12}|^2\cos^2(\phi_{12})}}{2}. \end{aligned} \tag{1.3.74}$$

To get rid of the square root we use the approximation $|\Gamma_{12}| \ll |M_{12}|$

$$\begin{aligned}\Delta M^2 &\approx \frac{\Big(4|M_{12}|^2-|\Gamma_{12}|^2\Big)}{2}\\ &\quad \pm\frac{4|M_{12}|^2}{2}\Big(1-\frac{|\Gamma_{12}|^2}{4|M_{12}|^2}+\frac{|\Gamma_{12}|^4}{32|M_{12}|^4}+\frac{|\Gamma_{12}|^2\cos^2(\phi_{12})}{2|M_{12}|^2}\Big). \end{aligned} \tag{1.3.75}$$

In order to get a real positive answer we pick the upper sign for the overall factor inside the second round bracket, and use the condition $|\Gamma_{12}| \ll |M_{12}|$ once more, to obtain

$$\Delta M \;=\; 2|M_{12}|. \tag{1.3.76}$$

The results obtained in Eq.(1.3.72) and Eq.(1.3.76) are basic when calculating for ΔM and $\Delta\Gamma$ in the B_d^0 and the B_s^0 systems because the condition $\Gamma_{12} \ll |M_{12}|$ is valid. However this inequality is not satisfied by D^0 mesons, we now derive the generic result [16]

$$2|\Gamma_{12}| \;>\; \Delta\Gamma. \tag{1.3.77}$$

The relation in Eq.(1.3.77) is useful for establishing theoretical bounds when comparing against the experiment even when we cannot make assumptions on the size of $|\Gamma_{12}|$ with respect to $|M_{12}|$.

To begin with the proof we solve for $|M_{12}|^2$ in Eq.(1.3.69) obtaining

$$|M_{12}|^2 \;=\; \frac{|\Gamma_{12}|^2 - \frac{1}{4}\Delta\Gamma^2}{4 - \frac{16|\Gamma_{12}|^2\cos^2(\phi_{12})}{\Delta\Gamma^2}}. \tag{1.3.78}$$

Now, $|M_{12}|^2$ should be real and positive, therefore there are two possibilities:

1. $|\Gamma_{12}|^2 - \frac{1}{4}\Delta\Gamma^2 < 0$ and $4 - \frac{16|\Gamma_{12}^2|\cos^2(\phi_{12})}{\Delta\Gamma^2} < 0$.

2. $|\Gamma_{12}|^2 - \frac{1}{4}\Delta\Gamma^2 > 0$ and $4 - \frac{16|\Gamma_{12}^2|\cos^2(\phi_{12})}{\Delta\Gamma^2} > 0$.

The first set of inequalities is inconsistent because it requires simultaneously

$$|\Delta\Gamma| > 2|\Gamma_{12}| \quad \text{and} \quad 2|\Gamma_{12}||\cos(\phi_{12})| > \Delta\Gamma. \tag{1.3.79}$$

On the other hand, the second set is self consistent as long as

$$2|\Gamma_{12}| > |\Delta\Gamma| \quad \text{and} \quad \Delta\Gamma > 2|\Gamma_{12}||\cos(\phi_{12})|. \tag{1.3.80}$$

The result we are looking for is just the first inequality in Eq.(1.3.80).

1.3.4 Time dependent and flavour specific decays

This subsection is devoted to the calculation of different formulae that will prove to be very useful during our discussion on the classification of $\mathcal{CP}$ violation. We focus

on $M^0 = B_q^0$ mesons for $q = d, s$. We start our discussion by rewriting the functions in Eq.(1.3.62) in a more convenient way that exhibits the explicit dependence on ΔM and $\Delta\Gamma$. We first introduce the following definitions

$$M = \frac{M_H + M_L}{2}, \qquad \Gamma = \frac{\Gamma_H + \Gamma_L}{2}. \tag{1.3.81}$$

Then using Eq.(1.3.64) we can write

$$M_{L/H} = M \mp \frac{\Delta M}{2}, \qquad \Gamma_{L/H} = \Gamma \pm \frac{\Delta\Gamma}{2}, \tag{1.3.82}$$

and Eq.(1.3.62) becomes

$$\begin{aligned} g_\pm(t) &= \frac{1}{2}\Big(\exp\Big[-i(M - \frac{\Delta M}{2})t - \frac{1}{2}(\Gamma + \frac{\Delta\Gamma}{2})t\Big] \\ &\quad \pm\exp\Big[-i(M + \frac{\Delta M}{2})t - \frac{1}{2}(\Gamma - \frac{\Delta\Gamma}{2})t\Big]\Big) \\ &= \frac{1}{2}\exp\Big[-(iM + \frac{1}{2}\Gamma)t\Big]\Big(\exp\Big[(\frac{i\Delta M}{2} - \frac{\Delta\Gamma}{4})t\Big] \\ &\quad \pm\exp\Big[-(\frac{i\Delta M}{2} - \frac{\Delta\Gamma}{4})t\Big]\Big). \end{aligned} \tag{1.3.83}$$

And we can immediately calculate

$$\begin{aligned} |g_\pm(t)|^2 &= \frac{1}{4}\exp(-\Gamma t)\Big(\exp(-\frac{\Delta\Gamma}{2}t) \pm \exp(-i\Delta M t) \pm \exp(i\Delta M t) + \exp(\frac{\Delta\Gamma}{2}t)\Big) \\ &= \frac{1}{2}\exp(-\Gamma t)\Big(\cosh\frac{\Delta\Gamma}{2}t \pm \cos\Delta M t\Big), \end{aligned} \tag{1.3.84}$$

$$\begin{aligned} g_+^* g_- &= \frac{1}{4}\exp(-\Gamma t)\Big(\exp(-\frac{\Delta\Gamma}{2}t) - \exp(-i\Delta M t) + \exp(i\Delta M t) - \exp(\frac{\Delta\Gamma}{2}t)\Big) \\ &= \frac{1}{2}\exp(-\Gamma t)\Big(-\sinh\frac{\Delta\Gamma}{2}t + i\sin\Delta M t\Big). \end{aligned} \tag{1.3.85}$$

Based on the definitions in Eq.(1.3.61) and Eq.(1.3.63) we can identify $|g_+(t)|^2$ and $|g_-(t)|^2$ with the probability densities for the transitions $B_q^0 \to B_q^0(\bar{B}_q^0 \to \bar{B}_q^0)$ and $B_q^0 \to \bar{B}_q^0(\bar{B}_q^0 \to B_q^0)$ respectively.

Considering a decay B_q^0 $(\bar{B}_q^0)$ to f, we write the transition amplitudes from the flavour states $\{|B_q^0\rangle, |\bar{B}_q^0\rangle\}$ to the final states $\{f, |\bar{f}\rangle = \{f, \mathcal{CP}|f\rangle\}$ as

$$\begin{aligned} A_f^q &:= \langle f|B_q^0\rangle, \quad \bar{A}_f^q := \langle f|\bar{B}_q^0\rangle, \\ A_{\bar{f}}^q &:= \langle \bar{f}|B_q^0\rangle, \quad \bar{A}_{\bar{f}}^q := \langle \bar{f}|\bar{B}_q^0\rangle. \end{aligned} \tag{1.3.86}$$

Next we study in more detail the calculation of the time dependent decay of a neutral meson B_q^0 to a final state f

$$\frac{d\Gamma[B_q^0 \to f](t)}{dt} = N_f |\langle f|B_q^0(t)\rangle|^2, \tag{1.3.87}$$

where N_f is a time-independent normalization factor and the time dependent state $|B_q^0(t)\rangle$ can be read off Eq.(1.3.61). We find

$$\begin{aligned}
\frac{d\Gamma[B_q^0 \to f](t)}{dt} &= N_f \Big| g_+(t) A_f^q + \frac{q}{p} g_-(t) |\bar{A}_f^q \Big|^2 \\
&= \frac{N_f}{2} \exp(-\Gamma t) \Big(|A_f^q|^2 \Big[\cosh \frac{\Delta\Gamma_q}{2} t + \cos \Delta M_q t \Big] \\
&\quad + A_f^{q,*} \bar{A}_f^q \frac{q}{p} \Big[- \sinh \frac{\Delta\Gamma_q}{2} t + i \sin \Delta M_q t \Big] \\
&\quad + A_f^q \bar{A}_f^{q,*} \frac{q^*}{p^*} \Big[- \sinh \frac{\Delta\Gamma_q}{2} t - i \sin \Delta M_q t \Big] \\
&\quad + |\bar{A}_f^q|^2 \Big| \frac{q}{p} \Big|^2 \Big[\cosh \frac{\Delta\Gamma_q}{2} t - \cos \Delta M_q t \Big] \Big) \\
&= \frac{N_f}{2} \exp(-\Gamma_q t) \Big(\Big[|A_f^q|^2 + \Big| \bar{A}_f^q \frac{q}{p} \Big|^2 \Big] \cosh \frac{\Delta\Gamma_q}{2} t \\
&\quad + \Big[|A_f^q|^2 - \Big| \bar{A}_f^q \frac{q}{p} \Big|^2 \Big] \cos \Delta M_q t - 2\mathcal{R}e \Big[A_f^{q,*} \bar{A}_f^q \frac{q}{p} \Big] \sinh \frac{\Delta\Gamma_q}{2} t \\
&\quad - 2\mathcal{I}m \Big[A_f^{q,*} \bar{A}_f^q \frac{q}{p} \Big] \sin \Delta M_q t \Big).
\end{aligned} \tag{1.3.88}$$

To simplify the expression above we introduce the definition

$$\lambda_f^q := \frac{\bar{A}_f^q q}{A_f^q p} \tag{1.3.89}$$

and the final result is

$$\begin{aligned}
\frac{d\Gamma[B_q^0 \to f](t)}{dt} &= N_f |A_f^q|^2 \exp(-\Gamma_q t) \Big[\frac{1 + |\lambda_f^q|^2}{2} \cosh \frac{\Delta\Gamma_q}{2} t + \frac{1 - |\lambda_f^q|^2}{2} \cos \Delta M_q t \\
&\quad - \mathcal{R}e(\lambda_f^q) \sinh \frac{\Delta\Gamma_q}{2} t - \mathcal{I}m(\lambda_f^q) \sin \Delta M_q t \Big].
\end{aligned} \tag{1.3.90}$$

Using Eq.(1.3.63) we can proceed in an analogous way to calculate the transition for the process $\bar{B}_q^0$ into the same final state f

$$\begin{aligned}
\frac{d\Gamma[\bar{B}_q^0 \to f](t)}{dt} &= N_f |\langle f|\bar{B}_q^0(t)\rangle|^2 \\
&= N_f |A_f|^2 \Big| \frac{p}{q} \Big|^2 \exp(-\Gamma t) \Big[\frac{1 + |\lambda_f^q|^2}{2} \cosh \frac{\Delta\Gamma_q}{2} t - \frac{1 - |\lambda_f^q|^2}{2} \cos \Delta M_q t \\
&\quad - \mathcal{R}e(\lambda_f^q) \sinh \frac{\Delta\Gamma_q}{2} t + \mathcal{I}m(\lambda_f^q) \sin \Delta M_q t \Big].
\end{aligned} \tag{1.3.91}$$

To obtain $d\Gamma[B_q^0 \to \bar{f}](t)/dt$ we use Eq.(1.3.90), replacing λ_f^q by

$$\lambda_{\bar{f}}^{q} = \frac{\bar{A}_{\bar{f}}^{q}}{A_{\bar{f}}^{q}}\frac{q}{p} \tag{1.3.92}$$

and extract a global factor $|\lambda_{\bar{f}}^{q}|^2$

$$\begin{aligned}\frac{d\Gamma[B_q^0 \to \bar{f}](t)}{dt} &= N_f|A_{\bar{f}}^{q}|^2\exp(-\Gamma_q t)\Big[\frac{1+|\lambda_{\bar{f}}^{q}|^2}{2}\cosh\frac{\Delta\Gamma_q}{2}t + \frac{1-|\lambda_{\bar{f}}^{q}|^2}{2}\cos\Delta M_q t \\ &\quad -\mathcal{R}e(\lambda_{\bar{f}}^{q})\sinh\frac{\Delta\Gamma_q}{2}t + \mathcal{I}m(\lambda_{\bar{f}}^{q})\sin\Delta M_q t\Big] \\ &= N_f|\bar{A}_{\bar{f}}^{q}|^2\Big|\frac{q}{p}\Big|^2\exp(-\Gamma_q t)\Big[\frac{1+|\lambda_{\bar{f}}^{q}|^{-2}}{2}\cosh\frac{\Delta\Gamma_q}{2}t - \frac{1-|\lambda_{\bar{f}}^{q}|^{-2}}{2}\cos\Delta M_q t \\ &\quad -\mathcal{R}e\Big(\lambda_{\bar{f}}^{q-1}\Big)\sinh\frac{\Delta\Gamma_q}{2}t + \mathcal{I}m\Big(\lambda_{\bar{f}}^{q-1}\Big)\sin\Delta M_q t\Big].\end{aligned} \tag{1.3.93}$$

There is only one transition left to be determined $d\Gamma[\bar{B}_q^0 \to \bar{f}](t)/dt$. This can be obtained following the same procedure as for Eq.(1.3.93); however in this case we start with Eq.(1.3.91), replace λ_f^q with $\lambda_{\bar{f}}^{q}$ and extract a global factor $|\lambda_{\bar{f}}^{q}|^2$, the result is

$$\begin{aligned}\frac{d\Gamma[\bar{B}_q^0 \to \bar{f}](t)}{dt} &= N_f|\bar{A}_{\bar{f}}^{q}|^2\exp(-\Gamma_q t)\Big[\frac{1+|\lambda_{\bar{f}}^{q}|^{-2}}{2}\cosh\frac{\Delta\Gamma_q}{2}t + \frac{1-|\lambda_{\bar{f}}^{q}|^{-2}}{2}\cos\Delta M_q t \\ &\quad -\mathcal{R}e\Big(\lambda_{\bar{f}}^{q-1}\Big)\sinh\frac{\Delta\Gamma_q}{2}t - \mathcal{I}m\Big(\lambda_{\bar{f}}^{q-1}\Big)\sin\Delta M_q t\Big].\end{aligned} \tag{1.3.94}$$

Notice that in Eq.(1.3.93) and Eq.(1.3.94) we have taken $N_f = N_{\bar{f}}$ because the normalization factor is only dependent on the kinematics.

The main results of this section are the formulas in Eq.(1.3.90, 1.3.91, 1.3.93) and Eq.(1.3.94), they can be simplified in certain cases, e.g. flavour specific decays. A decay $B_q^0 \to f_{fs}$ is considered flavour specific if two conditions hold:

1. $\langle f_{fs}|\bar{B}_q^0\rangle = 0$ and $\langle \bar{f}_{fs}|B_q^0\rangle = 0$ leading to $\lambda_f^q = 0$ and $(\lambda_{\bar{f}}^{q})^{-1} = 0$
2. there is no direct $\mathcal{CP}$ violation, then $|A_f^q| = |\bar{A}_{\bar{f}}^{q}|$.

Examples of flavour specific decays are $B_s^0 \to D_s^-\pi^+$, $B_s^0 \to X_s l^+\nu_l$ and $B_d^0 \to X_d l^+\nu_l$. If we apply the first set of conditions defining direct $\mathcal{CP}$ violation we get

$$\begin{aligned}
\frac{d\Gamma[B_q^0 \to f_{fs}](t)}{dt} &= \frac{1}{2}N_f|A_f^q|^2\exp(-\Gamma_q t)\Big(\cosh\frac{\Delta\Gamma_q}{2}t + \cos\Delta M_q t\Big)\\
\frac{d\Gamma[\bar{B}_q^0 \to f_{fs}](t)}{dt} &= \frac{1}{2}N_f|A_f^q|^2\Big|\frac{p}{q}\Big|^2\exp(-\Gamma_q t)\Big(\cosh\frac{\Delta\Gamma_q}{2}t - \cos\Delta M_q t\Big)\\
\frac{d\Gamma[B_q^0 \to \bar{f}_{fs}](t)}{dt} &= \frac{1}{2}N_f|\bar{A}_{\bar{f}}^q|^2\Big|\frac{q}{p}\Big|^2\exp(-\Gamma_q t)\Big(\cosh\frac{\Delta\Gamma_q}{2}t - \cos\Delta M_q t\Big)\\
\frac{d\Gamma[\bar{B}_q^0 \to \bar{f}_{fs}](t)}{dt} &= \frac{1}{2}N_f|\bar{A}_{\bar{f}}^q|^2\exp(-\Gamma_q t)\Big(\cosh\frac{\Delta\Gamma_q}{2}t + \cos\Delta M_q t\Big) \qquad (1.3.95)
\end{aligned}$$

we will come back to these formulas soon when studying $\mathcal{CP}$ violation in mixing.

1.3.5 CP violation in decay

$\mathcal{CP}$ violation in decay is also called direct $\mathcal{CP}$ violation and is defined by $|\bar{A}_{\bar{f}}^q/A_f^q| \neq 1$, this can be translated to the following inequality in terms of decay probabilities $P(B_q^0 \to f) \neq P(\bar{B}_q^0 \to \bar{f})$. If $\mathcal{CP}$ violation in decay occurs the following asymmetry is non-vanishing

$$\mathcal{A}_{\text{decay}} = \frac{\Gamma[\bar{B}_q^0 \to \bar{f}] - \Gamma[B_q^0 \to f]}{\Gamma[\bar{B}_q^0 \to \bar{f}] + \Gamma[B_q^0 \to f]}. \qquad (1.3.96)$$

If the effects of mixing are neglected as a first approximation, i. e. $\Delta\Gamma_q = 0$ and $\Delta M_q = 0$, we get the following simplified formula for the previous asymmetry

$$\mathcal{A}_{\text{decay}} = \frac{\Big|\frac{\bar{A}_{\bar{f}}}{A_f}\Big|^2 - 1}{\Big|\frac{\bar{A}_{\bar{f}}}{A_f}\Big|^2 + 1}. \qquad (1.3.97)$$

This type of $\mathcal{CP}$ violation is only posssible if the decay amplitude has contributions from at least two diagrams with partial amplitudes A_1 and A_2 with different weak $\phi_{1,2}$ and strong $\delta_{1,2}$ phases such that the final amplitude and its $\mathcal{CP}$ conjugate are

$$\begin{aligned}
A_f &= |A_1|\exp(i[\delta_1 + \phi_1]) + |A_2|\exp(i[\delta_2 + \phi_2]),\\
\bar{A}_{\bar{f}} &= |A_1|\exp(i[\delta_1 - \phi_1]) + |A_2|\exp(i[\delta_2 - \phi_2]). \qquad (1.3.98)
\end{aligned}$$

If we define $\Delta\delta = \delta_2 - \delta_1$ and $\Delta\phi = \phi_2 - \phi_1$, we can square the amplitudes to obtain

$$
\begin{aligned}
|A_f|^2 &= |A_1|^2 + |A_2|^2 + 2|A_1||A_2|\cos(\Delta\delta + \Delta\phi) \\
&= |A_1|^2 + |A_2|^2 + 2|A_1||A_2|\Big(\cos\Delta\delta\cos\Delta\phi - \sin\Delta\delta\sin\Delta\phi\Big), \\
|\bar{A}_{\bar{f}}|^2 &= |A_1|^2 + |A_2|^2 + 2|A_1||A_2|\Big(\cos\Delta\delta\cos\Delta\phi + \sin\Delta\delta\sin\Delta\phi\Big). \quad (1.3.99)
\end{aligned}
$$

Plugging Eq.(1.3.99) into Eq.(1.3.97) we get

$$
\mathcal{A}_{decay} = \frac{2|A_1||A_2|\sin\Delta\delta\ \sin\Delta\phi}{|A_1|^2 + |A_2|^2 + 2|A_1||A_2|\cos\Delta\delta\ \cos\Delta\phi}. \quad (1.3.100)
$$

As an specific example consider the transition $B_s^0 \to K^-\pi^+$ and its $\mathcal{CP}$ conjugate version $\bar{B}_s^0 \to K^+\pi^-$, in this case the individual amplitudes get contributions from penguins and tree level topologies. We then make the following identifications in our formula Eq.(1.3.99): $A_1 \to A_{tree}$ and $A_2 \to A_{penguin}$; in this case the difference $\Delta\delta$ corresponds to the CKM angle $\gamma = \arg\Big(-\frac{V_{ud}V_{ub}^*}{V_{cd}V_{cb}^*}\Big)$.

1.3.6 CP violation in mixing

The definition of $\mathcal{CP}$ violation in mixing is given in terms of the condition $|q/p| \neq 1$ and it implies the following inequality for the oscillation probabilities $P(B_q^0 \to \bar{B}_q^0) \neq P(\bar{B}_q^0 \to B_q^0)$. To get a deeper understanding of $\mathcal{CP}$ violation in mixing, using Eq.(1.3.54) and (1.3.48) we calculate the ratio

$$
\begin{aligned}
\Big|\frac{q}{p}\Big|^4 &= \Big(\frac{2M_{12} + i\Gamma_{12}}{2M_{12}^* + i\Gamma_{12}^*}\Big)\Big(\frac{2M_{12}^* - i\Gamma_{12}^*}{2M_{12} - i\Gamma_{12}}\Big) \\
&= \frac{|M_{12}|^2 + |\Gamma_{12}|^2/4 - |M_{12}||\Gamma_{12}|\sin\phi_{12}}{|M_{12}|^2 + |\Gamma_{12}|^2/4 + |M_{12}||\Gamma_{12}|\sin\phi_{12}}. \quad (1.3.101)
\end{aligned}
$$

From the previous equation we can see that there is no $\mathcal{CP}$ violation in mixing if $\phi_{12} = 0$. As for Eq.(1.3.100) we construct an asymmetry to quantify the effects of $\mathcal{CP}$ violation in mixing for flavour specific decays f_{fs} with the help of Eq.(1.3.95)

$$
\begin{aligned}
\mathcal{A}_{CP_{mix}} &= \frac{d\Gamma[\bar{B}_q^0 \to f_{fs}](t)/dt - d\Gamma[B_q^0 \to \bar{f}_{fs}](t)/dt}{d\Gamma[\bar{B}_q^0 \to f_{fs}](t)/dt + d\Gamma[B_q^0 \to \bar{f}_{fs}](t)/dt} \\
&= \frac{\Big|\frac{p}{q}\Big|^2 - \Big|\frac{q}{p}\Big|^2}{\Big|\frac{p}{q}\Big|^2 + \Big|\frac{q}{p}\Big|^2} = \frac{1 - \Big|\frac{q}{p}\Big|^4}{1 + \Big|\frac{q}{p}\Big|^4} = -\frac{2|M_{12}||\Gamma_{12}|\sin\phi_{12}}{2|M_{12}|^2 + \frac{|\Gamma_{12}|^2}{2}} \quad (1.3.102)
\end{aligned}
$$

In the case of B_d^0 and B_s^0 mesons we can simplify the previous equation a bit further considering that $|\Gamma_{12}| \ll |M_{12}|$, then we obtain

$$\mathcal{A}_{CP_{mix}} \approx \frac{|\Gamma_{12}|}{|M_{12}|}\sin\phi_{12} = a_{sl}. \tag{1.3.103}$$

Where a_{sl} is called semileptonic asymmetry since it is common to use flavour specific semileptonic decays such as $B_s^0 \to X_s l^+ \nu_l$ and $B_d^0 \to X_d l^+ \nu_l$ for the measurement of $\mathcal{A}_{CP_{mix}}$. We will discuss in more detail the semileptonic asymmetries a_{sl}^s and a_{sl}^d corresponding to the neutral B_s^0 and B_d^0 respectively in the next chapter.

1.3.7 CP violation in interference between a decay with and without mixing

We are now interested in $\mathcal{CP}$ violation arising from the interference between mixing and decay, this is also called mixing induced $\mathcal{CP}$ violation. We consider final states f into which both the B_q^0 and the $\bar{B}_q^0$ can decay. This allows interference between the transitions $B_q^0 \to f$ and $B_q^0 \to \bar{B}_q^0 \to f$, leading to a relative phase responsible for the $\mathcal{CP}$ violation effect. In this section our analysis is given in terms of the following asymmetry

$$\mathcal{A}_{fCP}(t) = \frac{d\Gamma[\bar{B}_q^0 \to f](t)/dt - d\Gamma[B_q^0 \to f](t)/dt}{d\Gamma[\bar{B}_q^0 \to f](t)/dt + d\Gamma[B_q^0 \to f](t)/dt}. \tag{1.3.104}$$

After substituting Eq.(1.3.90) and Eq.(1.3.91) in Eq.(1.3.104), neglecting $\mathcal{CP}$ violation in mixing $\left|\frac{p}{q}\right| \approx 1$ and taking into account that for neutral B_q^0 mesons $\Delta\Gamma_q < \Delta M_q$, we get

$$\begin{aligned}\mathcal{A}_{fCP}(t) &= -\frac{1-|\lambda_f^q|^2}{1+|\lambda_f^q|^2}\cos\Delta M_q t + \frac{2\mathcal{I}m(\lambda_f^q)}{1+|\lambda_f^q|^2}\sin\Delta M_q t \\ &= S_f \sin\Delta M_q t - C_f \cos\Delta M_q t,\end{aligned} \tag{1.3.105}$$

where

$$C_f = \frac{1-|\lambda_f^q|^2}{1+|\lambda_f^q|^2}, \qquad S_f = \frac{2\mathcal{I}m(\lambda_f^q)}{1+|\lambda_f^q|^2}. \tag{1.3.106}$$

Of particular interest are final states that are also $\mathcal{CP}$ eigenstates because the B_q^0 and the $\bar{B}_q^0$ mesons decay into them at equal rates. For $\mathcal{CP}$ eigenstates

$$|\bar{f}_{CP}\rangle = \mathcal{CP}|f_{CP}\rangle = \eta_f|f_{CP}\rangle \quad \text{and} \quad \bar{A}_{fCP} = \eta_f \bar{A}_{\bar{f}CP}, \tag{1.3.107}$$

with $\eta = 1$ for $\mathcal{CP}$ even states and $\eta = -1$ for $\mathcal{CP}$ odd states. We can then rewrite the λ^q factor in Eq.(1.3.89) as

$$\lambda^q_{fCP} \;=\; \eta_f \frac{\bar{A}_{\bar{f}CP}}{A_{fCP}} \frac{q}{p}, \tag{1.3.108}$$

and the coefficient C_f can be simplified to $C_{fCP} = (1-\left|\frac{\bar{A}_{\bar{f}CP}}{A_{fCP}}\right|^2)/(1+\left|\frac{\bar{A}_{\bar{f}CP}}{A_{fCP}}\right|^2)$. Up to one sign, the previous expression is the same as Eq.(1.3.97) obtained from CP violation in decay, therefore C_f determines the $\mathcal{CP}$ violation in decay component inside Eq.(1.3.104). In the case of $\mathcal{CP}$ eigenstates there is no $\mathcal{CP}$ violation in mixing and no $\mathcal{CP}$ violation in decay (this last condition holds because according to Eq.(1.3.107) $|\bar{A}_{\bar{f}CP}| = |A_{fCP}|$), consequently $C_f = 0$ and we get the simplified Equation for the asymmetry Eq.(1.3.105)

$$\mathcal{A}_{fCP}(t) \;=\; S_{fCP} \sin \Delta M t \tag{1.3.109}$$

where

$$S_f \;=\; \mathcal{I}m(\lambda_{fCP}) = \eta_f \mathcal{I}m\Big(\frac{\bar{A}_{\bar{f}CP}}{A_{fCP}} \frac{q}{p}\Big). \tag{1.3.110}$$

If in addition there is only one CKM structure contributing to the decay amplitude (this holds when the effect from penguins can be neglected) we write the amplitudes in Eq.(1.3.110) in terms of a single strong ϕ^{strong} and a single weak phase ϕ^{CKM}

$$A_{fCP} = A_j e^{i(\phi^{strong}+\phi^{CKM})}, \qquad \bar{A}_{\bar{f}CP} = A_j e^{i(\phi^{strong}-\phi^{CKM})}. \tag{1.3.111}$$

As it has been stated already for B_q^0 ($q = s, d$) systems $|\Gamma_{12}| \ll |M_{12}|$, then Eq.(1.3.57) can be simplified to

$$\frac{q}{p} \approx \frac{M_{12}^*}{|M_{12}|}. \tag{1.3.112}$$

For neutral $B_{s,d}^0$ mesons the phase of M_{12}^* is twice the negative value of the CKM phase $\beta_{s,d}$ defined in Eq.(1.4.116) [1], therefore

[1] In Eq.(1.4.116) we define the CKM phase β_d corresponding to B_d^0 mesons (conventionally denoted as β [1, 17]). The analogous phase β_s for B_s^0 mesons is determined according to $\beta_s := -\arg\Big(-(V_{cs}V_{cb}^*)/(V_{ts}V_{tb}^*)\Big)$ [17] (notice the extra overall minus sign with respect to Eq.(1.4.116)).

$$\frac{q}{p} \approx e^{-2i\beta_q}. \tag{1.3.113}$$

Combining the complex phases from Eq.(1.3.111) and Eq.(1.3.113) we can finally write

$$S_f \;=\; \eta_f \sin(-2\beta_q - 2\phi_j^{CKM}). \tag{1.3.114}$$

As an example we quote the value for the asymmetry S_f when it is calculated from the decay $B_s^0 \to J/\psi\phi$, in this case the leading CKM structure is just β_s and we obtain

$$S_f = -\eta_f \sin 2\beta_s. \tag{1.3.115}$$

1.4 The CKM angles

In this section we center our discussion on the measurement of the CKM angles defined by the second of the unitarity conditions in Eq.(1.2.34) whose graphical representation corresponds to the triangle shown in Fig.1.1. The definition of the angles in terms of the CKM elements can be read directly from Fig.1.1. Moreover, they can be written at leading order using the Wolfenstein parameterization introduced in Eq.(1.2.37) as

$$\begin{aligned}
\beta &= \phi_1 = \arg\Big(-\frac{V_{cd}V_{cb}^*}{V_{td}V_{tb}^*}\Big) \approx \arg\Big(\frac{1}{1-\rho-i\eta}\Big),\\
\alpha &= \phi_2 = \arg\big(-\frac{V_{td}V_{tb}^*}{V_{ud}V_{ub}^*}\Big) \approx \arg\Big(-\frac{1-\rho-i\eta}{\rho+i\eta}\Big),\\
\gamma &= \phi_3 = \arg\Big(-\frac{V_{ud}V_{ub}^*}{V_{cd}V_{cb}^*}\Big) \approx \arg\Big(\rho+i\eta\Big).
\end{aligned} \tag{1.4.116}$$

In the following subsections we elaborate briefly on how these angles are determined, the CKM angle γ will be of particular interest in Chapter 4 where we will analyse how possible new physics effects at tree level can affect the precision on its determination.

1.4.1 β/ϕ_1

The CKM angle β is measured as an effect of $\mathcal{CP}$ violation in interference through the following asymmetry for neutral $B_d^0, \bar{B}_d^0$ mesons - see Eq.(1.3.105) -

$$\begin{aligned}\mathcal{A}_{fCP}(t) &= \frac{d\Gamma[\bar{B}_d^0 \to f](t)/dt - d\Gamma[B_d^0 \to f](t)/dt}{d\Gamma[\bar{B}_d^0 \to f](t)/dt + d\Gamma[B_d^0 \to f](t)/dt} \\ &= S_f \sin \Delta M_d t - C_f \cos \Delta M_d t. \end{aligned} \tag{1.4.117}$$

We are interested in final $\mathcal{CP}$ eigenstates f for which $C_f = 0$ and $S_f = 2\mathcal{I}m\lambda_f^d/(1 + |\lambda_f^d|^2) = -\eta_f \sin 2\phi$ where λ_f^d is the ratio of the transition amplitudes introduced in Eq.(1.3.89), η_f is the $\mathcal{CP}$ eigenvalue of f and 2ϕ is the phase difference between the decay paths $B_d^0 \to f$ and $B_d^0 \to \bar{B}_d^0 \to f$, see Section 1.3.7. β can be determined through $b \to c\bar{c}s$ transitions to final $\mathcal{CP}$ eigenstates such as $B_d^0 \to J/\psi K_L^0$ for which the ratio of amplitudes λ_f^d is

$$\lambda_f^d = \Big(\frac{V_{tb}^* V_{td}}{V_{tb} V_{td}^*}\Big)\Big(\eta_f \frac{V_{cb} V_{cs}^*}{V_{cb}^* V_{cs}}\Big)\Big(\frac{V_{cd}^* V_{cs}}{V_{cd} V_{cs}^*}\Big) = -\eta_f \sin 2\beta. \tag{1.4.118}$$

The combination of CKM factors inside the first round bracket arises from the ratio q/p introduced in Eq.(1.3.55). The content of the second bracket comes from the tree level B decay amplitude, finally the third bracket is the result of $K^0 - \bar{K}^0$ mixing [18].

In addition to the tree level amplitude T there are also contributions from penguin diagrams with partial amplitudes $V_{ub}V_{us}^* P^u$, $V_{cb}V_{cs}^* P^c$, $V_{tb}V_{ts}^* P^t$ where the quarks running inside the loop are the up, the charm and the top respectively. Schematically we can write

$$\begin{aligned} A_{c\bar{c}s} &= V_{cb}V_{cs}^* T + V_{ub}V_{us}^* P^u + V_{cb}V_{cs}^* P^c + V_{tb}V_{ts}^* P^t \\ &= V_{cb}V_{cs}^*(T + P^c - P^t) + V_{ub}V_{us}^*(P^u - P^t), \end{aligned} \tag{1.4.119}$$

where we have used the third unitarity condition in Eq.(1.2.34) to eliminate the product $V_{tb}V_{ts}^*$ in terms of $V_{cb}V_{cs}^*$ and $V_{ub}V_{us}^*$. Considering $\Big|(V_{ub}V_{us}^*)/(V_{cb}V_{cs}^*)\Big| \approx \mathcal{O}(\lambda^3)$ we see that, the weak phase contribution arising from penguins is suppressed in comparison with the tree level weak phase by a factor of at least order λ^3. The current world average for β based on the decay channels $B_d^0 \to$ charmonium $K_{S,L}^0$ using data from ALEPH, OPAL, CDF, LHCb, Babar and Belle is [1]

$$\sin 2\beta = 0.691 \pm 0.017. \tag{1.4.120}$$

Other options for the measurement of β are decays mediated by the transition $b \to c\bar{c}d$ such as $B_d^0 \to J/\psi\pi^0$, $B_d^0 \to D^+D^-$ and $B_d^0 \to D^{(*)+}D^{(*)-}$; however, in

these cases the contributions from tree level and penguin diagrams are of the same order in the CKM structure and each one of them introduces a different weak phase arising from the CKM combinations $V_{cb}^* V_{cd}$ and $V_{tb}^* V_{td}$ respectively. Consequently these options are less clean than the ones based on charmonium.
The CKM phase β can also be determined from the penguin free transition $b \to c\bar{u}d$ for final states common to both B_d^0 and $\bar{B}_d^0$. The world average value available at the moment uses data from BABAR and Belle and is based on the $\mathcal{CP}$ even final states: $D\pi^0$, $D\eta$, $D\omega$, $D^*\pi^0$ and $D^*\eta$ with the secondary decays $D^* \to D\pi^0$ and $D \to K_S\pi^+\pi^-$. Based on this method the final world average available is $\sin 2\beta = 0.63 \pm 0.11$ [1].

Considering that the penguin dominated transitions $b \to s\bar{q}q$ have the same weak phase as the tree level decay chain $b \to c\bar{c}s$,$V_{tb}^* V_{ts} = -V_{cb}^* V_{cs}\Big(1 + \mathcal{O}(\lambda^2)\Big)$. Decays such as $B_s^0 \to \phi\phi$, $B^0 \to \phi K^0$ and $B^0 \to \eta' K^0$ can be used to extract β in the SM. These penguins are sensitive to possible BSM phases that could result into $S_f \neq -\eta_f \sin 2\beta$ and $C_f \neq 0$. Among the decays used in [1] within this category we have $B \to \pi^0 K_S^0, K_S^0 K_S^0 K_S^0, \rho^0 K_S, \omega K_S$ leading to the current naive penguin average $\sin 2\beta = 0.655 \pm 0.032$ [1].

1.4.2 γ/ϕ_3

As can be seen in the third of Eq.(1.4.116) the phase γ does not depend on the CKM elements involving the top quark, this is one of reasons that make its determination from tree level processes possible. The experimental extraction of γ takes advantage of the interference between the transitions $B^- \to D^0 K^-$ and $B^- \to \bar{D}^0 K^-$, with D^0 and $\bar{D}^0$ decaying to common final states f_D. At quark level the transitions $B^- \to D^0 K^-$ and $B^- \to \bar{D}^0 K^-$ correspond to the decay chains $b \to c\bar{u}s$ and $b \to u\bar{c}s$ respectively; the CKM angle γ can be extracted from the ratio

$$r_B e^{(\delta_B - \gamma)} = \frac{\mathcal{A}(B^- \to \bar{D}^0 K^-)}{\mathcal{A}(B^- \to D^0 K^-)}, \tag{1.4.121}$$

where the weak phase arises from $(V_{ub}V_{cs}^*)/(V_{cb}V_{us}^*)$ and δ_B is the relative strong phase.

The different experimental methods available for the determination of γ depend on the final state f_D considered. In the GLW method proposed by Gronau, London and Wyler [19], [20] decays of the D^0 and the $\bar{D}^0$ meson to common $\mathcal{CP}$ eigenstates are taken into account: this includes $\mathcal{CP}$ even states such as K^+K^- as well as $\mathcal{CP}$ odd states such as $K^0_S\pi^0$. One of the problems with the GLW method is that the process $B^- \to K^-\bar{D}^0$ is colour suppressed whereas $B^- \to K^-D^0$ is colour allowed, consequently the ratio r_B is relatively small ($r_B \approx 0.1 - 0.2$) making it difficult to measure. In order to deal with this technical issue Atwood, Dunietz and Soni [21], [22] -ADS- suggested to focus on final decay states where Cabibbo allowed decay $\bar{D}^0$ and doubly Cabibbo-suppressed D^0 decays interfere. One example is the transition $B^- \to [K^+\pi^-]_D K^-$, that can be obtained through two channels: the Cabibbo favored decay $B^- \to D^0K^-$ followed by the double Cabibbo suppressed process $D^0 \to K^+\pi^-$, or the Cabibbo suppressed transition $B^- \to \bar{D}^0K^-$ followed by the Cabibbo favored decay $\bar{D}^0 \to K^+\pi^-$. Several studies using the GLW and the ADS method have been made by the B factories [23], the CDF collaboration [24] and the LHCb collaboration [25].

Another method for the determination of γ was proposed by Giri, Grossman, Soffer and Zupan (GGSZ) [26] and is based on the Dalitz plot study of three body decays of the D meson in $B^\pm \to DK^\pm$ to final states such as $K^0_S\pi^+\pi^-$, $K^0_SK^+K^-$ and $\pi^+\pi^-\pi^0$. In particular the mode $D^0 \to K^0_S\pi^+\pi^-$ has three advantages:

- large branching fraction,
- high sensitivity to γ because of the large interference between the processes $D^0 \to K^0_S\pi^+\pi^-$ and $\bar{D}^0 \to K^0_S\pi^+\pi^-$,
- rich resonant structure, which provides large variations of the strong phase in D decays leading to a good sensitivity in the measurement of γ and low dependency on the strong phase δ_B.

With the GGSZ method Belle and BABAR measured $\gamma = (78.4^{+10.8^\circ}_{-11.6^\circ} \pm 3.6^\circ \pm 8.9)^\circ$ [27] and $\gamma = (68 \pm 14 \pm 4 \pm 3)^\circ$ [28] respectively where the last uncertainty arises from the D-decay modeling.

Combining the results from the three methods the values for γ reported by BaBar, Belle and LHCb collaborations are $(69^{+17}_{-16})^\circ$ [29] , $(68^{+15}_{-14})^\circ$ [30] and $(70.9^{+7.1}_{-8.5})^\circ$ [31] respectively, all the numbers quoted in this paragraph are summarized in the Section "Unitarity Triangle Parameters" of [1].

1.4.3 α/ϕ_2

The CKM angle α is measured using time-dependent $\mathcal{CP}$ asymmetries in $b \to u\bar{u}d$ dominated transitions. One complication arises from the fact that the $b \to d$ penguin decays and the tree level $b \to u\bar{u}d$ have a different CKM phase and their magnitudes are of the same size in λ. Among the different channels used for the extraction of α we have $B \to \pi\pi, \rho\pi, \rho\rho$.

The $B \to \pi\pi$ decays get a sizable contribution from $b \to d$ penguin amplitudes then if we use the asymmetry in Eq.(1.4.117) with $f = \pi^+\pi^-$ the coefficient S_f will no longer be proportional to $\sin(2\alpha)$ but rather to $\sin(2\alpha_{eff})$ where $\alpha_{eff} = \alpha + \Delta\alpha$ (in contrast with the results found for β), here $\Delta\alpha$ quantifies the effect from penguins. Due to the non negligible contribution from penguins we will have direct $\mathcal{CP}$ violation, thus $A_f \neq \bar{A}_{\bar{f}}$ as explained in Section 1.3.5 implying $C_f \neq 0$ in Eq.(1.4.117). The determination of α from the final states $\pi\pi$ uses the isospin analysis based on the relationship $\frac{1}{\sqrt{2}}A_{\pi^+\pi^-} + A_{\pi^0\pi^0} - A_{\pi^+\pi^0} = 0$ introduced in [32]. Using this method Belle excludes the range $23.8^\circ < \alpha < 66.8^\circ$ at 1σ level [33], on the other hand BaBar quotes $71.0^\circ < \alpha < 109^\circ$ at the 68% C. L. [34] as stated in [1].

The determination of α through the decay $B \to \rho\rho$ is also based on an isospin analysis. Using the longitudinal polarization fractions in $B^+ \to \rho^+\rho^0$ and $B^0 \to \rho^+\rho^-$ it was found that the final states are almost $\mathcal{CP}$-even only and also that the effect of penguins is small. The averages for the asymmetry coefficients $S_{\rho^+\rho^-}$ and $C_{\rho^+\rho^-}$ in Eq.(1.4.117) based on measurements from BaBar [35] and Belle [36] give -0.14 ± 0.13 and 0.00 ± 0.09 respectively [1]. The results for α from BaBar based on $\rho\rho$ final states read $\alpha = (92.4^{+6.0}_{-6.5})^\circ$ and $\alpha = (93.7 \pm 10.6)^\circ$ in the case of Belle [36]. Finally it is possible to determine α using the decays $B^0_d \to \pi^+\pi^-\pi^0$ [37], [38]. In this case the study is performed using a time dependent Dalitz plot analysis of the three body final state. One of the advantages of this method is that there is only

one discrete ambiguity since the variations of the strong phases in the interference regions of the $\rho^+\pi^-$, $\rho^-\pi^+$ and $\rho^0\pi^0$ amplitudes are known. Using this method Belle reported [39] $68^\circ < \alpha < 95^\circ$ at the 68.3% confidence level.

Chapter 2

Effective field theories in flavour physics

In this chapter we introduce the basics of the formalism of effective hamiltonians used in the calculation of hadronic amplitudes in flavour physics. In the first section we present the method in the case of current-current [1] transitions, followed by a discussion on the determination of the Wilson coefficients by matching the effective theory with the full SM calculation. We will see that this step leads to expressions with logarithms that can potentially break the perturbative expansions if there is a big gap between the matching scale and the effective scale. We show how this problem is solved using the renormalization group equations at leading and next to leading order in α_s. Then we present the full $\Delta F = 1$ effective Hamiltonian including electroweak and QCD penguins. We conclude with an overview on the $\Delta F = 2$ Hamiltonian and show briefly its usage in the determination of the mixing observables $\Delta\Gamma_q$ and ΔM_q associated with neutral B_q^0 mesons. The approach followed here is based mainly on [10], [40] and the references cited therein.

[1] Here the term "current" makes reference to weak currents $\bar{\psi}'\gamma^\mu(1-\gamma^5)\psi$ defined in analogy to the QED electromagnetic currents $j^\mu = \bar{\psi}'\gamma^\mu\psi$; where ψ' and ψ are two fermionic fields.

2.1 Current-current effective field theories

In order to illustrate the construction and application of effective Hamiltonians we consider the amplitude for the transition $b \to c\bar{u}d$. In the SM this decay is given by the diagram shown in Fig.2.1 and the corresponding amplitude is

$$A_{b\to c\bar{u}d} = iM_W^2 \frac{G_F}{\sqrt{2}} V_{cb}V_{ud}^* \frac{\left[\bar{c}_\alpha \gamma^\mu (1-\gamma_5) b_\alpha\right]\left[\bar{d}_\beta \gamma_\mu (1-\gamma_5) u_\beta\right]}{k^2 - M_W^2}, \quad (2.1.1)$$

where α, β are colour indices and G_F is the Fermi coupling defined in terms of the electroweak coupling constant g as

$$G_F := \frac{\sqrt{2} g^2}{8\ M_W^2}. \quad (2.1.2)$$

We can expand the denominator in Eq.(2.1.1) in powers of $\frac{k^2}{M_W^2}$ considering that for the process of interest $k^2 \ll M_W^2$ so that $A_{b\to c\bar{u}d}$ becomes

$$\begin{aligned} A_{b\to c\bar{u}d} &= -i\frac{G_F}{\sqrt{2}} V_{cb}V_{ud}^* \left[\bar{c}_\alpha \gamma^\mu (1-\gamma_5) b_\alpha\right]\left[\bar{d}_\beta \gamma_\mu (1-\gamma_5) u_\beta\right] + \mathcal{O}(\frac{k^2}{M_W^2}) \\ &= -i\frac{G_F}{\sqrt{2}} V_{cb}V_{ud}^* \Big(\bar{c}_\alpha b_\alpha\Big)_{V-A} \Big(\bar{d}_\beta u_\beta\Big)_{V-A} + \dots . \end{aligned} \quad (2.1.3)$$

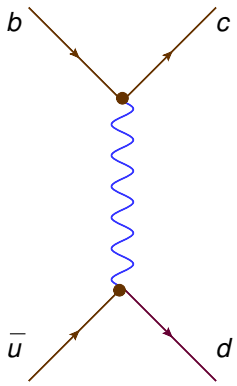

Figure 2.1: Current-current transition $b \to c\bar{u}d$.

The result is then an "effective amplitude" where the W boson has been "integrated out", the graphical representation of Eq.(2.1.3) is shown in Fig.2.2.

The amplitude in Eq.(2.1.3) can be obtained through the following "effective Hamiltonian"

$$\hat{\mathcal{H}}_{eff} = \frac{G_F V_{cb}V_{ud}^*}{\sqrt{2}} \Big(\bar{c}_\alpha b_\alpha\Big)_{V-A} \Big(\bar{d}_\beta u_\beta\Big)_{V-A}. \quad (2.1.4)$$

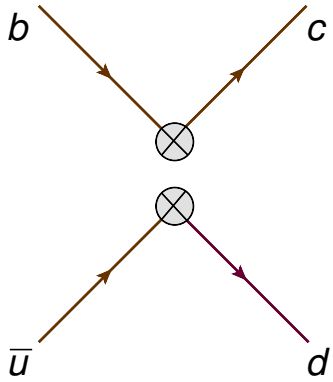

Figure 2.2: Effective diagram for the current-current transition $b \to c\bar{u}d$.

Next, we generalize Eq.(2.1.4) in order to account for higher order QCD perturbative corrections by writing $\hat{\mathcal{H}}_{eff}$ as

$$\hat{\mathcal{H}}_{eff} = \frac{G_F V_{cb} V_{ud}^*}{\sqrt{2}} \Big(C_1 \hat{Q}_1 + C_2 \hat{Q}_2 \Big). \tag{2.1.5}$$

The operators $\hat{Q}_1$ and $\hat{Q}_2$ include the quark fields relevant to our process. The coefficients C_1 and C_2 in Eq.(2.1.5) are called "Wilson coefficients" [41–44], they can be thought as the coupling constants for the effective interactions in the operators $\hat{Q}_1$ and $\hat{Q}_2$.

Unless stated otherwise, in this thesis we follow the convention

$$\hat{Q}_1 = \Big(\bar{c}_\alpha b_\beta \Big)_{V-A} \Big(\bar{d}_\beta u_\alpha \Big)_{V-A} \qquad \hat{Q}_2 = \Big(\bar{c}_\alpha b_\alpha \Big)_{V-A} \Big(\bar{d}_\beta u_\beta \Big)_{V-A}. \tag{2.1.6}$$

Notice that the definitions in Eq.(2.1.6) are not unique, sometimes the colour structures of $\hat{Q}_1$ and $\hat{Q}_2$ appear interchanged in the literature, see for example [45].

In principle, to reproduce Eq.(2.1.3) only $\hat{Q}_2$ is required; however, $\hat{Q}_1$ arises when QCD loops are included, we will show this below.

Our expression for the effective Hamiltonian in Eq.(2.1.5) is an example of an Operator Product Expansion because the product of two charged current operators is expanded as a series of local operators multiplied by effective coupling constants C_1 and C_2. We will see at the end of this section that one of the most attractive features of the OPE is the factorization into short distance and long distance contributions given by the matrix elements of the effective operators and the Wilson coefficients respectively.

Now we present the procedure for the determination of the Wilson coefficients C_1 and C_2 at one loop in α_s. To begin with we have to determine, in the full theory,

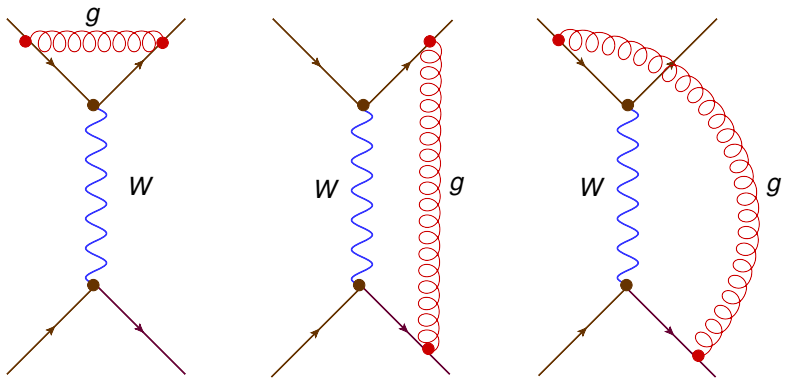

Figure 2.3: One loop QCD corrections to the current-current transition $b \to c\bar{u}d$ (their symmetric counterparts should also be taken into account).

the amplitude for the process $b \to c\bar{u}d$ including the set of topologies in Fig.2.1 and Fig.2.3. After doing the corresponding calculations the final expression for the amplitude in the full theory is

$$A^{(0)}_{\text{full}} = \frac{G_F V_{cb} V^*_{ud}}{\sqrt{2}} \Big(\Big[1 + 2C_F \frac{\alpha_s}{4\pi} \Big(\frac{1}{\varepsilon} + \ln\Big[-\frac{\mu^2}{p^2} \Big] \Big) + \frac{3}{N} \frac{\alpha_s}{4\pi} \ln\Big[-\frac{M_W^2}{p^2} \Big] \Big] \langle \hat{Q}_2 \rangle_{\text{Tree}} + -3 \frac{\alpha_s}{4\pi} \ln\Big[-\frac{M_W^2}{p^2} \Big] \langle \hat{Q}_1 \rangle_{\text{Tree}} \Big) = A'^{(0)} \langle \hat{Q}_2 \rangle_{\text{Tree}} + B'^{(0)} \langle \hat{Q}_1 \rangle_{\text{Tree}}, \quad (2.1.7)$$

where

$$A'^{(0)} = 1 + 2C_F \frac{\alpha_s}{4\pi} \Big(\frac{1}{\varepsilon} + \ln\Big[-\frac{\mu^2}{p^2} \Big] \Big) + \frac{3}{N} \frac{\alpha_s}{4\pi} \ln\Big[-\frac{M_W^2}{p^2} \Big],$$
$$B'^{(0)} = -3 \frac{\alpha_s}{4\pi} \ln\Big[-\frac{M_W^2}{p^2} \Big]. \quad (2.1.8)$$

In Eq.(2.1.7) and Eq.(2.1.8) p is the four momentum of the decaying b-quark, N is the number of colours (here we consider $N = 3$) and $C_F = (N^2 - 1)/(2\ N)$. The flux of colour mediated by the gluon in the second and third diagrams in Fig.2.3 leads to the operator $\hat{Q}_1$ as an effect of $\mathcal{O}(\alpha_s)$. The tree level matrix elements of the operators $\hat{Q}_1$ and $\hat{Q}_2$ are given by $\langle \hat{Q}_1 \rangle_{\text{Tree}}$ and $\langle \hat{Q}_2 \rangle_{\text{Tree}}$ respectively. The loop integrals were calculated using dimensional regularization. It is found that only the first topology in Fig.2.3 is divergent and the corresponding pole is the $1/\varepsilon$ factor in Eq.(2.1.7), the other loop topologies are finite and do not need to be regularized.

The next step is to focus our attention on the calculation within the effective theory; we will use our results from Eq.(2.1.7) and Eq.(2.1.8) later. Firstly we evaluate the insertion of $\hat{Q}_1$ and $\hat{Q}_2$ in the diagrams shown in Fig.2.4, they are the effective version of the full theory diagrams presented in Fig.2.3, the results are

$$
\begin{aligned}
\langle \hat{Q}_1 \rangle^{(0)} &= \left(1 + 2C_F \frac{\alpha_s}{4\pi}\left(\frac{1}{\varepsilon} + \ln\left[-\frac{\mu^2}{p^2}\right]\right)\right)\langle \hat{Q}_1 \rangle_{\text{Tree}} \\
&\quad + \frac{3}{N}\frac{\alpha_s}{4\pi}\left(\frac{1}{\varepsilon} + \ln\left[-\frac{\mu^2}{p^2}\right]\right)\langle \hat{Q}_1 \rangle_{\text{Tree}} \\
&\quad - 3\frac{\alpha_s}{4\pi}\left(\frac{1}{\varepsilon} + \ln\left[-\frac{\mu^2}{p^2}\right]\right)\langle \hat{Q}_2 \rangle_{\text{Tree}} \\
\\
\langle \hat{Q}_2 \rangle^{(0)} &= \left(1 + 2C_F \frac{\alpha_s}{4\pi}\left[\frac{1}{\varepsilon} + \ln\left[-\frac{\mu^2}{p^2}\right]\right]\right)\langle \hat{Q}_2 \rangle_{\text{Tree}} \\
&\quad + \frac{3}{N}\frac{\alpha_s}{4\pi}\left(\frac{1}{\varepsilon} + \ln\left[-\frac{\mu^2}{p^2}\right]\right)\langle \hat{Q}_2 \rangle_{\text{Tree}} \\
&\quad - \frac{3\alpha_s}{4\pi}\left(\frac{1}{\varepsilon} + \ln\left(-\frac{\mu^2}{p^2}\right)\right)\langle \hat{Q}_1 \rangle_{\text{Tree}}. \qquad (2.1.9)
\end{aligned}
$$

Notice that the leading terms in Eq.(2.1.9) are obtained from the insertion of $\hat{Q}_1$ and $\hat{Q}_2$ in the diagram in Fig.2.2. Also there are now more $1/\varepsilon$ poles, the reason is that the second and third topologies in Fig.2.4 lead to new divergences when calculated using dimensional regularization.

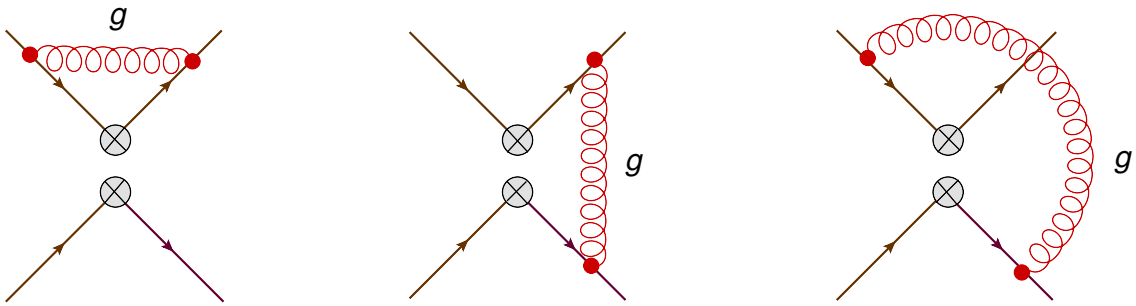

Figure 2.4: One loop QCD current-current diagrams in the effective theory, the $\otimes\ \otimes$ symbols denote the insertion of a 4 fermion operator $\hat{Q}_i$ (their symmetric counterparts should also be taken into account).

Before continuing it is convenient to discuss how the different $1/\varepsilon$ divergences are removed from Eq.(2.1.9). The contribution $2C_F\alpha_s/(4\pi\varepsilon)$ can be eliminated when doing the matching with the full SM calculation because it also appears in the full theory amplitude in Eq.(2.1.7) and Eq.(2.1.8); it can also be removed by renormalizing the quark fields through the renormalization constant $Z_q^{-1/2}$ (see below). To get rid of the remaining divergences we have to perform an additional operator renor-

malization through the matrix Z_{ij}. Then we write the following equation between the bare $\langle Q_j^{(0)}\rangle$ and the renormalized matrix element $\langle Q_j\rangle$

$$\langle \hat{Q}_i^{(0)}\rangle \;=\; Z_q^2 Z_{ij}\langle \hat{Q}_j\rangle. \tag{2.1.10}$$

Where Z_{ij} are the elements of the renormalization matrix $\hat{Z}$; in our case we can easily identify

$$\hat{Z} = 1 + \frac{\alpha_s}{4\pi N\varepsilon}\begin{bmatrix} 3 & -3N \\ -3N & 3 \end{bmatrix}, \tag{2.1.11}$$

where we have only considered the $1/\varepsilon$ poles not multiplying the factor $2C_F\alpha_s/(4\pi)$. The renormalized operators $\hat{Q}_j$ read

$$\langle \hat{Q}_1\rangle = A\langle \hat{Q}_1\rangle_{\text{Tree}} + B\langle \hat{Q}_2\rangle_{\text{Tree}}, \qquad \langle \hat{Q}_2\rangle = B\langle \hat{Q}_1\rangle_{\text{Tree}} + A\langle \hat{Q}_2\rangle_{\text{Tree}}, \tag{2.1.12}$$

where

$$A = 1 + \frac{\alpha_s}{4\pi}\ln\Big[-\frac{\mu^2}{p^2}\Big]\Big(2C_F + \frac{3}{N}\Big), \qquad B = -\frac{3\alpha_s}{4\pi}\ln\Big[-\frac{\mu^2}{p^2}\Big]. \tag{2.1.13}$$

And the effective amplitude corresponding to the process $b \to c\bar{u}d$ can be written as

$$\begin{aligned}\langle \hat{H}_{\text{eff}}\rangle \;&=\; C_1\langle \hat{Q}_1\rangle + C_2\langle \hat{Q}_2\rangle \\ &=\; \Big(C_1A + C_2B\Big)\langle \hat{Q}_1\rangle_{\text{Tree}} + \Big(C_1B + C_2A\Big)\langle \hat{Q}_2\rangle_{\text{Tree}}.\end{aligned} \tag{2.1.14}$$

Before doing the matching between the effective theory and the full SM calculation we have to eliminate the ε pole appearing in the amplitude in Eq.(2.1.7); here we remove this divergence by renormalizing the quark operators in the full SM as we did in Eq.(2.1.10), the new renormalized SM amplitude A_{full} is identical to Eq.(2.1.7) but without the term including the divergent term $2C_F\alpha_s/(4\pi\varepsilon)$.

We are ready to match the renormalized SM amplitude $A_{\text{full}}^{(0)}$ in Eq.(2.1.7) with the effective theory determination in Eq.(2.1.14), the required condition reads

$$A_{\text{full}}^{(0)} \;=\; \langle \hat{H}_{\text{eff}}\rangle. \tag{2.1.15}$$

Using Eq.(2.1.8) and Eq.(2.1.13) we find

$$C_1A + C_2B = B', \qquad C_1B + C_2A = A', \tag{2.1.16}$$

where the coefficient $A^{'}$ is the same as $A^{'(0)}$ up to the term $2C_F\alpha_s/(4\pi\varepsilon)$ and $B^{'} = B^{'(0)}$ in Eq.(2.1.8), and we can solve for C_1 and C_2 to get at order α_s

$$\begin{aligned} C_1 &= \frac{AB' - A'B}{A^2 - B^2} \approx B' - B \approx -\frac{3\alpha_s}{4\pi}\ln\Big[\frac{M_W^2}{\mu^2}\Big], \\ C_2 &= \frac{A'A - B'B}{A^2 - B^2} \approx \frac{A'}{A} \approx 1 + 3\frac{\alpha_s}{4\pi N}\ln\Big[\frac{M_W^2}{\mu^2}\Big]. \end{aligned} \tag{2.1.17}$$

This is the set of equations we were looking for, however they should be improved. The logarithms $\ln\Big[\frac{M_W^2}{\mu^2}\Big]$ can break our naive perturbative expansion if the difference between the scales M_W and μ is large. We will discuss in Section 2.2.1 the resummation of these logarithms using the renormalization group equations.

As we mentioned at the beginning of this chapter one of the most attractive features of the OPE is the factorization into short distance and long distance contributions, this can be verified explicitly by looking at the logarithms appearing in the equations for the Wilson coefficients in Eq.(2.1.17) and in the renormalized versions of the matrix elements for the operators $\hat{Q}_1$ and $\hat{Q}_2$ shown next

$$\begin{aligned} \langle\hat{Q}_1\rangle &= \Big(1 + 2C_F\frac{\alpha_s}{4\pi}\ln\Big[-\frac{\mu^2}{p^2}\Big] + \frac{3}{N}\frac{\alpha_s}{4\pi}\ln\Big[-\frac{\mu^2}{p^2}\Big]\Big)\langle\hat{Q}_1\rangle_{\text{Tree}} \\ &\quad -3\frac{\alpha_s}{4\pi}\ln\Big[-\frac{\mu^2}{p^2}\Big]\langle\hat{Q}_2\rangle_{\text{Tree}}, \\ \\ \langle\hat{Q}_2\rangle &= -\frac{3\alpha_s}{4\pi}\ln\Big[-\frac{\mu^2}{p^2}\Big]\langle\hat{Q}_1\rangle_{\text{Tree}} \\ &\quad +\Big(1 + 2C_F\frac{\alpha_s}{4\pi}\ln\Big[-\frac{\mu^2}{p^2}\Big] + \frac{3}{N}\frac{\alpha_s}{4\pi}\ln\Big[-\frac{\mu^2}{p^2}\Big]\Big)\langle\hat{Q}_2\rangle_{\text{Tree}}. \end{aligned} \tag{2.1.18}$$

The logarithms $\ln\Big[-M_W^2/p^2\Big]$ appearing in the full theory amplitude Eq.(2.1.7) can be factorized, at $\mathcal{O}(\alpha_s)$, according to the following schematic equation

$$1 + \alpha_s\ln\Big[-M_W^2/p^2\Big] = \Big(1 + \alpha_s\ln\Big[M_W^2/\mu^2\Big]\Big)\Big(1 + \alpha_s\ln\Big[-\mu^2/p^2\Big]\Big), \tag{2.1.19}$$

where all the short distance scales are in the factor $\Big(1 + \alpha_s\ln\Big[M_W^2/\mu^2\Big]\Big)$ and the long distance ones in $\Big(1 + \alpha_s\ln\Big[-\mu^2/p^2\Big]\Big)$. It can be seen that as a consequence of the effective theory approach described in this section, the short distance scales end up in the Wilson coefficients in Eq.(2.1.17) whereas the long distance contributions are contained in the matrix elements of the effective operators in Eq.(2.1.18).

2.1.1 Operator renormalization

We make a small digression in order to compare two possible options to renormalise the effective amplitude computed from Eq.(2.1.9). The first one called composite operator renormalization was applied in the previous section, here the bare operators are renormalized according to

$$\hat{Q}_i^{(0)} = Z_{ij}\hat{Q}_j, \tag{2.1.20}$$

where in this section repeated indices are implicitly summed over.
For the matrix elements we have

$$\langle\hat{Q}_i\rangle^{(0)} = Z_{ij}Z_q^{-2}\langle\hat{Q}_j\rangle, \tag{2.1.21}$$

or equivalently

$$\langle\hat{Q}_j\rangle = Z_{ji}^{-1}Z_q^2\langle\hat{Q}_i\rangle^{(0)}, \tag{2.1.22}$$

where we have used

$$\hat{q}^{(0)} = Z_q^{1/2}\hat{q}.$$

Finally, we can express the fully renormalized amplitude as

$$A_{\text{eff}} = C_j\langle\hat{Q}_j\rangle = Z_{ji}^{-1}Z_q^2C_j\langle\hat{Q}_i\rangle^{(0)}, \tag{2.1.23}$$

where for simplicity we have dropped CKM factors and an overall constant G_F.
Now we can show the relationship between this approach and the conventional counterterm procedure, for which the bare Wilson coefficients $C_i^{(0)}$ are renormalized according to $C_i^{(0)} = Z_{ij}^c C_j$ so that the effective Hamiltonian reads

$$\hat{H}_{\text{eff}} = C_i^{(0)}\hat{Q}_i(\hat{q}^{(0)}) = Z_{ij}^c C_j Z_q^2\hat{Q}_i^{(0)}(\hat{q}), \tag{2.1.24}$$

and the renormalized effective amplitude is given by

$$A_{\text{eff}} = \langle H_{\text{eff}}\rangle = Z_{ij}^c C_j Z_q^2\langle\hat{Q}_i\rangle^{(0)}. \tag{2.1.25}$$

If we compare Eq.(2.1.23) with Eq.(2.1.25) we find the following equality between Z_{ij}^{-1} and Z_{ij}^c

$$Z_{ji}^{-1} = Z_{ij}^c. \tag{2.1.26}$$

2.2 Renormalization group equations

In Eq.(2.1.17) the Wilson coefficients were calculated by matching the effective theory with the full SM calculation. It can be seen that large logarithms can occur when there is a big difference between the renormalization and the matching scales, μ and M_W respectively, leading to a potential breakdown of perturbation theory. To cure this problem we should resum the logarithms to all orders through the renormalization group equations for the Wilson coefficients, this section is devoted to the description of this formalism.

To begin with, consider again Eq.(2.1.20) for composite operator renormalization

$$\hat{Q}_i^{(0)} \;=\; Z_{ij}\hat{Q}_j.$$

As usual in quantum field theory, the bare operator $\hat{Q}_i^{(0)}$ should be scale independent, consequently

$$\mu\frac{d\hat{Q}_i^{(0)}}{d\mu} = Z_{ij}\mu\frac{d\hat{Q}_j}{d\mu} + \mu\frac{dZ_{ij}}{d\mu}\hat{Q}_j = 0 \implies \mu\frac{d\hat{Q}_j}{d\mu} = -Z^{-1}_{jk}\mu\frac{dZ_{ki}}{d\mu}\hat{Q}_i \quad (2.2.27)$$

and we define the anomalous dimension matrix as

$$\gamma_{ij} \;:=\; Z^{-1}_{jk}\mu\frac{dZ_{ki}}{d\mu}. \quad (2.2.28)$$

The effective weak hamiltonian should also be independent of the renormalization scale μ, therefore

$$\mu\frac{d\hat{H}_{\text{eff}}}{d\mu} = \mu\frac{d}{d\mu}\Big(C_j\hat{Q}_j\Big) = 0 \implies \mu\frac{dC_j}{d\mu}\hat{Q}_j = -C_j\mu\frac{d\hat{Q}_j}{d\mu} \quad (2.2.29)$$

and using Eq.(2.2.27) and Eq.(2.2.28) we get

$$\mu\frac{dC_j}{d\mu}\hat{Q}_j \;=\; -C_j\mu\frac{d\hat{Q}_j}{d\mu} = C_jZ^{-1}_{jk}\mu\frac{dZ_{ki}}{d\mu}\hat{Q}_i = C_j\gamma_{ji}\hat{Q}_i. \quad (2.2.30)$$

Then the renormalization group equations for C_i read

$$\mu\frac{dC_i}{d\mu} = \gamma_{ji}C_j. \quad (2.2.31)$$

2.2.1 Resummed Wilson coefficients for tree level processes

We can now obtain generalized solutions for the Wilson coefficients C_1 and C_2 where the logarithms appearing in Eq.(2.1.17) are resummed to all orders in perturbation

theory. As a first step we proceed with the explicit determination of the anomalous dimension matrix defined in Eq.(2.2.28), this requires the calculation of the derivative of Eq.(2.1.11) with respect to the renormalization scale μ

$$\mu\frac{d\hat{Z}}{d\mu} = \frac{d\hat{Z}}{d\ln\mu} = \frac{1}{4\pi N\varepsilon}\frac{d\alpha_s}{d\ln\mu}\begin{bmatrix} 3 & -3N \\ -3N & 3 \end{bmatrix}. \tag{2.2.32}$$

To simplify Eq.(2.2.32) it is convenient to introduce the QCD β function. In this work we use the following definition expressed in terms of α_s [13], [40]

$$\beta \;:=\; \frac{\mu}{2}\frac{d\alpha_s}{d\mu} = \frac{1}{2}\frac{d\alpha_s}{d\ln\mu} = -\varepsilon\alpha_s - \frac{\beta_0}{4\pi}\alpha_s^2 - \frac{\beta_1}{(4\pi)^2}\alpha_s^3 + \mathcal{O}(\alpha_s^4). \tag{2.2.33}$$

Where the required coefficients are

$$\beta_0 = \frac{11N-2f}{3}, \quad \beta_1 = \tfrac{34}{3}N^2 - \tfrac{10}{3}Nf - 2C_F f, \quad C_F = \frac{N^2-1}{2N}, \tag{2.2.34}$$

being N the number of colours and f the number of quark flavours.

Using Eq.(2.2.33) we write Eq.(2.2.32) at $\mathcal{O}(\alpha_s)$, as

$$\mu\frac{d\hat{Z}}{d\mu} = -\frac{1}{2\pi N}\alpha_s\begin{bmatrix} 3 & -3N \\ -3N & 3 \end{bmatrix}, \tag{2.2.35}$$

and applying the definition of the anomalous dimension matrix in Eq.(2.2.28) we get at $\mathcal{O}(\alpha_s)$

$$\hat{\gamma} = \hat{Z}^{-1}\mu\frac{d\hat{Z}}{d\mu} = -\frac{1}{2\pi N}\alpha_s\begin{bmatrix} 3 & -3N \\ -3N & 3 \end{bmatrix} = \frac{\alpha_s}{4\pi}\hat{\gamma}^{(0)}, \tag{2.2.36}$$

with

$$\hat{\gamma}^{(0)} = \frac{1}{N}\begin{bmatrix} -6 & 6N \\ 6N & -6 \end{bmatrix}. \tag{2.2.37}$$

The vector version of Eq.(2.2.31) for the tree level Wilson coefficients $\vec{C} = \begin{pmatrix} C_1 \\ C_2 \end{pmatrix}$ reads

$$\mu\frac{d\vec{C}}{d\mu} = \hat{\gamma}^T\vec{C}. \tag{2.2.38}$$

Using the chain rule and substituting the definition of the β function given in Eq.(2.2.33) the left hand side of the previous equation can be rewritten as

$$\mu\frac{d\vec{C}}{d\mu}=\mu\frac{d\alpha_s}{d\mu}\frac{d\vec{C}}{d\alpha_s}=2\beta\frac{d\vec{C}}{d\alpha_s}. \tag{2.2.39}$$

This allows us to obtain an alternative version of the renormalization group equations in terms of the strong coupling constant α_s

$$\frac{d\vec{C}}{d\alpha_s}=\frac{\hat{\gamma}^T}{2\beta}\vec{C}. \tag{2.2.40}$$

To solve Eq.(2.2.40) we first diagonalize $\hat{\gamma}^{(0)T}$ through a similarity transformation according to

$$\hat{\gamma}^{(0)T}=\hat{V}\hat{\gamma}_D^{(0)}\hat{V}^{-1}, \tag{2.2.41}$$

with the rotation matrix given by

$$\hat{V}=\hat{V}^{-1}=\frac{1}{\sqrt{2}}\begin{bmatrix}1 & 1\\ 1 & -1\end{bmatrix}\quad\text{and}\quad\hat{\gamma}_D^{(0)}=\begin{bmatrix}\frac{6N-6}{N} & 0\\ 0 & -\frac{6N+6}{N}\end{bmatrix}:=\begin{bmatrix}\gamma_+^{(0)} & 0\\ 0 & \gamma_-^{(0)}\end{bmatrix}.$$

In the diagonal basis Eq.(2.2.40) becomes

$$\frac{d\vec{C}'}{d\alpha_s}=\frac{\alpha_s}{4\pi}\frac{\hat{\gamma}_D^{(0)}}{2\beta}\vec{C}'=-\frac{1}{2\beta_0\alpha_s}\hat{\gamma}_D^{(0)}\vec{C}', \tag{2.2.42}$$

where

$$\vec{C}'=\sqrt{2}\hat{V}^{-1}\vec{C}=\begin{pmatrix}C_1+C_2\\ C_1-C_2\end{pmatrix}:=\begin{pmatrix}C_+\\ C_-\end{pmatrix}. \tag{2.2.43}$$

The current-current operators in the diagonal and non diagonal basis are connected through

$$\hat{Q}_+=\frac{\hat{Q}_1+\hat{Q}_2}{2},\qquad\hat{Q}_-=\frac{\hat{Q}_1-\hat{Q}_2}{2}. \tag{2.2.44}$$

The solution of Eq.(2.2.42) is completely straightforward considering that in the diagonal basis we are dealing with a pair of decoupled equations. We write the final result as

$$C_\pm(\mu)=U_\pm(\mu,M_W)C_\pm(M_W), \tag{2.2.45}$$

with the LO transition factor given by

$$\begin{aligned}U_\pm(\mu,M_W)&=\exp\Big(\int_{\alpha_s(M_W)}^{\alpha_s(\mu)}d\alpha_s\frac{\gamma_\pm}{2\beta}\Big)=\exp\Big(-\int_{\alpha_s(M_W)}^{\alpha_s(\mu)}\frac{d\alpha_s}{\alpha_s}\frac{\gamma_\pm^{(0)}}{2\beta_0}\Big)\\&=\Big(\frac{\alpha_s(\mu)}{\alpha_s(M_W)}\Big)^{-\frac{\gamma_\pm^{(0)}}{2\beta_0}}.\end{aligned} \tag{2.2.46}$$

For the purposes of future generalization it is convenient to write Eq.(2.2.45) in matrix notation as follows

$$\vec{C}'(\mu) \;=\; \Big(\frac{\alpha_s(\mu)}{\alpha_s(M_W)}\Big)^{-\frac{\hat{\gamma}_D^{(0)}}{2\beta_0}}\vec{C}'(M_W), \tag{2.2.47}$$

and for completeness we display explicitly the structure of the transition matrix in order to appreciate the connection with Eq.(2.2.46)

$$\Big(\frac{\alpha_s(\mu)}{\alpha_s(M_W)}\Big)^{-\frac{\hat{\gamma}_D^{(0)}}{2\beta_0}} \;=\; e^{-\ln\Big(\frac{\alpha_s(\mu)}{\alpha_s(M_W)}\Big)\frac{\hat{\gamma}_D^{(0)}}{2\beta_0}} = \begin{bmatrix} \Big(\frac{\alpha_s(\mu)}{\alpha_s(M_W)}\Big)^{-\frac{\gamma_+^{(0)}}{2\beta_0}} & 0 \\ 0 & \Big(\frac{\alpha_s(\mu)}{\alpha_s(M_W)}\Big)^{-\frac{\gamma_-^{(0)}}{2\beta_0}} \end{bmatrix}.$$

To return to the original basis $\{C_1, C_2\}$ we use the rotation matrix $\hat{V}$ to obtain

$$\vec{C}(\mu) \;=\; \vec{V}\Big(\frac{\alpha_s(\mu)}{\alpha_s(M_W)}\Big)^{-\frac{\hat{\gamma}_D^{(0)}}{2\beta_0}}\hat{V}^{-1}\vec{C}(M_W) = \hat{U}^{(0)}(\mu, M_W)\vec{C}(M_W), \tag{2.2.48}$$

where the full expression for the transition matrix is

$$\hat{U}^{(0)}(\mu, M_W) \;=\; \hat{V}\Big(\frac{\alpha_s(\mu)}{\alpha_s(M_W)}\Big)^{-\frac{\hat{\gamma}_D^{(0)}}{2\beta_0}}\hat{V}^{-1} = \exp\Big(-\frac{\gamma^{(0)T}}{2\beta_0}\ln\Big[\frac{\alpha_s(\mu)}{\alpha_s(M_W)}\Big]\Big). \tag{2.2.49}$$

We have achieved our main target since the logarithms appearing in Eq.(2.1.17) are now summed at all orders in perturbation theory (instead of a truncated series of logs we ended with a closed expression given by the exponential in Eq.(2.2.49)). To provide a full solution we should obtain the initial conditions $C_1(M_W)$ and $C_2(M_W)$, in this case we can safely use (2.1.17) since for $\mu = M_W$ large logarithms do not arise, we get

$$C_1(M_W) = 0 \qquad C_2(M_W) = 1 \tag{2.2.50}$$

and our result for the current-current Wilson coefficients at the scale $\mu \sim m_b$ is just

$$\begin{aligned} C_1(\mu) &= 1/2\Big(\eta^{-\frac{6}{23}} - \eta^{\frac{12}{23}}\Big), \\ C_2(\mu) &= 1/2\Big(\eta^{-\frac{6}{23}} + \eta^{\frac{12}{23}}\Big), \end{aligned} \tag{2.2.51}$$

with the ratio of strong coupling constants written as $\eta = \alpha_s(\mu)/\alpha_s(M_W)$.
With the inputs shown in Appendix A we find the following numerical values

$$C_1(\mu) = -0.27, \qquad C_2(\mu) = 1.12. \tag{2.2.52}$$

2.2.2 Wilson coefficients beyond leading logarithms

There are different motivations behind the calculation of the Wilson coefficients at NLO in perturbation theory, for instance we have to reduce the ambiguities associated with the renormalization scale arising at leading order in physical quantities such as $m_t(\mu)$, $m_b(\mu)$, $m_c(\mu)$ and the strong coupling constant $\alpha_s(\mu)$. Also the scheme dependence introduced in matrix elements of effective operators should be cancelled by the Wilson coefficients where the scheme dependence first enters at NLO. To get acquainted with the formalism we will start studying the case where the anomalous dimension matrix is diagonal considering only current-current operators, nevertheless our final formulas will be valid in more generic situations where the operators mix under the renormalization group equations and where we have other effective operators in addition to the tree level ones.

Diagonal case

To calculate the NLO version of the transition factors given in Eq.(2.2.46) we consider the formal NLO formula for the components of the diagonal anomalous dimension matrix $\gamma_\pm$

$$\gamma_\pm(\alpha_s) \;=\; \gamma_\pm^{(0)}\frac{\alpha_s}{4\pi}+\gamma_\pm^{(1)}\Big(\frac{\alpha_s}{4\pi}\Big)^2. \tag{2.2.53}$$

We then substitute this expression inside the argument of the exponential in Eq.(2.2.46) and expand in powers of α_s to obtain

$$\begin{aligned}\frac{\gamma_\pm}{2\beta} &= \frac{\gamma_\pm^{(0)}\alpha_s+\gamma_\pm^{(1)}\frac{\alpha_s^2}{4\pi}}{-2\beta_0\alpha_s^2-\frac{2\beta_1\alpha_s^3}{4\pi}}\approx-\frac{1}{2\beta_0\alpha_s^2}\Big(\gamma_\pm^{(0)}\alpha_s+\gamma_\pm^{(1)}\frac{\alpha_s^2}{4\pi}\Big)\Big(1-\frac{\beta_1\alpha_s}{4\pi\beta_0}\Big)\\ &= -\frac{1}{2\beta_0}\Big(\frac{\gamma_\pm^{(0)}}{\alpha_s}+\frac{\gamma_\pm^{(1)}}{4\pi}\Big)\Big(1-\frac{\beta_1\alpha_s}{4\pi\beta_0}\Big)=\frac{1}{4\pi}J_\pm-\frac{\gamma_\pm^{(0)}}{2\beta_0\alpha_s}+\mathcal{O}(\alpha_s),\end{aligned} \tag{2.2.54}$$

with

$$J_\pm \;=\; \frac{\gamma_\pm^{(0)}}{2\beta_0^2}\beta_1-\frac{\gamma_\pm^{(1)}}{2\beta_0}. \tag{2.2.55}$$

By exponentiating the integral of Eq.(2.2.54) with respect to α_s we get the following result for the transition factors

$$\begin{aligned}
\exp\Big(\int_{\alpha_s(M_W)}^{\alpha_s(\mu)}\frac{\gamma_\pm}{2\beta}d\alpha_s\Big) &= \exp\Big(\frac{1}{4\pi}\Big[\alpha_s(\mu)-\alpha_s(M_W)\Big]J_\pm+\frac{\gamma^{(0)}}{2\beta_0}\ln\Big(\frac{\alpha_s(M_W)}{\alpha_s(\mu)}\Big)\Big)\\
&= \exp\Big(\frac{1}{4\pi}\alpha_s(\mu)J_\pm\Big)\exp\Big(\frac{\gamma^{(0)}_\pm}{2\beta_0}\ln\Big[\frac{\alpha_s(M_w)}{\alpha_s(\mu)}\Big]\Big)\exp\Big(-\frac{1}{4\pi}\alpha_s(M_W)J_\pm\Big)\\
&\simeq \Big(1+\frac{\alpha_s(\mu)}{4\pi}J_\pm\Big)\Big(\frac{\alpha_s(M_W)}{\alpha_s(\mu)}\Big)^{\frac{\gamma^{(0)}_\pm}{2\beta_0}}\Big(1-\frac{\alpha_s(M_W)}{4\pi}J_\pm\Big)\\
&= \Big(1+\frac{\alpha_s(\mu)}{4\pi}J_\pm\Big)U^{(0)}_\pm(\mu,M_W)\Big(1-\frac{\alpha_s(M_W)}{4\pi}J_\pm\Big) \qquad (2.2.56)
\end{aligned}$$

where $U^{(0)}_\pm(\mu,M_W)=\Big(\frac{\alpha_s(M_W)}{\alpha_s(\mu)}\Big)^{\frac{\gamma^{(0)}_\pm}{2\beta_0}}$. The expression shown in Eq.(2.2.56) is the main result of this subsection; it will be used in the next subsection as our prototype in the construction of the evolution matrix at NLO when there is operator mixing under the renormalization group equations.

Non diagonal case

Consider the generic evolution equation for the Wilson coefficients

$$\vec{C}(\mu) = \hat{U}(\mu,M_W)\vec{C}(M_W) \qquad (2.2.57)$$

where the array of Wilson coefficients $\vec{C}$ can have an arbitrary number of components; then in addition to the pure tree level contributions $\{C_1,C_2\}$ we can include other topologies such as QCD and electroweak penguins. Even though Eq.(2.2.40) was constructed within the context of tree level transitions the arguments used on its determination were totally general, then we can easily translate this condition into the following master formula for the transition matrix

$$\frac{d\hat{U}(\mu,M_W)}{d\alpha_s(\mu)}=\frac{\hat{\gamma}^T\hat{U}(\mu,M_W)}{2\beta}. \qquad (2.2.58)$$

The solution of the previous equation can be formally written in terms of a series in the coupling constant α_s as follows

$$\begin{aligned}
\hat{U}(\mu,M_W) &= \hat{1}+\int_{\alpha_s(M_W)}^{\alpha_s(\mu)}d\alpha'_s\frac{\hat{\gamma}^T}{2\beta}+\int_{\alpha_s(M_W)}^{\alpha_s(\mu)}d\alpha'_s\int_{\alpha'_s(M_W)}^{\alpha'_s(\mu)}d\alpha''_s\frac{\hat{\gamma}^T(\alpha'_s)}{2\beta}\frac{\hat{\gamma}^T(\alpha''_s)}{2\beta}\\
&\quad +... \qquad (2.2.59)
\end{aligned}$$

We can write Eq.(2.2.59) in a simpler way by introducing the strong coupling constant ordering operator $\hat{T}_\alpha$ defined as

$$\hat{T}_\alpha\Big(\hat{M}(\alpha_{s,1})\hat{M}(\alpha_{s,2})...\hat{M}(\alpha_{s,n})\Big) := \sum_{\text{perm}} \Theta(\alpha_{s,i_1}-\alpha_{s,i_2})...\Theta(\alpha_{s,i_n}-\alpha_{s,i_{n-1}})\times \hat{M}(\alpha_{s,i_1})\hat{M}(\alpha_{s,i_2})...\hat{M}(\alpha_{s,i_n}), \quad (2.2.60)$$

where the summation symbol runs over all the possible permutations of the indices $\{i_1, i_2, ..., i_n\} = \{1, 2, 3, ..., n\}$ and we find the formal solution

$$\hat{U}(\mu, M_W) = \hat{T}_{\alpha_s}\Big(\exp\Big[\int d\alpha_s' \frac{\hat{\gamma}^T(\alpha_s')}{2\beta}\Big]\Big). \quad (2.2.61)$$

Although the previous equation is the general answer at all orders in perturbation theory here we are only interested in the NLO calculation, for practical purposes it is more useful to start with a matrix version of Eq.(2.2.56) and then to proceed with the explicit calculation of the different components involved

$$\begin{aligned}\hat{U}(\mu,\mu_W) &= \Big(1+\frac{\alpha_s(\mu)}{4\pi}\hat{J}\Big)\hat{U}^{(0)}(\mu,\mu_W)\Big(1-\frac{\alpha_s(\mu_W)}{4\pi}\hat{J}\Big)\\ &= \hat{K}(\alpha_s(\mu))\hat{U}^{(0)}(\mu,\mu_W)\hat{K}^{-1}(\alpha_s(\mu_W)),\end{aligned} \quad (2.2.62)$$

where we have introduced

$$\hat{K}(\alpha_s(\mu') = 1+\frac{\alpha_s(\mu')}{4\pi}\hat{J}. \quad (2.2.63)$$

Notice that the previous equation reproduces correctly in the leading order limit the result shown in Eq.(2.2.49).

In the remaining part of this section all our attention will be centred on the detailed calculation of the matrix $\hat{J}$ appearing in (2.2.62). We begin by substituting (2.2.49) into Eq.(2.2.62) and evaluating the derivative with respect to α_s

$$\begin{aligned}\frac{d\hat{U}(\mu,\mu_W)}{d\alpha_s} &= \frac{d\hat{K}(\alpha_s(\mu))}{d\alpha_s}\hat{U}^{(0)}(\mu,\mu_W)\hat{K}^{-1}(\alpha_s(\mu_W))\\ &\quad -\hat{K}(\alpha_s(\mu))\frac{\gamma^{(0)T}}{2\beta_0\alpha_s(\mu)}\hat{U}^{(0)}(\mu,\mu_W)\hat{K}^{-1}(\alpha_s(\mu_W)).\end{aligned} \quad (2.2.64)$$

then we plug this result together with Eq.(2.2.62) into Eq.(2.2.58) and perform some simplifications in order to establish the following equality

$$\frac{\hat{\gamma}^T}{2\beta}\hat{K}(\alpha_s(\mu)) = \frac{d\hat{K}(\alpha_s(\mu))}{d\alpha_s} - \hat{K}(\alpha_s(\mu))\frac{\hat{\gamma}^{(0)T}}{2\beta_0\alpha_s(\mu)},$$

or equivalently

$$\frac{d\hat{K}(\alpha_s(\mu))}{d\alpha_s(\mu)} + \frac{1}{2\beta_0\alpha_s(\mu)}\Big[\hat{\gamma}^{(0)T}, \hat{K}(\alpha_s(\mu))\Big] = \frac{\gamma^T}{2\beta}\hat{K}(\alpha_s(\mu)) + \frac{\hat{\gamma}^{(0)T}}{2\beta_0\alpha_s(\mu)}\hat{K}(\alpha_s(\mu)). \tag{2.2.65}$$

Using Eq.(2.2.63) we get the following equation for $\hat{J}$

$$\hat{J} + \frac{\Big[\hat{\gamma}^{(0)T}, \hat{J}\Big]}{2\beta_0} = 4\pi\Big(\frac{\hat{\gamma}^T}{2\beta} + \frac{\hat{\gamma}^{(0)T}}{2\beta_0\alpha_s(\mu)}\Big)\Big(\hat{1} + \frac{\alpha_s(\mu)}{4\pi}\hat{J}\Big). \tag{2.2.66}$$

We can further simplify the previous equations considering the $\alpha_s(\mu)$ expansion for β (2.2.33) and $\hat{\gamma}^T$ up to NLO

$$\frac{\hat{\gamma}^T}{2\beta} = -\frac{1}{2\alpha_s(\mu)\beta_0}\Big(\hat{\gamma}^{(0)T} + \frac{\alpha_s(\mu)}{4\pi}\hat{\gamma}^{(1)T} - \frac{\alpha_s(\mu)\beta_1}{4\pi\beta_0}\hat{\gamma}^{(0)T}\Big), \tag{2.2.67}$$

so we get

$$\hat{J} + \Big[\frac{\hat{\gamma^{(0)}}^T}{2\beta_0}, \hat{J}\Big] = -\frac{\hat{\gamma}^{(1)T}}{2\beta_0} + \frac{\beta_1}{\beta_0^2}\hat{\gamma}^{(0)T}. \tag{2.2.68}$$

To complete the determination of $\hat{J}$ we follow [46], then it is convenient to perform a similarity transformation using the matrix $\hat{V}$ introduced in Eq.(2.2.41) such that $\hat{\gamma}^{(0)T}$ becomes diagonal, in this new basis Eq.(2.2.68) becomes

$$\hat{H} + \Big[\frac{\hat{\gamma}_D^{(0)}}{2\beta_0}, \hat{H}\Big] = -\frac{\hat{G}}{2\beta_0} + \frac{\beta_1}{2\beta_0^2}\hat{\gamma}_D^{(0)}, \tag{2.2.69}$$

with

$$\hat{J} = \hat{V}\hat{H}\hat{V}^{-1}, \qquad \hat{G} = \hat{V}^{-1}\hat{\gamma}^{(1)T}\hat{V}. \tag{2.2.70}$$

We propose the following ansatz for the matrix $\hat{H}$

$$\hat{H} = \hat{M} + a\gamma_D^{(0)T}, \tag{2.2.71}$$

where by direct substitution into Eq.(2.2.69) the constant a is found to be $a = \beta_1/(2\beta_0^2)$. And we are left with a simpler version of Eq.(2.2.69) in terms of the matrix $\hat{M}$

$$\hat{M} + \Big[\frac{\hat{\gamma}_D^{(0)}}{2\beta_0}, \hat{M}\Big] = -\frac{\hat{G}}{2\beta_0}. \tag{2.2.72}$$

Next we provide a step by step solution for the components of $\hat{M}$. Firstly we develop the left hand side of Eq.(2.2.72) using index notation to obtain

$$M_{ij} + \frac{1}{2\beta_0}\sum_k \gamma_{i,D}^{(0)}\delta_{ik}M_{kj} - \frac{1}{2\beta_0}\sum_k M_{ik}\delta_{kj}\gamma_{j,D}^{(0)} = M_{ij} + \frac{1}{2\beta_0}\gamma_{i,D}^{(0)}M_{ij} - \frac{1}{2\beta_0}M_{ij}\gamma_{j,D}^{(0)}, \tag{2.2.73}$$

next we substitute back this result into Eq.(2.2.72) and express the right hand side in terms of components

$$M_{ij}\Big(1+\frac{1}{2\beta_0}\gamma^{(0)}_{i,D}M_{ij}-\frac{1}{2\beta_0}\gamma^{(0)}_{j,D}\Big) \;=\; -\frac{G_{ij}}{2\beta_0},$$

finally we solve for the different components M_{ij} of $\hat{M}$ to get

$$M_{ij} \;=\; -\frac{G_{ij}}{2\beta_0+\gamma^{(0)}_{i,D}-\gamma^{(0)}_{j,D}}. \tag{2.2.74}$$

By substituting into Eq.(2.2.71) we arrive at

$$H_{ij} \;=\; \frac{\beta_1}{2\beta_0^2}\delta_{ij}\gamma_i^{(0),T}-\frac{G_{ij}}{2\beta_0+\gamma^{(0)}_{i,D}-\gamma^{(0)}_{j,D}}. \tag{2.2.75}$$

All the ingredients required for the full calculation of the NLO version of the evolution matrix in Eq.(2.2.62) are summarized in Eq.(2.2.70) and Eq.(2.2.75. Here we assume that the anomalous dimension matrix $\hat{\gamma}$ is known up to NLO. The results presented in this section will be essential in Chapter 4 in order to evaluate possible New Physics contributions in tree level operators in observables involving other topologies as well.

2.3 The effective $\Delta F = 1$ Hamiltonian

Up to now our discussion for the effective Hamiltonians has focused mostly on the current-current operators $\hat{Q}_1$ and $\hat{Q}_2$ in Eq.(2.1.6), this set of operators is however quite limited for phenomenological purposes, realistic studies require other topologies such as electroweak and QCD penguins. Nevertheless the ideas introduced in the previous sections can straightforwardly be generalized when all these contributions are taken into account. In this subsection we introduce the full effective Hamiltonian for $\Delta B = 1$ transitions in the case of neutral B_s^0 mesons, we also provide the generic renormalization group equations required when electroweak corrections are included at NLO. All the results presented here can easily be adapted to B_d^0 mesons by replacing the CKM elements including the strange quark with the analogous components for the down quark and by substituting the strange quark field for the down quark field inside the corresponding operators.

2.3.1 The $\Delta B = 1$ Hamiltonian for neutral B_s^0 mesons

The effective Hamiltonian for $\Delta B = 1$ transitions in the case of neutral B_s^0 mesons is

$$\begin{aligned}\mathcal{H}_{eff} &= \frac{G_F}{\sqrt{2}}\Big(\sum_{p,p'=u,c}\lambda^s_{pp'}\sum_{i=1,2}C_i^{pp'}(\mu)\hat{Q}_i^{pp'} \\ &\quad + \sum_{p=u,c}\lambda^s_p\sum_{i=3}^{10}C_i(\mu)\hat{Q}_i + C_{7\gamma}\hat{Q}_{7\gamma} + C_{8g}\hat{Q}_{8g}\Big) + h.c.\,, \end{aligned} \tag{2.3.76}$$

with the following CKM combinations

$$\lambda^s_p = V_{pb}V^*_{ps}, \qquad \lambda^s_{pp'} = V_{pb}V^*_{p's}. \tag{2.3.77}$$

Here $p, p' = u, c$ and C_i denotes the Wilson coefficient for the corresponding dimension six operator, unless stated otherwise in this thesis we will refer to the following basis

$$\begin{aligned}
\hat{Q}_1^{pp'} &= \Big(\bar{\hat{s}}_\alpha\hat{p}_\beta\Big)_{V-A}\Big(\bar{\hat{p}}'_\beta\hat{b}_\alpha\Big)_{V-A}, & Q_2^{pp'} &= \Big(\bar{\hat{s}}\hat{p}\Big)_{V-A}\Big(\bar{\hat{p}}'\hat{b}\Big)_{V-A}, \\
\hat{Q}_3 &= \Big(\bar{\hat{s}}\hat{b}\Big)_{V-A}\sum_q\Big(\bar{\hat{q}}\hat{q}\Big)_{V-A}, & \hat{Q}_4 &= \Big(\bar{\hat{s}}_\alpha\hat{b}_\beta\Big)_{V-A}\sum_q\Big(\bar{\hat{q}}_\beta\hat{q}_\alpha\Big)_{V-A}, \\
\hat{Q}_5 &= \Big(\bar{\hat{s}}\hat{b}\Big)_{V-A}\sum_q\Big(\bar{\hat{q}}\hat{q}\Big)_{V+A}, & \hat{Q}_6 &= \Big(\bar{\hat{s}}_\alpha\hat{b}_\beta\Big)_{V-A}\sum_q\Big(\bar{\hat{q}}_\beta\hat{q}_\alpha\Big)_{V+A}, \\
\hat{Q}_7 &= \Big(\bar{\hat{s}}\hat{b}\Big)_{V-A}\sum_q\frac{3}{2}e_q\Big(\bar{\hat{q}}\hat{q}\Big)_{V+A}, & \hat{Q}_8 &= \Big(\bar{\hat{s}}_\alpha\hat{b}_\beta\Big)_{V-A}\sum_q\frac{3}{2}e_q\Big(\bar{\hat{q}}_\beta\hat{q}_\alpha\Big)_{V+A}, \\
\hat{Q}_9 &= \Big(\bar{\hat{s}}\hat{b}\Big)_{V-A}\sum_q\frac{3}{2}e_q\Big(\bar{\hat{q}}\hat{q}\Big)_{V-A}, & \hat{Q}_{10} &= \Big(\bar{\hat{s}}_\alpha\hat{b}_\beta\Big)_{V-A}\sum_e\frac{3}{2}\Big(\bar{\hat{q}}_\beta\hat{q}_i\Big)_{V-A}, \\
\hat{Q}_{7\gamma} &= \frac{e}{8\pi^2}m_b\bar{\hat{s}}\sigma_{\mu\nu}\Big(1+\gamma_5\Big)F^{\mu\nu}\hat{b}\,, & \hat{Q}_{8g} &= \frac{g_s}{8\pi^2}m_b\bar{\hat{s}}\sigma_{\mu\nu}\Big(1+\gamma_5\Big)G^{\mu\nu}\hat{b}\,.
\end{aligned} \tag{2.3.78}$$

Where α and β are colour indices, e_q is the electric charge of the quark q, e is the $U(1)_Y$ coupling and g the $SU(3)_C$ one, m_b is the mass of the b-quark and $F^{\mu\nu}$ and $G^{\mu\nu}$ are the electro-magnetic and chromo-magnetic field strength tensors respectively. $\hat{Q}_1^{pp'}$ and $\hat{Q}_2^{pp'}$ are the tree-level operators, $\hat{Q}_2^{pp'}$ being the colour singlet. $\hat{Q}_{3-6}$ denote the QCD penguin operators and $\hat{Q}_{7-10}$ the electro-weak penguin operators. The electro-magnetic operator is given by $\hat{Q}_{7\gamma}$ and the chromo-magnetic operator by $\hat{Q}_{8g}$. Our notation agrees with the one used in [47] and [48], it corresponds to a

negative value of C_{8g} because of $-ig\gamma_\mu T^a$ being the Feynman rule for the quark-gluon vertex. In [45] a different basis is used, where $\hat{Q}_1$ and $\hat{Q}_2$ are interchanged and $Q_{7\gamma}$ and Q_{8g} have a different sign (this is equivalent to the sign convention $iD^\mu = i\partial^\mu + g_s A^\mu_a T^a$ for the gauge-covariant derivative).

Generalized Wilson coefficient running

In analogy with Section 2.1 the Wilson coefficients C_i with $i = 1, 2, ..., 10, 7\gamma, 8g$ in Eq. (2.3.76) are obtained by matching the calculations of the effective theory and the SM at the scale $\mu = M_W$ and then evolving down to the scale $\mu \sim m_b$ using the renormalization group equations according to

$$\vec{C}(\mu) \;=\; \hat{\boldsymbol{U}}(\mu, \mu_W, \alpha)\vec{C}(M_W). \tag{2.3.79}$$

The NLO evolution matrix is given by

$$\boldsymbol{U}(\mu, M_W, \alpha) \;=\; \hat{U}(\mu, \mu_W) + \frac{\alpha}{4\pi}\hat{R}(\mu, \mu_W), \tag{2.3.80}$$

in this case we are dealing with square matrices of dimensionality 10×10; here $\hat{U}(\mu, \mu_W)$ contains all the QCD evolution and its formal NLO expression coincides with Eq.(2.2.62). Nevertheless it should be calculated using the 10 dimensional version of the NLO anomalous dimension QCD matrix quoted as $\hat{\gamma}_s$ in [47]. In addition to pure QCD contributions also NLO electroweak effects are introduced through $\hat{R}(\mu, \mu_W)$

$$\hat{R}(\mu, M_W) \;=\; -\frac{2\pi}{\beta_0}\hat{V}\Big(\hat{K}^{(0)}(\mu, M_W) + \frac{1}{4\pi}\sum_i^3 K_i^{(1)}(\mu, M_W)\Big)\hat{V}^{-1}. \tag{2.3.81}$$

the components β_0, β_1 of the β function involved in Eq.(2.3.81) and in Eq. (2.3.84) can be found in Eq.(2.2.34). The leading order part of the full evolution matrix corresponds to

$$\boldsymbol{U}^{(0)}(\mu, M_W, \alpha) \;=\; \hat{U}^{(0)}(\mu, \mu_W) + \frac{\alpha}{4\pi}\hat{R}^{(0)}(\mu, M_W), \tag{2.3.82}$$

with $\hat{U}^{(0)}(\mu, \mu_W)$ given by Eq.(2.2.49) and

$$\hat{R}^{(0)}(\mu, M_W) \;=\; -\frac{2\pi}{\beta_0}\hat{V}\hat{K}^{(0)}(\mu, M_W)\hat{V}^{-1}. \tag{2.3.83}$$

In analogy with (2.2.41) the matrix $\hat{V}$ is the one that diagonalizes the leading order part $\hat{\gamma}_s^{(0)}$ of $\hat{\gamma}_s$. Because of the electroweak interaction new anomalous dimension

matrices $\hat{\gamma}_{se}$ and $\hat{\gamma}_e$ [47] are needed. We now provide the full set of matrices required for the evaluation of Eq.(2.3.81)

$$
\begin{aligned}
(\hat{K}^{(0)}(\mu, M_W))_{ij} &= \frac{M^{(0)}_{ij}}{a_i - a_j - 1}\Big[\Big(\frac{\alpha_s(M_W)}{\alpha_s(\mu)}\Big)^{a_j}\frac{1}{\alpha_s(\mu)} - \Big(\frac{\alpha_s(M_W)}{\alpha_s(\mu)}\Big)^{a_i}\frac{1}{\alpha_s(M_W)}\Big], \\
(\hat{K}^{(1)}(\mu, M_W))_{ij} &= \begin{cases} \frac{M^{(1)}_{ij}}{a_i - a_j}\Big[\Big(\frac{\alpha_s(M_W)}{\alpha_s(\mu)}\Big)^{a_j} - \Big(\frac{\alpha_s(M_W)}{\alpha_s(\mu)}\Big)^{a_i}\Big], & i \neq j \\ \\ M^{(1)}_{ii}\Big(\frac{\alpha_s(M_W)}{\alpha_s(\mu)}\Big)^{a_i}\ln\frac{\alpha_s(\mu)}{\alpha_s(M_W)}, & i = j \end{cases}, \\
\hat{K}^{(1)}_2(\mu, M_W) &= -\alpha_s(M_W)\hat{K}^{(0)}(\mu, M_W)\hat{H}, \\
\hat{K}^{(1)}_3(\mu, M_W) &= -\alpha_s(M_W)\hat{H}\hat{K}^{(0)}(\mu, M_W), \\
\hat{M}^{(0)} &= \hat{V}^{-1}\hat{\gamma}^{(0)T}_e\hat{V}, \\
\hat{M}^{(1)} &= \hat{V}^{-1}\Big(\gamma^{(1)T}_{se} - \frac{\beta_1}{\beta_0}\gamma^{(0)T}_e + [\hat{\gamma}^{(0)T}_e, \hat{J}]\Big)\hat{V}, \qquad (2.3.84)
\end{aligned}
$$

where the formula for $\hat{H}$ can be read from Eq.(2.2.75) under the replacement $\hat{\gamma} \to \hat{\gamma}_s$. The only missing piece for the full determination of $\vec{C}(\mu)$, in Eq.(2.3.79), are the NLO initial conditions $\vec{C}(M_W)$

$$
\begin{aligned}
\vec{C}(M_W) &= \vec{C}^{(0)}_s(M_W) + \frac{\alpha_s(M_W)}{4\pi}\vec{C}^{(1)}_s(M_W) \\
&\quad + \frac{\alpha}{4\pi}\Big(\vec{C}^{(0)}_e(M_W) + \frac{\alpha_s(M_W)}{4\pi}\vec{C}^{(1)}_e(M_W) + \vec{R}^{(0)}_e(M_W)\Big). \qquad (2.3.85)
\end{aligned}
$$

As pointed out in [45] the electroweak contributions in Eq.(2.3.85) can be $x_t = m_t^2/M_W^2$ and/or $1/\sin^2\theta_W$ enhanced (these terms will be denoted by $\vec{C}^{(0)}_e$). Consequently it is fair to treat the product $\alpha\ \vec{C}^{(0)}_e$, as a LO contribution. Consistency requires then the inclusion of $\vec{C}^{(1)}_e$ as a NLO effect. The remainder $\vec{R}^{(0)}_e$ is numerically smaller in comparison with $\vec{C}^{(0)}_e$ and therefore considered a NLO effect, it contains the NLO scheme dependency of the Wilson coefficients. This approach differs from the one followed by [47] where $\vec{C}^{(0)}_e(M_W) + \vec{R}^{(0)}_e(M_W)$ is introduced as a NLO effect and then $\vec{C}^{(1)}_e$ is omitted. The explicit expressions for the contributions $\vec{C}^{(0)}_s$, $\vec{C}^{(1)}$, $\vec{C}^{(0)}_e$, $\vec{C}^{(1)}_e$ and $\vec{R}^{(0)}_e$ of $\vec{C}(M_W)$ are given in appendix C.

It should be further stressed that when applying Eq. (2.3.79) we consistently dropped products between NLO contributions from $\boldsymbol{U}(\mu, M_W, \alpha)$ and NLO effects from $\vec{C}(M_W)$ but we have taken into account products between NLO contributions from $\boldsymbol{U}(\mu, M_W, \alpha)$ and LO contributions from $\vec{C}(M_W)$ and vice versa.

2.4 Calculation of B mixing observables ΔM

The non-diagonal mixing component M_{12} in Eq.(1.3.47) is given by the matrix element

$$M_{12}^q = \frac{\langle B_q^0|\hat{\mathcal{H}}_q^{|\Delta B|=2}|\bar{B}_q^0\rangle}{2M_{B_q}} \tag{2.4.86}$$

for $q = d, s$. Where the effective Hamiltonian $\mathcal{H}_q^{|\Delta B|=2}$ is given as

$$\hat{\mathcal{H}}^{|\Delta B|=2} = \frac{G_F^2}{16\pi^2}(V_{tb}V_{tq}^*)^2 C^{|\Delta B|=2}(m_t, M_W, \mu)\hat{Q}^{|\Delta B|=2} + h.c.. \tag{2.4.87}$$

The effective four quark operator $\hat{Q}^{|\Delta B|=2}$ is

$$\hat{Q}^{|\Delta B|=2} = \Big(\bar{\hat{q}}\hat{b}\Big)_{V-A}\Big(\bar{\hat{q}}\hat{b}\Big)_{V-A}, \tag{2.4.88}$$

and the Wilson coefficient has a perturbative expansion in α_s according to

$$C^{|\Delta B|=2} = C^{|\Delta B|=2,(0)} + \frac{\alpha_s(\mu)}{4\pi}C^{|\Delta B|=2,(1)} + \dots. \tag{2.4.89}$$

Denote the SM amplitude by

$$\mathcal{M} = \mathcal{M}^{(0)} + \frac{\alpha_s}{4\pi}\mathcal{M}^{(1)} + \dots. \tag{2.4.90}$$

Then the matching condition between the effective and the full theory reads

$$\begin{aligned} -\mathcal{M}^{(0)} - \frac{\alpha_s(\mu)}{4\pi}\mathcal{M}^{(1)} + \dots = {} & \frac{G_F^2}{16\pi^2}(V_{tb}V_{tq}^*)^2\Big[C^{|\Delta B|=2,(0)} + \frac{\alpha_s}{4\pi}C^{|\Delta B|=2,(1)}\Big]\times \\ & \Big[\langle\hat{Q}^{|\Delta B|=2}\rangle^{(0)} + \frac{\alpha_s}{4\pi}\langle\hat{Q}^{|\Delta B|=2}\rangle^{(1)}\Big]\times\Big[1 + \mathcal{O}\Big(\frac{m_b^2}{M_W^2}\Big)\Big] \\ & +\mathcal{O}(\alpha_s^2), \end{aligned} \tag{2.4.91}$$

where

$$\langle\hat{Q}^{|\Delta B|=2}\rangle := \langle B_q^0|\hat{Q}^{|\Delta B|=2}|\bar{B}_q^0\rangle. \tag{2.4.92}$$

From explicit calculations in the SM it is found

$$\begin{aligned} \mathcal{M}^{(0)} &= \sum_{\alpha,\beta=u,c,t} V_{\alpha b}^* V_{\alpha q} V_{\beta b}^* V_{\beta q}\mathcal{M}_{\alpha\beta}^{(0)}\langle\hat{Q}^{|\Delta B|=2}\rangle^{(0)} \\ &= -\frac{G_F^2}{16\pi^2}M_W^2\langle\hat{Q}^{|\Delta B|=2}\rangle^{(0)}\sum_{\alpha,\beta=u,c,t}\lambda_\alpha^{(q)}\lambda_\beta^{(q)}F(x_\alpha, x_\beta), \end{aligned} \tag{2.4.93}$$

with $\lambda_\alpha^{(q)} = V_{\alpha b}V_{\alpha q}^*$ for $q = d, s$ and

$$\mathcal{M}_{\alpha\beta}^{(0)} = -\frac{G_F^2}{16\pi^2}M_W^2 F(x_\alpha, x_\beta), \tag{2.4.94}$$

with $x_\alpha = m_\alpha^2/M_W^2$ and $F(x_\alpha, x_\beta) = F(x_\beta, x_\alpha)$.

To simplify the notation we introduce the Inami-Lim functions [49]

$$\begin{aligned} S_0(x_\alpha, x_\beta) &= F(x_\alpha, x_\beta) - F(x_\alpha, 0) - F(0, x_\beta) + F(0,0) = \\ &= x_\alpha\Big(-\frac{3x_\beta}{4(1-x_\beta)} + \ln\Big[\frac{x_\beta}{x_\alpha}\Big] - \frac{3x_\beta^2 \ln\, x_\beta}{4(1-x_\beta)^2}\Big), \\ S_0(x_\alpha) &= \lim_{x_\beta \to x_\alpha} S_0(x_\alpha, x_\beta) = \frac{x_\beta}{(1-x_\beta)^2}\Big(1 - \frac{11}{4}x_\beta + \frac{x_\beta^2}{4} - \frac{3x_\beta^2 \ln\, x_\beta}{(1-x_\beta)}\Big). \end{aligned} \tag{2.4.95}$$

From the analysis of the asymptotic behaviour of $S_0(x_c)$ and $S_0(x_c, x_t)$ in Eq.(2.4.95) we find

$$\begin{aligned} S_0(x_c) &\approx x_c, \\ S_0(x_c, x_t) &\approx x_c \ln\Big(\frac{x_t}{x_c}\Big), \end{aligned} \tag{2.4.96}$$

these equations show that the charm quark contributions are suppressed by a factor $x_c \sim \mathcal{O}(10^{-4})$ with respect to the ones from the quark top $x_t \approx 4.5$ and therefore can be neglected.

Then Eq.(2.4.93) simplifies to

$$-\mathcal{M}^{(0)} = \frac{G_F^2}{16\pi^2} M_W^2 \lambda_t^2 S_0(x_t) \langle \hat{Q}^{|\Delta B|=2} \rangle. \tag{2.4.97}$$

If we substitute Eq.(2.4.97) into Eq.(2.4.91) we can calculate explicitly the Wilson coefficient $C^{|\Delta B|=2}$ at the lowest order in α_s

$$C^{|\Delta B|=2,(0)}(m_t, M_W, \mu) = M_W^2 S_0(x_t). \tag{2.4.98}$$

Our leading order Wilson coefficient does not depend explicitly on the renormalization scale μ, this enters indirectly through the mass of the top quark. Big logarithms will be absent as long as we pick the matching scale $\mu_{tW} \sim \mathcal{O}(M_W, m_t)$. On the other hand the absence of large logarithms in the matrix element $\langle Q \rangle$ requires $\mu_b \sim m_b$. Since we should use the same scale μ for both $C^{|\Delta B|=2,(0)}$ and $\langle Q \rangle$ we need to evolve both contributions to a common scale using the renormalization group equations in order to resum large logarithms of the form $\alpha_s^n \ln^n \mu_{tW}/\mu_b$.

The renormalization group equations lead to (see Eq.(2.2.46))

$$C^{|\Delta B|=2,(0)}(m_t, M_W, \mu_b) = \Big(\frac{\alpha_s(\mu_b)}{\alpha_s(\mu_{tW})}\Big)^{-\frac{\gamma_+^{(0)}}{2\beta_0}} C^{|\Delta B|=2,(0)}(m_t, M_W, \mu_{tW}),$$
$$\langle \hat{Q}(\mu_b)\rangle = \Big(\frac{\alpha_s(\mu_b)}{\alpha_s(\mu_{tW})}\Big)^{\frac{\gamma_+^{(0)}}{2\beta_0}} \langle Q(\mu_W)\rangle. \quad (2.4.99)$$

Alternatively the Wilson coefficient $C^{|\Delta B|=2}$ can be written as

$$C^{|\Delta B|=2}(m_t, M_W, \mu_b) = \eta_B b_B(\mu_b) C^{|\Delta B|=2,(0)}(m_t, M_W, \mu_{tW}), \quad (2.4.100)$$

where all the μ_b dependence is contained inside $b_B(\mu_b)$ and all the high scales in η_B [50].

The μ_b dependence of b_B and the chosen renormalisation scheme should cancel in the product $b_B(\mu_b)\langle\hat{Q}(\mu_b)\rangle$. The only missing ingredient is the matrix element of the operator $\hat{Q}$, the standard parameterization is

$$\langle B_q^0|\hat{Q}^{|\Delta B|=2}(\mu_b)|\bar{B}_q^0\rangle = \frac{8}{3} M_{B_q}^2 f_{B_q}^2 \frac{\hat{B}_{B_q}}{b_{B_q}(\mu_b)}, \quad (2.4.101)$$

where f_{B_q} is the B_q^0 meson decay constant and $\hat{B}_{B_q}$ is the bag parameter.

If we combine Eq.(2.4.86), (2.4.87), (2.4.98) ,(2.4.100) and (2.4.101) we finally get

$$M_{12} = \frac{\langle B_q|\hat{\mathcal{H}}_q^{|\Delta B|=2}|\bar{B}_q\rangle}{2M_{B_q}} = \frac{G_F^2}{12\pi^2}\eta_B M_{B_q} B_{B_q} f_{B_q}^2 M_W^2 S\Big(\frac{m_t^2}{M_W^2}\Big)(V_{tb}V_{tq}^*)^2.$$

2.4.1 Calculation of Γ_{12}

In this section we briefly summarize the steps that lead to the calculation of Γ_{12}^q for $q = s, d$, in particular we focus in the B_s^0 system. The results derived can be easily generalized to the B_d^0 system as well.

The determination of Γ_{12}^s is given through the optical theorem by [51]

$$\Gamma_{12}^s = \frac{1}{2M_{B_s}}\langle B_s^0|\mathcal{I}m\Big(i\int d^4x \hat{T}\Big[\mathcal{H}^{|\Delta B|=1}(x)\mathcal{H}^{|\Delta B|=1}(0)\Big]\Big)|\bar{B}_s^0\rangle, \quad (2.4.102)$$

where $\hat{T}$ is the time ordered operator.

After doing the explicit calculations the following result is found

$$\Gamma_{12}^s = -\Big((\lambda_c^s)^2\Gamma_{12}^{s,cc} + \lambda_u^s\lambda_c^s\Gamma_{12}^{s,uc} + (\lambda_u^s)^2\Gamma_{12}^{s,uu}\Big)$$
$$= -\Big((\lambda_t^s)^2\Gamma_{12}^{s,cc} + 2\lambda_t^s\lambda_u^s\Big[\Gamma_{12}^{s,cc} - \Gamma_{12}^{s,uc}\Big] + (\lambda_u^s)^2\Big[\Gamma_{12}^{s,cc} - 2\Gamma_{12}^{s,uc} + \Gamma_{12}^{s,uu}\Big]\Big), \quad (2.4.103)$$

where we have made use of the unitarity relationship $\lambda_u^s + \lambda_c^s + \lambda_t^s = 0$ in order to express λ_c in terms of λ_t.

The different "up" type quark labels in the Γ_{12}^{ab} structures in Eq.(2.4.103) (for $ab = cc, uc, uu$) denote the quarks in the loops of the effective diagrams after the integration of the W bosons. As an example we show in Fig.2.5 [15] the set of topologies contributing to $\Gamma_{12}^{cc,s}$ up to NLO in QCD interactions.

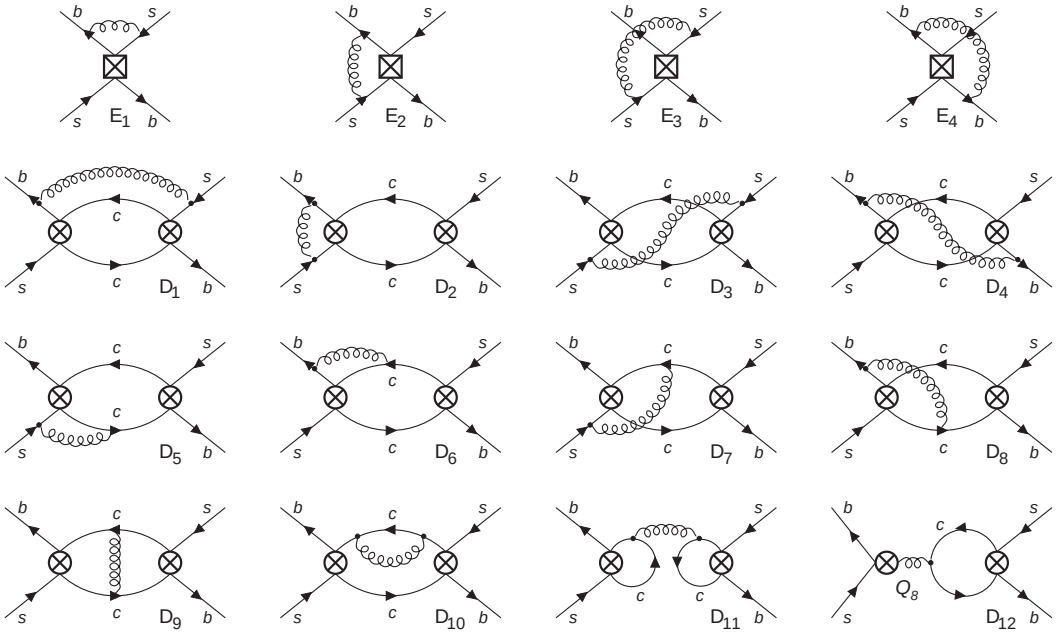

Figure 2.5: Standard Model diagrams contributing to $\Gamma_{12}^{cc,s}$ up to NLO in QCD [15].

The components $\Gamma_{12}^{ab,s}$ have the following structure

$$\Gamma_{12}^{s,ab} = \Gamma_{ab}^{s,Q}\langle\hat{Q}\rangle + \Gamma_{ab}^{s,Q_S}\langle\hat{Q}_S\rangle + \Gamma_{ab}^{s,\tilde{Q}_S}\langle\tilde{\hat{Q}}_S\rangle + \mathcal{O}(1/m_b), \qquad (2.4.104)$$

with the following $\Delta B = 2$ operators

$$\begin{aligned}
\hat{Q} &= \Big(\bar{\hat{s}}\gamma^\mu[1-\gamma_5]\hat{b}\Big)\times\Big(\bar{\hat{s}}\gamma_\mu[1-\gamma_5]\hat{b}\Big), \\
\hat{Q}_S &= \Big(\bar{\hat{s}}[1+\gamma_5]\hat{b}\Big)\times\Big(\bar{\hat{s}}[1+\gamma_5]\hat{b}\Big), \\
\tilde{\hat{Q}}_S &= \Big(\bar{\hat{s}}_\alpha[1+\gamma_5]\hat{b}_\beta\Big)\times\Big(\bar{\hat{s}}_\beta[1+\gamma_5]\hat{b}_\alpha\Big), \qquad (2.4.105)
\end{aligned}$$

and the corresponding matrix elements

$$\begin{aligned}
\langle\hat{Q}\rangle &= \langle B_S|\hat{Q}|\bar{B}_s\rangle = \frac{8}{3}M_{B_s}^2 f_{B_s}^2 B, \\
\langle\hat{Q}_S\rangle &= \langle B_s|\hat{Q}_S|\bar{B}_s\rangle = -\frac{5}{3}M_{B_s}^2 f_{B_s}^2 B'_S, \\
\langle\hat{\tilde{Q}}_S\rangle &= \langle B_s|\hat{\tilde{Q}}_S|\bar{B}_s\rangle = \frac{1}{3}M_{B_s}^2 f_{B_s}^2 \tilde{B}'_S. \qquad (2.4.106)
\end{aligned}$$

Here f_{B_s} is the decay constant of the B_s meson and the modified bag parameters B'_S and $\tilde{B}'_S$ are defined as

$$B'_X = \frac{M_{B_s}^2}{\bar{m}_b(\bar{m}_b)+\bar{m}_s(\bar{m}_b)}B_X. \qquad (2.4.107)$$

The three operators introduced in Eq.(2.4.105) are not independent, it is found that they are connected through the $1/m_b$ suppressed operator

$$\hat{R}_0 = \hat{Q}_S + \alpha_1\tilde{Q}_S + \frac{\alpha_2}{2}\hat{Q} = 0 + \mathcal{O}\Big(\frac{\Lambda}{m_b}\Big), \qquad (2.4.108)$$

where $\alpha_{1,2}$ contain NLO corrections; the corresponding expressions in the $\overline{MS}$ scheme are [48]

$$\begin{aligned}
\alpha_1 &= 1 + \frac{\alpha_s(\mu_2)}{3\pi}\Big(12\ln\frac{\mu_2}{m_b}+6\Big), \\
\alpha_2 &= 1 + \frac{\alpha_s(\mu_2)}{3\pi}\Big(6\ln\frac{\mu_2}{m_b}+\frac{13}{2}\Big). \qquad (2.4.109)
\end{aligned}$$

We can write $\Gamma_{12}^{ab,s}$ more explicitly in terms of $\hat{Q}$ and $\hat{Q}_S$ as [52]

$$\Gamma_{12}^{ab,s} = \frac{G_F^2 m_b^2}{24\pi M_{Bs}}\Big[G^{ab}\langle B_s|\hat{Q}|\bar{B}_s\rangle - G_S^{ab}\langle B_s|\hat{Q}_S|\bar{B}_s\rangle\Big] + \Gamma_{12,1/m_b}^{ab,s}, \qquad (2.4.110)$$

with

$$G^{ab} = F^{ab} + P^{ab}, \qquad G_S^{ab} = -F_S^{ab} - P_S^{ab}. \qquad (2.4.111)$$

Here F^{ab} and F_S^{ab} arise from the double insertion of current-current operators $\hat{Q}_{1,2}$, whereas P^{ab} and P_S^{ab} are the result of the insertion of the penguin operators $\hat{Q}_{3,\ldots,6}$ and $\hat{Q}_8$.

At leading order the coefficients $G^{s,xy}$ and $G_S^{s,xy}$ have the following universal structure in terms of the current-current Wilson coefficients

$$\begin{aligned}
G^{s,xy} &= 3C_1^2 + 2C_1C_2 + \frac{1}{2}C_2^2, \\
G_S^{s,xy} &= -(3C_1^2 + 2C_1C_2 - C_2^2). \qquad (2.4.112)
\end{aligned}$$

The quadratic dependence on the tree level Wilson coefficients is not a surprise given that according to Eq.(2.4.102) these calculations are derived from the double insertion of $\Delta B = 1$ operators.

CKM	B_s^0	B_d^0
$\frac{\lambda_u}{\lambda_t}$	$-8.0486 \cdot 10^{-3} + 1.81082 \cdot 10^{-2} i$	$7.5543 \cdot 10^{-3} - 4.04703 \cdot 10^{-1} i$
$\left(\frac{\lambda_u}{\lambda_t}\right)^2$	$-2.63126 \cdot 10^{-4} - 2.91491 \cdot 10^{-4} i$	$-1.63728 \cdot 10^{-1} - 6.1145 \cdot 10^{-3} i$

Table 2.1: CKM ratios λ_u/λ_c for neutral B mesons; where $\lambda_p^q = V_{pb}V_{pq}^*$ for $q = s, d$ and $p = u, c$. The numerical inputs used in this calculations are provided in Appendix A.

Finally $\Gamma_{12,1/m_b}^{ab,s}$ stands for the sub-leading $1/m_b$ corrections calculated from the following set of operators

$$\begin{aligned}
\hat{R}_1 &= \frac{m_s}{m_b}\Big(\bar{s}_\alpha[1+\gamma_5]b_\alpha\Big)\times\Big(\bar{s}_\beta[1-\gamma_5]b_\beta\Big) \\
\hat{R}_2 &= \frac{1}{m_b^2}\Big(\bar{s}_\alpha \overleftarrow{D}_\rho\gamma^\mu[1-\gamma_5]D^\rho b_\alpha\Big)\times\Big(\bar{s}_\beta\gamma_\mu[1-\gamma_5]b_\beta\Big) \\
\hat{R}_3 &= \frac{1}{m_b^2}\Big(\bar{s}_\alpha \overleftarrow{D}_\rho[1+\gamma_5]D^\rho b_\alpha\Big)\times\Big(\bar{s}_\beta[1+\gamma_5]b_\beta\Big) \qquad (2.4.113)
\end{aligned}$$

In addition operators with mixed colour indices should also be included, they are denoted by $\tilde{\hat{R}}_1$, $\tilde{\hat{R}}_2$ and $\tilde{\hat{R}}_3$. Finally there is also the contribution from the operator $\hat{R}_0$ introduced in Eq.(2.4.108).

To cancel the dependency in Γ_{12}^s and M_{12}^s on the decay constant f_{B_s} the following ratio is considered

$$\begin{aligned}
-\frac{\Gamma_{12}^s}{M_{12}^s} &= \frac{\lambda_c^2\Gamma_{12}^{s,cc} + 2\lambda_c\lambda_u\Gamma_{12}^{s,uc} + \lambda_u^2\Gamma_{12}^{s,uu}}{\lambda_t^2\tilde{M}_{12}^s} \\
&= \frac{\Gamma_{12}^{s,cc}}{\tilde{M}_{12}^s} + 2\Big(\frac{\lambda_u}{\lambda_t}\Big)\frac{\Gamma_{12}^{s,cc} - \Gamma_{12}^{s,uc}}{\tilde{M}_{12}^s} + \Big(\frac{\lambda_u}{\lambda_t}\Big)^2\frac{\Gamma_{12}^{s,cc} - 2\Gamma_{12}^{s,uc} + \Gamma_{12}^{s,uu}}{\tilde{M}_{12}^s} \\
&= -10^{-4}\Big[c + a\frac{\lambda_u}{\lambda_t} + b\Big(\frac{\lambda_u}{\lambda_t}\Big)^2\Big]. \qquad (2.4.114)
\end{aligned}$$

In Eq.(2.4.114) we are introducing the a, b and c notation [53], in the SM these coefficients are real . The way of writing Γ_{12}^s/M_{12}^s in Eq.(2.4.114) can be viewed as a Taylor expansion in the small CKM parameter λ_u/λ_t, for which we get the numerical ratios shown in Tab. 2.1 (we use the same CKM inputs as in [15], see Appendix A; the values were taken in 2015 from CKMfitter [17], similar results can be obtained from UTfit [54]).

In addition to the CKM suppression a pronounced GIM-cancellation [55] is arising

	B_s^0	B_d^0
c	-48.0 ± 8.3	-49.5 ± 8.5
a	$+12.3 \pm 1.4$	$+11.7 \pm 1.3$
b	$+0.79 \pm 0.12$	$+0.24 \pm 0.06$

Table 2.2: Numerical values for the coefficients a, b, c used in the determination of Γ_{12}^q [53] for the neutral B_q^0 systems for $q = u, c$. All the inputs required for the explicit numerical evaluations are presented in Appendix A.

in the coefficients a and b in Eq.(2.4.114). With the input parameters in Appendix A we get the numerical values presented in Tab.2.2.

We now make direct contact with the mixing observables $\Delta\Gamma_s$ and ΔM_s. To begin with we take the real part of Eq.(2.4.114) and use the definitions given in Eq.(1.3.72) and Eq.(1.3.76) to obtain

$$\mathcal{R}e\Big[\frac{\Gamma_{12}^s}{M_{12}^s}\Big] \;=\; -\frac{\Delta\Gamma_s}{\Delta M_s} \approx -10^{-4} c. \tag{2.4.115}$$

On the other hand, the imaginary part of Eq.(2.4.114) allows to calculate the semileptonic asymmetries introduced in Eq.(1.3.103)

$$\mathcal{I}m\Big[\frac{\Gamma_{12}^s}{M_{12}^s}\Big] \;=\; a_{sl}^s \approx 10^{-4} a \cdot \mathcal{I}m\Big[\frac{\lambda_u}{\lambda_t}\Big]. \tag{2.4.116}$$

We present the explicit values for mixing observables $\Delta\Gamma_{s,d}$, $\Delta M_{s,d}$ and $a_{sl}^{s,d}$ in Section 4.7 and Section 6.3.

When the NLO-QCD and the sub-leading $1/m_b$ corrections are included, it is found that $\Delta\Gamma_s$ does not have a good behaviour: the corrections are large and have the same sign. To solve this problem in [52] the operator basis is changed from $\{\hat{Q}, \hat{Q}_S\}$ to $\{\hat{Q}, \hat{\tilde{Q}}_S\}$, this has the effect of changing the dependence on the bag parameters from $\{B, B_S\}$ to $\{B, \tilde{B}_S\}$.

We can solve for $\hat{Q}_S$ in terms of $\hat{R}_0$ in Eq.(2.4.108) to get

$$\begin{aligned}
\Gamma_{12}^{ab} &= \frac{G_F^2 m_b^2}{24\pi M_{Bs}}\Big[G^{ab}\langle B_s|\hat{Q}|\bar{B}_s\rangle - G_S^{ab}\langle B_s|\Big(\hat{R}_0 - \alpha_1\hat{\tilde{Q}}_S - \frac{1}{2}\alpha_2\hat{Q}\Big)|\bar{B}_s\rangle\Big] + \Gamma_{12,1/m_b}^{ab} \\
&= \frac{G_F^2 m_b^2}{24\pi M_{Bs}}\Big[\Big(G^{ab} + \frac{1}{2}\alpha_2 G_S^{ab}\Big)\langle B_s|\hat{Q}|\bar{B}_s\rangle + \alpha_1 G_S^{ab}\langle B_S|\hat{\tilde{Q}}_S|\bar{B}_S\rangle\Big] + \tilde{\Gamma}_{12,1/m_b}^{ab}
\end{aligned}$$

where

$$\tilde{\Gamma}_{12}^{ab} = \Gamma_{12,1/m_b}^{ab} - \frac{G_F^2 m_b^2}{24\pi M_{Bs}} G_S^{ab} \langle B_s | \hat{R}_0 | \bar{B}_s \rangle. \tag{2.4.117}$$

The effect of changing the set of operators from $\{\hat{Q}, \hat{Q}_S\}$ to $\{\hat{Q}, \hat{\tilde{Q}}_S\}$ can be appreciated in the following equations for the ratio $\Delta\Gamma_s/\Delta M_s$ calculated in the old and the new basis [15].

$$\begin{aligned} \frac{\Delta\Gamma_s^{Old}}{\Delta M_s} &= 10^{-4} \cdot \left[2.6 + 69.7\frac{B_S}{B} - 24.3\frac{B_R}{B}\right] \\ \frac{\Delta\Gamma_s^{New}}{\Delta M_s} &= 10^{-4} \cdot \left[44.8 + 16.4\frac{\tilde{B}_S}{B} - 13.0\frac{B_R}{B}\right] \end{aligned} \tag{2.4.118}$$

As can be seen in the second of Eq.(2.4.118), the leading numerical term in the calculation based on the new basis is not multiplying any ratio of bag parameters, hence it is free from hadronic uncertainties. The second and third terms, containing the ratios $\tilde{B}_S/B$ and B_R/B respectively, have smaller contributions because they are multiplied by smaller numerical factors. In contrast, in the old basis the leading numerical contribution enhances the uncertainties from the ratio B_S/B and it is quite sizeable in comparison with the rest of the terms included. The calculations for neutral B mixing in Chapters 4, 5 and 6 are based on this approach.

Chapter 3

Basics on QCD Factorization

3.1 Introduction

As will be discussed in Chapter 4, we have performed a global fit to determine possible new physics effects manifesting as deviations on the current-current Wilson coefficients C_1 and C_2 for B-meson decays. This analysis includes constraints from neutral B-meson mixing as well as from non-leptonic B-meson decays such as $B \to \pi\pi$, $B \to \pi\rho$, $B \to \rho\rho$ and $B \to D\pi$. The amplitudes for the non-leptonic decays included in our analysis were calculated using the QCD Factorization formalism (QCDF) [56]. In this chapter we present a brief summary of the QCDF results relevant to our investigations.

3.2 QCD Factorization

The main idea of factorization is to disentangle physical effects from different length and momentum scales. When studying B meson decays we are faced with two energy scales m_b and Λ_{QCD} determining the perturbative and non-perturbative regimes of the processes of interest, respectively.

In order to introduce the main QCDF formulas let us first define "light" and "heavy" mesons according to [57]. A meson with mass m is considered "heavy" if m scales with m_b in the heavy quark limit such that m/m_b remains fixed. On the other hand a meson is regarded as "light" if its mass remains finite in the heavy quark limit,

for a light meson $m \sim \mathcal{O}(\Lambda_{QCD})$.

Consider the transition $B \to M_1 M_2$ where M_1 and M_2 are two final state mesons, then under the application of the effective theory formalism introduced in Chapter 2 the corresponding amplitude can be expressed in terms of the matrix elements of different dimension six operators $\langle M_1 M_2|\hat{Q}_i|B\rangle$ (where $\hat{Q}_i$ is any of the operators in Eq.(2.3.78)). According to QCDF the structure of these matrix elements depends on whether the final states are "light" or "heavy" (see Fig.3.1). For instance if M_1 and M_2 are light then the corresponding matrix element is

$$\begin{aligned}\langle M_1 M_2|\hat{Q}_i|B\rangle &= \sum_j F_j^{B\to M_1}(0)\int_0^1 du T_{ij}^I(u)\Phi_{M_2}(u) + (M_1 \leftrightarrow M_2) \\ &\quad + \int_0^1 d\xi du dv T_i^{II}(\xi,u,v)\Phi_B(\xi)\Phi_{M_1}(v)\Phi_{M_2}(u). \qquad (3.2.1)\end{aligned}$$

In the right hand side of the previous equation $F_j^{B\to M_{1,2}}(m_{2,1}^2)$ represents a form factor for the transition $B \to M_1 M_2$ and $\Phi_M(u)$ is the non-perturbative Light-Cone Distribution Amplitude (LDCA) for the meson M.

We have written Eq.(3.2.1) in such a way that it can be applied to situations where the spectator quark can end in any of the two final state light mesons. If the spectator can go into only one of the final mesons, this one will be labelled as M_1 and just the first and the third terms on the right hand side of Eq.(3.2.1) should be included.

If in the final hadronic states M_1 is "heavy" and M_2 is "light" then, according to QCDF the corresponding matrix element is

$$\langle M_1 M_2|\hat{Q}_i|B\rangle = \sum_j F_j^{B\to M_1}(m_2^2)\int_0^1 du T_{ij}^I(u)\Phi_{M_2}(u). \qquad (3.2.2)$$

The meaning of different factors inside Eq.(3.2.2) are analogous to those given for Eq.(3.2.1).

Physically the LCDA [58] $\Phi_M(u)$ describes the momentum fraction of the partons for a particular Fock state associated with M. The partons of the Fock state under consideration should be taken at zero transverse separation in the light cone coordinates, this is one of the requirements for the factorizability of the hadronic amplitudes. The LCDA are ordered using the quantum number twist t. The twist of an operator $\hat{O}$ is given by $t = d - s$, being d the canonical mass dimension of $\hat{O}$

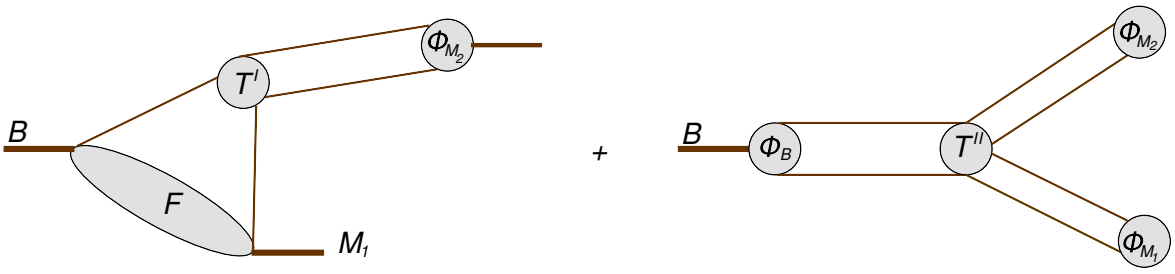

Figure 3.1: Factorization of matrix elements for B decays into "light"-"light" mesons (both diagrams included) and "heavy"-"light" (only left diagram) in QCDF.

and s its Lorentz Spin. The leading twist $t = 2$ LCDA corresponds to the lowest Fock state used in the description of M, thus for this particular case only the valence quark q and the valence antiquark $\bar{q}'$ are included. The symbol u in the argument of Φ_M is the fraction of longitudinal momentum carried by q and $\bar{u} = 1 - u$ is the fraction of longitudinal momentum corresponding to $\bar{q}'$. The functions $T^{I,II}$ are called hard-scattering kernels, T^I contains nonfactorizable gluon exchange, including penguin topologies. On the other hand, hard interactions involving the spectator quark are part of T^{II}. One of the main features of the QCDF formula is that all the non-perturbative effects can be absorbed into the form factor and the LCDA.
At leading power in α_s the factorization formula can be simplified considering that $T^I = constant + \mathcal{O}(\alpha_s)$ and $T^{II} = \mathcal{O}(\alpha_s)$. Then the convolution integral containing T^I reduces to a decay constant f_{M_2} and we can drop the contribution containing T^{II} to obtain

$$\langle M_1 M_2 | \hat{Q} | B \rangle \approx F^{B \to M_1}(0) f_{M_2}. \tag{3.2.3}$$

This is the result obtained in naive factorization [59, 60]. It ignores final state interactions and consequently does not account for strong rescattering phases. The naive factorization formalism corresponds to the leading terms in the α_s and $1/m_b$ expansion in QCDF. We will refer to naive factorization in Section 4.4.2 and 4.8.5 in order to get an estimation on the possible size of amplitudes that have not been calculated from first principles yet.
Returning to our main line of discussion, we now present the structure of the amplitude for the process $\bar{B}_d^0 \to M_1 M_2$ within the context of QCDF,

$$\mathcal{A}(\bar{B}_d^0 \to M_1 M_2) \;=\; \frac{G_F}{\sqrt{2}} \sum_{p=u,c} \lambda_p \langle M_1 M_2 | \hat{\mathcal{T}}_p^{(d)} + \mathcal{T}_p^{ann,(d)} | B \rangle. \qquad (3.2.4)$$

Using the basis in Eq.(2.3.78) (adapted for B_d^0 instead of B_s^0) and including QCD and electroweak penguins, the operator $\hat{\mathcal{T}}_p^{(d)}$ in Eq.(3.2.4) is [45]

$$\begin{aligned}
\hat{\mathcal{T}}_p^{(d)} &= \alpha_1(M_1M_2)\delta_{pu}\Big(\bar{\hat{d}}\hat{b}\Big)_{V-A}\otimes\Big(\bar{\hat{u}}\hat{u}\Big)_{V-A} \\
&+ \alpha_2(M_1M_2)\delta_{pu}\Big(\bar{\hat{u}}\hat{b}\Big)_{V-A}\otimes\Big(\bar{\hat{d}}\hat{u}\Big)_{V-A} \\
&+ \alpha_3(M_1M_2)\sum_q\Big(\bar{\hat{d}}\hat{b}\Big)_{V-A}\otimes\Big(\bar{\hat{q}}\hat{q}\Big)_{V-A} \\
&+ \alpha_4^p(M_1M_2)\sum_q\Big(\bar{\hat{q}}\hat{b}\Big)_{V-A}\otimes\Big(\bar{\hat{d}}\hat{q}\Big)_{V-A} \\
&+ \alpha_5(M_1M_2)\sum_q\Big(\bar{\hat{d}}\hat{b}\Big)_{V-A}\otimes\Big(\bar{\hat{q}}\hat{q}\Big)_{V+A} \\
&+ \alpha_6^p(M_1M_2)\sum_q\Big(-2\Big)\Big(\bar{\hat{q}}\hat{b}\Big)_{S-P}\otimes\Big(\bar{\hat{d}}\hat{q}\Big)_{S+P} \\
&+ \alpha_7^p(M_1M_2)\sum_q\Big(\bar{\hat{d}}\hat{b}\Big)_{V-A}\otimes\frac{3}{2}e_q\Big(\bar{\hat{q}}\hat{q}\Big)_{V+A} \\
&+ \alpha_8^p(M_1M_2)\sum_q\Big(-2\Big)\Big(\bar{\hat{q}}\hat{b}\Big)_{S-P}\otimes\frac{3}{2}e_q\Big(\bar{\hat{d}}\hat{q}\Big)_{S+P} \\
&+ \alpha_9^p(M_1M_2)\sum_q\Big(\bar{\hat{d}}\hat{b}\Big)_{V-A}\otimes\frac{3}{2}e_q\Big(\bar{\hat{q}}\hat{q}\Big)_{V-A} \\
&+ \alpha_{10}^p(M_1M_2)\sum_q\Big(\bar{\hat{q}}\hat{b}\Big)_{V-A}\otimes\frac{3}{2}e_q\Big(\bar{\hat{d}}\hat{q}\Big)_{V-A}, \qquad (3.2.5)
\end{aligned}$$

with $(\bar{\hat{q}}_1\hat{q}_2)_{S\pm P} = \bar{\hat{q}}_1(1\pm\gamma_5)\hat{q}_2$. The previous expression can easily be applied to $\bar{B}_s^0$ mesons by substituting the field of the down quark by the corresponding one of the strange quark. The symbol $\otimes$ indicates that the matrix elements for the operators have to be evaluated in the factorized form $\langle M_1M_2|j_1\otimes j_2|B\rangle \equiv \langle M_1|j_1|B\rangle\langle M_2|j_2|0\rangle$ or $\langle M_1|j_2|B\rangle\langle M_2|j_1|0\rangle$ depending on the specific case. The nonfactorizable contributions are kept inside the topological amplitudes $\alpha_i^p(M_1M_2)$ to be described in more detail below.

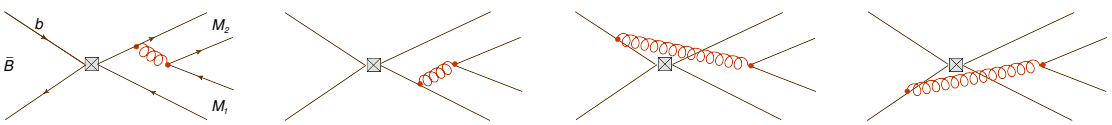

Figure 3.2: Weak annihilation diagrams.

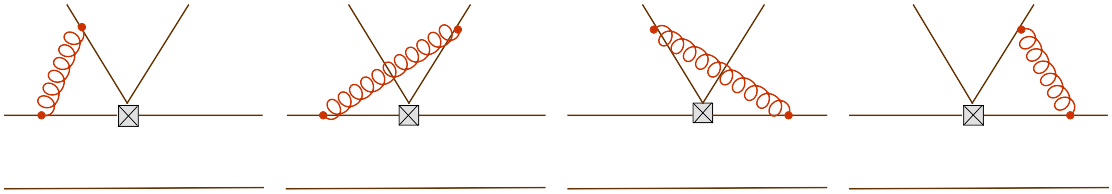

Figure 3.3: NLO vertex corrections included in the topological amplitudes α_i^p.

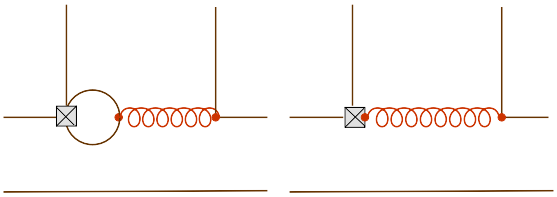

Figure 3.4: NLO penguin topologies included in α_i^p.

The matrix elements of $\mathcal{T}_p^{(d),ann}$ correspond to weak annihilation contributions (see Fig.3.2) and cannot be calculated using QCDF. Regarding the scaling behaviour in the heavy quark limit, the annihilation contributions are found to be suppressed by Λ_{QCD}/m_b [57], hence they are classified as power corrections. The following example attempts to explain how the argument works. Consider for instance the process $\bar{B}_d^0 \to \pi^+\pi^-$. As shown in [57], the form factors and decay constants relevant to this process have the following scaling behaviour in the heavy quark limit

$$F^{B\to\pi}(0) \sim \left(\frac{\Lambda_{QCD}}{m_b}\right)^{3/2}, \quad f_\pi \sim \Lambda_{QCD}, \quad f_B \sim \frac{\Lambda_{QCD}^{3/2}}{m_b^{1/2}}, \tag{3.2.6}$$

therefore for the amplitude of the factorizable diagrams we get

$$\mathcal{A}(\bar{B}_d^0 \to \pi^+\pi^-) \sim G_F\ m_b^2\ F^{B\to\pi}(0) f_\pi \sim G_F\ \Lambda_{QCD}^{5/2} m_b^{1/2}. \tag{3.2.7}$$

On the other hand, for the annihilation topologies the following asymptotic expression is expected

$$\mathcal{A}(\bar{B}_d^0 \to \pi^+\pi^-) \sim G_F f_B f_\pi^2 \alpha_s \sim G_F \frac{\Lambda_{QCD}^{7/2}}{m_b^{1/2}} \alpha_s. \tag{3.2.8}$$

Considering the scaling behaviour given in Eq.(3.2.6) we see that the annihilation contribution in Eq.(3.2.8) is suppressed by one power in Λ_{QCD}/m_b with respect to the factorizable amplitude in Eq.(3.2.7).

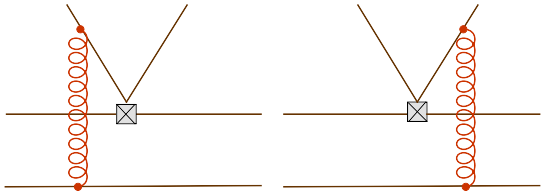

Figure 3.5: Hard scattering contributions to the topological amplitudes α_i^p.

3.3 Topological amplitudes

The topological amplitudes $\alpha_i^p(M_1M_2)$ have the following generic structure at NLO in α_s [61]

$$\begin{aligned}\alpha_i^{p,M_1M_2} &= \Big(C_i(\mu_b)+\frac{C_{i\pm1}(\mu_b)}{N_c}\Big)N_i(M_2)+\frac{\alpha_s(\mu_b)}{4\pi}\frac{C_{i\pm1}(\mu_b)C_F}{N_c}V_i(M_2)+P_i^p(M_2)\\ &\quad+\frac{\alpha_s(\mu_h)}{4\pi}\Big(\frac{4\pi^2C_{i\pm1}(\mu_h)C_F}{N_c^2}H_i(M_1M_2)\Big).\end{aligned} \tag{3.3.9}$$

Where the superscript $p=u,c$ should be removed for $i=1,2$. For some processes quoted in the literature [45] alternative versions of this formula are used. However, for the purposes of the QCDF amplitudes required in this Thesis we will refer to Eq.(3.3.9) unless stated otherwise. In Eq.(3.3.9) C_i are the Wilson coefficients calculated at the scale $\mu\sim m_b$ (see Section 2.3.1). For the subindices of the coefficients $C_{i\pm1}$ we have

$$C_{i\pm1}=\begin{cases}C_{i+1}: & \text{if } i \text{ is odd},\\ C_{i-1}: & \text{if } i \text{ is even.}\end{cases}$$

The normalization of the light-cone distribution $N_i(M_2)$ for the meson M_2 is determined according to the following rule

$$N_i(M_2)=\begin{cases}0: & i=6,8 \text{ and } M_2=V,\\ 1: & \text{in any other case.}\end{cases}$$

The symbol $V_i(M_2)$ in Eq.(3.3.9) stands for the one loop vertex corrections shown in Fig.3.3. The Penguin contributions presented in Fig.3.4 are given by $P_i^p(M_2)$. Finally the hard spectator interactions appearing in Fig.3.5 are introduced through $H_i(M_1M_2)$.

3.4 Power corrections in Hard spectator functions

The hard scattering functions $H_i(M_1M_2)$ get a divergence from the twist-3 distribution amplitude $\Phi_{m_1}(y)$ of the meson M_1. We now provide a brief explanation on how this divergence is treated in QCDF. To begin with, the contribution of $\Phi_{m_1}(y)$ to $H_i(M_1M_2)$ has the following structure

$$\delta H_i(M_1M_2) \;\propto\; r_\chi^{M_1}\int_0^\infty d\xi\frac{\Phi_B(\xi)}{\xi}\int_0^1 dx\frac{\Phi_{M_2}(x)}{\bar{x}}\int_0^1 dy\frac{\Phi_{m_1}(y)}{\bar{y}}, \quad (3.4.10)$$

for $\bar{x}=1-x$ and $\bar{y}=1-y$. The factor $r_\chi^{M_1}$ in Eq.(3.4.10) provides a suppression of the order Λ_{QCD}/m_b in the heavy quark limit. This can be seen for example in the case of $M_1=\pi$ for which we have

$$\begin{aligned} r_\chi^\pi(\mu) &= \frac{2m_\pi^2}{m_b(\mu)(m_u+m_d)(\mu)} \approx \frac{2\Lambda_{QCD}^2}{m_b(\mu)\Lambda_{QCD}} \\ &\sim \frac{\Lambda_{QCD}}{m_b}. \end{aligned} \quad (3.4.11)$$

The main problem is that $\Phi_{m_1}(y)$ does not vanish at $y=1$ leading to a divergent term in Eq.(3.4.10). Conventionally the divergence is extracted according to the following prescription

$$\begin{aligned} \int_0^1\frac{dy}{\bar{y}}\Phi_{m_1}(y) &= \Phi_{m_1}(1)\int_0^1\frac{dy}{\bar{y}}+\int_0^1\frac{dy}{\bar{y}}\Big[\Phi_{m_1}(y)-\Phi_{m_1}(1)\Big] \\ &= \Phi_{m_1}(1)X_H^{M_1}+\int_0^1\frac{dy}{[\bar{y}]_+}\Phi_{m_1}(y). \end{aligned} \quad (3.4.12)$$

In Eq.(3.4.12) the divergence is parameterized inside X_H, physically X_H represents a soft gluon interaction with the spectator quark. It is expected that $X_H\sim\ln(m_b/\Lambda_{QCD})$ because the divergence appearing is regulated by a physical scale of the order Λ_{QCD}. In addition a complex coefficient cannot be excluded since multiple soft scatterings can introduce a strong interaction phase. The standard parameterization for X_H from Beneke-Buchalla-Neubert-Sachrajda (BBNS) [57] is

$$X_H \;=\; \Big(1+\rho_H e^{i\phi_H}\Big)\ln\frac{m_B}{\Lambda_h}, \quad (3.4.13)$$

where $\Lambda_h\approx\mathcal{O}(\Lambda_{QCD})$ and $\rho_H\approx\mathcal{O}(1)$. We will deal with X_H in Chapter 4, where X_H will be assumed to be the same for all mesons M_1 and all topological amplitudes α_i^p. The remaining integral $\int_0^1 dy/[\bar{y}]_+\Phi_{m_1}(y)$, in Eq.(3.4.12), is finite. For instance for pseudoscalar mesons $\Phi_{m_1}(y)=1$, and trivially

$$\int_0^1 \frac{dy}{[\bar{y}]_+}\Phi_{m_1}(y) \;=\; \int_0^1 \frac{dy}{\bar{y}}\Big[\Phi_{m_1}(y)-\Phi_{m_1}(1)\Big]=0. \tag{3.4.14}$$

Unfortunately X_H cannot be determined from first principles, so the parameterization in Eq.(3.4.13) accounts for our ignorance on the underlying hard scattering mechanisms described by the integral of Φ_{m_1} in Eq.(3.4.12). Another important source of uncertainty in Eq.(3.4.10) is the inverse moment of the LCDA of the B meson

$$\int_0^1 d\xi \frac{\Phi_B(\xi)}{\xi} \;=\; \frac{m_B}{\lambda_B}, \tag{3.4.15}$$

where λ_B is an unknown quantity parameterizing our ignorance on the LCDA Φ_B.

3.5 Weak annihilation contributions

The contribution from the weak annihilation topologies shown in Fig.3.2 are taken into account using linear combinations of the basic "building blocks" $A_k^{i,f}$. They result from the calculation of divergent integrals including the twist 2 and twist 3 LCDA of the final mesons M_1 and M_2, see Eqn. (3.5.16). The superscripts "i, f" indicate whether the gluon emission comes from an initial or a final quark state, respectively. The subscripts describe the Dirac structure under consideration: $k = 1$ for $(V-A)\otimes(V-A)$, $k = 2$ for $(V-A)\otimes(V+A)$ and $k = 3$ for $(-2)(S-P)\otimes(S+P)$.

$$\begin{aligned}
b_1 &= \frac{C_F}{N_c^2}C_1A_1^i,\\
b_2 &= \frac{C_F}{N_c^2}C_2A_1^i,\\
b_3^p &= \frac{C_F}{N_c^2}\Big(C_3A_1^i + C_5(A_3^i + A_3^f) + N_cC_6A_3^f\Big),\\
b_4^p &= \frac{C_F}{N_c^2}\Big(C_4A_1^i + C_6A_2^i\Big),\\
b_{3,\mathrm{EW}}^p &= \frac{C_F}{N_c^2}\Big(C_9A_1^i + C_7(A_3^i + A_3^f) + N_cC_8A_3^f\Big),\\
b_{4,\mathrm{EW}}^p &= \frac{C_F}{N_c^2}\Big(C_{10}A_1^i + C_8A_2^i\Big)
\end{aligned} \tag{3.5.16}$$

In Eq. 3.5.16 b_1 and b_2 correspond to the annihilation amplitudes due to current-current topologies. The amplitudes b_3^p and b_4^p account for QCD penguin annihilation. Finally $b_{3,\mathrm{EW}}^p$ and $b_{4,\mathrm{EW}}^p$ are the result of electroweak penguin annihilation.

BBNS treat the endpoint singularities arising in the annihilation topologies in an analogous way as for the hard scattering contributions, i.e. they introduce

$$X_A = \left(1+\rho_A e^{i\phi_A}\right)\ln\frac{m_B}{\Lambda_h}, \tag{3.5.17}$$

which corresponds to the regularized integral

$$\int_0^1 \frac{dx}{x} \to \int_{\Lambda_h/m_B}^1 \frac{dx}{x} = \ln\frac{m_B}{\Lambda_h}, \tag{3.5.18}$$

modified by ρ_A and the phase ϕ_A. The hard scattering contributions and the weak annihilation contributions are evaluated at the scale $\mu = \sqrt{\Lambda_h m_b}$.

Chapter 4

New Physics at tree level decays

The possibility of new physics in non leptonic tree level decays has already been considered in e.g. [2,3,62]; however, to the best of our knowledge there has not been a rigorous study so far. For instance the results in [2, 3] are based on a scan over the parameter space defined by new physics contributions only and the correlations between other input parameters such as decay constants, masses and so on were not included. The analysis presented here improves the study in [2, 62] on possible new effects in the $b \to q\bar{q}'d$ and $b \to q\bar{q}'s$ decays ($q, q' = u, c$) in two different ways. Firstly we make a more profound statistical analysis, in addition it also includes full NLO formulae for the different physical observables considered (previously only simplified expressions were used in most of the cases). As far as we know this is the first systematic study on the subject. We perform two analyses, in the first one we study the new physics effects on the different decay transitions $b \to q\bar{q}'d$ and $b \to q\bar{q}'s$ independently; we focus in particular on the inclusive decays $b \to u\bar{u}d$, $b \to c\bar{u}d$ and $b \to c\bar{c}d$ ($b \to u\bar{c}d$ is rather unconstrained and is not included). As a second step we make a universal treatment by assuming that new physics has the same effect over the channels $b \to q\bar{q}'d$ and $b \to q\bar{q}'s$. Following this approach, we found the strongest constraints possible within our investigation. Finally, we assess the phenomenological impact of new physics at tree level on two physical observables: the decay width difference for B_d^0 meson mixing $\Delta\Gamma_d$ and on the CKM angle γ.

4.1 Basic formalism

Our starting point is the effective Hamiltonian in Eq.(2.3.76) written in terms of the basis in Eq.(2.3.78). We introduce new physics in tree level decays by modifying the Wilson coefficients of the operators $\hat{Q}_1$ and $\hat{Q}_2$ with respect to their SM values according to

$$C_{1,2}^{SM} \to C_{1,2}^{NP} := C_{1,2}^{SM} + \Delta C_{1,2}. \tag{4.1.1}$$

We present the possible bounds for ΔC_1 and ΔC_2 at the matching scale $\mu = M_W$ and work under the assumption of "single operator dominance" by considering changes to each Wilson coefficient independently. E.g. to establish constraints on $\Delta C_1(M_W)$ we fix $\Delta C_2(M_W) = 0$ and vice versa, this is the most conservative approach, if we allow both parameters to change simultaneously this results in partial cancellations leading to bigger new physics regions. Taking into account that, the theoretical formulae for our observables are calculated at the scale $\mu = m_b$, we evolve the new Wilson coefficients $C_1^{NP}(M_W)$ and $C_2^{NP}(M_W)$ using the renormalization group formalism described in Section 2.3.1. We consider new physics to be leading order only, then we treat the SM contribution $C_{1,2}^{SM}(M_W)$ and the new physics components $\Delta C_{1,2}$ differently under the renormalization group equations. For instance the evolution of $C_{1,2}^{SM}(M_W)$ is done using the full NLO expressions in Eq.(2.3.80) whereas $\Delta C_{1,2}(M_W)$ are evolved using only the LO version in Eq.(2.3.82). Notice that even though at $\mu = M_W$ there is only new physics in C_1 and C_2, the non diagonal nature of the evolution equations propagate these effects to all the other Wilson coefficients undergoing mixing at the scale $\mu = m_b$.

4.2 Statistical analysis

The new physics contributions $\Delta C_1(M_W)$ and $\Delta C_2(M_W)$ compatible with experimental data are calculated using a likelihood ratio test as given by Eq.(B.0.1) and Eq.(B.0.3), where the chi-squared function is

$$\chi^2(\vec{\omega}) \;=\; \sum_i \Big(\frac{\hat{O}_{i,exp} - \hat{O}_{i,theo}(\vec{\omega})}{\sigma_{i,exp}} \Big)^2. \tag{4.2.2}$$

Here $\hat{O}_{i,exp}$ and $\hat{O}_{i,theo}$ are the experimental and theoretical determinations of the ith observable respectively. The vector $\vec{\omega}$ includes all the inputs necessary for the determination of $\hat{O}_{i,theo}$. We want to make a distinction among the different components of $\vec{\omega}$; we will define a subvector $\vec{\lambda}$ containing only the SM inputs (e.g. quarks masses, decay constants, form factors, etc), leaving separate the new physics contributions $\Delta C_{1,2}$, thus we write

$$\vec{\omega} \;=\; (\vec{\lambda}, \Delta C_1(M_W), \Delta C_2(M_W)). \tag{4.2.3}$$

During our global fit $\vec{\lambda}$ and $\Delta C_{1,2}(M_W)$ are treated differently. We are not really interested in the SM components entering $\vec{\lambda}$; however, they are crucial in defining the uncertainties of our observables. Hence in our analysis they have the status of nuisance parameters. On the other hand $\Delta C_{1,2}(M_W)$ play a central role in our study, as a matter of fact we want to probe for the possible values of $\Delta C_{1,2}(M_W)$ compatible with data. Technically speaking we profile the likelihood with respect to $\Delta C_{1,2}(M_W)$. In practice this means that we first partially minimize our likelihood estimator (see Appendix B) with respect to the components in $\vec{\lambda}$ and then we study the behaviour of the resulting estimator with respect to different values for $\Delta C_{1,2}(M_W)$.

The new physics contributions $\Delta C_1(M_W)$ and $\Delta C_2(M_W)$ are assumed to be complex and the possible values of their real and imaginary components, determined at the scale $\mu = M_W$, are supposed to obey a Gaussian distribution with mean $\overline{\Delta C}_{1,2} = 0$ and standard deviation $\sigma_{\Delta C_{1,2}} = 1$.

As already mentioned in the previous section, during our statistical analysis we used the single operator dominance assumption by fitting independently the contributions $\Delta C_1(M_W)$ and $\Delta C_2(M_W)$. Then if we want to estimate the possible values of $\Delta C_1(M_W)$ we take $\Delta C_2(M_W) = 0$ and vice-versa. Next we describe step-by-step the fitting method for $\Delta C_1(M_W)$, an analogous procedure was followed for $\Delta C_2(M_W)$ (the necessary statistical concepts are presented in Appendix B).

1. Define the confidence level (CL) for the statistical fit and estimate the p value according to

$$p \;=\; 1 - CL. \tag{4.2.4}$$

2. Establish a sampling region on the plane defined by the real and the imaginary components of $\Delta C_1(M_W)$. Our main aim here is to determine which values in the test region are allowed at the confidence level given in the first step. The sampling region is observable dependent, in our case we always use rectangular grids around the origin of the complex plane defined by $\Delta C_1(M_W)$ (the origin of this plane corresponds to the SM value). The number of points on the grid depends on the numerical stability of our algorithms, on the time required to compute a particular combination of observables and on the size of the new physics regions determined by them.

3. Obtain the combination of values $\vec{\omega}'$ that minimize the χ^2 function in Eq.(4.2.2), here we are interested in the global minimum of χ^2, hence the minimization takes into account all the entries in $\vec{\omega}'$ including $\Delta C_1(M_W)$ and $\Delta C_2(M_W)$. Using the notation given in Appendix B we will label the global minimum of χ^2 as $\min\limits_{\vec{\omega}'\in\Omega} \chi^2$, where Ω denotes the parameter space for all the inputs.

4. Each one of the points on the grid constructed in Step 2 is a null hypothesis for $\Delta C_1(M_W)$, we will refer to them individually as $\Delta C_1^{NH}(M_W)$. For every $\Delta C_1^{NH}(M_W)$ apply Steps 5 to 7.

5. Determine the set of values for the nuisance parameters $\vec{\lambda}_0$ that minimizes the χ^2 function in Eq.(4.2.2) under the assumption $\Delta C_1(M_W) = \Delta C_1^{NH}(M_W)$. We will label this new result as $\min\limits_{\vec{\omega}_0\in\Omega_0} \chi^2$. Here Ω_0 is the subregion of the parameter space where $\Delta C_1(M_W) = \Delta C_1^{NH}(M_W)$ and $\vec{\omega}_0 = (\vec{\lambda}_0, \Delta C_1^{NH}(M_W), 0)$.

6. Perform a likelihood ratio test as defined in Eq.(B.0.3). The $\Delta\chi^2$ function should be computed using the global minimum estimated in Step 3 and the partial minimization for the χ^2 obtained in Step 5.

7. Estimate the $p(\vec{\omega_0})$ value associated with $\vec{\omega_0}$ using Eq.(B.0.6). Accept the null hypothesis for $\Delta C_1(M_W)$ only if

$$p(\vec{\omega_0}) > p. \tag{4.2.5}$$

We implement the steps previously described with the package MyFitter [63]. To minimize the computational time invested in the combined fits we make use of the

parallelization option available on MyFitter, this allows us to divide one particular "fitting process" into several computing "jobs". With this procedure we are able to execute up to 130 jobs simultaneously using the local computer cluster of the Institute for Particle Physics and Phenomenology (Durham University). The time invested in each one of the fits depends on the combination of observables considered and on the availability of the computer resources at the institute. The combined fits in Section 4.8.4 are particularly demanding requiring up to 4 days to be finished with an average of 100 jobs running simultaneously.

4.3 Constraints from $b \to u\bar{u}d$ transitions

We begin our analysis by deriving constraints on the new physics contributions $\Delta C_{1,2}^{uu}(M_W)$ entering in the quark level transition $b \to u\bar{u}d$. Our bounds are calculated taking into account the decays $B \to \pi\pi$, $\rho\pi$, $\rho\rho$. We include different observables calculated to leading power in $\Lambda_{\rm QCD}/m_b$ using the QCD Factorization (QCDF) formalism introduced briefly in Chapter 3. The reliability of the factorization predictions is a subject of debate [62], and in the following we only include observables that can be argued to be under good theoretical control in this approach.

Consider the exclusive decay $\bar{B}_d^0 \to M_1 M_2$, where M_1 and M_2 are final state mesons. As described in Chapter 3, within the context of QCDF the Wilson coefficients $C_{1,2}$ enter in the amplitudes $\mathcal{A}(\bar{B}_d^0 \to M_1 M_2)$ for the different $\bar{B}_d^0$ hadronic decays through the topological amplitudes α_i^{p,M_1M_2} (Eq.(4.3.6)) whose updated expressions using the new physics versions of the tree level Wilson Coefficients $C_i^{NP} = C_i^{SM} + \Delta C_i$ (for $i = 1, .., 10$) are

$$\begin{aligned}\alpha_i^{p,M_1M_2} &= \Big(C_i^{NP}(\mu_b) + \frac{C_{i\pm1}^{NP}(\mu_b)}{N_c}\Big) N_i(M_2) + \frac{\alpha_s(\mu_b)}{4\pi}\frac{C_{i\pm1}(\mu_b)C_F}{N_c} V_i(M_2) + P_i^p(M_2) \\ &\quad + \frac{\alpha_s(\mu_h)}{4\pi}\Big(\frac{4\pi^2 C_{i\pm1}(\mu_h)C_F}{N_c^2} H_i(M_1M_2)\Big). \end{aligned} \tag{4.3.6}$$

Here it should be stressed that even though new physics is introduced only in C_1 and C_2 at the scale $\mu = M_W$, it actually propagates to the Wilson Coefficients of other operators as well at the scale $\mu = m_b$, this is the result of the operator mixing given by the non-diagonal structure of the anomalous dimension matrices described

in Section 2.2. Consequently when writing Eq.(4.3.6) it makes sense to also consider new physics effects in C_i for $i \neq 1, 2$. Another important remark is that in this work new physics is supposed to be leading order in α_s and α only; since all the vertex corrections V_i^M, penguins $P_i^{p,M}$ and hard scattering spectator interactions $H_i^{M_1 M_2}$ are already suppressed by factors of $\mathcal{O}(\alpha_s)$ and $\mathcal{O}(\alpha)$ we will always drop the extra contributions $\Delta C_1(M_W)$ and $\Delta C_2(M_W)$ in the Wilson coefficients multiplying or included in any of these terms. Finally notice that all the factors included in the last term of Eq.(4.3.6) are evaluated at the scale $\mu_h = \sqrt{\Lambda_h m_b}$.

For the observables related with the exclusive decays $B \to \pi\pi$, $\rho\pi$, $\rho\rho$ we perform two analyses depending on our treatment of the first moment of the light cone distribution λ_B and the magnitudes ρ_H and ρ_A used to parameterize the power corrections arising in the hard spectator interactions and the annihilation topologies, respectively (see Section 3.4 and Section 3.5). For the "standard analysis" we consider

$$\lambda_B = 400 \pm 150 \text{ MeV [64]} \quad 0 < \rho_H < 2 \quad 0 < \rho_A < 2, \tag{4.3.7}$$

alternatively, we make a second estimation taking into account a more "aggressive" version of the previous inputs

$$\lambda_B = 400 \pm 50 \text{ MeV} \quad 0 < \rho_H < 1 \quad 0 < \rho_A < 1. \tag{4.3.8}$$

Based on the idea proposed in [65], bounds for λ_B have been obtained experimentally from Belle using the decay channel $B^+ \to l^+ \nu_l \gamma$ [66]. The most recent determination gives $\lambda_B > 238$ MeV at 90% C.L.. This is above the value of $\lambda_B \simeq 200$ MeV preferred by QCDF in order to describe the data within the theoretical and experimental uncertainties [67]. However, this bound is consistent with old theoretical calculations such as [68] and [69], which give $\lambda_B = 460 \pm 110$ MeV and $\lambda_B = 476.19 \pm 113.38$ MeV, respectively. For our standard analysis we adopted the value used in [64], which results from a combination of these and other studies. On the other hand in our aggressive analysis we considered a possible future scenario where the uncertainty drops by 2/3 while keeping the same central value. Having a relatively big value for λ_B has the advantage of reducing the uncertainty by suppressing the power corrections of the hard spectator interactions. To determine the error contributions

from the power correction parameters X_A and X_H in Eq.(3.4.13) and Eq.(3.5.17) respectively, we calculated the difference between the maximum and the minimum value of each one of our QCDF observables within the intervals for $\rho_{A,H}$ defined in Eq.(4.3.7, 4.3.8) and $0 < \phi_{A,H} < 2\pi$. To estimate the partial errors from the rest of the input parameters used in the determination of a given observable we fixed X_A and X_H to the common value $X_H = X_A = \ln m_B/\Lambda_h$ as performed in [61].

4.3.1 $R_{\pi\pi}$

We include the precision observable

$$\begin{aligned} R_{\pi\pi} &= \frac{\Gamma(B^- \to \pi^0\pi^-)}{d\Gamma(\bar{B} \to \pi^+ l^- \bar{\nu}_l)/dq^2|_{q^2=0}} \\ &\simeq 3\pi^2 f_\pi^2 |V_{ud}|^2 |\alpha_1^{\pi\pi} + \alpha_2^{\pi\pi}|^2, \end{aligned} \tag{4.3.9}$$

which offers several advantages from the calculational point of view, for instance the transition $B^- \to \pi^-\pi^0$ is, to a good degree of precision, a pure tree level process; in addition, $R_{\pi\pi}$ is free from the uncertainty associated with the CKM element $|V_{ub}|$. The topological amplitudes $\alpha_{1,2}^{\pi\pi}$ in Eq.(4.3.9) are available in the literature up to NNLO [70], [64], [67]. In this project we include the NNLO results as a re-scaling effect according to

$$\frac{\alpha_i^{\pi\pi}}{\alpha_i^{\mathrm{NNLO},\pi\pi}} = \frac{\alpha_i^{\mathrm{NLO},\pi\pi}(\mu_0)}{\alpha_{0,i}^{\mathrm{NLO},\pi\pi}}, \tag{4.3.10}$$

where $i = 1, 2$ and:

- $\alpha_{0,i}^{\mathrm{NLO},\pi\pi}$ is the NLO version of the amplitude $\alpha_i^{\pi\pi}$ evaluated at the central value of all the input parameters and kept constant during the fit.

- $\alpha_i^{\mathrm{NLO},\pi\pi}(\mu_0)$ is the NLO version of the amplitude $\alpha_i^{\pi\pi}$ with the renormalization scale fixed at $\mu_0 = m_b$ and the rest of the input parameters allowed to float when doing the statistical fit.

- $\alpha_{1,2}^{NNLO,\pi\pi}$ is the NNLO version of the amplitude $\alpha_i^{\pi\pi}$. To our knowledge the NNLO calculation for the amplitude $\alpha_i^{\pi\pi}$ has been derived at different stages during the last eleven years including new effects each time. To begin with the NNLO correction to the hard spectator scattering was introduced in [70].

Then in [64], the NNLO contributions to the vertices were also calculated and improved afterwards in [67] by taking into account the charm and bottom mass dependency arising from massive quark loop insertions into the gluon propagator.

Our interest in the NNLO determination arises because of the reduction in the renormalization scale dependency with respect to the NLO result, therefore during the statistical fit we treat the scaling coefficients $\alpha_{1,2}^{\mathrm{NNLO},\pi\pi}$ as nuisance parameters allowed to float within the limits established by the renormalization scale error only. As described at the beginning of this section we work under two possible scenarios depending on the values allowed for the power correction parameters $\rho_{H,A}$ and the first moment of the distribution amplitude associated with the B_d^0 meson λ_B, we also take into account two possible scaling factors $\alpha_{1,2}^{NNLO,\pi\pi}$. For the standard fit we considered [64]

$$\begin{aligned}\alpha_1^{\mathrm{NNLO},\pi\pi} &= 0.195^{+0.119+0.025+0.055}_{-0.066-0.025-0.055} - \left(0.101^{+0.017+0.021+0.055}_{-0.010-0.029-0.055}\right)i,\\ \alpha_2^{\mathrm{NNLO},\pi\pi} &= 1.013^{+0.017+0.008+0.014}_{-0.031-0.011-0.014} + \left(0.027^{+0.006+0.020+0.014}_{-0.010-0.013-0.014}\right)i,\end{aligned} \tag{4.3.11}$$

where only the second component of the error budget is due to higher order perturbative corrections (the first component estimates the uncertainty from hadronic input parameters and the third component the effect of the power corrections). To illustrate our treatment of the renormalization scale errors consider $\alpha_1^{NNLO,\pi\pi}$, taking into account that the renormalization scale dependency is the only component of the total error we are interested in, the real and the imaginary parts of $\alpha_1^{NNLO,\pi\pi}$ are allowed to vary within the intervals $[0.195-0.025, 0.195+0.025]$ and $[-0.101-0.029, -0.101+0.021]$ respectively.

Alternatively for the aggressive analysis we tested a second set of NNLO topological amplitudes $\alpha_{1,2}^{\mathrm{NNLO},\pi\pi}$ [67]

$$\begin{aligned}\alpha_1'^{\mathrm{NNLO},\pi\pi} &= 0.240^{+0.018+0.026}_{-0.010-0.023} - \left(0.077^{+0.021+0.005}_{-0.030-0.004}\right)i,\\ \alpha_2'^{\mathrm{NNLO},\pi\pi} &= 1.000^{+0.009+0.006}_{-0.012-0.007} + \left(0.011^{+0.019+0.002}_{-0.012-0.003}\right)i.\end{aligned} \tag{4.3.12}$$

where the first component of the uncertainty arises from the hard renormalization scale dependency μ and the second component from the hard

collinear-scale $\mu_{hc} = \sqrt{\Lambda_{QCD} m_b}$. In [67] and [71] μ is treated independently of $\mu_{hc} = \sqrt{\Lambda_{QCD} m_b}$; the first scale affects the vertex corrections whereas the latter only the hard scattering contributions. We became aware of the set of values in Eq.(4.3.12) during the late stages of our investigation. Considering the time required to implement these updated results we decided to keep our old set of numbers in Eq.(4.3.11) for the standard analysis and to include the updated versions in Eq.(4.3.12) only in the aggressive study. One of the most important differences between Eq.(4.3.11) and Eq.(4.3.12) is the result for the colour suppressed amplitude $\alpha_1^{\pi\pi}$. However, by comparing the central values for the standard and the aggressive estimations for the observables $R_{\pi\pi}$ and $S_{\pi\pi}$, defined in Eq.(4.3.9) and Eq.(4.3.17) respectively, and by looking at the renormalization scale effects, in Tab.4.1 and Tab.4.2, we can see that using an old set of numbers for $\alpha_{1,2}^{\pi\pi}$ does not have a significant impact on the final results.

To estimate the effect of μ on the error budget inside Eq.(4.3.12) we use the information for the real and imaginary parts of $\alpha_{1,2}^{\pi\pi}$ presented in Fig. 3 of [67]. Since the μ_h dependence is not displayed explicitly in [67] we include the results shown in Tab.2 of [71]. Notice that our μ partial errors determined from Fig. 3 in [67] are not that different in comparison with those reported in Tab.2 of [71].

Our theoretical estimation based on the inputs for the standard and the aggressive analyses are

$$R^{SM}_{\pi\pi;\ std.} = \Big(0.70 \pm 0.12\Big), \qquad R^{SM}_{\pi\pi;\ agr.} = \Big(0.67 \pm 0.08\Big). \tag{4.3.13}$$

and they agree with the experimental determination presented in [67]

$$R^{Exp}_{\pi\pi} \;=\; \Big(0.81 \pm 0.14\Big). \tag{4.3.14}$$

The regions allowed for new physics in the tree level Wilson coefficients are presented in Fig.4.1 and Fig.4.2 for the standard and the aggressive analyses, respectively. As expected, the new physics regions in the second set of plots are more constrained, the contributions of the different inputs to the total error are presented in Tab.4.1.

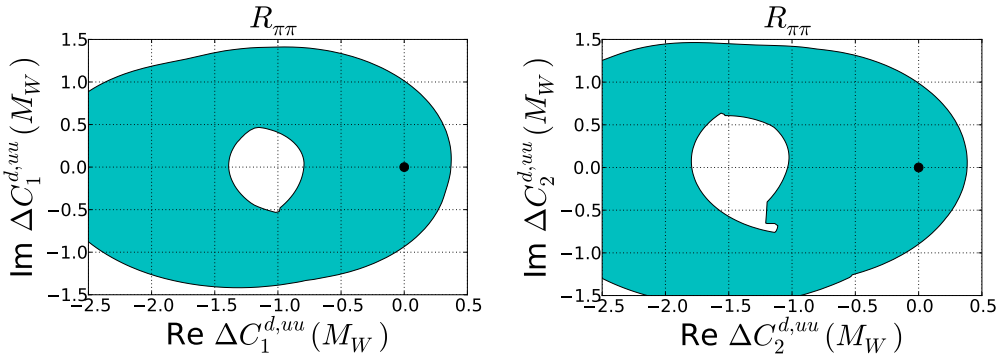

Figure 4.1: Regions for new physics, at 90% C. L., in the $\mathcal{R}e\ \Delta C_1^{d,uu}$ - $\mathcal{I}m\ \Delta C_1^{d,uu}$ (left) and $\mathcal{R}e\ \Delta C_2^{d,uu}$ - $\mathcal{I}m\ \Delta C_2^{d,uu}$ (right) planes allowed by the observable $R_{\pi\pi}$ in the standard analysis. The black point corresponds to the SM value.

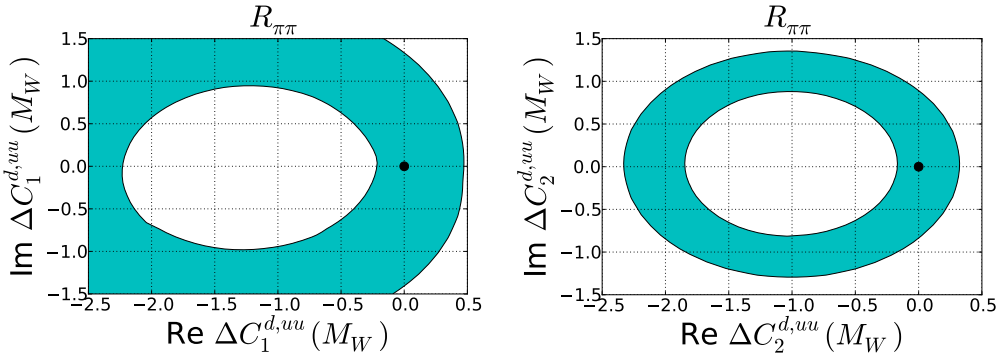

Figure 4.2: Regions for new physics, at 90% C. L., in the $\mathcal{R}e\ \Delta C_1^{d,uu}$ - $\mathcal{I}m\ \Delta C_1^{d,uu}$ (left) and $\mathcal{R}e\ \Delta C_2^{d,uu}$ - $\mathcal{I}m\ \Delta C_2^{d,uu}$ (right) planes allowed by the observable $R_{\pi\pi}$ in the aggressive analysis. The black point corresponds to the SM value.

Parameter	Standard analysis	Aggressive analysis
$\delta(\mu)$	5.26%	5.06%
$\delta(\Lambda_5)$	0.20%	0.19%
$\delta(m_s)$	0.21%	0.09%
$\delta(m_b)$	0.05%	0.03%
$\delta(\lvert V_{us}\rvert)$	0.02%	0.02%
$\delta(\lvert V_{cb}\rvert)$	$< 0.01\%$	$< 0.01\%$
$\delta(f_B)$	0.47%	0.20%
$\delta(f_\pi)$	0.39%	0.37%
$\delta(\alpha_{2\pi})$	2.86%	1.20%
$\delta(F_0^{B\to\pi})$	3.98%	1.69%
$\delta(\lambda_B)$	9.55%	1.16%
$\delta(X_H)^{max}$	13.09%	10.88%
$\left(\sum \delta\right)_1$	11.98%	5.61%
$\sum \delta$	17.74%	12.24%

Table 4.1: Error budget for the observable $R_{\pi\pi}$; $\left(\sum \delta\right)_1$ corresponds to the relative uncertainty excluding the contributions from power corrections; $\sum \delta$ is the relative uncertainty including the effect from power corrections of hard-spectator scattering $\delta(X_H)^{max}$.

4.3.2 $S_{\pi\pi}$ and $S_{\rho\pi}$

A very effective way to constrain possible new physics phases in the Wilson coefficients C_1, C_2 in addition to their magnitudes is by studying the mixing-induced $\mathcal{CP}$ asymmetries S_f (see Eq.(1.3.106)) for $B \to \pi\pi, \pi\rho$ transitions. The direct $\mathcal{CP}$ asymmetries, C_f , are suppressed by powers of α_s and/or Λ_{QCD}/m_b in QCD factorization and are difficult to predict quantitatively. We can calculate the indirect asymmetries in the $B \to \pi\pi, \pi\rho$ sectors at NLO in QCD factorization using the information provided in [61]. For the $B \to \pi\pi$ decays we get

$$S_{\pi\pi} = \frac{2\mathcal{I}m\Big(e^{-2i\beta}\frac{\bar{\mathcal{A}}_{\pi^+\pi^-}}{\mathcal{A}_{\pi^+\pi^-}}\Big)}{1+|\frac{\bar{\mathcal{A}}_{\pi^+\pi^-}}{\mathcal{A}_{\pi^+\pi^-}}|^2}, \tag{4.3.15}$$

where $\mathcal{A}_{\pi^+\pi^-}$ is the transition amplitude for the process $\bar{B}^0_d \to \pi^+\pi^-$ that can be written in terms of the corresponding topological amplitudes as

$$\begin{aligned}\mathcal{A}_{\pi^+\pi^-} = A_{\pi\pi}\Big(&\lambda_u\alpha_2^{\pi\pi} + \lambda_u\beta_2^{\pi\pi} + \sum_{p=u,c}\lambda_p\Big[\tilde{\alpha}_4^{p,\pi\pi} + \tilde{\alpha}_{4,EW}^{p,\pi\pi} \\ &+ \beta_3^{p,\pi\pi} - 1/2\beta_{3,EW}^{p,\pi\pi} + 2\beta_4^{p,\pi\pi} + 1/2\beta_{4,EW}^{p,\pi\pi}\Big]\Big).\end{aligned} \tag{4.3.16}$$

To introduce NNLO effects in $\alpha_2^{\pi\pi}$ we follow the procedure described in Section 4.3.1 for $R_{\pi\pi}$. In addition to the tree level contributions $\alpha_2^{\pi\pi}$, we have to include QCD and electroweak penguins given by $\tilde{\alpha_4}^{p,\pi\pi}$ and $\tilde{\alpha_4}_{EW}^{p,\pi\pi}$ respectively. Finally $\beta_4^{\pi\pi}$ accounts for QCD penguin annihilation and $\beta_{4,EW}^{\pi\pi}$ for electroweak penguin annihilation. The global normalization factor $A_{\pi\pi}$ can be found in Eq.(D.1.1). The explicit expressions for all the amplitudes can be constructed using Eq.(4.3.6) and the information provided in Appendix D.

Using the numerical inputs shown in Appendix A we obtain the following results for our standard and the aggressive analysis

$$S^{SM}_{\pi\pi;\ std.,\ agr.} = -0.53 \pm 0.41. \tag{4.3.17}$$

The contributions from each of the input parameters to the total error is displayed in Tab.4.2. Notice that the central values and the final error in both studies coincide even though the ranges for the parameters $\rho_{A,H}$ are different as indicated in

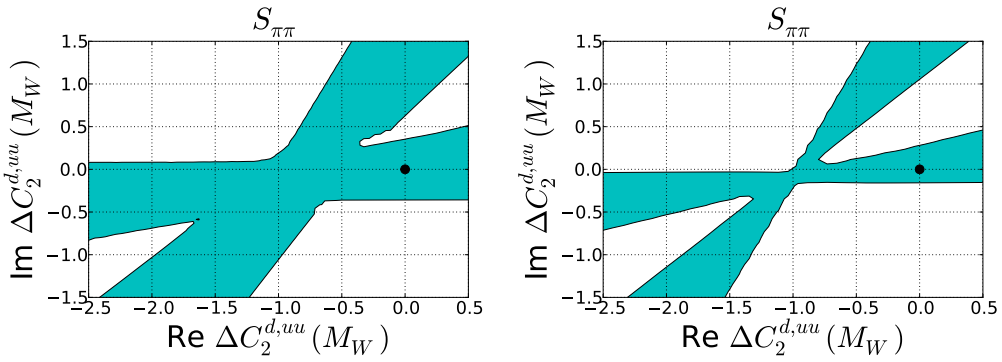

Figure 4.3: Regions for new physics, at 90% C. L, in the $\mathcal{R}e\ \Delta C_2^{d,uu}$ - $\mathcal{I}m\ \Delta C_2^{d,uu}$ plane allowed by the observable $S_{\pi\pi}$ in the standard (left) and the aggressive (right) analysis. The black point corresponds to the SM value.

Eq.(4.3.7) and Eq.(4.3.8). This can be explained by noting that $S_{\pi\pi}$ reaches its maximum and minimum value within $0 < \rho_{A,H} < 1$ which is a subset of $0 < \rho_{A,H} < 2$. The corresponding experimental value is [1]

$$S_{\pi\pi}^{Exp} = -0.66 \pm 0.06, \tag{4.3.18}$$

showing consistency with the SM estimations in Eq.(4.3.17).
The bounds on $\Delta C_1^{d,uu}(M_W)$ obtained from $S_{\pi\pi}$ are weaker than those obtained considering other observables, consequently $S_{\pi\pi}$ is useful for constraining $\Delta C_2^{d,uu}(M_W)$ only, the allowed new physics regions are shown in Fig.4.3. In spite of having the same numerical results for the standard and the aggressive analysis (see Eq.(4.3.17)), the statistical fit is sensitive to the differences in the input parameters. As a matter of fact the reduced interval for λ_B in the aggressive analysis shrinks the new physics regions for $\Delta C_2^{d,uu}(M_W)$ as shown on the right plot of Fig.4.3.

The indirect $\mathcal{CP}$ asymmetry for the decay $B \to \rho\pi$ is

$$S_{\rho\pi} = \frac{1}{2}\Big(S_{\rho^+\pi^-} + S_{\rho^-\pi^+}\Big), \tag{4.3.19}$$

with the partial contributions given by

$$S_{\pi^+\rho^-} = \frac{2\ \mathcal{I}m\Big(e^{-2i\beta}\frac{\bar{\mathcal{A}}_{\pi^+\rho^-}}{\mathcal{A}_{\pi^+\rho^-}}\Big)}{1 + |\frac{\bar{\mathcal{A}}_{\pi^+\rho^-}}{\mathcal{A}_{\pi^+\rho^-}}|^2}, \qquad S_{\pi^-\rho^+} = \frac{2\ \mathcal{I}m\Big(e^{-2i\beta}\frac{\bar{\mathcal{A}}_{\pi^-\rho^+}}{\mathcal{A}_{\pi^-\rho^+}}\Big)}{1 + |\frac{\bar{\mathcal{A}}_{\pi^-\rho^+}}{\mathcal{A}_{\pi^-\rho^+}}|^2}. \tag{4.3.20}$$

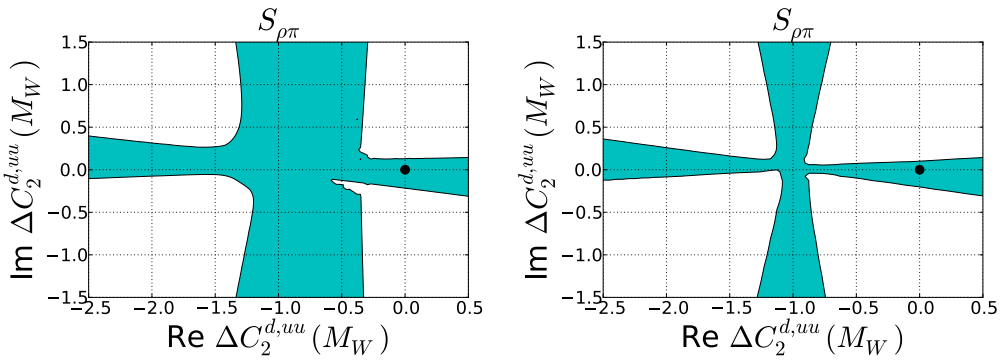

Figure 4.4: Regions for new physics, at 90% C. L., in the $\mathcal{R}e\ \Delta C_2^{d,uu}$ - $\mathcal{I}m\ \Delta C_2^{d,uu}$ plane allowed by the observable $S_{\rho\pi}$ in the standard (left) and the aggressive (right) analysis. The black point corresponds to the SM value.

The individual amplitudes $\mathcal{A}_{\pi^+\rho^-}$ and $\mathcal{A}_{\pi^-\rho^+}$ for the processes $\bar{B}_d^0 \to \pi^+\rho^-$ and $\bar{B}_d^0 \to \pi^-\rho^+$ respectively are

$$\begin{aligned}
\mathcal{A}_{\pi^+\rho^-} &= A_{\pi\rho}\Big(\lambda_u\alpha_2^{\pi\rho} + \sum_{p=u,c}\lambda_p\Big[\tilde{\alpha}_4^{p,\pi\rho} + \tilde{\alpha}_{4,EW}^{p,\pi\rho} \\
&\quad + \beta_3^{p,\pi\rho} + \beta_4^{p,\pi\rho} - \frac{1}{2}\beta_{3,EW}^{p,\pi\rho} - \frac{1}{2}\beta_{4,EW}^{p,\pi\rho}\Big]\Big) \\
&\quad + A_{\rho\pi}\Big(\lambda_u\beta_1^{\rho\pi} + \sum_{p=u,c}\lambda_p\Big[\beta_4^{p,\rho\pi} + \beta_{4,EW}^{p,\rho\pi}\Big]\Big), \\
\mathcal{A}_{\pi^-\rho^+} &= A_{\rho\pi}\Big(\lambda_u\alpha_2^{\rho\pi} + \sum_{p=u,c}\lambda_p\Big[\tilde{\alpha}_4^{p,\rho\pi} + \tilde{\alpha}_{4,EW}^{p,\rho\pi} + \beta_3^{p,\rho\pi} \\
&\quad + \beta_4^{p,\rho\pi} - \frac{1}{2}\beta_{3,EW}^{p,\rho\pi} - \frac{1}{2}\beta_{4,EW}^{p,\rho\pi}\Big]\Big) \\
&\quad + A_{\pi\rho}\Big(\lambda_u\beta_1^{\pi\rho} + \sum_{p=u,c}\lambda_p\Big[\beta_4^{p,\pi\rho} + \beta_{4,EW}^{p,\pi\rho}\Big]\Big).
\end{aligned} \tag{4.3.21}$$

As for the case of $S_{\pi\pi}$, $\alpha_2^{\rho\pi,\pi\rho}$ are tree level amplitudes while $\alpha_4^{\rho\pi,\pi\rho}$ and $\tilde{\alpha}_4^{\rho\pi,\pi\rho}$ are QCD penguin and electroweak penguin amplitudes respectively. The coefficients $\beta_1^{\rho\pi,\pi\rho}$ correspond to current-current annihilation, $\beta_{3,4}^{\pi\rho,\rho\pi}$ to QCD penguin annihilation and $\beta_{4,EW}^{\rho\pi,\pi\rho}$ to electroweak penguin annihilation. The full expressions for the amplitudes can be obtained using Eq.(4.3.6) and the information given in Appendix D.

Our SM determinations are

$$S_{\rho\pi,std.}^{SM} = \Big(-2.8 \pm 8.1\Big)\times 10^{-2}, \qquad S_{\rho\pi,agr.}^{SM} = \Big(-2.8 \pm 7.1\Big)\times 10^{-2}, \tag{4.3.22}$$

and they are compatible with the current experimental average [1]

$$S_{\rho\pi}^{Exp} = \Big(6.0 \pm 7.0\Big) \times 10^{-2}. \tag{4.3.23}$$

The relative errors from each of the inputs for $S_{\rho\pi}$ are presented in Tab.4.3, where it can be seen that this observable is highly sensitive to the CKM inputs γ and $|V_{ub}/V_{cb}|$. The allowed new physics regions for $\Delta C_2^{d,uu}(M_W)$ are displayed in Fig.4.4. In spite of having an uncertainty above 100% the observable $S_{\rho\pi}$ rules out large sections in the complex plane of $\Delta C_2^{d,uu}(M_W)$ and consequently deserves to be included in the analysis of $C_2^{d,uu}$. In contrast we find weak bounds for $\Delta C_1^{d,uu}(M_W)$ that are not worthy to be taken into account.

4.3.3 $R_{\rho\rho}$

Extra constraints for the tree level Wilson coefficients of the transition $b \to u\bar{u}d$ can be obtained with the ratio of hadronic decays

$$R_{\rho\rho} = \mathcal{B}_r(B^- \to \rho_L^- \rho_L^0)/\mathcal{B}_r(\bar{B}_d^0 \to \rho_L^+ \rho_L^-) = \frac{|\mathcal{A}_{\rho^-\rho^0}|^2}{|\mathcal{A}_{\rho^+\rho-}|^2}. \tag{4.3.24}$$

Where $\mathcal{A}_{\rho^-\rho^0}$ and $\mathcal{A}_{\rho^+\rho-}$ are the amplitudes for the processes $B^- \to \rho_L^-\rho_L^0$ and $\bar{B}_d^0 \to \rho_L^+\rho_L^-$ respectively, given by [72, 73]

$$\begin{aligned}
\mathcal{A}_{\rho^-\rho^0} &= \frac{A_{\rho\rho}}{\sqrt{2}}\Big[\lambda_u\Big(\alpha_1^{\rho\rho} + \alpha_2^{\rho\rho}\Big) + \frac{3}{2}\sum_{p=u,c}\lambda_p\Big(\alpha_7^{p,\rho\rho} + \alpha_9^{p,\rho\rho} + \alpha_{10}^{p,\rho\rho}\Big)\Big], \\
\mathcal{A}_{\rho^+\rho^-} &= A_{\rho\rho}\Big[\lambda_u\Big(\alpha_2^{\rho\rho} + \beta_2^{\rho\rho}\Big) + \sum_{p=u,c}\lambda_p\Big(\alpha_4^{p,\rho\rho} + \alpha_{10}^{p,\rho\rho} \\
&\quad + \beta_3^{p,\rho\rho} + 2\beta_4^{p,\rho\rho} - \frac{1}{2}\beta_{3,EW}^{p,\rho\rho} + \frac{1}{2}\beta_{4,EW}^{p,\rho\rho}\Big)\Big].
\end{aligned} \tag{4.3.25}$$

In Eq.(4.3.25) we can identify tree level amplitudes $\alpha_{1,2}^{\rho\rho}$, QCD penguins $\alpha_4^{\rho\rho}$ and electroweak penguins $\alpha_{7,9,10}^{\rho\rho}$. In addition we also have QCD penguin annihilation $\beta_{3,4}^{\rho\rho}$ and electroweak penguin annihilation $\beta_{3,4,EW}^{\rho\rho}$. The full expressions for all the topological amplitudes can be obtained using the information provided in Eq.(4.3.6) and Appendix D.

To include NNLO effects in the amplitudes $\alpha_{1,2}^{\rho\rho}$ we use the formula

$$\frac{\alpha_i^{\rho\rho}}{\alpha_i^{\mathrm{NNLO},\rho_L\rho_L}} = \frac{\alpha_i^{\mathrm{NLO},\rho_L\rho_L}(\mu_0)}{\alpha_{0,i}^{\mathrm{NLO},\rho\rho}}, \tag{4.3.26}$$

Parameter	Standard analysis	Aggressive analysis
$\delta(\mu)$	3.87%	4.06%
$\delta(\Lambda_5)$	1.10%	1.08%
$\delta(m_t(m_t))$	0.01%	0.01%
$\delta(m_c)$	0.06%	0.07%
$\delta(m_s)$	1.45%	1.45%
$\delta(m_b)$	0.58%	0.58%
$\delta(\lvert V_{us}\rvert)$	0.47%	0.47%
$\delta(\lvert V_{cb}\rvert)$	0.01%	0.01%
$\delta(\lvert V_{ub}/V_{cb}\rvert)$	10.22%	10.13%
$\delta(\gamma)$	44.67%	44.11%
$\delta(f_B)$	0.24%	0.23%
$\delta(f_\pi)$	0.02%	0.02%
$\delta(\alpha_{2\pi})$	0.12%	0.12%
$\delta(F_0^{B\to\pi})$	1.97%	1.97%
$\delta(\lambda_B)_\pm$	1.55%	0.44%
$\delta(X_H)^{max}$	2.67%	1.33%
$\delta(X_A)^{max}$	62.96%	62.79%
$\left(\sum \delta\right)_1$	46.10%	45.53%
$\sum \delta$	78.08%	77.58%

Table 4.2: Error budget for the observable $S_{\pi\pi}$; $\left(\sum \delta\right)_1$ corresponds to the relative uncertainty excluding the contributions from the power corrections; $\sum \delta$ is the relative uncertainty including the effect of power corrections from hard spectator scattering $\delta(X_H)^{max}$ and annihilation topologies $\delta(X_A)^{max}$.

Parameter	Standard analysis	Aggressive analysis
$\delta(\mu)$	30.69%	
$\delta(\Lambda_5)$	5.01%	
$\delta(m_t(m_t))$	0.01%	
$\delta(m_c)$	0.08%	
$\delta(m_s)$	15.18%	
$\delta(m_b)$	4.41%	
$\delta(\lvert V_{us}\rvert)$	6.52%	
$\delta(\lvert V_{cb}\rvert)$	0.08%	
$\delta(\lvert V_{ub}/V_{cb}\rvert)$	140.60%	
$\delta(\gamma)$	189.59%	
$\delta(f_B)$	1.25%	
$\delta(f_\pi)$	0.09%	
$\delta(a_{2\pi})$	9.59%	
$\delta(a_{2\rho})$	4.75%	
$\delta(a_{2\rho}^\perp)$	0.07%	
$\delta(F_0^{B\to\pi})$	8.83%	
$\delta(A_0^{B\to\rho})$	17.62%	
$\delta(\lambda_B)$	11.00%	3.15%
$\delta(f_\rho^\perp)$	0.15%	
$\delta(f_\rho)$	2.60%	
$\delta(X_H)^{max}$	23.21%	12.75%
$\delta(X_A)^{max}$	153.73%	69.95%
$\left(\sum\delta\right)_1$	240.01%	239.78%
$\sum\delta$	285.97%	250.10%

Table 4.3: Error budget for the observable $S_{\rho\pi}$; $\left(\sum\delta\right)_1$ corresponds to the relative uncertainty excluding the contributions from the power corrections; $\sum\delta$ is the relative uncertainty including the effect of power corrections from hard spectator scattering $\delta(X_H)^{max}$ and annihilation topologies $\delta(X_A)^{max}$. For the aggressive analysis we only quote the results when the numerics are different with respect to the standard analysis.

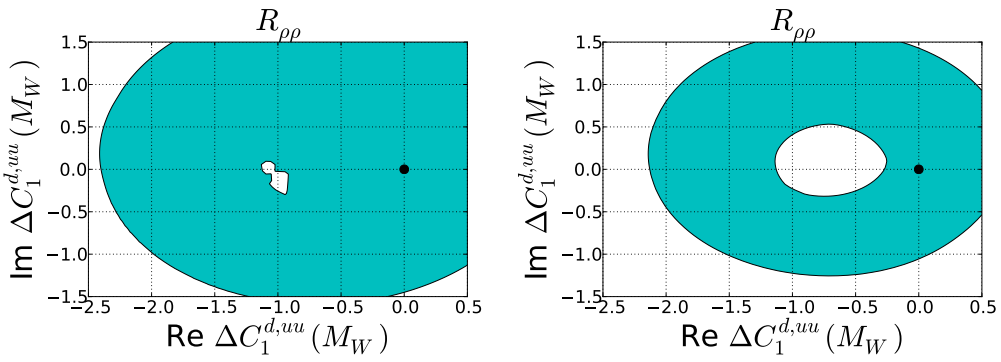

Figure 4.5: Regions for new physics, at 90% C. L., in the $\mathcal{R}e\ \Delta C_1^{d,uu}$ - $\mathcal{I}m\ \Delta C_1^{d,uu}$ plane allowed by the observable $R_{\rho\rho}$ in the standard (left) and the aggressive (right) analysis. The black point corresponds to the SM value.

with $i = 1, 2$, and follow a treatment analogous to the one described in Section 4.3.1 for $\alpha_{1,2}^{\pi\pi}$.

For the NNLO components in (4.3.26) we use the values in [64]

$$\alpha_1^{\text{NNLO},\rho_L\rho_L} = 0.177^{+0.110+0.025+0.055}_{-0.063-0.029-0.055} - \left(0.097^{+0.021+0.021+0.055}_{-0.012-0.029-0.055}\right)i,$$
$$\alpha_2^{\text{NNLO},\rho_L\rho_L} = 1.017^{+0.017+0.010+0.014}_{-0.029-0.011-0.014} + \left(0.025^{+0.007+0.019+0.014}_{-0.013-0.013-0.014}\right)i. \qquad (4.3.27)$$

During the fit these topological amplitudes were allowed to float within the limits defined by the second entry of the error budget providing the renormalization scale uncertainty.

Our theoretical estimation for this observable is

$$R^{SM}_{\rho\rho;\ std.} = \Big(67.6 \pm 29.2\Big)\times 10^{-2}, \qquad R^{SM}_{\rho\rho;\ agr.} = \Big(67.6 \pm 13.6\Big)\times 10^{-2}, \quad (4.3.28)$$

on the experimental side we use

$$R^{Exp}_{\rho\rho} \quad = \quad \Big(89.0 \pm 14.0\Big)\times 10^{-2}. \qquad (4.3.29)$$

The partial contributions to the error budget are presented in Tab.4.4 and the constraints for $\Delta C_1^{d,uu}(M_W)$ in Fig.4.5. We do not show the regions for $\Delta C_2^{d,uu}(M_W)$ because they lead to weak bounds.

Parameter	Standard analysis	Aggressive analysis
$\delta(\mu)$	2.99%	
$\delta(\Lambda_5)$	0.21%	
$\delta(m_t(m_t))$	$7.77 \cdot 10^{-5}$%	
$\delta(m_c)$	0.13%	
$\delta(m_b)$	0.23%	
$\delta(V_{us})$	$2.0 \cdot 10^{-3}$%	
$\delta(V_{cb})$	$3.77 \cdot 10^{-4}$%	
$\delta(V_{ub}/V_{cb})$	0.05%	
$\delta(\gamma)$	0.38%	
$\delta(f_B)$	0.53%	
$\delta(a_{2\rho})$	2.38%	
$\delta(A_0^{B\to\rho})$	4.04%	
$\delta(\lambda_B)$	13.15%	3.69%
$\delta(f_\rho)$	0.56%	
$\delta(X_H)^{max}$	27.01%	14.77%
$\delta(X_A)^{max}$	30.54%	11.75%
$\left(\sum \delta\right)_1$	14.31%	6.74%
$\sum \delta$	43.21%	20.05%

Table 4.4: Error budget for the observable $R_{\rho\rho}$; $\left(\sum \delta\right)_1$ corresponds to the overall uncertainty excluding the contributions from the power corrections; $\sum \delta$ is the relative uncertainty including the effect of power corrections from hard spectator scattering $\delta(X_H)^{max}$ and annihilation topologies $\delta(X_A)^{max}$. For the aggressive analysis we only quote the results when the numerics are different with respect to the standard analysis.

4.4 Constraints from $b \to c\bar{u}d$ transitions

4.4.1 $\bar{B}_d^0 \to D^{*+}\pi^-$

Our first bounds for possible new physics effects $\Delta C_{1,2}^{cu}(M_W)$, affecting the quark level transition $b \to c\bar{u}d$ at tree level, will be derived using the ratio between the non-leptonic decay $\bar{B}_d^0 \to D^{(*)+}\pi^-$ and the differential semi-leptonic process $\bar{B}_d^0 \to D^{(*)+}l^-\bar{\nu}_l$ evaluated at $q^2 = m_\pi^2$ for $l = e, \mu$

$$R_{D^*\pi} = \frac{\Gamma(\bar{B}^0 \to D^{*+}\pi^-)}{d\Gamma(\bar{B}^0 \to D^{*+}l^-\bar{\nu}_l)/dq^2|_{q^2=m_\pi^2}} \simeq 6\pi^2 f_\pi^2 |V_{ud}|^2 |\alpha_2^{D^*\pi}|^2. \quad (4.4.30)$$

This observable was proposed by Bjorken to test the factorization hypothesis [74], it is free from the uncertainties associated with the form factor $F^{B\to D}$ and offers the possibility of comparing directly the coefficient $\alpha_2^{D^*\pi}$ calculated using QCDF against experimental observations

At NLO the topological amplitude $\alpha_2^{D^*\pi}$ [57] is given by

$$\alpha_2^{D^*\pi} = C_2^{NP}(\mu_b) + \frac{C_1^{NP}(\mu_b)}{3} + \frac{\alpha_s(\mu_b)}{4\pi}\frac{C_F}{N_c}C_1(\mu_b)\Big[-B - 6\ln\frac{\mu^2}{m_b^2} + \int_0^1 du F(u,-z)\Phi_\pi(u)\Big], \quad (4.4.31)$$

where the term B inside the square bracket cancels the renormalization scheme dependence of the Wilson coefficients C_1 and C_2, which in naive dimensional regularization requires $B = 11$. The kernel $F(u,z)$ includes QCD vertex corrections arising in the $b \to c\bar{u}d$ transition and has to be evaluated at $z = m_c(m_b)/m_b$ before being convoluted with the light-cone distribution Φ_π associated with the π^- meson in the final state. The NNLO calculation of the amplitude $\alpha_2^{D^*\pi}$ in [75], showed a marginal correction of 2% with respect to the NLO result, consequently for the purpose of this project the NLO calculation is enough.

To implement Eq.(4.4.31) we follow the conventions established in Section 4.1 and Section 4.3, hence we evaluate all the scale dependent quantities at $\mu_b \sim m_b$ while the Wilson coefficient in front of the square bracket is estimated at leading order in α_s assuming no new physics contributions.

Using the asymptotic form of Φ_π and the expression for $F(u,z)$ provided in [57] we find

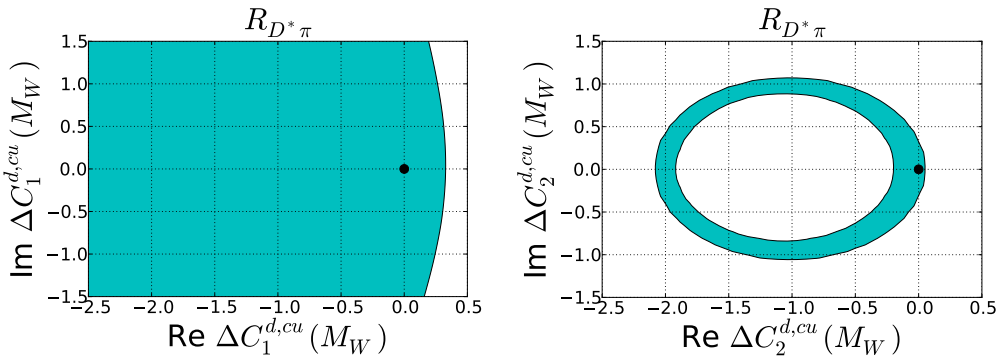

Figure 4.6: Regions for new physics, at 90% C. L., in the $\mathcal{R}e\ \Delta C_1^{d,cu}$ - $\mathcal{I}m\ \Delta C_1^{d,cu}$ and the $\mathcal{R}e\ \Delta C_2^{d,cu}$ - $\mathcal{I}m\ \Delta C_2^{d,cu}$ planes allowed by the observable $R_{D^*\pi}$ in the standard analysis. The black point corresponds to the SM value.

$$R_{D^*\pi}^{SM} = \Big(1.076 \pm 0.046\Big)\text{GeV}^2, \tag{4.4.32}$$

corresponding to $z = 0.233$, while the experimental result available in the literature is [76]

$$R_{D^*\pi} = \Big(0.96 \pm 0.08\Big)\text{GeV}^2. \tag{4.4.33}$$

Hence there is a good agreement between theory and experiment. Our statistical fit provides the 90 % confidence level regions allowed for $\Delta C_1^{cu}(M_W)$ and $\Delta C_2^{cu}(M_W)$ displayed in Fig.4.6, the individual contributions to the total error are presented in Tab.4.5.

4.4.2 S_{D^*h}

We include the indirect CP asymmetry associated to the colour suppressed decay $B^0 \to D^{(*)}h^0$ dominated by the transition $b \to c\bar{u}d$, where $h^0 = \pi^0, \eta, \omega$ giving

$$S_{D^*h^0} = \frac{2\ \mathcal{I}m\Big(e^{-2i\beta}\frac{\mathcal{A}_{D^*h^0}}{\bar{\mathcal{A}}_{D^*h^0}}\Big)}{1 + \Big|\frac{\mathcal{A}_{D^*h^0}}{\bar{\mathcal{A}}_{D^*h^0}}\Big|^2}. \tag{4.4.34}$$

There is no theoretical estimation from QCD factorization for the amplitudes required by Eq.(4.4.34), we then use naive factorization to write [2]

Parameter	Standard analysis
$\delta(\mu)$	4.24%
$\delta(\Lambda_5)$	0.22%
$\delta(f_\pi)$	0.35%
$\delta(\lvert V_{ub}/V_{cb}\rvert)$	$1.36 \cdot 10^{-4}$%
$\delta(\lvert V_{cb}\rvert)$	$6.56 \cdot 10^{-5}$%
$\delta(\lvert V_{us}\rvert)$	0.02%
$\delta(z)$	$2.00 \cdot 10^{-3}$%
$\delta(m_b)$	0.03%
$\sum \delta$	4.26%

Table 4.5: Error budget for the observable $R_{D^*\pi}$

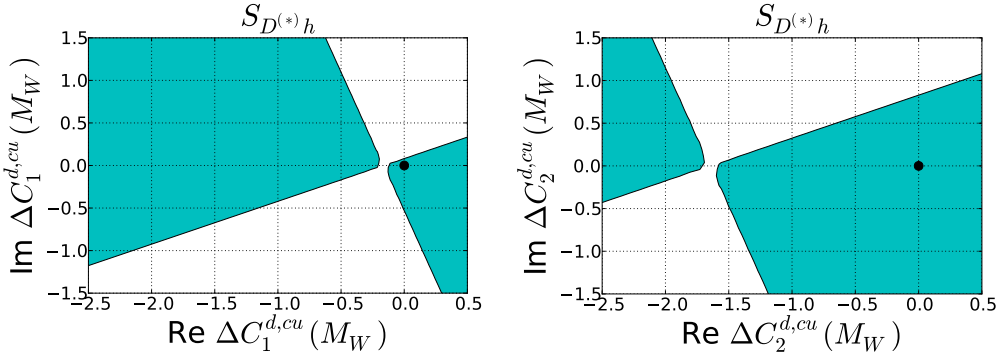

Figure 4.7: Regions for new physics, at 90% C. L., in the $\mathcal{R}e\ \Delta C_1^{d,cu}$ - $\mathcal{I}m\ \Delta C_1^{d,cu}$ (left) and $\mathcal{R}e\ \Delta C_2^{d,cu}$ - $\mathcal{I}m\ \Delta C_2^{d,cu}$ (right) planes allowed by the observable S_{D^*h} in the standard analysis. The black point corresponds to the SM value.

$$\frac{\mathcal{A}_{D^*h^0}}{\bar{\mathcal{A}}_{D^*h^0}} = \frac{C_1^{NP} + \frac{C_2^{NP}}{3}}{(C_1^{NP})^* + \frac{(C_2^{NP})^*}{3}}. \tag{4.4.35}$$

The experimental result delivered by BABAR is

$$S_{D^*h} = -0.56 \pm 0.23. \tag{4.4.36}$$

Under the approximations made, the theoretical central value for our observable is $S_{D^*h} = \sin(2\beta) = -0.69$, with an uncertainty of ± 0.06 based only on the CKM inputs V_{us}, V_{cb}, γ and V_{ub}/V_{cb}. Using this error in the fit can lead to an underestimation of the uncertainty, leading us to follow a more conservative approach and consider a theoretical error equal to the experimental one [2]. This can be achieved by fitting this observable using the experimental result in Eq.(4.4.36) with the inflated error $\sqrt{2} \times 0.23$.

We include the Wilson coefficients C_1 and C_2 at NLO in Eq.(4.4.34) to obtain the contours shown in Fig.4.7, where the red regions correspond to the space allowed for new physics at 90% C. L. .

4.5 Observables constraining $b \to c\bar{c}d$ transitions

4.5.1 M_{12}^d

The observable (see Section 1.4.1)

$$S_{B_d^0 \to J/\Psi K_{S,L}} = \frac{2\,\mathcal{I}m(\lambda_{J/\Psi K_{S,L}})}{1 + |\lambda_{J/\Psi K_{S,L}}|^2} = \sin(2\beta_d), \tag{4.5.37}$$

with

$$\lambda_{J/\Psi K_{S,L}} = \frac{q}{p}\frac{\bar{\mathcal{A}}_{B_d^0 \to J/\Psi K_{S,L}}}{\mathcal{A}_{B_d^0 \to J/\Psi K_{S,L}}}, \tag{4.5.38}$$

and

$$\frac{q}{p} = \frac{M_{12}^d}{|M_{12}^d|}, \tag{4.5.39}$$

allows us to constrain new physics at tree level in two different ways. Firstly by modifying the $|\Delta B| = 2$ effective Hamiltonian in Eq. (2.4.87) used in the determination of M_{12}^d and secondly by introducing new weak phases in the amplitude $\mathcal{A}_{B_d^0 \to J/\Psi K_{S,L}}$ leading to modifications on the ratio $\frac{\bar{\mathcal{A}}_{B_d^0 \to J/\Psi K_{S,L}}}{\mathcal{A}_{B_d^0 \to J/\Psi K_{S,L}}}$ with respect to its SM value.

Let us consider first the corrections on the $|\Delta B| = 2$ effective Hamiltonian, this will allow us to constrain new physics on the decay channel $b \to c\bar{c}d$, the second possibility will be explored later in Section 4.6.2. According to Eq.(2.4.86)

$$M_{12}^d = \frac{\langle B_d^0 | \hat{\mathcal{H}}_d^{|\Delta B|=2} | \bar{B}_d^0 \rangle}{2 M_{B_d^0}}, \tag{4.5.40}$$

in addition to the main contribution to $\hat{\mathcal{H}}_d^{|\Delta B|=2}$ given in terms of the $|\Delta B| = 2$ operator in Eq.(2.4.88) we can include double insertions of the $|\Delta B| = 1$ Hamiltonian [77]

$$\begin{aligned} \hat{\mathcal{H}}_{eff}^{|\Delta B|=1} &= \frac{4G_F}{\sqrt{2}} \Big[V_{cb}^* V_{cd} \Big(\bar{\hat{b}}_L \gamma_\mu \hat{c}_L\Big)\Big(\bar{\hat{c}}_L \gamma^\mu \hat{d}_L\Big) C_2^{cc} + V_{cb}^* V_{ud} \Big(\bar{\hat{b}} \gamma_\mu \hat{c}_L\Big)\Big(\bar{\hat{u}} \gamma^\mu \hat{d}_L\Big) C_2^{cu} \\ &\quad + V_{ub}^* V_{cd} \Big(\bar{\hat{b}}_L \gamma_\mu u_L\Big)\Big(\bar{\hat{c}}_L \gamma^\mu \hat{d}_L\Big) C_2^{uc} + V_{ub}^* V_{ud} \Big(\bar{\hat{b}}_L \gamma_\mu \hat{u}_L\Big)\Big(\bar{\hat{u}}_L \gamma^\mu \hat{d}_L\Big) C_2^{uu} \Big], \end{aligned} \tag{4.5.41}$$

giving

$$\hat{T}^{|\Delta B|=2} = -\frac{i}{2} \int d^4x \hat{T}\Big[\hat{\mathcal{H}}_{eff}^{|\Delta B|=1}(x) \hat{\mathcal{H}}_{eff}^{|\Delta B|=1}(0) \Big]. \tag{4.5.42}$$

The double insertions in Eq.(4.5.42) lead to the following set of operators

$$\begin{aligned} \hat{T}_1 &= -\frac{i}{2} \int d^4x \hat{T}\Big[\Big(\bar{\hat{b}}_L \gamma_\mu \hat{c}_L\Big)(x)\Big(\bar{\hat{c}}_L \gamma^\mu \hat{d}_L\Big)(x)\Big(\bar{\hat{b}}_L \gamma^\nu \hat{c}_L\Big)(0)\Big(\bar{\hat{c}}_L \gamma_\nu \hat{d}_L\Big)(0)\Big] \\ \hat{T}_2 &= -\frac{i}{2} \int d^4x \hat{T}\Big[\Big(\bar{\hat{b}}_L \gamma_\mu \hat{c}_L\Big)(x)\Big(\bar{\hat{u}}_L \gamma^\mu \hat{d}_L\Big)(x)\Big(\bar{\hat{b}}_L \gamma^\nu \hat{u}_L\Big)(0)\Big(\bar{\hat{c}}_L \gamma_\nu \hat{d}_L\Big)(0)\Big] \\ \hat{T}_3 &= -\frac{i}{2} \int d^4x \hat{T}\Big[\Big(\bar{\hat{b}}_L \gamma_\mu \hat{u}_L\Big)(x)\Big(\bar{\hat{u}}_L \gamma^\mu \hat{d}_L\Big)(x)\Big(\bar{\hat{b}}_L \gamma^\nu \hat{u}_L\Big)(0)\Big(\bar{\hat{u}}_L \gamma_\nu \hat{d}_L\Big)(0)\Big]. \end{aligned} \tag{4.5.43}$$

The set $\hat{T}_{1,2,3}$ in Eq.(4.5.43) mix with the following local $|\Delta B| = 2$ dimension 8 operators

$$\begin{aligned} \hat{\hat{Q}}_1' &= \Box\Big(\bar{\hat{b}}_L \gamma_\mu \hat{d}_L\Big)\Big(\bar{\hat{b}} \gamma^\mu \hat{d}_L\Big) \\ \hat{\hat{Q}}_2' &= \partial^\mu \partial^\nu \Big(\bar{\hat{b}}_L \gamma_\mu \hat{d}_L\Big)\Big(\bar{\hat{b}} \gamma^\mu \hat{d}_L\Big) \\ \hat{\hat{Q}}_3' &= m_c^2 \Big(\bar{\hat{b}}_L \gamma_\mu \hat{d}_L\Big)\Big(\bar{\hat{b}} \gamma^\mu \hat{d}_L\Big). \end{aligned} \tag{4.5.44}$$

If we arrange the operators in Eq.(4.5.43) and Eq.(4.5.44) into the vector $\vec{\hat{O}} = (\hat{Q}'_1, \hat{Q}'_2, \hat{Q}'_3, \hat{T}_1, \hat{T}_2, \hat{T}_3)^T$ then the corresponding vector of Wilson coefficients is $\vec{C} = (C'_1, C'_2, C'_3, C'_4, C'_5, C'_6)$ and the operator mixing is determined by the anomalous dimension matrix

$$\hat{\gamma} = \frac{1}{48\pi^2} \begin{pmatrix} 0 & 0 & 0 & 0 & 0 & 0 \\ 0 & 0 & 0 & 0 & 0 & 0 \\ 0 & 0 & 0 & 0 & 0 & 0 \\ 1 & 2 & 6 & 0 & 0 & 0 \\ 1 & 2 & 3 & 0 & 0 & 0 \\ 1 & 2 & 0 & 0 & 0 & 0 \end{pmatrix}. \tag{4.5.45}$$

The renormalization scale running of the elements in $\vec{C}$ can be calculated through the renormalization group equations

$$\Big(\mu\frac{\partial}{\partial\mu} - \gamma^T\Big)\vec{C} \;\; = \;\; 0. \tag{4.5.46}$$

The initial conditions are determined from matching at the scale $\mu \sim m_t \sim M_W$ and are given by

$$\begin{aligned} C'_1(M_W, x_t) &= -\frac{\lambda_t^2}{96\pi^2}C_{12}(x_t), \qquad & C'_2(M_W, x_t) &= -\frac{\lambda_t^2}{48\pi^2}C'_{12}(x_t), \\ C'_3(M_W, x_t) &= \frac{1}{32\pi^2}\Big(2\lambda_c\lambda_t C_3(x_t) + \lambda_c^2\Big), \qquad & C'_4(M_W) &= \lambda_c^2\Big(C_2^{d,cc}(M_W)\Big)^2, \\ C'_5(M_W) &= 2\lambda_c\lambda_u C_2^{d,cu}(M_W)C_2^{d,uc}(M_W), \qquad & C'_6(M_W) &= \lambda_u^2\Big(C_2^{d,uu}(M_W)\Big)^2, \end{aligned} \tag{4.5.47}$$

where

$$C_3(x_t) \;\; = \;\; \ln\, x_t - \frac{3x_t}{4(1-x_t)} - \frac{3x_t^2\,\ln\, x_t}{4(1-x_t)^2}. \tag{4.5.48}$$

We are interested in phases correcting the leading contribution provided by the CKM combination $V_{tb}V_{td}^*$ in Eq.(2.4.88). It is found [78] that the first corrections arise from weak phases appearing in terms proportional to $\left(\frac{m_c}{M_W}\right)^2$, therefore in what follows the mass of the charm quark is not taken to zero and we evolve the renormalization scale down to $\mu \sim m_c$ using Eq.(4.5.46).

According to [77] the contribution from the functions $C_{12}(x_t)$ and $C'_2(M_W, x_t)$ can be neglected after solving Eq.(4.5.46) since they are small in comparison with the

logarithms $\ln\left[\frac{\mu^2}{M_W^2}\right]$ arising in the solution of Eq.(4.5.46), with $\mu \sim m_c$, consequently their explicit expressions are not required. The Wilson coefficients in Eq.(4.5.47) are, after the introduction of new physics contributions,

$$\begin{aligned} C_2^{d,cc}(M_W) &= 1 + \Delta C_2^{d,cc}(M_W), \qquad C_2^{d,cu}(M_W) = 1 + \Delta C_2^{d,cu}(M_W), \\ C_2^{d,uc}(M_W) &= 1 + \Delta C_2^{d,uc}(M_W), \qquad C_2^{d,uu}(M_W) = 1 + \Delta C_2^{d,uu}(M_W). \end{aligned} \tag{4.5.49}$$

Notice that in Eq.(4.5.49) we can introduce independent new physics contributions in the different channels $b \to c\bar{c}d$, $b \to c\bar{u}d$, $b \to u\bar{c}d$ and $b \to u\bar{u}d$ through $\Delta C_2^{d,cc}$, $\Delta C_2^{d,cu}$, $\Delta C_2^{d,uc}$ and $\Delta C_2^{d,uu}$ respectively. In this section we are interested in the bounds on $\Delta C_2^{d,cc}$ only; the observables in Sections 4.3 and 4.4 give stronger constraints over the other channels.

We want to evolve the Wilson coefficients down to the scale $\mu \sim m_c$, at this scale we have to consider the following operator matching $\hat{Q}'_i \to \hat{P}_i$ for $i = 0, 1, 2, 3$ with

$$\begin{aligned} \hat{P}_0 &= \left(\bar{\hat{h}}^{(+)}_{v,L}\gamma_\mu \hat{d}_L\right)\left(\bar{\hat{h}}^{(-)}_{v,L}\gamma^\mu \hat{d}_L\right) \\ \hat{P}_1 &= m_b^2\left(\bar{\hat{h}}^{(+)}_{v,L}\gamma_\mu \hat{d}_L\right)\left(\bar{\hat{h}}^{(-)}_{v,L}\gamma^\mu \hat{d}_L\right) \\ \hat{P}_2 &= m_b^2\left(\bar{\hat{h}}^{(+)}_{v,R}\hat{d}_L\right)\left(\bar{\hat{h}}^{(-)}_{v,R}\hat{d}_L\right) \\ \hat{P}_3 &= m_c^2\left(\bar{\hat{h}}^{(+)}_{v,R}\gamma_\mu \hat{d}_L\right)\left(\bar{\hat{h}}^{(-)}_{v,L}\gamma^\mu \hat{d}_L\right), \end{aligned} \tag{4.5.50}$$

where the heavy quark limit was used in order to write $i\partial_\mu b \to (m_b v_\mu + i\partial_\mu)h_v$, and $h_v^{(+/-)}$ denotes the static b quark/antiquark field moving with velocity v.

The full solution of the renormalization group equations for the Wilson coefficients in Eq.(4.5.46) is

$$\begin{aligned} C'_1(\mu) &= \frac{1}{48}\ln\left[\frac{\mu^2}{M_W^2}\right]\left\{\frac{\lambda_c^2}{2}\left(C_2^{d,cc}\right)^2 - \lambda_c^2 C_2^{d,cu}C_2^{d,uc} - \lambda_c\lambda_t C_2^{d,cu}C_2^{d,uc}\right. \\ &\quad \left. + \frac{\lambda_c^2}{2}\left(C_2^{d,uu}\right)^2 + \lambda_c\lambda_t\left(C_2^{d,uu}\right)^2 + \frac{\lambda_t^2}{2}\left(C_2^{d,uu}\right)^2\right\} \\ C'_2(\mu) &= \frac{1}{48}\ln\left[\frac{\mu^2}{M_W^2}\right]\left\{\lambda_c^2\left(C_2^{d,cc}\right)^2 - 2\lambda_c^2 C_2^{d,cu}C_2^{d,uc} - 2\lambda_c\lambda_t C_2^{d,cu}C_2^{d,uc}\right. \\ &\quad \left. + \lambda_c^2\left(C_2^{d,uu}\right)^2 + 2\lambda_c\lambda_t\left(C_2^{d,uu}\right)^2 + \lambda_t^2\left(C_2^{d,uu}\right)^2\right\} \\ C'_3(\mu) &= \frac{1}{48}\ln\left[\frac{\mu^2}{M_W^2}\right]\left\{3\lambda_c^2\left(C_2^{d,cc}\right)^2 - 3\lambda_c^2 C_2^{d,cu}C_2^{d,uc} - 3\lambda_c\lambda_t C_2^{d,cu}C_2^{d,uc}\right\}, \end{aligned} \tag{4.5.51}$$

where all the coefficients $C_2^{d,cc}, C_2^{d,uc}, C_2^{d,cu}, C_2^{d,uu}$ are evaluated at the scale $\mu \sim M_W$, i.e. are given by the set in Eq.(4.5.49). We can now construct the extra contribution, arising from double insertions of $\Delta B = 1$ operators, to the $\Delta B = 2$ Hamiltonian. We get at the scale $\mu = m_c$

$$\begin{aligned}\mathcal{H}_{eff}^{\hat{|\Delta B|=2,extra}} &= 8G_F^2\Big(\Big[\frac{\lambda_t^2}{96\pi^2}C_{12}(x_t) + C_1'(m_c)\Big]\hat{P}_1 + \Big[-\frac{\lambda_t^2}{48\pi^2}C_{12}'(x_t) + C_2'(m_c)\Big]\hat{P}_2 \\ &\quad + \Big[\frac{1}{32\pi^2}\Big(2\lambda_c\lambda_t C_3(x_t) + \lambda_c^2\Big) + C_3'(m_c)\Big]\hat{P}_3\Big), \qquad (4.5.52)\end{aligned}$$

where we have included the functions $C_{12}(x_t)$, $C_{12}'(x_t)$ and $C_3(x_t)$ to reproduce the initial conditions in Eq.(4.5.47) for $C_1'(M_W, x_t), C_2'(M_W, x_t)$ and $C_3'(M_W, x_t)$. If we take $\Delta C_2^{uu} = \Delta C_2^{uc} = \Delta C_2^{cu} = \Delta C_2^{cc} = 0$ and $\mu = m_c$, we reproduce Eq.(19) in [77]

$$\begin{aligned}\hat{\mathcal{H}}_{eff}^{|\Delta B|=2,extra} &= \frac{G_F^2}{4\pi^2}\Big[\frac{\lambda_t^2}{3}\Big(C_{12}(x_t) - \ln\Big[\frac{m_c^2}{M_W^2}\Big]\Big)\hat{P}_1 \\ &\quad -\frac{2\lambda_t^2}{3}\Big(C_{12}'(x_t) - \ln\Big[\frac{m_c^2}{M_W^2}\Big]\Big)\hat{P}_2 \\ &\quad +\Big(2\lambda_c\lambda_t\Big\{C_3(x_t) - \ln\Big[\frac{m_c^2}{M_W^2}\Big]\Big\} + \lambda_c^2\Big)\hat{P}_3\Big]. \qquad (4.5.53)\end{aligned}$$

Our new result for M_{12}^d is then

$$M_{12}^d = \frac{\langle B_d^0|\hat{\mathcal{H}}_d^{|\Delta B|=2} + \hat{\mathcal{H}}_{eff}^{|\Delta B|=2,extra}|\bar{B}_d^0\rangle}{2M_{B_d^0}}, \qquad (4.5.54)$$

where $\mathcal{H}_d^{|\Delta B|=2}$ is given by Eq.(2.4.88) and $\mathcal{H}_{eff}^{\Delta B=2,extra}$ by Eq.(4.5.52). For the matrix elements of the operators $\hat{P}_1$, $\hat{P}_2$, $\hat{P}_3$ we use [79]

$$\begin{aligned}\langle\hat{P}_1\rangle &= \frac{2}{3}m_b^2 f_{B_d}^2 M_{B_d}^2 B_{B_d}^{(1)}(\mu), \\ \langle\hat{P}_2\rangle &= -\frac{5}{12}m_b^2\Big(\frac{M_{B_d}}{m_b(\mu) + m_d(\mu)}\Big)^2 f_{B_d}^2 M_{B_d}^2 B_{B_d}^{(2)}(\mu), \\ \langle\hat{P}_3\rangle &= \frac{m_c^2}{m_b^2}\langle\hat{P}_1\rangle. \qquad (4.5.55)\end{aligned}$$

We consider two possibilities for the numerical evaluation of $M_{12}^d/|M_{12}^d|$ depending on the set of CKM inputs used. If we take into account the numerical data quoted in Appendix A then we find

$$\mathcal{I}m\Big(M_{12}^d/|M_{12}^d|\Big)^{SM,1} = \Big(69.15 \pm 3.00\Big)\times 10^{-2}. \qquad (4.5.56)$$

If we turn off the double $|\Delta B| = 1$ insertion given in Eq.(4.5.53) we get

$$\mathcal{I}m\Big(M_{12}^d/|M_{12}^d|\Big)^{SM,0} = \Big(69.09 \pm 3.00\Big)\times 10^{-2}. \qquad (4.5.57)$$

Therefore $\mathcal{H}_{eff}^{|\Delta B|=2,extra}$ in Eq.(4.5.53) accounts for corrections of $\mathcal{O}(10^{-3})$, in agreement with the result found in [77].

The current fit for the determination of $\sin(2\beta_d)$ including the direct measurement as reported in [17] is

$$\sin(2\beta_d^{dir}) = \Big(71.0 \pm 1.1\Big)\times 10^{-2}. \tag{4.5.58}$$

On the other hand the fit for the determination of $\sin(2\beta_d)$ excluding the direct measurement is [17]

$$\sin(2\beta_d^{ind}) = \Big(74.8^{+3.0}_{-3.2}\Big)\times 10^{-2}. \tag{4.5.59}$$

The fact that Eq.(4.5.57) and Eq.(4.5.58) are very close suggest that the direct measurement of $\sin(2\beta_d)$ was used in the determination of the CKM inputs $|V_{cs}|$, $|V_{cb}|$, $|V_{ub}/V_{cb}|$ and γ quoted in Appendix A. A fairer comparison between theory and experiment can be done if the theoretical formula for $M_{12}^d/|M_{12}^d|$ is evaluated using CKM inputs where the direct measurement of $\sin(2\beta_d)$ is not involved, unfortunately we do not have such information. One possibility is to use the weak phase given by Eq.(4.5.59) by modifying Eq.(4.5.54) according to

$$M_{12}^d \;=\; \frac{|\langle B_d^0|\mathcal{H}_d^{|\Delta B|=2}|\bar{B}_d^0\rangle|e^{-2i\beta_d} + \langle B_d^0|\mathcal{H}_{eff}^{|\Delta B|=2,extra}|\bar{B}_d^0\rangle}{2M_{B_d^0}}. \tag{4.5.60}$$

Notice that Eq.(4.5.60) includes the indirect determination for $\sin(2\beta_d)$ in the leading part given by the matrix element of $\mathcal{H}_d^{|\Delta B|=2}$. However, $\langle B_d^0|\mathcal{H}_{eff}^{|\Delta B|=2,extra}|\bar{B}_d^0\rangle$ still contains the weak phases arising from the CKM inputs quoted in Appendix A. So Eq.(4.5.60) does not use a consistent set of CKM entries. Following this approach we obtain

$$\mathcal{I}m\Big(M_{12}^d/|M_{12}^d|\Big)^{SM,2} = 74.19 \pm 3.14. \tag{4.5.61}$$

The double insertions cause a deviation of $\mathcal{O}(1\%)$ with respect to the result presented in Eq.(4.5.59), this is 10 times bigger than the estimation reported in the literature [77]. It should be stressed though, that in the determination of Eq.(4.5.61) there was not a consistent treatment of the CKM inputs as explained in the previous paragraph.

Parameter	Main CKM Inputs	$\sin(2\beta_d)$
$\delta(\mu_b)$	$< 0.01\%$	0.04%
$\delta(\mu_c)$	0.01%	0.13%
$\delta(\lvert V_{us}\rvert)$	0.20%	$< 0.01\%$
$\delta(\lvert V_{cb}\rvert)$	0.01%	0.04%
$\delta(\lvert V_{ub}/V_{cb}\rvert)$	4.33%	$< 0.01\%$
$\delta(\gamma)$	0.07%	$< 0.01\%$
$\delta(m_t(m_t))$	$< 0.01\%$	$< 0.01\%$
$\delta(m_c(m_c))$	$< 0.01\%$	0.01%
$\delta(m_b(m_b))$	$< 0.01\%$	$< 0.01\%$
$\delta(\Lambda_5)$	$< 0.01\%$	$< 0.01\%$
$\sin(2\beta_d^{ind})$	—	4.22%
$\sum \delta_T$	4.33%	4.23%

Table 4.6: Error budget for the observable $M_{12}^d/|M_{12}^d|$. The second column refers to the determination given in Eq.(4.5.56) where our main CKM inputs were used. The third column refers to Eq.(4.5.61) where the indirect measurement for $\sin(2\beta_d)$ was used to evaluate the leading contribution in M_{12}^d.

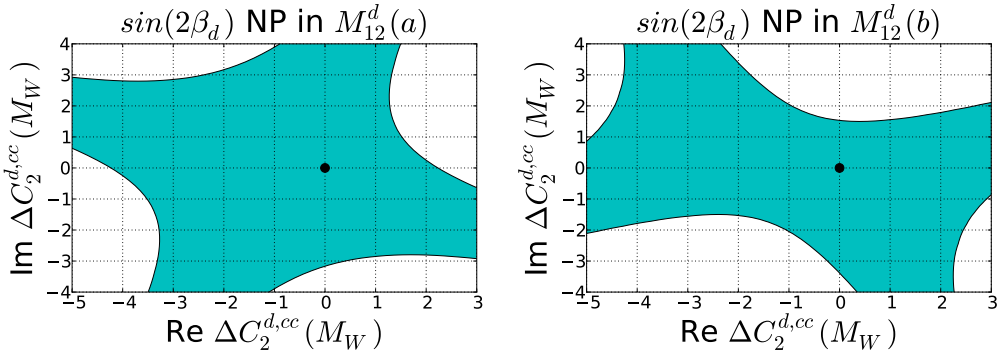

Figure 4.8: Regions for new physics, at 90% C. L., in the $\mathcal{R}e\ \Delta C_2^{d,cc}$ - $\mathcal{I}m\ \Delta C_2^{d,cc}$ plane allowed by the observable $M_{12}^d/|M_{12}^d|$ considering our main CKM inputs (a) and the direct measurement of $\sin(2\beta_d)$ (b). The black point corresponds to the SM value.

4.5.2 $B \to X_d\gamma$

The branching ratio of the process $B \to X_d\gamma$ is useful for constraining the new physics contribution $\Delta C_2^{d,cc}(M_W)$. As a first approximation for the calculation of $\mathcal{B}_r(B \to X_d\gamma)$ we use the formulas to be provided in Section 4.6.1 for $B \to X_s\gamma$ and replace the information related to the strange quark with the analogous information for the down quark [80]. In particular the operators $\hat{Q}_7$ and $\hat{Q}_8$ in Eq.(4.6.72) become [81]

$$\hat{Q}_7 = \frac{e}{16\pi^2} m_b \Big(\bar{d}_L \sigma^{\mu\nu} b_R\Big) F_{\mu\nu}, \qquad \hat{Q}_8 = \frac{g}{16\pi^2} m_b \Big(\bar{d}_L T^a \sigma^{\mu\nu} b_R\Big) G^a_{\mu\nu}, \quad (4.5.62)$$

and our theoretical determination is

$$\mathcal{B}_r(B \to X_d\gamma) \;=\; \Big(1.46^{+0.15}_{-0.28}\Big)\times 10^{-5}, \quad (4.5.63)$$

which can be compared against the experimental result [81–83]

$$\mathcal{B}_r(B \to X_d\gamma) \;=\; \Big(1.41 \pm 0.57\Big)\times 10^{-5}. \quad (4.5.64)$$

As explained in [84], during the calculation of the branching ratios for the processes $B \to X_{d,s}\gamma$ the following two CKM combinations arise $V_{tq}^* V_{tb}$ and $V_{uq}^* V_{ub}$ for $q = d, s$. In the calculation of Eq.(4.5.63) we are omitting the second type of CKM structure. It was considered in [81] leading to $\mathcal{B}_r(B \to X_d\gamma) = (1.54^{+0.26}_{-0.31}) \times 10^{-5}$ and thus it accounts for an overall 5% correction in the central value with respect to our result in Eq.(4.5.63). However, after combining the constraints imposed by $\mathcal{B}_r(B \to X_d\gamma)$ with those from the observables a_{sl}^d and M_{12}^d, we found weak bounds for $\Delta C_{1,2}^{d,cc}$, we then use $\Delta\Gamma_d$ to get stronger constraints. Notice that the theoretical determination of $\mathcal{B}_r(B \to X_d\gamma)$ in [81] shows more tension with respect to the experimental result in Eq.(4.5.64) than our computation in Eq.(4.5.63). This suggests that including all the CKM structures will lead to larger new physics regions, but this cannot affect our conclusions because our bounds, including only one CKM combination, already saturate the experimental uncertainty for $\Delta\Gamma_d$.

Parameter	Standard analysis
$\delta(\mu)_{\pm}$	7.97%
$\delta(\mathcal{B}_r(\bar{B} \to X_c e \bar{\nu}_e))_{\pm}$	3.96%
$\delta(\lvert V_{us}\rvert)_{\pm}$	0.46%
$\delta(\lvert V_{cb}\rvert)_{\pm}$	4.93%
$\delta(\lvert V_{ub}/V_{cb}\rvert)_{\pm}$	0.10%
$\delta(\gamma)_{\pm}$	2.20%
$\delta(m_d)_{\pm}$	0.11%
$\delta(\delta)_{-}$	16.46%
$\delta(m_t(m_W))_{\pm}$	0.37%
$\delta(\Lambda_5)_{\pm}$	0.65%
$\delta(m_b^{1S})_{\pm}$	0.55%
$\delta(m_c(m_c))_{\pm}$	1.29%
$\left(\sum \delta\right)_{+}$	10.54%
$\left(\sum \delta\right)_{-}$	19.55%

Table 4.7: Error budget for the observable $\mathcal{B}_r(\bar{B} \to X_d\gamma)$. The subindex $\pm$ stands for symmetric errors, notice that the parameter δ affects only the lower bound for the overall error so that we get different values for the total lower and upper uncertainties $\left(\sum \delta\right)_{-}$ and $\left(\sum \delta\right)_{+}$ respectively.

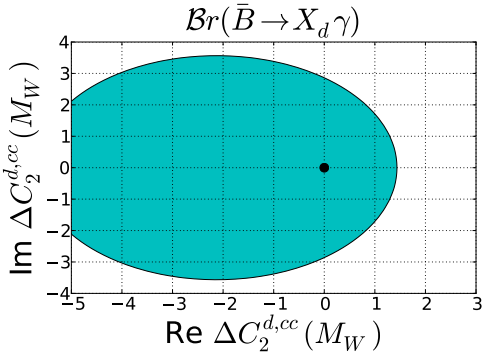

Figure 4.9: Regions for new physics, at 90% C. L. in the $\mathcal{R}e\ \Delta C_2^{d,cc}$ - $\mathcal{I}m\ \Delta C_2^{d,cc}$ plane allowed by the observable $B_s^0 \to X_d\gamma$. The black point corresponds to the SM value.

4.6 Constraints from $b \to c\bar{c}s$ transitions

4.6.1 $\bar{B} \to X_s\gamma$

The process $\bar{B} \to X_s\gamma$ is a very interesting transition for BSM phenomenology for several reasons. To begin with it is a loop generated flavour changing neutral current sensitive to new particles. In addition, the experimental and theoretical precision achieved on its determination have an accuracy of the same order; moreover, this process is useful to constrain CKM elements involving the top quark. The experimental world average up to date combines measurements from CLEO, Belle and Babar leading to [1]

$$\mathcal{B}_r(\bar{B} \to X_s\gamma) \quad = \quad \Big(3.43 \pm 0.21 \pm 0.07\Big) \times 10^{-4}. \tag{4.6.65}$$

On the theory side there has been a huge effort in the determination of this observable; the most precise results available are obtained at NNLO, here we consider [85]

$$\mathcal{B}_r^{SM}(\bar{B} \to X_s\gamma) \quad = \quad \Big(3.36 \pm 0.23\Big) \times 10^{-4}, \tag{4.6.66}$$

where the energy of the photon satisfies the cut $E_0^\gamma > 1.6$ GeV. Using the Heavy Quark Effective Theory (HQET) the calculation of the branching ratio for the process $\bar{B} \to X_s\gamma$ is written as [86]

$$\mathcal{B}_r(\bar{B} \to X_s\gamma) \quad = \mathcal{B}_r(\bar{B} \to X_c e\bar{\nu}_e) \times R_{quark}(\delta) \times \left(1 - \frac{\delta_{sl}^{NP}}{m_b^2} + \frac{\delta_{rad}^{NP}}{m_b^2}\right), \tag{4.6.67}$$

where $R_{quark}(\delta)$ is a perturbative quantity calculated from the ratio of the quark level decays

$$R_{quark}(\delta) \;=\; \frac{\Gamma(b \to X_s\gamma)^{E_\gamma > (1-\delta)E_{max}}}{\Gamma(b \to X_c e\bar{\nu}_e)}, \tag{4.6.68}$$

and δ_{sl}^{NP}, δ_{rad}^{NP} are two parameters accounting for non-perturbative corrections to the semileptonic and radiative B-meson decay rates respectively. They can be written in terms of the HQET parameter λ_2 as

$$\delta_{sl}^{NP} - \delta_{rad}^{NP} \;=\; \Big(\frac{3}{2} - \frac{6(1-z)^4}{g(z)}\Big)\lambda_2 + \frac{9}{2}\lambda_2,$$

where

$$\lambda_2 \;=\; \frac{1}{4}\Big(m_{B^*}^2 - m_B^2\Big). \tag{4.6.69}$$

The factor $\mathcal{B}_r(\bar{B} \to X_c e\bar{\nu}_e)$ in Eq.(4.6.68) is the branching ratio for the semileptonic process $\bar{B} \to X_c e\bar{\nu}_e$ and $(1-\delta)\frac{m_b}{2}$ determines the lower cut on the energy of the photon in the Bremsstrahlung correction E_γ; here we use

$$\delta_{min} < \delta < 0.99, \qquad \delta_{min} = \Big(m_c(m_c)/m_b^{1S}\Big)^2 \approx 0.075. \tag{4.6.70}$$

The normalization factor $\Gamma(b \to X_c e\bar{\nu}_e)$ in Eq.(4.6.68) allows us to eliminate the uncertainties associated with the pole mass of the b quark m_b and the CKM angles. The expression for the ratio $R_{quark}(\delta)$ inside Eq.(4.6.68) is

$$R_{quark}(\delta) \;= \frac{|V_{ts}^* V_{tb}|^2}{|V_{cb}|^2}\frac{6\alpha}{\pi g(z)} F\Big(|D|^2 + A\Big). \tag{4.6.71}$$

With $F = \frac{1}{k(z)}\Big(\frac{m_b(\mu=m_b)}{m_{b,pole}}\Big)^2$, $k(z)$ is the NLO correction and $g(z)$ is the phase space factor for the calculation of the semileptonic decay $\Gamma[b \to X_c e\bar{\nu}_e]$. Here we consider $z = (m_c(m_c)/m_b^{1S})^2$ [87].

Before describing the perturbative terms D and A inside Eq.(4.6.71) let us first discuss briefly the operator basis and the set of Wilson coefficients used during the calculations for this section.

The absence of Dirac traces containing γ_5 at leading order in G_F makes the following basis particularly useful in the computation of the perturbative contribution inside Eq.(4.6.71) [86]

$$\hat{Q}_1 = \Big(\bar{s}_L\gamma_\mu T^a c_L\Big)\Big(\bar{c}_L\gamma^\mu T^a b_L\Big)\,, \qquad \hat{Q}_2 = \Big(\bar{s}_L\gamma_\mu c_L\Big)\Big(\bar{c}_L\gamma^\mu b_L\Big),$$
$$\hat{Q}_3 = \Big(\bar{s}\gamma_\mu b_L\Big)\sum_q\Big(\bar{q}\gamma^\mu q\Big)\,, \qquad \hat{Q}_4 = \Big(\bar{s}_L\gamma_\mu T^a b_L\Big)\sum_q\Big(\bar{q}\gamma^\mu T^a q\Big),$$
$$\hat{Q}_5 = \Big(\bar{s}_L\Gamma_{\mu_1\mu_2\mu_3} b_L\Big)\sum_q\Big(\bar{q}\Gamma^{\mu_1\mu_2\mu_3} q\Big)\,, \quad \hat{Q}_6 = \Big(\bar{s}_L\Gamma_{\mu_1\mu_2\mu_3} T^a b_L\Big)\sum_q\Big(\bar{q}\Gamma^{\mu_1\mu_2\mu_3} T^a q\Big),$$
$$\hat{Q}_7 = \frac{e}{16\pi^2} m_b\Big(\bar{s}_L\sigma^{\mu\nu} b_R\Big)F_{\mu\nu}\,, \qquad \hat{Q}_8 = \frac{g}{16\pi^2} m_b\Big(\bar{s}_L T^a\sigma^{\mu\nu} b_R\Big)G^a_{\mu\nu}, \qquad (4.6.72)$$

with $\Gamma_{\mu_1\mu_2\mu_3} = \gamma^{\mu_1}\gamma^{\mu_2}\gamma^{\mu_3}$.

It is convenient to express $\mathcal{B}_r(\bar{B} \to X_s\gamma)$ in terms of the so-called effective coefficients $C_i^{eff}(\mu)$, constructed from linear combinations of the Wilson coefficients C_i associated with the operators in Eq.(4.6.72), according to

$$C_i^{eff}(\mu) \;=\; \begin{cases} C_i(\mu) \text{ for } i = 1..., 6 \\ C_7(\mu) + \sum_{i=1}^6 y_i C_i(\mu) \text{ for } i = 7 \\ C_8(\mu) + \sum_{i=1}^6 z_i C_i(\mu) \text{ for } i = 8, \end{cases} \qquad (4.6.73)$$

with $y = (0, 0, -\frac{1}{3}, -\frac{4}{9}, -\frac{20}{3}, -\frac{80}{9})$ and $z = (0, 0, 1, -\frac{1}{6}, 20, -\frac{10}{3})$.
The set of coefficients in Eq.(4.6.73) are specially useful since at leading order they are regularization and renormalization scheme independent [47], this does not hold for the original coefficients of the operators $Q_7(\mu)$ and $Q_8(\mu)$ in Eq.(4.6.72). The renormalization scale evolution for the coefficients in 4.6.73 is determined by

$$\mu\frac{d}{d\mu}C_i^{eff}(\mu) \;=\; C_j^{eff}(\mu)\gamma_{ji}^{eff}(\mu), \qquad (4.6.74)$$

where γ_{ij}^{eff} are the components of the effective anomalous dimension matrix introduced up to NLO in [86]. The corresponding renormalization scale evolution matrices can be constructed using the information provided in Section 2.2.2 by substituting the matrices $\hat{\gamma}^{(0)}$ and $\hat{\gamma}^{(1)}$ by $\hat{\gamma}^{(0)}_{eff}$ and $\hat{\gamma}^{(1)}_{eff}$ respectively (see [86]). The initial conditions used in the determination of $C_i^{eff}(\mu)$ have the following structure

$$C_i^{eff,NP}(M_W) \;= C_i^{eff,SM}(M_W) + \Delta C_i^{eff}(M_W), \qquad (4.6.75)$$

for $i = 1, ..., 8$; where the explicit values for $C_i^{eff,SM}(M_W)$ can be found in [86].
The new physics contributions $\Delta C_i^{eff}(M_W)$ in Eq.(4.6.75) are given in terms of the new effects $\Delta C_{1,2}^{s,cc}(M_W)$ in our old basis in Eq.(2.3.78) according to

$$\begin{aligned}\Delta C_1^{eff}(M_W) &= 2.0\ \Delta C_1^{s,cc}(M_W),\\ \Delta C_2^{eff}(M_W) &= 1/3\ \Delta C_1^{s,cc}(M_W) + \Delta C_2^{s,cc}(M_W).\end{aligned} \tag{4.6.76}$$

The coefficients $C_i^{eff,SM}(M_W)$ are evolved down to the renormalization scale $\mu \sim m_b$ using the full NLO evolution matrices defined in terms of $\hat{\gamma}_{eff}^{(0)}$ and $\hat{\gamma}_{eff}^{(1)}$, on the other hand $\Delta C_i^{eff}(M_W)$ are evolved down using only the LO versions in Eq.(2.3.82).
We can now complete the analysis of Eq.(4.6.71), the term D is

$$D = C_7^{eff,NP}(\mu) + \tfrac{\alpha_s(\mu)}{4\pi} \sum_{i=1}^{8} C_i^{eff}(\mu)\Big[r_i + \gamma_{eff,i7}^{(0)}\ \ln\tfrac{m_b}{\mu}\Big]. \tag{4.6.77}$$

Where $\mu \sim m_b$ and $C_7^{eff,NP}(\mu)$ is determined up to NLO, the coefficients r_2, r_7 and r_8 arise during the calculation of the virtual corrections of the matrix elements $\langle s\gamma|\hat{O}_2|b\rangle$, $\langle s\gamma|\hat{O}_7|b\rangle$ and $\langle s\gamma|\hat{O}_8|b\rangle$ they can be found in [86, 88]; the coefficient r_1 can be calculated from r_2 through $r_1 = -\frac{1}{6}r_2$. The rest of the coefficients r_i provide corrections of $\mathcal{O}(1\%)$ [86] therefore we omit them in this study, they were estimated in [89]. Finally the full expression for A in Eq.(4.6.71) is

$$A = \Big(e^{-\alpha_s(\mu)\ln\delta(7+2\ln\delta)/3\pi} - 1\Big)|C_7^{(0)eff}(\mu)|^2 + \tfrac{\alpha_s(\mu)}{\pi} \sum_{\substack{i,j=1\\ i\le j}}^{8} C_i^{(0)eff}(\mu) C_j^{(0)eff}(\mu) f_{ij}(\delta), \tag{4.6.78}$$

where the exponential contains all the infrared logarithms of δ remaining after the cancellation of all the infrared divergences between the virtual and the Bremsstrahlung corrections to $b \to X_s\gamma$. All the required set of functions f_{ij} in Eq.(4.6.78) are provided in [86].

We take into account the NNLO result in Eq.(4.6.66) by rescaling our NLO determinations according to the following formula

$$\frac{\mathcal{B}_r(\bar{B} \to X_s\gamma)}{\mathcal{B}_r^{\rm NNLO}(\bar{B} \to X_s\gamma)} = \frac{\mathcal{B}_r^{\rm NLO}(\bar{B} \to X_s\gamma)(\mu_0)}{\mathcal{B}_{r0}^{\rm NLO}(\bar{B} \to X_s\gamma)}, \tag{4.6.79}$$

where

- $\mathcal{B}_{r0}^{\rm NLO}(\bar{B} \to X_s\gamma)$ is the branching ratio of the process $\bar{B} \to X_s\gamma$ calculated at NLO and evaluated at the central values of all the input parameters and kept constant during the statistical fit.

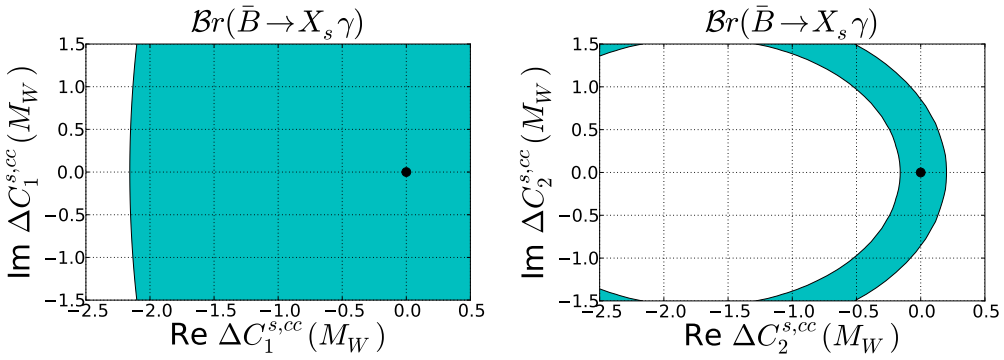

Figure 4.10: Regions for new physics, at 90% C. L., in the $\mathcal{R}e\ \Delta C_2^{s,cc}$ - $\mathcal{I}m\ \Delta C_2^{s,cc}$ allowed by the observable $\bar{B} \to X_s\gamma$. The black point corresponds to the SM value.

- $\mathcal{B}_r^{\rm NLO}(\bar{B} \to X_s\gamma)$ is the branching ratio of the process $\bar{B} \to X_s\gamma$ calculated at NLO with all the inputs allowed to float except the renormalization scale, which is fixed at $\mu_0 = m_b$.

- $\mathcal{B}_r^{\rm NNLO}(\bar{B} \to X_s\gamma)$ is the branching ratio of the process $\bar{B} \to X_s\gamma$ calculated at NNLO and allowed to float within the uncertainty associated with the renormalization scale. In the case of the theoretical result given in Eq.(4.6.66) [85] the renormalization scale uncertainty is equivalent to $\pm 3\%$ of the central value.

The partial contributions to the final error are described in Tab.4.8, our theoretical result after the NNLO rescaling is $\mathcal{B}_r(\bar{B} \to X_s\gamma) = (3.36^{+0.18}_{-0.45}) \times 10^{-4}$. The allowed regions for $\Delta C_1(M_W)$ and $\Delta C_2(M_W)$ are shown in Fig.4.10, it can be seen that this observable impose strong constraints over $\Delta C_2(M_W)$.

4.6.2 $\sin(2\beta_d)$

As shown in Eq. (4.5.37) and Eq. (4.5.38), the amplitude for the process $B \to J/\psi K$ is relevant in the calculation of the indirect CP asymmetry $S_{B_d^0 \to J/\psi K_{S,L}}$. On the experimental side it is constrained by the current value of $\sin(2\beta_d)$. At quark level the decay $B \to J/\psi K$ is given by the transition $b \to c\bar{c}s$, hence it allows us to establish bounds on the contributions $\Delta C_1^{s,cc}(M_W)$ and $\Delta C_2^{s,cc}(M_W)$; in particular, there is a high sensitivity to the imaginary part of $\Delta C_1^{s,cc}(M_W)$. This is particularly valuable

Parameter	Standard analysis
$\delta(\mu)_{\pm}$	3.00%
$\delta(\mathcal{B}_r(\bar{B} \to X_c e \bar{\nu}_e))_{\pm}$	3.96%
$\delta(\lvert V_{us}\rvert)_{\pm}$	0.02%
$\delta(\lvert V_{cb}\rvert)_{\pm}$	0.01%
$\delta(\lvert V_{ub}/V_{cb}\rvert)_{\pm}$	0.1%
$\delta(\gamma)_{\pm}$	0.10%
$\delta(m_s)_{\pm}$	0.04%
$\delta(\delta)_{-}$	12.26%
$\delta(m_t(m_W))_{\pm}$	0.19%
$\delta(\Lambda_5)_{\pm}$	0.62%
$\delta(m_b^{1S})_{\pm}$	0.60%
$\delta(m_c(m_c))_{\pm}$	1.39%
$\left(\sum \delta\right)_{+}$	5.24%
$\left(\sum \delta\right)_{-}$	13.34%

Table 4.8: Error budget for the observable $\mathcal{B}_r(\bar{B} \to X_s\gamma)$. The subindex $\pm$ stands for symmetric errors. Notice that the parameter δ affects only the lower bound for the overall error So that we get different values for the total lower and upper uncertainties $\left(\sum \delta\right)_{-}$ and $\left(\sum \delta\right)_{+}$ respectively.

because, as shown in [3], $\mathcal{I}m(\Delta C_1(M_W))$ can induce sizeable deviations of $\mathcal{O}(10^\circ)$ in the determination of the CKM phase γ (well within the current experimental precision).

Our approach in this section is based in the calculations of [90], where the amplitude for the process $B \to J/\psi K$ is written as

$$\mathcal{A}_{B\to J/\psi K} = \frac{G_F}{\sqrt{2}} V_{cb}V_{cs}^* \; \bar{\alpha}_2 \; A_{J/\psi K}, \tag{4.6.80}$$

with

$$\bar{\alpha}_2 \;\; = \;\; \alpha_2 + \alpha_3 + \alpha_5 + \alpha_7 + \alpha_9. \tag{4.6.81}$$

For the purposes of the asymmetry in Eq.(4.5.37), the explicit expression for the global factor $A_{J/\psi}$ is not required because it cancels in the ratio between $\mathcal{A}_{B\to J/\psi K}$ and $\bar{\mathcal{A}}_{B\to J/\psi K}$ given in Eq.(4.5.38). Notice that possible complex phases arising in $A_{J/\psi}$ also cancel in the ratio because they are "strong", hence they are left unaffected when taking the $\mathcal{CP}$ conjugate of $\mathcal{A}_{B\to J/\psi K}$ in Eq.(4.5.38). In addition, the weak phase from the CKM combination $V_{cb}V_{cs}^*$ can also be ignored regarding that it is tiny, $(\mathcal{O}(10^{-3})^\circ)$, in comparison with the $\mathcal{O}(10)^\circ$ phase induced by the imaginary components of ΔC_1 and ΔC_2.

Then our theoretical expression for the determination of $\sin(2\beta)$ is

$$\sin(2\beta) = \mathcal{I}m\Big(e^{-2i\beta_{indir.}} \frac{\hat{\mathcal{CP}}(\bar{\alpha}_2)}{\bar{\alpha}_2}\Big). \tag{4.6.82}$$

The topological amplitudes α_i $(i = 2, 3, 5, 7, 9)$ in Eq.(4.6.80) have the following dependence on the Wilson coefficients of the operators in Eq.(2.3.78)

$$\begin{aligned}
\alpha_2 &= C_1 + \frac{C_2}{N_c} + \frac{\alpha_s}{4\pi}\frac{C_F}{N_c} C_2 \times K_1, \\
\alpha_3 &= C_3 + \frac{C_4}{N_c} + \frac{\alpha_s}{4\pi}\frac{C_F}{N_c} C_4 \times K_1, \\
\alpha_5 &= C_5 + \frac{C_6}{N_c} - \frac{\alpha_s}{4\pi}\frac{C_F}{N_c} C_6 \times K_2, \\
\alpha_7 &= C_7 + \frac{C_8}{N_c} - \frac{\alpha_s}{4\pi}\frac{C_F}{N_c} C_8 \times K_2, \\
\alpha_9 &= C_9 + \frac{C_{10}}{N_c} + \frac{\alpha_s}{4\pi}\frac{C_F}{N_c} C_{10} \times K_1.
\end{aligned} \tag{4.6.83}$$

In naive dimensional regularization K_1 and K_2 are written in terms of the vertex correction functions (f_I, g_I) and the hard scattering spectator interaction contribution f_{II} as

$$
\begin{aligned}
K_1 &= -18 - 12\,\ln\frac{\mu}{m_b} + f_I + f_{II} + \frac{F_0^{BK}(m^2_{J/\psi})}{F_1^{BK}(m^2_{J/\psi})} g_I, \\
K_2 &= -6 - 12\,\ln\frac{\mu}{m_b} + f_I + f_{II} + \frac{F_0^{BK}(m^2_{J/\psi})}{F_1^{BK}(m^2_{J/\psi})} g_I.
\end{aligned} \tag{4.6.84}
$$

The equations for f_I and g_I are given in Eq.(D.6.11). We evaluate explicitly the integrals in Eq.(D.6.11) using the leading component of the LCDA of the J/ψ meson on its Gegenbauer polynomial expansion

$$
\phi^{J/\psi}(\xi) = 6\xi(1-\xi). \tag{4.6.85}
$$

Where ξ is the momentum fraction carried by the charm quark inside the J/ψ meson. The evaluation of the hard spectator interaction function f_{II} requires the twist-2 ϕ^K and twist-3 ϕ^K_σ LCDA for the Kaon [1]

$$
\begin{aligned}
f_{II} &= \frac{4\pi^2}{N_c} \frac{f_K f_B}{F_1^{BK}(m^2_{J/\psi}) m_B^2} \frac{1}{1-z} \int_0^1 \frac{d\bar{\rho}}{\bar{\rho}} \phi_1^B(\bar{\rho}) \int_0^1 \frac{d\xi}{\xi} \phi^{J/\psi}(\xi) \\
&\quad \times \int_0^1 \frac{d\bar{\eta}}{\bar{\eta}} \Big(\phi^K(\bar{\eta}) + \frac{2\mu_\chi}{m_b} \frac{1}{(1-z)} \frac{\phi^K_\sigma(\bar{\eta})}{6\bar{\eta}} \Big),
\end{aligned} \tag{4.6.86}
$$

where $z \in (m^2_{J/\psi}/m_b^2, m^2_{J/\psi}/m_B^2)$ and $\mu_\chi = 6\Lambda_{QCD}$.

For the first moment of the LCDA of the B meson we use the standard QCDF result $\int_0^1 d\bar{\rho}\phi^B(\bar{\rho})/\bar{\rho} = m_B/\lambda_B$ (Eq.(3.4.15)), and for the twist-2 and twist-3 distribution amplitudes ϕ^K and ϕ^K_σ we consider

$$
\phi^K(\bar{\eta}) = \phi^K_\sigma(\bar{\eta}) = 6\bar{\eta}(1-\bar{\eta}), \tag{4.6.87}
$$

such that

$$
\int_0^1 \frac{d\xi}{\xi} \phi^{J/\psi} = \int_0^1 \frac{d\bar{\eta}}{\bar{\eta}} \phi^K(\bar{\eta}) = 3. \tag{4.6.88}
$$

The integral of $\phi^K_\sigma(\bar{\eta})$ in Eq. (4.6.86) is divergent, as discussed in Chapter 3 this is a common feature of twist-3 LCDA. To parameterize the divergence we follow the prescription indicated by [90] and write

[1] During the writing process of this thesis we pointed out to the authors of [90] an inconsistency between the formulas for f_{II} and the numerical value of α_2 presented in the published version of their paper; this problem has been corrected in the latest version of the manuscript available in the Arxiv. [91]

Parameter	Standard analysis
$\delta(z)$	50.11%
$\delta(\mu)$	10.50%
$\delta(r)$	20.63%
$\delta(\delta)$	60.91%
$\sum \delta$	60.07%

Table 4.9: Error budget for the amplitude $|\bar{\alpha}_2|$.

$$\int_0^1 \frac{d\bar{\eta}}{\bar{\eta}} \;\; \to \;\; \ln\frac{m_B}{\Lambda_h} + r, \tag{4.6.89}$$

with

$$r \;\; = \;\; |r|\exp(i\delta). \tag{4.6.90}$$

Then we have

$$\int_0^1 \frac{d\bar{\eta}}{\bar{\eta}} \frac{\phi_\sigma^K}{\bar{\eta}} \to 6\Big(\ln\frac{m_B}{\Lambda_h} + r - 1\Big). \tag{4.6.91}$$

Our numerical ranges for the parameters r and δ are

$$3.0 < |r| < 6.0 \qquad 0.0 < \delta < 2.4. \tag{4.6.92}$$

We choose the interval for δ such that the sub amplitude $\bar{\alpha}_2$ (see Eq.(4.6.81)) reaches its maximum and minimum value inside. We get [2]

$$|\bar{\alpha_2}| = \Big(17.52 \pm 10.52\Big)\times 10^{-2}. \tag{4.6.93}$$

we are in agreement with the experimental value cited in [90]

$$|\bar{\alpha_2}(J/\psi K)|_{exp} = \Big(26.0 \pm 2.0\Big)\times 10^{-2}. \tag{4.6.94}$$

The error budget for $\bar{\alpha}_2$ is presented in Tab.4.9

[2] Our determination for the central value is $\bar{\alpha}_2 = 0.16 - 0.06i$.

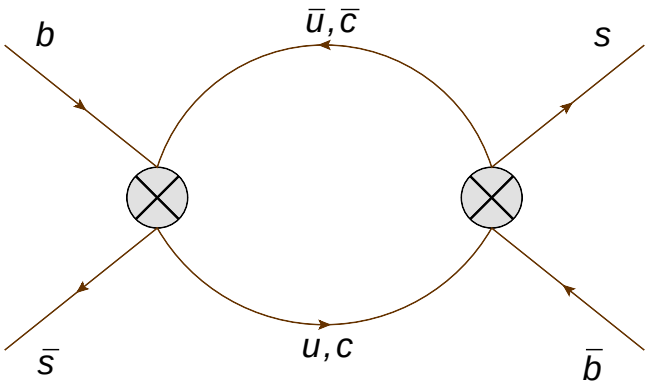

Figure 4.11: Effective diagrams arising from the double insertions of the operators $\hat{Q}_1 - \hat{Q}_6$.

4.7 Constraints using multiple channels observables: a^s_{sl}, a^d_{sl} and $\Delta\Gamma_s$

The semileptonic asymmetry a^s_{sl} and the decay width $\Delta\Gamma_s$ for neutral B^0_s meson mixing are sensitive to the quark level decay channels $b \to u\bar{u}s$, $b \to c\bar{u}s$ and $b \to c\bar{c}s$. In Section 2.4.1 these two observables were defined in terms of the non-diagonal elements Γ^s_{12} and M^s_{12} of the mixing matrix in Eq.(1.3.49) as

$$a^s_{sl} = \mathcal{I}m\Big[\frac{\Gamma^s_{12}}{M^s_{12}}\Big] \qquad \Delta\Gamma_s = 2|\Gamma^s_{12}|\cos\phi^s_{12}, \tag{4.7.95}$$

where ϕ^s_{12} is defined in Eq.(1.3.48) .

As explained in Section 2.4.1, the element Γ^s_{12} is determined from the double insertion of $\mathcal{H}^{|\Delta B|=1}$ Hamiltonians. As a matter of fact the dependence on the tree level Wilson coefficients $C^{uu,uc,uu}_{1,2}$ arises from the double insertion of the current-current operators $\left\{\hat{Q}^{ab}_{1,2}, \hat{Q}^{ab}_{1,2}\right\}$ and from the insertions between a single current-current and a penguin $\left\{\hat{Q}^{ab}_{1,2}, \hat{Q}_{3,4,5,6}\right\}$ (for $ab = uu, uc, cc$, see Eq.(2.3.78)). These double insertions lead to the effective topologies shown in Fig.4.11. According to Eq.(2.4.103) the element Γ^s_{12} is decomposed in terms of the partial contributions $\Gamma^{s,ab}_{12}$, where $ab = uu, uc, cc$, depending on the "up" type quarks running inside the loops as shown in Fig.4.11.

The Heavy Quark Expansion (HQE) allows us to reduce the different diagrams in Fig.4.11 to the generic $\Delta B = 2$ topology presented in Fig.4.12. Actually, Fig.4.12 is associated with the $\Delta B = 2$ operators $\hat{Q}$, $\hat{Q}_S$ and $\hat{\tilde{Q}}_S$ given in Eq.(2.4.105). The expressions for $\Gamma^{s,ab}_{12}$ written in terms of the matrix elements of $\hat{Q}$ and $\hat{Q}_S$ were

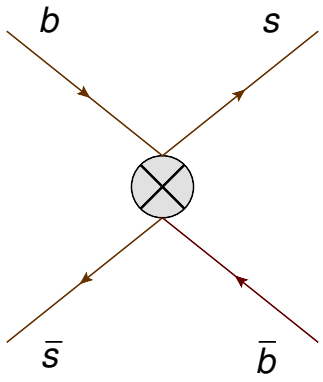

Figure 4.12: $\Delta B = 2$ operators arising after the HQE of the double insertions of $\hat{Q}_1 - \hat{Q}_6$.

introduced in Eq.(2.4.110). Here we are interested in the functions G^{ab} and G_S^{ab} given in Eq.(2.4.110). They are further decomposed in terms of the current-current coefficients F^{ab} and F_S^{ab} (double insertion of current-current operators), and the penguin coefficients P^{ab} and P_S^{ab} (insertion between a single current-current and a penguin operator).

The equations for F^{ab} and F_S^{ab} in terms of the tree-level Wilson coefficients $C_1^{s,ab}$ and $C_2^{s,ab}$ obey the following generic structure

$$F^{ab} = F_{11}^{ab}\Big(C_1^{ab}(\mu)\Big)^2 + F_{12}^{ab} C_1^{ab}(\mu) C_2^{ab}(\mu) + F_{22}^{ab}\Big(C_2^{ab}(\mu)\Big)^2, \tag{4.7.96}$$

where the individual factors $F_{11,12,22}^{ab}$ are available in the literature up to NLO

$$F_{ij}^{ab} = F_{ij}^{(0)} + \frac{\alpha_s(\mu)}{4\pi} F_{ij}^{(1)}. \tag{4.7.97}$$

To account for new physics effects, the Wilson coefficients inside Eq.(4.7.96) should be modified following Eq.(4.1.1). Notice that Eq.(4.7.96) is sensitive to the different transitions $b \to c\bar{c}s$, $b \to u\bar{c}s$, $b \to c\bar{u}s$ and $b \to u\bar{u}s$. To be consistent with the inclusion of new physics effects $\Delta C_1^{s,ab}$ and $\Delta C_2^{s,ab}$ at LO only, we drop products between $\alpha_s(\mu)$ and $\Delta C_1^{s,ab}$ and $\Delta C_2^{s,ab}$ inside Eq.(4.7.96).

New physics effects should also be introduced in the penguin functions P^{ab} and P_S^{ab}. For the purposes of illustration we present the explicit results for P^{cc} and P_S^{cc} for the B_s^0 system [48]

$$\begin{aligned} P^{cc} &= \sqrt{1-4\bar{z}}\Big((1-\bar{z})K_1'(\mu) + \frac{1}{2}(1-4\bar{z})K_2'(\mu) + 3\bar{z}K_3'(\mu)\Big) + \frac{\alpha_s(\mu)}{4\pi} F_p(\bar{z})\Big(C_2^{cc}(\mu)\Big)^2, \\ P_S^{cc} &= \sqrt{1-4\bar{z}}\Big(1+2\bar{z}\Big)\Big(K_1'(\mu) - K_2'(\mu)\Big) - \frac{\alpha_s(\mu)}{4\pi} 8F_p(\bar{z})\Big(C_2^{cc}(\mu)\Big)^2. \end{aligned} \tag{4.7.98}$$

With

$$\begin{aligned}
\bar{z} &= \Big(m_c(m_b)/m_b(m_b)\Big)^2 \text{ [52]} \\
K_1^{'cc}(\mu) &= 2\Big(3C_1^{cc}(\mu)C_3(\mu) + C_1^{cc}(\mu)C_4(\mu) + C_2^{cc}(\mu)C_3(\mu)\Big) \\
K_2^{'cc}(\mu) &= 2C_2^{cc}(\mu)C_4(\mu) \\
K_3^{'cc}(\mu) &= 2\Big(3C_1^{cc}(\mu)C_5(\mu) + C_1^{cc}(\mu)C_6(\mu) + C_2^{cc}(\mu)C_5(\mu) + C_2^{cc}(\mu)C_6(\mu)\Big)
\end{aligned} \tag{4.7.99}$$

and

$$\begin{aligned}
F_p^{cc}(z) &= -\frac{1}{9}\sqrt{1-4\bar{z}}\Big(1+2\bar{z}\Big)\Big[2\ln\frac{\mu}{m_b} + \frac{2}{3} + 4\bar{z} - \ln\bar{z} \\
&\quad + \sqrt{1-4\bar{z}}\Big(1+2\bar{z}\Big)\ln\frac{1-\sqrt{1-4\bar{z}}}{1+\sqrt{1+4\bar{z}}} + \frac{3C_8(\mu)}{C_2^{cc}(\mu)}\Big].
\end{aligned} \tag{4.7.100}$$

The Wilson coefficients inside $K_1^{'cc}(\mu)$, $K_2^{'cc}(\mu)$ and $K_3^{'cc}(\mu)$ should be modified according to Eq.(4.1.1) in order to include new physics effects $\Delta C_1^{s,ab}$ and $\Delta C_2^{s,ab}$.
As discussed in Section 4.5.1 new physics at tree level can be introduced in M_{12}^q (for $q = d, s$) as the result of double insertion of $\Delta B = 1$ operators. However, the overall contributions are rather weak and can be ignored in our analysis for a_{sl}^s, a_{sl}^d and $\Delta\Gamma_d$.
Even though we have focused our attention in the B_s^0 system, an analogous procedure can be followed to derive constraints from a_{sl}^d and $\Delta\Gamma_d$ in the case of the B_d^0 system.
Our theoretical predictions for a_{sl}^s and a_{sl}^d are [15]

$$\begin{aligned}
a_{sl}^{s,SM} &= \Big(2.22 \pm 0.27\Big)\times 10^{-5}, \\
a_{sl}^{d,SM} &= \Big(-4.7 \pm 0.6\Big)\times 10^{-4},
\end{aligned} \tag{4.7.101}$$

on the experimental side we consider [1]

$$\begin{aligned}
a_{sl}^{s} &= \Big(0.17 \pm 0.30\Big)\times 10^{-2}, \\
a_{sl}^{d} &= \Big(0.01 \pm 0.20\Big)\times 10^{-2}.
\end{aligned} \tag{4.7.102}$$

The theoretical determinations for $\Delta\Gamma_s$ and $\Delta\Gamma_d$ are [15]

$$\begin{aligned}
\Delta\Gamma_s^{SM} &= \Big(0.088 \pm 0.02\Big)\text{ps}^{-1}, \\
\Delta\Gamma_d^{SM} &= \Big(2.61 \pm 0.59\Big)\times 10^{-3}\ \text{ps}^{-1},
\end{aligned} \tag{4.7.103}$$

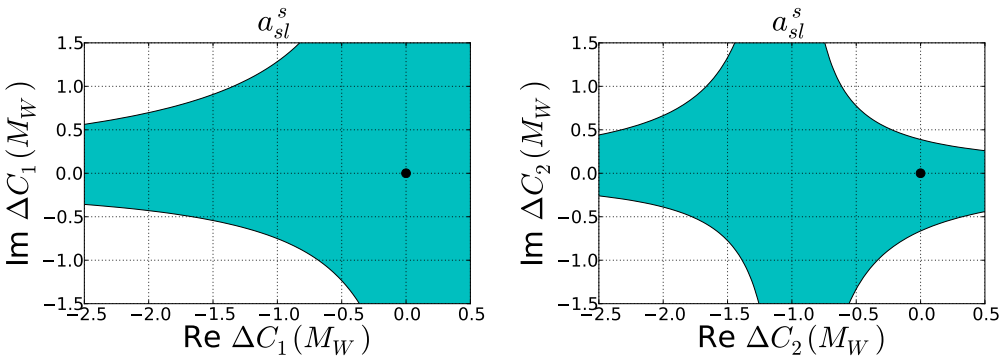

Figure 4.13: Regions for new physics, at 90% C. L., in the $\mathcal{R}e\ \Delta C_1$ - $\mathcal{I}m\ \Delta C_1$ (left) and $\mathcal{R}e\ \Delta C_2$ - $\mathcal{I}m\ \Delta C_2$ (right) planes allowed by the observable a^s_{sl} in the standard analysis. The black point corresponds to the SM value. Here we are assuming universality: $\Delta C_1^{s,uu} = \Delta C_1^{s,uc} = \Delta C_1^{s,cc} = \Delta C_1$.

and the corresponding experimental results are

$$\begin{aligned} \Delta\Gamma_s^{Exp} &= \Big(0.081 \pm 0.006\Big)\text{ps}^{-1},\ [1] \\ \Delta\Gamma_d^{Exp} &= \Big(-1.32 \pm 6.58\Big)\times 10^{-3}\ \text{ps}^{-1}, \end{aligned} \tag{4.7.104}$$

where $\Delta\Gamma_d^{Exp}$ was derived using [1]

$$\Big(\Delta\Gamma_d/\Gamma_d\Big)^{Exp} = -0.002 \pm 0.010, \qquad \tau^{Exp}_{B^0_d} = 1.520 \pm 0.004\ \text{ps}. \tag{4.7.105}$$

The regions allowed for $\Delta C_1(M_W)$ and $\Delta C_2(M_W)$ are presented in Fig.4.13, 4.14 and 4.15 for a^s_{sl}, a^d_{sl} and $\Delta\Gamma_s$ respectively. In all these cases the new contributions $\Delta C_{1,2}(M_W)$ are treated in a universal fashion assuming $\Delta C_1^{uu}(M_W) = \Delta C_1^{uc}(M_W) = \Delta C_1^{cc}(M_W) = \Delta C_1(M_W)$ (and the same for $\Delta C_2(M_W)$). The error budgets for a^s_{sl}, a^d_{sl} , $\Delta\Gamma_s$ and $\Delta\Gamma_d$ appear in Tab.4.10, 4.11, 4.12 and 4.13 respectively [15].

Parameter	Standard analysis
$\delta(\mu)$	9.5%
$\delta(\lvert V_{ub}/V_{cb}\rvert)$	5.0%
$\delta(\bar{z})$	4.6%
$\delta(B_{\tilde{R}_3})$	2.6%
$\delta(\gamma)$	1.3%
$\delta(B_{R_3})$	1.1%
$\delta(m_b)$	1.0%
$\delta(m_t)$	0.7%
$\delta(\alpha_s)$	0.5%
$\delta(B_{\tilde{R}_1})$	0.5%
$\delta(\widetilde{B}_S)$	0.3%
$\delta(\mathcal{B}_{R_0})$	0.2%
$\delta(\mathcal{B}_{R_2})$	0.1%
$\delta(m_s)$	0.1%
$\delta(\mathcal{B}_{R_1})$	$< 0.1\%$
$\delta(\lvert V_{cb}\rvert)$	0.0%
$\sum \delta$	12.2%

Table 4.10: Error budget for the observable a_{sl}^s.

Parameter	Standard analysis
$\delta(B_{\widetilde{R}_2})$	0.1%
$\delta(\mu)$	9.4%
$\delta(\lvert V_{cb}\rvert)$	0.0%
$\delta(\widetilde{B}_S)$	0.6%
$\delta(B_{R_0})$	0.2%
$\delta(\bar{z})$	4.9%
$\delta(m_b)$	1.3%
$\delta(B_{\tilde{R}_3})$	2.7%
$\delta(B_{R_3})$	1.2%
$\delta(\gamma)$	1.1%
$\delta(\alpha_s)$	0.5%
$\delta(\lvert V_{ub}/V_{cb}\rvert)$	5.2%
$\delta(\bar{m}_t(\bar{m}_t)$	0.7%
$\sum\delta$	12.3%

Table 4.11: Error budget for the observable $a_{\rm sl}^{d}$.

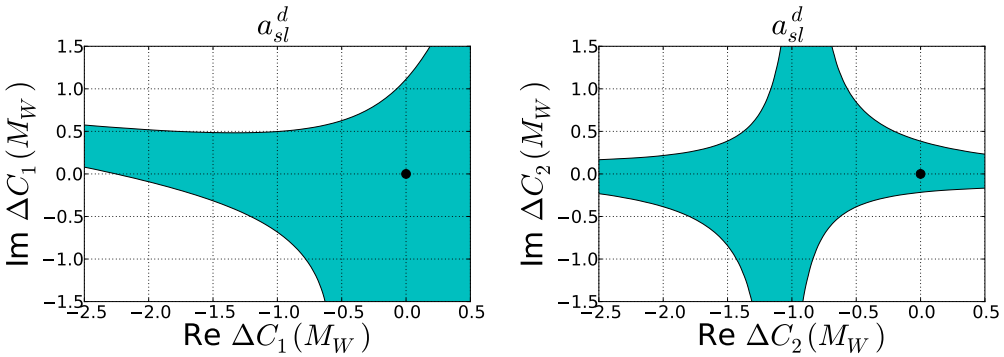

Figure 4.14: Regions for new physics, at 90% C. L., in the $\mathcal{R}e\ \Delta C_1$ - $\mathcal{I}m\ \Delta C_1$ (left) and $\mathcal{R}e\ \Delta C_2$ - $\mathcal{I}m\ \Delta C_2$ (right) planes allowed by the observable a_{sl}^{d} in the standard analysis. The black point corresponds to the SM value. Here we are assuming universality: $\Delta C_{1,2}^{d,uu} = \Delta C_{1,2}^{d,uc} = \Delta C_{1,2}^{d,cc} = \Delta C_{1,2}$.

Parameter	Standard analysis
$\delta(B_{\tilde{R}_2})$	14.8%
$\delta(f_{B_s}\sqrt{B})$	13.9%
$\delta(\mu)$	8.4%
$\delta(\lvert V_{cb}\rvert)$	4.9%
$\delta(\widetilde{B}_S)$	2.1%
$\delta(B_{R_0})$	2.1%
$\delta(\bar{z})$	1.1%
$\delta(m_b)$	0.8%
$\delta(B_{\tilde{R}_1})$	0.7%
$\delta(B_{\tilde{R}_3})$	0.6%
$\delta(B_{R_1})$	0.5%
$\delta(B_{R_3})$	0.2%
$\delta(m_s)$	0.1%
$\delta(\gamma)$	0.1%
$\delta(\alpha_s)$	0.1%
$\delta(\lvert V_{ub}/V_{cb}\rvert)$	0.1%
$\delta(\bar{m}_t(\bar{m}_t)$	0.0%
$\sum\delta$	22.8%

Table 4.12: Error budget for the observable $\Delta\Gamma_s$.

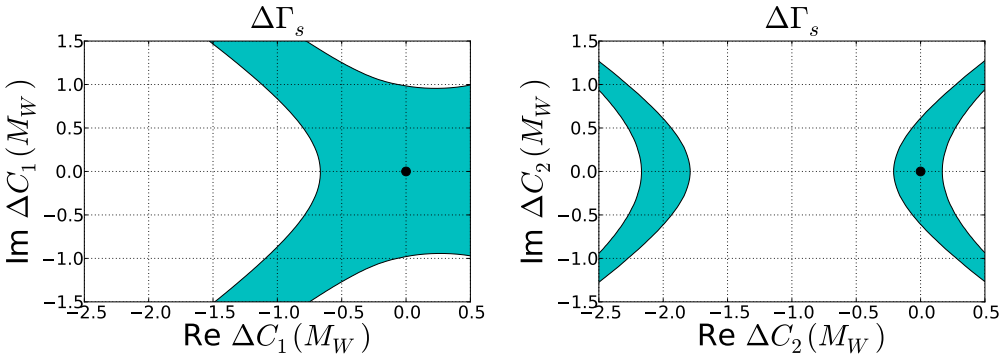

Figure 4.15: Regions for new physics, at 90% C. L., in the $\mathcal{R}e\ \Delta C_1$ - $\mathcal{I}m\ \Delta C_1$ (left) and $\mathcal{R}e\ \Delta C_2$ - $\mathcal{I}m\ \Delta C_2$ (right) planes allowed by the observable $\Delta\Gamma_s$ in the standard analysis. The black point corresponds to the SM value. Here we are assuming universality: $\Delta C_{1,2}^{s,uu} = \Delta C_{1,2}^{s,uc} = \Delta C_{1,2}^{s,cc} = \Delta C_{1,2}$.

Parameter	Standard analysis
$\delta(f_{B_d}\sqrt{B})$	13.7%
$\delta(\mu)$	7.9%
$\delta(\lvert V_{cb}\rvert)$	4.9%
$\delta(\widetilde{B}_S)$	4.0%
$\delta(B_{R_0})$	2.5%
$\delta(\bar{z})$	1.1%
$\delta(m_b)$	0.8%
$\delta(B_{\tilde{R}_1})$	0%
$\delta(B_{\tilde{R}_3})$	0.5%
$\delta(B_{R_1})$	0%
$\delta(B_{R_3})$	0.2%
$\delta(\gamma)$	0.2%
$\delta(\alpha_s)$	0.1%
$\delta(\lvert V_{ub}/V_{cb}\rvert)$	0.1%
$\delta(\bar{m}_t(\bar{m}_t)$	0.1%
$\sum\delta$	22.7%

Table 4.13: Error budget for the observable $\Delta\Gamma_d$.

4.8 Global fit results

In this section we present the overall regions for $\Delta C_1(M_W)$ and $\Delta C_2(M_W)$ obtained after combining observables for the different exclusive b quark transitions described within this chapter. We will start by updating the combinations for the decay channels $b \to u\bar{u}d$, $b \to c\bar{u}d$ and $b \to c\bar{c}d$ presented in [2]. New tree level physics contributions in these decay chains are of special interest in the investigation of BSM effects in decay width difference of neutral B_d^0 mesons, $\Delta\Gamma_d$. At the end of this section we will present results for our universal fit obtained when all the new physics contributions $\Delta C_1(M_W)$ and $\Delta C_2(M_W)$ are treated in the same way, this will allow us to determine the strongest bounds and to present an updated version on the possible impact on the measurement of the CKM phase γ reported in [92].

4.8.1 Global fit on $b \to u\bar{u}d$

Our first combined fit includes observables with the quark level transition $b \to u\bar{u}d$. In this case $\Delta C_1^{d,uu}(M_W)$ and $\Delta C_2^{d,uu}(M_W)$ are sensitive to different experimentally measurable quantities. For instance to calculate the regions for $\Delta C_1^{d,uu}(M_W)$ we included $R_{\pi\pi}$, $R_{\rho\rho}$ and a_{sl}^d (see left plot in Fig.4.16). On the other hand the constraints for $\Delta C_2^{d,uu}(M_W)$ (presented in the right plot in Fig. (4.16)) were derived considering $R_{\pi\pi}$, $S_{\pi\pi}$ and $S_{\rho\pi}$.

For $\Delta C_2^{d,uu}(M_W)$ we get the following limits

$$\begin{aligned} -2.38 < \mathcal{R}e\ \Delta C_1^{d,uu}(M_W) < 0.36, \qquad -1.27 < \mathcal{I}m\ \Delta C_1^{d,uu}(M_W) < 1.40. \\ -1.17 < \mathcal{R}e\ \Delta C_2^{d,uu}(M_W) < 0.38, \qquad -1.05 < \mathcal{I}m\ \Delta C_2^{d,uu}(M_W) < 1.00. \end{aligned} \tag{4.8.106}$$

The possible enhancements on $\Delta\Gamma_d$ due to $\Delta C_1^{d,uu}(M_W)$ and $\Delta C_2^{d,uu}(M_W)$ are

$$0.00 < \Delta\Gamma_d/\Delta\Gamma_d^{SM} < 1.44, \qquad 0.55 < \Delta\Gamma_d/\Delta\Gamma_d^{SM} < 1.76. \tag{4.8.107}$$

4.8.2 Global fit on $b \to c\bar{u}d$

To constrain $\Delta C_1^{d,cu}(M_W)$ and $\Delta C_2^{d,cu}(M_W)$, associated with the decay $b \to c\bar{u}d$, we included $R_{D^*\pi}$, S_{D^*h} and a_{sl}^d. The combined fit appears in Fig.4.17. The current

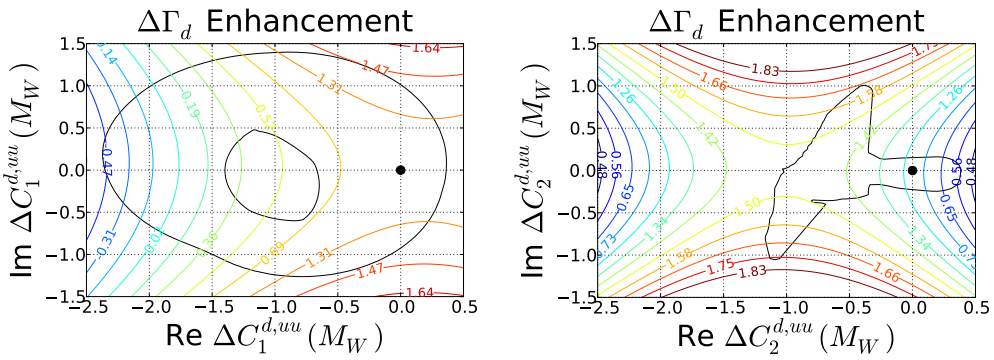

Figure 4.16: Combined fit for $\Delta C_1^{uu}(M_W)$ (black contours, left) and $\Delta C_2^{uu}(M_W)$ (black contours, right) at 90% C. L.. The coloured contour lines indicate the possible enhancements on $\Delta\Gamma_d$ with respect to the SM value. The black dot corresponds to the SM result.

experimental uncertainty associated with $\Delta\Gamma_d$ allows enhancement factors within the interval

$$-3.91 < \Delta\Gamma_d^{exp}/\Delta\Gamma_d^{SM} < 2.60. \tag{4.8.108}$$

However, the new physics regions for $\Delta C_1^{d,cu}(M_W)$ break the upper limit established in Eq.(4.8.108). Therefore, in order to be consistent with the experimental results available, we use $\Delta\Gamma_d$ to define the possible limits for $\Delta C_1^{d,cu}(M_W)$ and obtain

$$-1.12 < \mathcal{R}e\ \Delta C_1^{d,cu}(M_W) < 0.31 \qquad -0.70 < \mathcal{I}m\ \Delta C_1^{d,cu}(M_W) < 1.08. \tag{4.8.109}$$

The regions allowed for $\Delta C_2^{d,cu}(M_W)$ provide the following limits

$$-2.07 < \mathcal{R}e\ \Delta C_2^{d,cu}(M_W) < 0.06 \qquad -0.47 < \mathcal{I}m\ \Delta C_2^{d,cu}(M_W) < 0.63, \tag{4.8.110}$$

leading to enhancement factors on $\Delta\Gamma_d$ inside the interval

$$-0.93 < \Delta\Gamma_d/\Delta\Gamma_d^{SM} < 2.18. \tag{4.8.111}$$

4.8.3 Global fit on $b \to c\bar{c}d$

The allowed regions for $\Delta C_2^{d,cc}(M_W)$ are established using the observables $\mathcal{B}_r(B \to X_d\gamma)$, a_{sl}^d and M_{12}^d. As can be seen in Fig.4.18 the possible values for the real and the

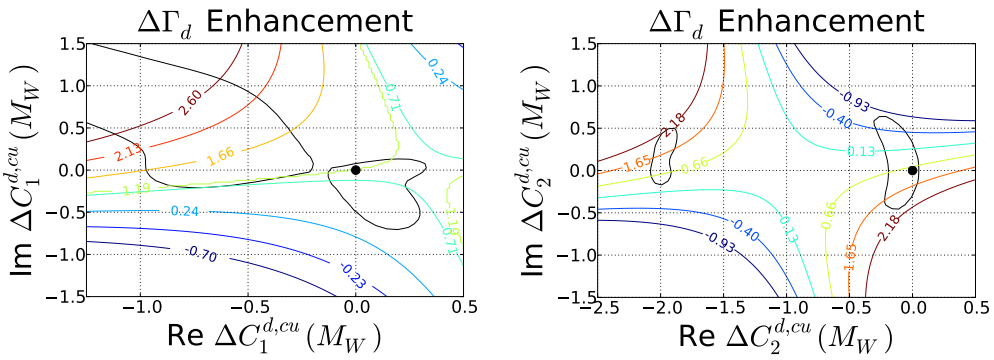

Figure 4.17: Combined fit for $\Delta C_1^{cu}(M_W)$ (black contours, left) and $\Delta C_2^{cu}(M_W)$ (black contours, right) at 90% C. L.. The coloured contour lines indicate the possible enhancements on $\Delta\Gamma_d$ with respect to the SM value. The black dot corresponds to the SM result.

imaginary components of $\Delta C_2^{d,cc}(M_W)$ completely saturate the experimental bounds on the enhancement for $\Delta\Gamma_d$ in Eq.(4.8.108). Hence we use the information on $\Delta\Gamma_d$ to establish limits on the real and the imaginary components of $\Delta C_2^{d,cc}(M_W)$. We get

$$-2.41 < \mathcal{R}e\ \Delta C_2^{d,cc}(M_W) < 0.43, \qquad -0.36 < \mathcal{I}m\ \Delta C_2^{d,cc}(M_W) < 1.34. \tag{4.8.112}$$

4.8.4 Universal fit on $\Delta C_1(M_W)$ and $\Delta C_2(M_W)$

Working under the assumptions $\Delta C_1^{s,ab}(M_W) = \Delta C_1^{d,ab}(M_W) = \Delta C_1(M_W)$ and $\Delta C_2^{s,ab}(M_W) = \Delta C_2^{d,ab}(M_W) = \Delta C_2(M_W)$ we are able to derive the strongest bounds on new physics at tree level b quark decays. Making a combined fit is time and resource consuming, consequently we select the set of observables that give the strongest constraints in $\Delta C_1(M_W)$ and $\Delta C_2(M_W)$ (the observables not included do not change our conclusions). For $\Delta C_1(M_W)$ the relevant set includes $R_{\pi\pi}$, $R_{D^*\pi}$, S_{D^*h}, $\mathcal{B}_r(\bar{B} \to X_s\gamma)$, $\sin(2\beta_d)$, a_{sl}^s, $\Delta\Gamma_s$ and a_{sl}^d. For $\Delta C_2(M_W)$ the corresponding measurable quantities are $S_{\rho\pi}$, $R_{D^*\pi}$, S_{D^*h}, $\mathcal{B}_r(\bar{B} \to X_s\gamma)$, a_{sl}^s, $\Delta\Gamma_s$ and a_{sl}^d. The new physics regions allowed for $\Delta C_{1,2}(M_W)$ are presented in Fig.4.19, these two plots are an upgrade of the ones reported in [3]. However, our approach here is by

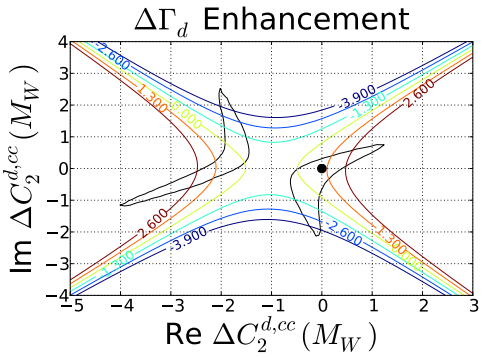

Figure 4.18: Regions for new physics in $\Delta C_2^{cc}(M_W)$ (black contours) allowed by the observables $B \to X_d\gamma$, M_{12}^d and a_{sl}^d. The contour lines indicate the possible enhancements on $\Delta\Gamma_d$ with respect to the SM value. The black dot corresponds to the SM result.

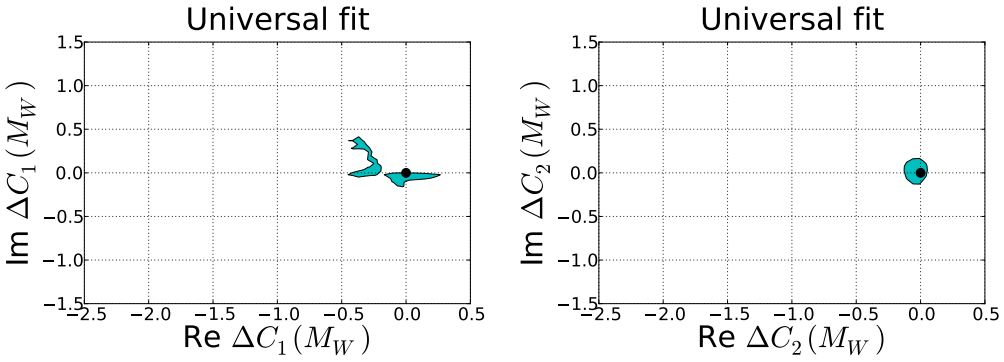

Figure 4.19: Universal constraints over $\Delta C_1(M_W)$ (left) and $\Delta C_2(M_W)$ (right). The black dot corresponds to the SM result.

far more rigorous than the one followed in that publication, in the end the results of both analyses are consistent. Based on the plots presented in Fig.4.19 we determine the following bounds on $\Delta C_1(M_W)$ and $\Delta C_2(M_W)$

$$-0.45 < \mathcal{R}e\ \Delta C_1(M_W) < 0.26 \qquad -0.16 < \mathcal{I}m\ \Delta C_1(M_W) < 0.41$$
$$-0.13 < \mathcal{R}e\ \Delta C_2(M_W) < 0.06 \qquad -0.12 < \mathcal{I}m\ \Delta C_2(M_W) < 0.17. \quad (4.8.113)$$

4.8.5 New Physics in the CKM phase γ

The determination of the CKM phase γ has already been discussed in Section 1.4.2. As it was mentioned, the sensitivity to γ arises from the interference between the

amplitudes associated with the quark level decay channels $b \to c\bar{u}s$ and $b \to u\bar{c}s$. At exclusive level the transitions of interest are $B^- \to D^0 K^-$ and $B^- \to \bar{D}^0 K^-$. Theoretical corrections to the extraction of γ have been investigated extensively in the literature, for instance the effects of $D - \bar{D}$ mixing and of CP violation in D and K decays (for final states with neutral kaons) have been studied in [93–98]. These effects lead to shifts in γ of at most a few degrees and can be taken into account by a suitable modification of the expressions for the amplitudes. The shifts can be larger in the $B \to D\pi$ modes. The irreducible theoretical uncertainty is due to higher-order electroweak corrections and has been found to be negligible for the extraction of γ using the $B \to DK$ modes $|\delta\gamma| < \mathcal{O}(10^{-7})$ [99]. It is expected to be tiny also in the $B \to D\pi$ case $|\delta\gamma/\gamma| < \mathcal{O}(10^{-4})$ [92].

Considering the expected precision of order 1° at LHCb [100] and Belle II [101] we now address the following question: How large of a shift in γ due to new-physics contributions in tree-level decays is still allowed by data? Our starting point for the computation of $\delta\gamma$ induced by ΔC_1 and ΔC_2, is the effective Hamiltonian for $b \to c\bar{u}s$ and $b \to u\bar{c}s$ decays. Denote by $\mathcal{H}^{\bar{u}_1 u_2 d_1}$ the effective Hamiltonian for the non-leptonic b-quark decays of the form $b \to u_1 \bar{u}_2 d_1$, where $u_{1,2}$ are up-type quarks and d_1 is a down-type quark:

$$\mathcal{H}^{\bar{u}_1 u_2 d_1} = \frac{G_F}{\sqrt{2}} V_{u_1 b} V^*_{u_2 d_1} \Big[C_1 \hat{Q}_1^{\bar{u}_1 u_2 d_1} + C_2 \hat{Q}_2^{\bar{u}_1 u_2 d_1} \Big] \tag{4.8.114}$$

with

$$Q_1^{\bar{u}_1 u_2 d_1} = (\bar{u}_1^\alpha b^\beta)_{V-A} (\bar{d}_1^\beta u_2^\alpha)_{V-A}, \qquad Q_2^{\bar{u}_1 u_2 d_1} = (\bar{u}_1^\alpha b^\alpha)_{V-A} (\bar{d}_1^\beta u_2^\beta)_{V-A} \tag{4.8.115}$$

where α and β are colour indices.

We will consider the amplitudes

$$\mathcal{A}(B^- \to D^0 K^-) = \langle D^0 K^- | \mathcal{H}_{\text{eff.}}^{\bar{c}us} | B^- \rangle \quad \text{and} \quad \mathcal{A}(B^- \to \bar{D}^0 K^-) = \langle \bar{D}^0 K^- | \mathcal{H}_{\text{eff.}}^{\bar{u}cs} | B^- \rangle \,. \tag{4.8.116}$$

The CKM angle γ can be extracted from the ratio of these two amplitudes via

$$r_B e^{i(\delta_B - \gamma)} = \frac{A(B^- \to \bar{D}^0 K^-)}{A(B^- \to D^0 K^-)} \,. \tag{4.8.117}$$

Inserting the expressions for the corresponding effective Hamiltonians we get

$$r_B e^{i(\delta_B - \gamma)} = \frac{V_{ub} V^*_{cs}}{V_{cb} V^*_{us}} \frac{\langle \bar{D}^0 K^- | Q_2^{\bar{u}cs} | B^- \rangle}{\langle D^0 K^- | Q_2^{\bar{c}us} | B^- \rangle} \left[\frac{C_2 + r_{A'} C_1}{C_2 + r_A C_1} \right] \,, \tag{4.8.118}$$

where we have defined the additional ratios

$$r_{A'} = \frac{\langle \bar{D}^0 K^- | Q_1^{\bar{u}cs} | B^- \rangle}{\langle \bar{D}^0 K^- | Q_2^{\bar{u}cs} | B^- \rangle} \,, \quad r_A = \frac{\langle D^0 K^- | Q_1^{\bar{c}us} | B^- \rangle}{\langle D^0 K^- | Q_2^{\bar{c}us} | B^- \rangle} \,. \tag{4.8.119}$$

New physics effects in C_1 and C_2 then modify $r_B e^{i(\delta_B - \gamma)}$ as

$$r_B e^{i(\delta_B-\gamma)} \to r_B e^{i(\delta_B-\gamma)} \cdot \left[\frac{C_2 + \Delta C_2 + r_{A'}(C_1 + \Delta C_1)}{C_2 + r_{A'} C_1} \frac{C_2 + r_A C_1}{C_2 + \Delta C_2 + r_A (C_1 + \Delta C_1)} \right] . \tag{4.8.120}$$

Thus any new complex contribution to C_1 and/or C_2 will introduce a shift in γ. Using the fact that $|C_1(m_b)/C_2(m_b)| \approx 0.22$ and that $|\Delta C_1(m_b)/C_2(m_b)|$ and $|\Delta C_2(m_b)/C_2(m_b)|$ are small we can further simplify Eq.(4.8.120) by expanding in these small ratios to obtain:

$$r_B e^{i(\delta_B-\gamma)} \to r_B e^{i(\delta_B-\gamma)} \cdot \left[1 + (r_{A'} - r_A) \frac{\Delta C_1}{C_2} \right] . \tag{4.8.121}$$

For the computations of $\delta\gamma$ in this section we use the full formula in Eq.(4.8.120). To proceed with the numerical evaluations we have to assign values to r_A and $r_{A'}$, considering that the corresponding matrix elements have not been calculated from first principles yet we made an estimation using colour counting and get $r_A \approx \mathcal{O}(1)$ and $r_{A'} \approx \mathcal{O}(3)$. Where the annihilation topologies have been omitted during the determination of $r_{A'}$; including the annihilation topologies gives a smaller value for $r_{A'}$. Using naive factorization arguments we get

$$r_A \approx \frac{f_D F_0^{B\to K}(0)}{f_K F_0^{B\to D}} \approx 0.4. \tag{4.8.122}$$

There are certainly large uncertainties on these estimates, but it seems very unlikely that the two ratios r_A and $r_{A'}$ cancel accidentally. As a conservative estimate we take $r_A - r_{A'} \approx -0.6$ [3] with r_A as in Eq.(4.8.122). Regarding the high experimental precision available in the determination of γ we use the results from the universal fit in Section 4.8.4 to analyse the effect of possible new physics deviations at tree level. The results are presented in Fig.4.20; since the possible values for $\delta\gamma$ induced by $\Delta C_1(M_W)$ saturate the current experimental uncertainty $-6.30^\circ < \delta\gamma < 7.00^\circ$ [17] we use CKM γ as an extra constraint on the complex components of $\Delta C_1(M_W)$, thus we update the bounds given in Eq.(4.8.113) to

$$-0.45 < \mathcal{R}e\ \Delta C_1(M_W) < 0.26 \qquad -0.16 < \mathcal{I}m\ \Delta C_1(M_W) < 0.10. \tag{4.8.123}$$

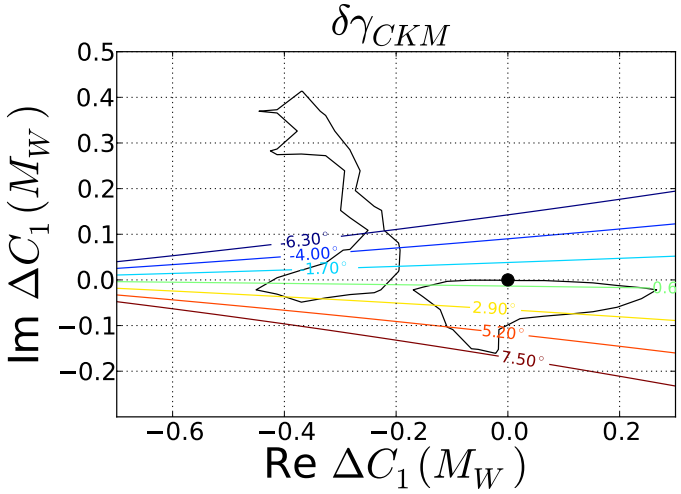

Figure 4.20: Possible deviations on the CKM phase γ due to new physics at tree level in $C_1(M_W)$. The black dot corresponds to the SM result.

Chapter 5

New physics in $\Delta\Gamma_d$

5.1 Introduction

In this chapter we devote our attention to investigate the possible sources of enhancement on the decay width difference of neutral B_d^0 mesons $\Delta\Gamma_d$ with respect to the value given in the SM. Our interest for this study was triggered by the possibility of using $\Delta\Gamma_d$ to reduce the tension between theory and experiment in the like-sign dimuon asymmetry [102], measured by the D0 collaboration [103–107]. In the latest experimental result [107] the $\mathcal{CP}$ violation component of the like sign dimuon measurement was reported in terms of the residual charge asymmetry A_{CP}. Unfortunately, as it will be discussed in Section 5.3.3, there are conceptual problems with the theoretical formula presented in [102] that can spoil the connection between A_{CP} and $\Delta\Gamma_d$. In spite of this fact the search for room for new physics in $\Delta\Gamma_d$ is well justified because its current experimental determination still allows an enhancement of several 100% with respect to its SM value.

We begin in Section 5.2 by showing how $\Delta\Gamma_d$ and $\Delta\Gamma_s$ are affected differently by possible new physics effects. Then in Section 5.3 we provide a brief review of A_{CP} as the result of $\mathcal{CP}$ violation in mixing and interference, explaining the connection between the interference component and $\Delta\Gamma_d$. In order to explore new physics effects we follow a model independent approach. We start by summarizing the results found in Section 4.8, where the enhancements on $\Delta\Gamma_d$ as the result of new physics in the tree level decay channels $b \to u\bar{u}d$, $b \to c\bar{u}d$ and $b \to u\bar{u}d$ were discussed.

Then as a second possibility we analyse in Section 5.5 the constraints on new-physics contributions from operators of the form $(\bar{d}b)(\bar{\tau}\tau)$. We show that since the existing constraints imposed by tree-level and loop-level mediated B-meson decays, such as $\bar{B}_d^0 \to \tau^+\tau^-$ and $B^+ \to \pi^+\mu^+\mu^-$ are quite loose, sizeable modifications of $\Delta\Gamma_d$ and a_{sl}^d are possible, in particular, if they arise from vector operators.

5.2 Comparison between $\Delta\Gamma_d$ and $\Delta\Gamma_s$

The first important observation is that $\Delta\Gamma_d$ is triggered by the CKM-suppressed decay $b \to c\bar{c}d$, whose inclusive branching ratio reads $(1.31 \pm 0.07)\%$ (based on the numerical evaluation in [108]), while $\Delta\Gamma_s$ receives the dominant contribution from the CKM-favoured decay $b \to c\bar{c}s$, which has an inclusive branching ratio of $(23.7 \pm 1.3)\%$ [108]. This means that a relative modification of $\Gamma(b \to c\bar{c}d)$ by 100% shifts the total b-quark decay rate $\Gamma_{\rm tot}$[1] by around 1% only, while a 100% variation in $\Gamma(b \to c\bar{c}s)$ results in an effect of roughly 25% in the same observable. Large enhancement of the $b \to c\bar{c}d$ decay rate can therefore be hidden in the hadronic uncertainties of $\Gamma_{\rm tot}$, while this is not possible in the case of the $b \to c\bar{c}s$ decay rate. The structure of $\Gamma_{12}^{q,\rm SM}$ and $(\Gamma_{12}^q/M_{12}^q)_{\rm SM}$ presented in Eq.(2.4.114) -for $q = d, s$- allows to draw some general conclusions on how new physics can modify $\Delta\Gamma_{d,s}$ and $a_{sl}^{d,s}$. Consider for instance the violation of the CKM unitarity $\lambda_u^q + \lambda_c^q + \lambda_t^q = \Delta_{\rm CKM}^q$, a property known from beyond the SM scenarios (see e.g. [109–111]) in which heavy fermions mix with the SM quarks and/or new charged gauge bosons mix with the W boson.[2] In such models Eq.(2.4.114) would receive a shift that can be approximated by

$$\Delta\left(\frac{\Gamma_{12}^q}{M_{12}^q}\right) \simeq (-48.75 \pm 8.35)\left[\left(1 - \frac{\Delta_{\rm CKM}^q}{\lambda_t^q}\right)^2 - 1\right] \cdot 10^{-4}\,. \tag{5.2.1}$$

Given our imperfect knowledge of some of the elements of the CKM matrix, deviations of the form $\Delta_{\rm CKM}^d \simeq \Delta_{\rm CKM}^s = \mathcal{O}(\lambda^3)$ are not excluded phenomenologically.

[1] We do not distinguish here between the total B-meson decay rates Γ_{B_d}, Γ_{B_s} and Γ_{B^+} and the total b-quark decay rate $\Gamma_{\rm tot}$, because the measured differences are smaller than the current theoretical uncertainties.

[2] See also [112] for a recent discussion of a similar point.

From Eq.(5.2.1) we then see that such a pattern of CKM unitarity violation can lead to a relative enhancement of $|\Gamma_{12}^d/M_{12}^d|$ by up to 300%, while in the case of $|\Gamma_{12}^s/M_{12}^s|$ the relative shifts can be 50% at most. Depending on the phase of $\Delta_{\rm CKM}^d/\lambda_t^d$ the new contribution in Eq.(5.2.1) could hence affect $\Delta\Gamma_d$ and a_{sl}^d in a significant way, while leaving ΔM_d, ΔM_s, $\Delta\Gamma_s$ and a_{sl}^s unchanged within the hadronic uncertainties.

5.3 The like-sign dimuon asymmetry

The $D0$ collaboration measured the like-sign dimuon charge asymmetry in $p\bar{p}$ collisions at $\sqrt{s} = 1.96$TeV [103–107] defined as

$$A \equiv \frac{N^{++} - N^{--}}{N^{++} + N^{--}}. \tag{5.3.2}$$

In Eq.(5.3.2) N^{++} and N^{--} represent the number of events containing pairs $\mu^+\mu^+$ and $\mu^-\mu^-$ respectively. In all the experimental measurements reported so far the $\mathcal{CP}$ violation component of A has shown discrepancies with respect to the SM expectations. In the latest experimental analysis [107] A is written in terms of the background term A_{bkg} and the residual dimuon charge asymmetry A_{CP} as

$$A = A_{CP} + A_{bkg}. \tag{5.3.3}$$

Then A_{CP} is further decomposed according to

$$A_{CP} = F_{SS}A_S + F_{SL}a_S, \tag{5.3.4}$$

where A_S is the result of B and $\bar{B}$ mesons decaying into $\mu^+\mu^+$ and $\mu^-\mu^-$ pairs, it does include contributions from $\mathcal{CP}$ violation in mixing (A_S^{mix}) and $\mathcal{CP}$ violation in interference (A_S^{int})

$$A_S = A_S^{mix} + A_S^{int}. \tag{5.3.5}$$

In addition, in Eq.(5.3.5) a_S quantifies the asymmetry from single muon production, F_{SS} is the experimental sensitivity to two "long" lived muons and F_{SL} determines

the sensitivity to one "short" and one "long" lived muon [3].

The semileptonic charge asymmetry is directly computed from the semileptonic asymmetries a^d_{sl} and a^d_{sl} as the result of $\mathcal{CP}$ violation in interference, this will be shown in Section 5.3.1

$$A^b_{sl} = C^s a^s_{sl} + C^d a^d_{sl}. \tag{5.3.6}$$

According to the information provided by D0 [104–107] A^{mix}_S and a_S can be expressed in terms of the semileptonic charge asymmetry A^b_{sl} as

$$A^{mix}_S = C_b A^b_{sl} \qquad a_S = c_b A^b_{sl}, \tag{5.3.7}$$

the coefficients C_b and c_b are obtained by experimentalist from simulation; as a rough estimation $C_b \in (0.45, 0.58)$ and $c_b \in (0.03, 0.11)$, the latest values can be found in [107].

Before 2013 the theoretical explanation behind A_S in Eq.(5.3.5) considered only A^{mix}_S, based on this interpretation the experimental result in [106] showed a 4.2 σ deviation with respect to the SM value. Then in [102] $\mathcal{CP}$ violation in interference was included A^{int}_S, as a matter of fact one of the conclusions of the analysis developed in [102] was $A^{int}_S \propto \frac{\Delta\Gamma_d}{\Gamma_d}$. Combining Eq.(5.3.4), Eq.(5.3.5), Eq.(5.3.7) and Eq.(5.3.6) we can formally write [107]

$$A_{CP} \;=\; C^s_{sl} a^s_{sl} + C^d_{sl} a^d_{sl} + C_{int} \frac{\Delta\Gamma_d}{\Gamma_d}. \tag{5.3.8}$$

The coefficients $C^s_{sl},\ C^d_{sl},\ C_{int}$ can be computed from the equations introduced in this section and the numerical inputs provided in e.g. [107], this will not be necessary for this chapter. The corresponding set of values used for our investigation of duality violation appears in Chapter 6 in Tab.6.4.

The formula presented in Eq.(5.3.8) has, in principle, potential for explaining the measured value for A_{CP} as the result of new physics in $\Delta\Gamma_d$. Nevertheless, a closer

[3] According to [107] "long" lived muons are those produced by particles travelling long distances before decaying within the detector. In contrast "short" lived muons are the result of the decay of particles within the beam pipe at small distances from the $p\bar{p}$ interaction point. Short lived muons are considered signal since their production is not affected by interactions in the detector material, on the other hand long lived muons are treated as background.

look at the derivation presented in [102] shows that some assumptions made should be reviewed before accepting Eq.(5.3.8) as the correct theoretical interpretation behind the measurements reported by D0. In order to gain a deeper understanding of the issues related with Eq.(5.3.8), we review in Section 5.3.1 and Section 5.3.2 how A_S^{mix} and A_S^{int} arise respectively. Finally in Section 5.3.3 we discuss the conceptual problems identified by the flavour physics community on the interference term $A_S^{int} = C_{int}\frac{\Delta\Gamma_d}{\Gamma_d}$.

5.3.1 $\mathcal{CP}$ violation in mixing contribution

To begin our discussion we write A_{sl}^b in Eq.(5.3.7) as

$$A_{sl}^b = \frac{\Gamma\Big(b\bar{b} \to \mu^+\mu^+X\Big) - \Gamma\Big(b\bar{b} \to \mu^-\mu^-X\Big)}{\Gamma\Big(b\bar{b} \to \mu^+\mu^+X\Big) + \Gamma\Big(b\bar{b} \to \mu^-\mu^-X\Big)}. \tag{5.3.9}$$

Where $\Gamma\Big(b\bar{b} \to \mu^{+(-)}\mu^{+(-)}X\Big)$ are the partial decay widths of the like-sign muon pairs produced from the decays of neutral B mesons. For the purposes of our discussion it is more convenient to address these contributions in terms of the $b(\bar{b})$ quarks inside the mesons rather than the mesons themselves. Here we assume that each one of the muons in a particular like-sign dimuon pair is generated by a different neutral B-meson; moreover, we assume that the μ particles are produced from the decay products of the b quarks inside the hadrons. A muon is considered to be "right sign" (RS) if the sign of its electric charge matches the sign of the charge of the b-quark inside the neutral meson from which it was generated. Otherwise the muon is labelled as "wrong sign" (WS). Consider the first term in the numerator of Eq.(5.3.9), we make the following factorization

$$\Gamma\Big(b\bar{b} \to \mu^+\mu^+X\Big) = \Gamma_{RS}^+\Gamma_{WS}^+. \tag{5.3.10}$$

Here Γ_{RS}^+ and Γ_{WS}^+ correspond to the partial widths associated with the production of a μ^+ out of a neutral meson containing a $\bar{b}$ and a b quark respectively. Being rigorous, for each one of the partial widths there are two possible $\mathcal{CP}$ violation mechanisms entering, to illustrate this point consider for example Γ_{WS}^+

$$\Gamma_{WS}^+ = \Gamma_{mix,WS}^+ + \Gamma_{int,WS}^+. \tag{5.3.11}$$

In Eq.(5.3.11) $\Gamma^{+}_{mix,WS}$ is the decay width of the decay chain $\bar{B}^0_{d,s} \to B^0_{d,s} \to \mu^+ + X$, i.e. is the result of the mixing process of neutral B-mesons. Using the notation followed in [102] we will denote the mixing subprocesses $\bar{B}^0_{d,s} \to B^0_{d,s}$ as $b \to \bar{b}$ and $B^0_{d,s} \to \bar{B}^0_{d,s}$ as $\bar{b} \to b$ whenever this becomes more convenient. The interference width $\Gamma^{+}_{int,WS}$ results from the inclusive decay chain $b \to f \to \mu + X'$ where f is a common state in which the $\bar{B}^0_{s,d}$ and the $B^0_{s,d}$ mesons can decay, we will elaborate on this contribution in Section 5.3.2, then in order to keep our explanation as simple as possible, we will ignore all the interference effects in the remainder of this section. The explicit formula for $\Gamma^{+}_{mix,WS}$ is

$$\Gamma^{+}_{mix,WS} = f_d T(\bar{B}^0_d \to B^0_d)\Gamma^d_{sl} + f_s T(\bar{B}^0_s \to B^0_s)\Gamma^s_{sl}, \tag{5.3.12}$$

where $f_{d,s}$ are the experimental production fractions of $B_{d,s}$; $T(\bar{B}^0_{d,s} \to B^0_{d,s})$ are the time integrated mixing probabilities and $\Gamma^{d,s}_{sl}$ are the semileptonic widths for $B^0_{d,s}$ decaying into μ^+ (the subindex "*sl*" stands for "semileptonic").
In a similar way we write for the right sign component in Eq.(5.3.10)

$$\Gamma^{+}_{mix,RS} = f_d T(B^0_d \to B^0_d)\Gamma^d_{SL} + f_s T(B^0_s \to B^0_s)\Gamma^s_{SL}, \tag{5.3.13}$$

the definitions of the different factors in Eq.(5.3.13) are analogous to those already introduced for Eq.(5.3.12).
The treatment for $\Gamma\Big(b\bar{b} \to \mu^-\mu^- X\Big)$ in the numerator of Eq.(5.3.9) is similar to the one followed for $\Gamma\Big(b\bar{b} \to \mu^+\mu^+ X\Big)$ in particular we have

$$\Gamma\Big(b\bar{b} \to \mu^-\mu^- X\Big) = \Gamma^-_{RS}\Gamma^-_{WS}, \tag{5.3.14}$$

with

$$\begin{aligned}
\Gamma^-_{mix,WS} &= f_d T(B^0_d \to \bar{B}_d)\Gamma^d_{sl} + f_s T(B^0_s \to \bar{B}_s)\Gamma^s_{sl}, \\
\Gamma^-_{mix,RS} &= f_d T(\bar{B}^0_d \to \bar{B}^0_d)\Gamma^d_{sl} + f_s T(\bar{B}^0_s \to \bar{B}^0_s)\Gamma^s_{sl}.
\end{aligned} \tag{5.3.15}$$

In our previous discussion we have followed the assumption made by experimentalists [104] of having the same production fractions f_d and semileptonic decay rates Γ^d_{sl} for B^0_d and $\bar{B}^0_d$ mesons (and correspondingly for B^0_s and $\bar{B}^0_s$), under this consideration the following equality holds

$$\Gamma^{+}_{mix,RS} = \Gamma^{-}_{mix,RS}, \tag{5.3.16}$$

and Eq.(5.3.9) becomes

$$A_{sl}^{b} = \frac{\Gamma_{mix,WS}^{+} - \Gamma_{mix,WS}^{-}}{\Gamma_{mix,WS}^{+} + \Gamma_{mix,WS}^{-}}. \tag{5.3.17}$$

The time integrated probabilities in Eq.(5.3.12) and Eq.(5.3.15) can be obtained from the time integrals of the functions $g_{\pm}(t)$ in Eq.(1.3.61) and Eq.(1.3.63) according to the following set of equations

$$\begin{aligned}
T(B_{d,s}^{0} \to \bar{B}_{d,s}^{0})(t) = \Big|\frac{q}{p} g_{-}(t)\Big|_{d,s}^{2} \quad &\to \quad T(B_{d,s}^{0} \to \bar{B}_{d,s}^{0}) = \Big(\Big|\frac{q}{p}\Big|^{2} \frac{Z^{-}}{2\Gamma}\Big)_{d,s}, \\
T(\bar{B}_{d,s}^{0} \to B_{d,s}^{0})(t) = \Big|\frac{p}{q} g_{-}(t)\Big|_{d,s}^{2} \quad &\to \quad T(\bar{B}_{d,s}^{0} \to B_{d,s}^{0}) = \Big(\Big|\frac{p}{q}\Big|^{2} \frac{Z^{-}}{2\Gamma}\Big)_{d,s}, \\
T(B_{d,s}^{0} \to B_{d,s}^{0})(t) = \Big|g_{+}(t)\Big|_{d,s}^{2} \quad &\to \quad T(B_{d,s}^{0} \to B_{d,s}^{0}) = \Big(\frac{Z^{+}}{2\Gamma}\Big)_{d,s}, \\
T(\bar{B}_{d,s}^{0} \to \bar{B}_{d,s}^{0})(t) = \Big|g_{+}(t)\Big|_{d,s}^{2} \quad &\to \quad T(\bar{B}_{d,s}^{0} \to \bar{B}_{d,s}^{0}) = \Big(\frac{Z^{+}}{2\Gamma}\Big)_{d,s}.
\end{aligned} \tag{5.3.18}$$

The set of extra functions required in Eq.(5.3.18) are

$$\begin{aligned}
x_{d,s} &= \Big(\frac{\Delta m}{\Gamma}\Big)_{d,s}, \\
y_{d,s} &= \Big(\frac{\Delta\Gamma}{2\Gamma}\Big)_{d,s}, \\
Z_{d,s}^{+} &= \Big(\frac{1}{1-y^{2}} + \frac{1}{1+x^{2}}\Big)_{d,s}, \\
Z_{d,s}^{-} &= \Big(\frac{1}{1-y^{2}} - \frac{1}{1+x^{2}}\Big)_{d,s}, \\
\Big(\frac{q}{p}\Big)_{d,s} &= e^{(-2i\beta_{d,s})}\Big[1 - \frac{a_{sl}^{d,s}}{2}\Big].
\end{aligned} \tag{5.3.19}$$

In the last equality of Eq.(5.3.19) we have used the connection between q/p and the semileptonic asymmetries $a_{sl}^{d,s}$ as given by Eq.(1.3.55) and Eq.(1.3.56).

If we substitute Eq.(5.3.19) inside Eq.(5.3.12) and inside the first expression in Eq.(5.3.15) we get

$$\begin{aligned}
\Gamma_{mix,WS}^{-} &= \sum_{q=d,s} f_{q}\Big(1 - a_{sl}^{q}\Big)\frac{Z^{-}}{2\Gamma}\Gamma_{sl}^{q}, \\
\Gamma_{mix,WS}^{+} &= \sum_{q=d,s} f_{q}\Big(1 + a_{sl}^{q}\Big)\frac{Z^{-}}{2\Gamma}\Gamma_{sl}^{q}.
\end{aligned} \tag{5.3.20}$$

Finally plugging Eq.(5.3.20) into Eq.(5.3.17) we obtain

$$A_{sl}^{b} = \frac{f_{d}\frac{Z_{d}^{-}}{\Gamma_{d}}\Gamma_{sl}^{d}\ a_{sl}^{d} + f_{s}\frac{Z_{s}^{-}}{\Gamma_{s}}\Gamma_{sl}^{s}\ a_{sl}^{s}}{f_{d}\frac{Z_{d}^{-}}{\Gamma_{d}}\Gamma_{sl}^{d} + f_{s}\frac{Z_{s}^{-}}{\Gamma_{s}}\Gamma_{sl}^{s}} = C^{d}a_{sl}^{d} + C^{s}a_{sl}^{s}, \tag{5.3.21}$$

with

$$C^q = \frac{f_q \frac{Z_q^-}{\Gamma_q} \Gamma_{sl}^q}{f_d \frac{Z_d^-}{\Gamma_d} \Gamma_{sl}^d + f_s \frac{Z_s^-}{\Gamma_s} \Gamma_{sl}^s}. \tag{5.3.22}$$

The result presented in Eq.(5.3.20) is just the standard expression for the semileptonic charge asymmetry A_{sl}^b and it is due entirely to $\mathcal{CP}$ violation in mixing.

5.3.2 Borissov-Hoeneisen derivation of the interference contribution

We now discuss the connection between the contribution from $\mathcal{CP}$ violation in interference A_S^{int} and the mixing observable $\Delta\Gamma_d$, the notation used in this section will be consistent with the one introduced in the original reference [102].

As it was mentioned in Section 1.3.7, $\mathcal{CP}$ violation in interference occurs when there are common hadronic states in which both the $\bar{B}_q^0$ and its $\mathcal{CP}$ conjugate can decay. In [102] the attention is centred on states f_{cc}^s (f_{cc}^d) achieved through the quark level transitions $b \to c\bar{c}s$ ($b \to c\bar{c}d$). The possible sources of single muons included in [102] are summarized on Tab. (5.1) where the weights w_i (for $i = 1, .., 6$) determine the probabilities for different decay channels. In particular, we are interested in the decay probability into intermediate states containing two charm quarks, this is given by $w_3 = w_{3d} + w_{3s}$, being w_{3d} and w_{3s} the partial contributions from $B_d^0(\bar{B}_d^0)$ and $B_s^0(\bar{B}_s^0)$ mesons respectively.

To begin with, we will estimate how likely it is to get pairs $\mu^-\mu^-$ in the final state; the probability that an initial b quark produces a "right sign" (RS) μ^- is

$$\begin{aligned} P_b &\propto 0.5 w_{3d}(f_i) \left[1 + S_i \frac{x_d}{1+x_d^2}\right] + w_{1a} + w_{2b} + 0.5\,(w_{3s} + w_{3fs} + w_4 + w_5) \\ &= 0.5 w_{3d}(f_i) S_i \frac{x_d}{1+x_d^2} + 0.5\,(w_3 + w_4 + w_5) + w_{1a} + w_{2b}. \end{aligned} \tag{5.3.23}$$

In the same way the probability of obtaining a "wrong sign" (WS) μ^- out of a $\bar{b}$ is

$$\begin{aligned} P_{\bar{b}} &\propto 0.5 w_{3d}(f_i) \left[1 - S_i \frac{x_d}{1+x_d^2}\right] + w_{1b} + w_{2a} + 0.5\,(w_{3s} + w_{3fs} + w_4 + w_5) \\ &= -0.5 w_{3d}(f_i) S_i \frac{x_d}{1+x_d^2} + 0.5\,(w_3 + w_4 + w_5) + w_{1b} + w_{2a}. \end{aligned} \tag{5.3.24}$$

In the case of $\mu^+\mu^+$ production we consider the following two probabilities

Process	Weight
$b \to \mu^- X$	$w_1 \equiv 1$
$b \to \mu^- X(non-osc)$	$w_{1a} = (1-\chi_0)w_1$
$\bar{b} \to b \to \mu^- X(osc)$	$w_{1b} = \chi_0 w_1$
$b \to c \to \mu^+ X$	$w_2 = 0.096 \pm 0.012$
$b \to c \to \mu^+ X(non-osc)$	$w_{2a} = (1-\chi_0)w_2$
$\bar{b} \to b \to c \to \mu^+ X(osc)$	$w_{2b} = \chi_0 w_2$
$b \to c\bar{c}q$ with $c \to \mu^+ X$ or $\bar{c} \to \mu^- X$	$w_3 = 0.064 \pm 0.006$
$\eta, \omega, \rho^0, \phi(1020), J/\psi, \psi' \to \mu^+\mu^-$	$w_4 = 0.021 \pm 0.002$
$b\bar{b}c\bar{c}$ with $c \to \mu^+ X$ or $\bar{c} \to \mu^- X$	$w_5 = 0.013 \pm 0.002$
$c\bar{c}$ with $c \to \mu^+ X$ or $\bar{c} \to \mu^- X$	$w_6 = 0.675 \pm 0.101$

Table 5.1: Sources of single muons included in the Borissov-Hoeneisen analysis.

$$
\begin{aligned}
P_b^{'} &\propto 0.5 w_{3d}(f_i)\left[1 - S_i \frac{x_d}{1+x_d^2}\right] + w_{1a} + w_{2b} + 0.5\left(w_{3s} + w_{3fs} + w_4 + w_5\right) \\
&= -0.5 w_{3d}(f_i) S_i \frac{x_d}{1+x_d^2} + 0.5\left(w_3 + w_4 + w_5\right) + w_{1a} + w_{2b} \\
P_{\bar{b}}^{'} &\propto 0.5 w_{3d}(f_i)\left[1 + S_i \frac{x_d}{1+x_d^2}\right] + w_{1b} + w_{2a} + 0.5\left(w_{3s} + w_{3fs} + w_4 + w_5\right) \\
&= 0.5 w_{3d}(f_i) S_i \frac{x_d}{1+x_d^2} + 0.5\left(w_3 + w_4 + w_5\right) + w_{1b} + w_{2a} \qquad (5.3.25)
\end{aligned}
$$

where $P_b^{'}$ and $P_{\bar{b}}^{'}$ correspond to the "wrong sign" (WS) and the "right sign" (RS) contributions respectively.

The extra factors $1 \pm S_i \frac{x_d}{1+x_d^2}$ in Eq.(5.3.23), Eq.(5.3.24) and Eq.(5.3.25) allow us to make a distinction between the contributions from B_d^0 and $\bar{B}_d^0$, they are required since w_{3d} was calculated including both contributions together [113]; S_i accounts for the eigenvalue of the intermediate states $f_{cc}^{s,d}$ under $\mathcal{CP}$ transformations and for the weak phase arising in the decays $B_q^0 \to f_{cc}^{s,d}$, in the SM

$$S_i = \pm \sin(2\beta_d). \qquad (5.3.26)$$

In principle there should be analogous factors $1 \pm S_i \frac{x_s}{1+x_s^2}$ multiplying the weights w_{3s} from B_s^0 and $\bar{B}_s^0$ mesons; however, in this case the ratio $\frac{x_s}{1+x_s^2}$ is roughly ten times smaller than $\frac{x_d}{1+x_d^2}$ and its overall contribution to Eq.(5.3.23), Eq.(5.3.24) and

Eq.(5.3.25) can be neglected.

The number of events with pairs of $\mu^-\mu^-$ and $\mu^+\mu^+$ arising from $\mathcal{CP}$ violation in interference are proportional to $P_b P_{\bar{b}}$ and $P_b^{'} P_{\bar{b}}^{'}$ respectively, therefore A_S^{int} in Eq.(5.3.5) is computed as

$$A_S^{int} = \frac{P_b P_{\bar{b}} - P_b^{'} P_{\bar{b}}^{'}}{P_b P_{\bar{b}} + P_b^{'} P_{\bar{b}}^{'}}. \tag{5.3.27}$$

After some algebra we write the numerator in Eq.(5.3.27)

$$P_b P_{\bar{b}} - P_b^{'} P_{\bar{b}}^{'} \;=\; w_{3d}(f_i) S_i \frac{x_d}{1+x_d^2} \left[w_{1a} + w_{2b} - w_{1b} - w_{2a} \right]. \tag{5.3.28}$$

We simplify the expression inside the square braket in Eq.(5.3.28) using Eq.(5.3.23) and Eq.(5.3.24); we find

$$w_{1a} + w_{2b} - w_{1b} - w_{2a} \;=\; P_b - P_{\bar{b}} - w_{3d}(f_i) S_i \frac{x_d}{1+x_d^2}. \tag{5.3.29}$$

Plugging Eq.(5.3.29) into Eq.(5.3.28) and neglecting the factor $\left(w_{3d}(f_i) S_i \frac{x_d}{1+x_d^2} \right)^2$ we get for the numerator in Eq.(5.3.27)

$$P_b P_{\bar{b}} - P_b^{'} P_{\bar{b}}^{'} \;=\; w_{3d}(f_i) S_i \frac{x_d}{1+x_d^2} \left(P_b - P_{\bar{b}} \right), \tag{5.3.30}$$

and for the denominator we use the following approximation

$$P_b P_{\bar{b}} + P_b^{'} P_{\bar{b}}^{'} \approx 2 P_b P_{\bar{b}}. \tag{5.3.31}$$

Substituting Eq.(5.3.30) and Eq.(5.3.31) into Eq.(5.3.27) we arrive to the master equation

$$A_S^{int,d} \;\approx\; \frac{w_{3d}(f_i)}{2} S_i \frac{x_d}{1+x_d^2} \frac{(P_b - P_{\bar{b}})}{P_b P_{\bar{b}}}. \tag{5.3.32}$$

We now focus or attention on the weight w_{3d}, its expression is provided in [102]

$$w_{3d}(f_i) \;=\; f_d \alpha \frac{\mathcal{B}r(B_d^0 \to f_i)\mathcal{B}r(f_i \to \mu X)}{\mathcal{B}r(b \to \mu X)}, \tag{5.3.33}$$

where $\mathcal{B}r(B_d^0 \to f_i)$ and $\mathcal{B}r(f_i \to \mu X)$ are the branching fractions of the processes $B_d^0 \to f_i$ and $f_i \to \mu X$ respectively. As a matter of fact $\mathcal{B}r(B_d^0 \to f_i)$ is an averaged branching fraction that takes into account contributions from both B_d^0 and $\bar{B}_d^0$. $\mathcal{B}r(b \to \mu X)$ is the average branching fraction of the direct decay of all B hadrons to muons weighted with the relative production rate of different B hadrons at the

hadron collider; f_d is the fraction of B_d^0 plus $\bar{B}_d^0$ in the mixture of b-hadrons; the coefficient α is the ratio of detector acceptances of muons from D^+ and B_d^0 decays. The expression for α as given in [102] is

$$\alpha = w_3 \frac{\mathcal{B}r(b \to \mu X)}{\mathcal{B}r(b \to c\bar{c}X)\mathcal{B}r(c\bar{c}q\bar{q}' \to \mu X)}. \tag{5.3.34}$$

In Eq.(5.3.34) $\mathcal{B}r(b \to c\bar{c}X)$ stands for the branching fraction of B hadron decays with a $c\bar{c}$ pair and $\mathcal{B}r(c\bar{c}q\bar{q}' \to \mu X)$ is the average branching fraction of the direct decay of all charmed hadrons to muons weighted with the relative production rate of different pairs of c hadrons in B decays.

Inserting Eq.(5.3.34) inside Eq.(5.3.33) and identifying the experimentally determined parameter $\delta = \frac{\mathcal{B}r(B_d^0 \to \mu X)}{\mathcal{B}r(b \to c\bar{c}X)}$ we obtain the final version for the formula of $w_{3d}(f_i)$

$$w_{3d}(f_i) = f_d w_3 \frac{\mathcal{B}r(B_d^0 \to f_i)}{\mathcal{B}r(b \to c\bar{c}X)}\delta. \tag{5.3.35}$$

We are interested in the combination of factors $w_{3d}(f_i)S_i$ inside Eq.(5.3.32), we include all the intermediate states decaying into muons by summing over the index i. Following the procedure indicated in [102], the final states f_i are divided depending on their behaviour under $\mathcal{CP}$ transformations into $\mathcal{CP}$ even and $\mathcal{CP}$ odd, then using Eq.(5.3.35) and Eq.(5.3.26) we can write

$$\begin{aligned}\sum_i w_{3d}(f_i)S_i &= \frac{f_d w_3 \delta}{\mathcal{B}r(b \to c\bar{c}X)} \sum_i \mathcal{B}r(B^0 \to f_i)S_i \\ &= -\frac{\sin(2\beta_d) f_d w_3 \delta}{\mathcal{B}r(b \to c\bar{c}X)}\Big[\mathcal{B}r(B_d^{0,even}) - \mathcal{B}r(B_d^{0,odd})\Big]. \end{aligned}\tag{5.3.36}$$

Considering that in the SM the $\mathcal{CP}$ violation of neutral B mesons in mixing is small, the mass eigenstates of the B^0 system coincide approximately with the $\mathcal{CP}$ eigenstates [114] this allow us to establish the following equality between the decay width differences

$$\Delta\Gamma_d = \Delta\Gamma_{d,CP} = \Gamma(B_d^{0,even}) - \Gamma(B_d^{0,odd}) = \Gamma_d\Big(\mathcal{B}r(B_d^{0,even}) - \mathcal{B}r(B_d^{0,odd})\Big). \tag{5.3.37}$$

Plugging Eq.(5.3.37) into Eq.(5.3.36) we obtain

$$\sum_i w_{3d}(f_i)S_i = -\frac{\sin(2\beta_d) f_d w_3 \delta}{\mathcal{B}r(b \to c\bar{c}X)} \frac{\Delta\Gamma_d}{\Gamma_d}.$$

We have reached the end of our derivation, we substitute back Eq.(5.3.38) into Eq. 5.3.32 to get

$$A_S^{int} = -\Big(\frac{\sin(2\beta_d) f_d w_3 \delta}{2\ \mathcal{B}r(b\to c\bar{c}X)}\frac{x_d}{1+x_d^2}\frac{(P_b - P_{\bar{b}})}{P_b P_{\bar{b}}}\Big)\frac{\Delta\Gamma_d}{\Gamma_d}. \tag{5.3.38}$$

5.3.3 Issues with the Borissov-Hoeneisen derivation

As discussed previously in Section 1.2.2 there is $\mathcal{CP}$ violation in the SM if and only if the Jarlskog commutator in Eq.(1.2.40) gives a non null value. If we take the formal limit $m_c \to m_u$, we have degeneracy between the 1st and the second families of quarks. Then as expected the Jarlskog commutator in Eq.(1.2.40) is identically zero and $\mathcal{CP}$ violation is removed from the SM. To test the consistency of our formulas we should verify that all the $\mathcal{CP}$ asymmetries vanish in this limit. As pointed out in [115] this holds for the semileptonic asymmetries, so that $A_{sl}^b = 0$; however, if we consider the result in Eq.(5.3.38) for A_S^{int} we find $A_S^{int} \neq 0$. This suggest that during our derivation in Section 5.3.2 the contributions from the up quark that were left out should be taken into account. This is not a surprise considering that during the determination of $A_S^{int} \neq 0$ it was always assumed that the leading term in interference is dominated by the hadronic states arising in the quark level transition $b \to c\bar{c}d$, and the effects from the channels $b \to c\bar{u}d$, $b \to u\bar{c}d$ and $b \to u\bar{u}d$ were completely ignored. The main conclusions from [115] are

- The contributions from $\mathcal{CP}$ violation in interference A_S^{int} should be included in the theoretical interpretation of the like-sign dimuon asymmetry.

- The physical quantities A_S^{int} and $\Delta\Gamma_d$ have a different dependency on $\Gamma^{d,cc}$, $\Gamma^{d,uc}$ and $\Gamma^{d,uu}$. The extra components involving the up quark, neglected in the study [102], will allow us to fulfil the Jarlskog criteria in the limit case $m_c \to m_u$.

- Based on a simple analysis of the CKM structure of Eq.(5.3.38) it is suggested that as a first correction an extra factor of 1/2 should be introduced.

To conclude this section let us outline a possible path towards the inclusion of the up quark contributions in A_S^{int}. To begin with we write the interference decay widths

considering intermediate states f^d_{cc}, f^d_{cu}, f^d_{uc} and f^d_{uu} accessible through the quark level transitions $b \to c\bar{c}d$, $b \to c\bar{u}d$, $b \to u\bar{c}d$ and $b \to u\bar{u}d$, respectively (and analogously for the $b \to s$ decays). For the purposes of illustration we consider the widths for the "right sign" (RS) and the "wrong sign" (WS) muons μ^+

$$\begin{aligned}
\Gamma^+_{int,RS} &= \Gamma(B^0_d \to f^d_{c\bar{c}} \to \mu^+ X_{c\bar{c}}) + \Gamma(B^0_d \to f^d_{u\bar{u}} \to \mu^+ X_{u\bar{u}}) \\
&+ \Gamma(B^0_d \to f^d_{u\bar{c}} \to \mu^+ X_{u\bar{c}}) + \Gamma(B^0_d \to f^d_{\bar{u}c} \to \mu^+ X_{\bar{u}c}) \\
&+ \Big(d \to s\Big) \\
\Gamma^+_{int,WS} &= \Gamma(\bar{B}^0_d \to f^d_{c\bar{c}} \to \mu^+ X_{c\bar{c}}) + \Gamma(\bar{B}^0_d \to f^d_{u\bar{u}} \to \mu^+ X_{u\bar{u}}) \\
&+ \Gamma(\bar{B}^0_d \to f^d_{u\bar{c}} \to \mu^+ X_{u\bar{c}}) + \Gamma(\bar{B}^0_d \to f^d_{\bar{u}c} \to \mu^+ X_{\bar{u}c}) \\
&+ \Big(d \to s\Big). \qquad (5.3.39)
\end{aligned}$$

To understand how the different mixing structures $\Gamma^{d,ab}_{12}$ may arise consider for example

$$\sum_{f^d_{c\bar{c}}} \Gamma(\bar{B}^0_d \to f^d_{c\bar{c}} \to \mu^+ X_{\bar{c}c}) \;\propto\; \sum_{f^d_{c\bar{c}}} \int_0^\infty | < f^d_{c\bar{c}} | \bar{B}^0_d(t) > |^2 dt \times Prob(c \to \mu^+). \qquad (5.3.40)$$

The summation in Eq.(5.3.40) runs over all the possible intermediate hadronic states that can be obtained through the decay chain $b \to c\bar{c}d$. When writing the right hand side of Eq.(5.3.40) we are expressing the amplitude for the process $\bar{B}^0_d \to f^d_{c\bar{c}} \to \mu^+ X_{cc}$ as the product of two subamplitudes. The first one, given by $< f_{c\bar{c}} | \bar{B}^0_d(t) >$, has to do with the purely hadronic transition $\bar{B}^0_d \to f_{c\bar{c}}$. The second one, accounting for the semileptonic decay process $f^d_{c\bar{c}} \to \mu^+ X_{cc}$, is introduced through $Prob(c \to \mu^+)$. One of the central assumptions make by [102] and [115] is that the probability for the decays $f^d_{c\bar{c}} \to \mu^+ X_{cc}$ is the same independently of the intermediate state $f^d_{c\bar{c}}$, so that the factor $Prob(c \to \mu^+)$ can be taken out of the summation symbol in Eq.(5.3.40). However this is not totally justified because at exclusive level the hadronic states $f^d_{c\bar{c}}$ have different probabilities for decaying into muons. In order to make progress in our discussion, let us assume that this technicality is already solved and that we can indeed assume an universal factor $Prob(c \to \mu^+)$ in Eq.(5.3.40). Then we can write

$$\begin{aligned}\sum_{f^d_{c\bar{c}}} |< f^d_{c\bar{c}}|\bar{B}(t)>|^2 \times Prob(c\to\mu^+) &= Prob(c\to\mu^+)\sum_{f^d_{c\bar{c}}}|< f_{c\bar{c}}|\bar{B}(t)>|^2 \\ &= \sum_{f^d_{c\bar{c}}}\Big\{|\frac{p}{q}g_-(t)A_{f_{c\bar{c}}}|^2 + |g_+(t)\bar{A}_{f^d_{c\bar{c}}}|^2 \\ &\quad +2\mathcal{R}e\Big[\Big(\frac{p}{q}\Big)^* g_+(t)g^*_-(t)A^*_{f_{c\bar{c}}}\bar{A}_{f_{c\bar{c}}}\Big]\Big\} \\ &\quad \times Prob(c\to\mu^+). \qquad (5.3.41)\end{aligned}$$

Here we are particularly interested in the last term on the right hand side of Eq.(5.3.41). After summing over all the intermediate states $f_{c\bar{c}}$ we obtain the final result

$$\sum_{f^d_{c\bar{c}}} A^*_{f^d_{c\bar{c}}}\bar{A}_{f^d_{c\bar{c}}} \;\propto\; \Gamma^{d,cc}_{12}. \qquad (5.3.42)$$

Analogous expressions proportional to $\Gamma^{d,uc}_{12}$ and $\Gamma^{d,uu}_{12}$ are obtained when calculating for the intermediate states $f^d_{c\bar{u}}$, $f^d_{u\bar{c}}$ and $f^d_{u\bar{u}}$.

5.4 New physics in $\Delta\Gamma_d$: current-current operators

The possibility of enhancing $\Delta\Gamma_d$ through new physics in the tree level Wilson coefficients C_1 and C_2 was considered for the first time in [2]. In Chapter 4 we made a deeper and more careful analysis by using a full statistical fit (in contrast the investigation in [2] was based on a naive parameter space scan). Considering the outcomes of this analysis we can now formulate stronger and more refined conclusions. Our channel by channel study in Section 4.8 is summarized in Tab.5.4 depending on the new physics effects in ΔC_1 and ΔC_2. The enhancement factors in Tab.5.4 for the channels $b\to u\bar{u}d$ and $b\to c\bar{u}d$ are bigger in comparison with our previous results in [2]. This is totally understandable since the statistical fit permits bigger new physics regions when taking into account the errors in different input parameters simultaneously. This is particularly relevant for observables calculated within the QCD factorization framework where the effects of the power corrections become important. As a matter of fact these contributions were completely omitted in [2]. In addition, in our new analysis we have excluded the total life time of the B mesons,

Channel	Enhancement due to ΔC_1	Enhancement due to ΔC_2
$b \to u\bar{u}d$	—	$(0.55, 1.76)$
$b \to c\bar{u}d$	$(0.24, 2.60)$	$(-0.93, 2.18)$
$b \to c\bar{c}d$	—	$(-3.90, 2.60)$

Table 5.2: Enhancements on $\Delta\Gamma_d$ based on $b \to d$ transitions.

this automatically increases the upper bounds for $\Delta\Gamma_d$ in the $b \to c\bar{u}d$ channel when fitting for ΔC_2^{cu}. In [2] an enhancement factor greater than 10 was claimed originating from the decay channel $b \to c\bar{c}d$. Now according to our study in Section 4.8.3 the enhancement bounds do not go beyond 2.6 (see Fig. 4.18). The reason for this is that bigger enhancement factors will violate the current experimental bounds in $\Delta\Gamma_d$: $-3.90 < \Delta\Gamma_d^{exp}/\Delta\Gamma_d^{SM} < 2.6$. All in all, the possible new physics enhancements in $\Delta\Gamma_d$ due to our uncertainty in tree level b-quarks decays are sizeable and saturate the bounds established by the most recent experimental measurements.

5.5 New physics in $\Delta\Gamma_d$: $\left(\bar{d}b\right)(\bar{\tau}\tau)$ operators

In this section we study possible effects on $\Delta\Gamma_d$ related to effective operators of the form $\left(\bar{d}b\right)(\bar{\tau}\tau)$. The analogous operators for the B_s-meson system (i.e. those obtained by replacing $d \to s$) were introduced in [116] and used in studying $\Delta\Gamma_s$. The corresponding effective Hamiltonian reads

$$\mathcal{H}_{\text{eff}}^{b\to d\tau^+\tau^-} = -\frac{4G_F}{\sqrt{2}}\,\lambda_t^d \sum_{i,j} C_{i,j}(\mu) Q_{i,j}\,, \tag{5.5.43}$$

and involves the following complete set of operators

$$\begin{aligned} Q_{S,AB} &= (\bar{d}\,P_A\,b)(\bar{\tau}\,P_B\,\tau)\,,\\ Q_{V,AB} &= (\bar{d}\,\gamma^\mu P_A\,b)(\bar{\tau}\,\gamma_\mu P_B\,\tau)\,,\\ Q_{T,A} &= (\bar{d}\,\sigma^{\mu\nu} P_A\,b)(\bar{\tau}\,\sigma_{\mu\nu} P_B\,\tau)\,, \end{aligned} \tag{5.5.44}$$

where $P_{L,R} = (1\mp\gamma_5)/2$ and $A, B = L, R$. In addition to these operators, our analysis uses the dimension-six effective Hamiltonian describing $b \to d\ell^+\ell^-$ transitions ($\ell =$

e, μ, τ). We write this as

$$\mathcal{H}_{\text{eff}}^{b\to d\ell^+\ell^-} = -\frac{4G_F}{\sqrt{2}}\,\lambda_t^d \sum_i C_i(\mu) Q_i\,. \tag{5.5.45}$$

The most important operators in what follows are

$$\begin{aligned} Q_7 &= \frac{e}{(4\pi)^2}\, m_b \left(\bar{d}\,\sigma^{\mu\nu} P_R\, b\right)\, F_{\mu\nu}\,, \\ Q_9 &= \frac{e^2}{(4\pi)^2} \left(\bar{d}\,\gamma^\mu P_L\, b\right) \left(\bar{\ell}\,\gamma_\mu\,\ell\right)\,, \\ Q_{10} &= \frac{e^2}{(4\pi)^2} \left(\bar{d}\,\gamma^\mu P_L\, b\right) \left(\bar{\ell}\,\gamma_\mu\gamma_5\,\ell\right)\,, \end{aligned} \tag{5.5.46}$$

and their chirality-flipped counterparts Q_i' obtained through the interchange $P_L \leftrightarrow P_R$.

The operators in Eq.(5.5.44) are interesting because they can give large contributions to $\Delta\Gamma_d$, but are only weakly constrained by experimental data. We will see that in the case of the B_d-meson system the various direct and indirect bounds on the Wilson coefficients of the operators in Eq.(5.5.44) are generally weaker than in the $\bar{B}_s^0$-meson system and that large enhancements of $\Delta\Gamma_d$ due to such operators are not yet ruled out. We derive direct bounds, where the operators contribute to tree-level matrix elements, from the decays $\bar{B}_d^0 \to \tau^+\tau^-$, $B \to X_d\tau^+\tau^-$ and $B^+ \to \pi^+\tau^+\tau^-$. Indirect bounds, where the operators contribute either through operator mixing and loop-level matrix elements, are based on $B \to X_d\gamma$ and $B^+ \to \pi^+\mu^+\mu^-$ decays. We discuss the two cases in turn.

5.5.1 Direct bounds

We first investigate direct constraints from the decay $B_d \to \tau^+\tau^-$. At present, the only experimental information on this decay is the 90% CL bound from [117]:

$$\mathcal{B}r\left(B_d \to \tau^+\tau^-\right) < 4.1 \cdot 10^{-3}\,. \tag{5.5.47}$$

The theory prediction, including both SM and the effects of the operators in Eq. (5.5.44) can be extracted from [118]. The result depends on the SM coefficient C_{10} in addition to the Wilson coefficients $C_{S,AB}$ and $C_{V,AB}$, but not on the tensor coefficients $C_{T,A}$. Moreover, due to a loop suppression factor of α/π, the SM contribution alone

is quite small, $\mathcal{B}r\,(B_d \to \tau^+\tau^-)_{\rm SM} \simeq 2.3 \cdot 10^{-8}$ [119]. We therefore neglect it in obtaining bounds on the coefficients of the new operators. Furthermore, as before we assume the dominance of a single operator at a time, neglecting interference terms of the new operators both with the SM contribution and with themselves. Following this procedure, we can set bounds on the absolute values of the coefficients $C_{S,AB}$ and $C_{V,AB}$, independent of the chirality structure. Giving up this assumption, would lead to considerably larger bounds on $\Delta\Gamma_d$. In that respect our estimates are very conservative.

The branching ratio depends on a number of input parameters. Some of these are common to the other decays discussed in this section: for these we use the values of G_F, M_{B_d}, τ_{B_d}, f_{B_d}, $|\lambda_d^t|$, m_τ, $\alpha(M_Z)$, $m_b^{\rm pole}$ and m_d summarised in Tab.3 of [2]. We then obtain at $m_b = \overline{m}_b(\overline{m}_b) \simeq 4.2$ GeV the results $|C_{S,AB}(m_b)| < 1.1$ and $|C_{V,AB}(m_b)| < 2.2$, which are also collected in Tab.5.3. These are the strongest bounds on the scalar and vector coefficients that will emerge from our analysis.

We next consider inclusive and exclusive $b \to d\tau^+\tau^-$ decays. In this case, there are no direct experimental bounds on the branching ratios. However, we can use information from the $B_{d,s}$-meson lifetimes to estimate the potential size of new-physics contributions to these decays. We first note that the SM prediction for the lifetime ratio is very close to unity [16, 120–123]

$$\left(\frac{\tau_{B_s}}{\tau_{B_d}} - 1\right)_{\rm SM} = (0.050 \pm 0.108)\,\% \,. \tag{5.5.48}$$

Current experimental measurements [1] show some tension with this prediction:

$$\left(\frac{\tau_{B_s}}{\tau_{B_d}} - 1\right) = (-1.0 \pm 0.4)\,\% \,. \tag{5.5.49}$$

Comparing the results and assuming no new physics in the B_s^0 system, one can get a rough bound on the size of possible new-physics contributions $\Gamma_d^{\rm NP}$ to the total B_d-meson decay rate Γ_d, namely

$$\frac{\Gamma_d^{\rm NP}}{\Gamma_s} = (1.05 \pm 0.41)\,\% \,. \tag{5.5.50}$$

At 90% CL one obtains

$$\mathcal{B}r\,(B_d \to X) \leq 1.72\% \,. \tag{5.5.51}$$

We now turn this estimate into bounds on Wilson coefficients using the theoretical expressions for the $B \to X_d\tau^+\tau^-$ and $B^+ \to \pi^+\tau^+\tau^-$ branching ratios. In contrast to $B_d \to \tau^+\tau^-$ decays, in these cases all operators contribute, so we also gain information on the tensor coefficients. However, once again the results are independent of the chirality structure and allow us to constrain only absolute values of the coefficients. For the inclusive decay $B \to X_d\tau^+\tau^-$, we use the expressions for the branching ratios given in Section 3 and the appendix of [116] after appropriate modifications. Most of the inputs to the branching ratio are common to B_d-meson and B_s-meson decays. Apart from trivial differences related to meson masses and lifetimes (for the exclusive decay we use τ_{B^+} and the CKM factor $|V_{td}^*V_{tb}|/|V_{cb}|$ given in Tab.3 of [2]). The exclusive decay $B^+ \to \pi^+\tau^+\tau^-$ depends on these parameters and also three $B \to \pi$ form factors ($f_{+,T,0}$), as a function of the dilepton invariant mass, denoted as q^2. For these we use the results of [124].[4] Moreover, we integrate over the full kinematic range $q^2 \in [4m_\tau^2, (M_{B+} - M_{\pi^+})^2]$.

We must also decide on a value for the experimental branching ratios. At present, we can only use Eq.(5.5.51) to estimate the size of the $B \to X_d\tau^+\tau^-$ and $B^+ \to \pi^+\tau^+\tau^-$ branching ratios, which most likely overestimates their allowed ranges. Here, a direct experimental bound would be very helpful. For reference, we collect the obtained bounds on the Wilson coefficients using the 90% CL estimates in Tab.5.3. In Section 5.5.3, we will show the size of possible enhancement of $\Delta\Gamma_d$ as a function of measured branching ratios. Compared to the bounds on the $B \to X_d\tau^+\tau^-$ and $B^+ \to \pi^+\tau^+\tau^-$ branching ratios estimated through (5.5.51), we find tiny SM predictions

$$\begin{aligned} \mathcal{B}r\left(B \to X_d\tau^+\tau^-\right)_{\rm SM} &= (1.2 \pm 0.3) \cdot 10^{-8}\,, \\ \mathcal{B}r\left(B^+ \to \pi^+\tau^+\tau^-\right)_{\rm SM} &= (1.5 \pm 0.5) \cdot 10^{-8}\,. \end{aligned} \tag{5.5.52}$$

In both cases our results refer to the fully-integrated and non-resonant branching ratios. The inclusive decay includes just the LO corrections, but accounts for contributions proportional to the tau mass that are of kinematic origin [125]. As for

[4] We have also derived bounds using the form factors from [126], which yield similar but slightly more stringent bounds.

the exclusive mode, we stayed within naive factorisation and the error reflects the uncertainty due to the use of different $B \to \pi$ form-factor determinations [124, 126].

5.5.2 Indirect bounds

Indirect bounds arise from cases where the operators in Eq.(5.5.44) do not give tree-level contributions to the decays, but contribute either through operator mixing, through loop-level matrix elements or through both. The theoretical expressions needed to set various indirect bounds can be adapted from [116]. It turns out that the most stringent indirect bounds on the Wilson coefficients can be derived from $B \to X_d\gamma$ and $B^+ \to \pi^+\mu^+\mu^-$ decays. We have also examined constraints from $B_d \to \gamma\gamma$ decays, but these are rather weak compared to the other decays and in some cases they depend very strongly on hadronic input parameters, so we do not discuss them further.

We first derive bounds from $B \to X_d\gamma$ decays. The structure of branching ratios for these decays is discussed in [84, 127]. We find that the perturbative quantity $P(E_0)$ introduced in the estimation of $\mathcal{B}_r(B \to X_d\gamma)$ can be written as

$$P(E_0) = \left|C_7^{\mathrm{SM}(0)}(m_b) + \Delta C_7^{\mathrm{eff}}(m_b)\right|^2 + \left|\Delta C_7^{\mathrm{eff}\prime}(m_b)\right|^2 , \tag{5.5.53}$$

where

$$\Delta C_7^{\mathrm{eff}(\prime)}(m_b) = \sqrt{x_\tau}\left(0.62 - 1.09\,\eta_6^{-1} + 4\ln x_\tau\right) C_{T,R(L)}(m_b)\,. \tag{5.5.54}$$

We have defined $\sqrt{x_\tau} \equiv m_\tau/m_b^{\mathrm{pole}}$ and the quantity $\eta_6 \equiv \alpha_s(\Lambda_{\mathrm{NP}})/\alpha_s(m_t)$, where α_s is to be evaluated with six active flavours. The first two terms in Eq.(5.5.54) arise from operator mixing and the third is the matrix element of $Q_{T,A}$. In order to derive 90% CL constraints on the Wilson coefficients $C_{T,A}(m_b)$, we insert Eq.(5.5.53) into the formula for $\mathcal{B}_r(B \to X_d\gamma)$ provided in e.g. [84] and compare with the experimental result in Eq.(4.5.64), as usual considering the dominance of one operator at a time. This procedure yields for $\Lambda_{\mathrm{NP}} \simeq 1$ TeV the bounds $|C_{T,R}(m_b)| < 0.2$ and $|C_{T,L}(m_b)| < 0.1$, which translate to $|\Delta C_7^{\mathrm{eff}}(m_b)| < 0.7$ and $|\Delta C_7^{\mathrm{eff}\prime}(m_b)| < 0.3$.

The rare decay $B^+ \to \pi^+\mu^+\mu^-$ has been observed by LHCb [128] in the 2011 data sample of $1\,\mathrm{fb}^{-1}$ with $(25.3^{+6.7}_{-6.4})$ events. This provides the first measurement of the

non-resonant branching ratio

$$\mathcal{B}r\left(B^+ \to \pi^+\mu^+\mu^-\right) = (2.3 \pm 0.6)\cdot 10^{-8}\,, \tag{5.5.55}$$

integrated over the whole dilepton invariant mass range $q^2 \in [4m_\mu^2, (M_{B^+} - M_{\pi^+})^2]$. In principle, the calculation of exclusive $B \to M\ell^+\ell^-$ $(M = P, V)$ decays is advanced, see [129] for the most recent prediction of $B^+ \to \pi^+\mu^+\mu^-$ in the SM, where $B \to \pi\ell\nu_\ell$ data have been used to extract information on the form factors. The inclusion of corrections beyond naive factorisation in QCD factorisation at low q^2 has been discussed in [130] (see also [131]), whereas at high q^2 a local operator product expansion can be applied to account for resonant contributions [132, 133]. However, in the absence of experimental measurements for either region separately and in view of the large experimental uncertainty, we evaluate the branching ratio in the naive factorisation approximation following [134]. Employing the $B \to \pi$ form factors of [124], we obtain

$$\mathcal{B}r\left(B^+ \to \pi^+\mu^+\mu^-\right)_{\rm SM} = (2.1 \pm 0.4)\cdot 10^{-8}\,. \tag{5.5.56}$$

The given uncertainty encodes the error related to differences in the existing $B \to \pi$ form-factor determinations [124, 126]. Our prediction in Eq.(5.5.56) is close both to the measured value given in Eq.(5.5.55) and the SM value obtained in [129].

Like in the case of the inclusive decay $B \to X_d\gamma$, the effective operators in Eq.(5.5.44) contribute to $B^+ \to \pi^+\mu^+\mu^-$ via mixing into the operators mediating $b \to d\gamma$ and $b \to d\ell^+\ell^-$ $(\ell = e, \mu)$. The case of $b \to s$ transitions has been previously discussed in [116] and can be adopted with appropriate replacements to $b \to d$ transitions. One then finds contributions from the tensor coefficients $C_{T,A}$, and also on the linear combination $(C_{V,AL} + C_{V,AR})$ of the vector coefficients. The scalar Wilson coefficients $C_{S,AB}$ are not subject to constraints from $B^+ \to \pi^+\mu^+\mu^-$.

In Fig.5.1, we show the 90% CL regions in the planes of complex-valued $C_{T,A}(m_b)$ and $\big(C_{V,AL}(m_b) + C_{V,AR}(m_b)\big)$ allowed by $\mathcal{B}r\,(B^+ \to \pi^+\mu^+\mu^-)$. In the plots a theory uncertainty of 20% of the SM prediction is assumed and the form-factor predictions [124] are used. We see that in the case of the tensor Wilson coefficients, $B^+ \to \pi^+\mu^+\mu^-$ provides at present the constraint $|C_{T,A}(m_b)| \lesssim 1.2$, which as indicated is clearly weaker than the sensitivity of the inclusive decay $B \to X_d\gamma$. Assuming

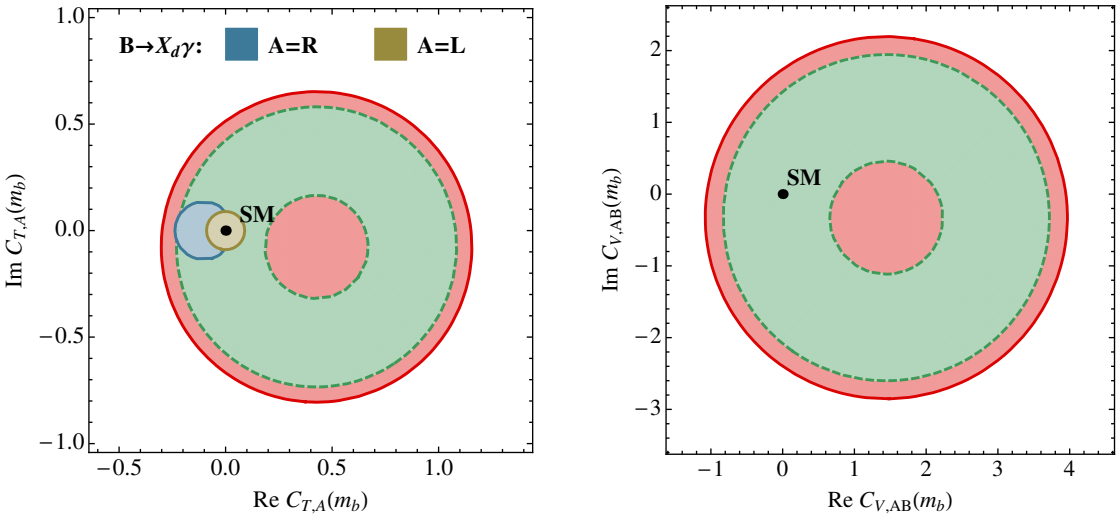

Figure 5.1: The 90% CL regions of $C_{T,A}(m_b)$ (left) and $\left(C_{V,AL}(m_b) + C_{V,AR}(m_b)\right)$ (right) from $\mathcal{B}r\,(B^+ \to \pi^+\mu^+\mu^-)$ (red) and $\mathcal{B}r\,(B \to X_d\gamma)$ for $T, A = T, R$ (blue) and $T, A = T, L$ (brown). The prospects assuming a measurement of $\mathcal{B}r\,(B^+ \to \pi^+\mu^+\mu^-)$ with 7 fb^{-1} at LHCb are shown as dashed (green) contours.

single operator dominance, the current constraint on the vector Wilson coefficients $|C_{V,AB}(m_b)| \lesssim 4.0$ is not as strong as the one from $B_d \to \tau^+\tau^-$. For comparison we also show contours assuming that LHCb has collected 7 fb^{-1} of data by 2017. For this purpose the current statistical errors have been rescaled by a factor $1/\sqrt{7}$. This exercise shows the potential of this decay mode to reduce further the allowed ranges of $b \to d\tau^+\tau^-$ Wilson coefficients. Depending on the central value of the measurement, it will provide complementary constraints to $B \to X_d\gamma$ for the tensor Wilson coefficients.

5.5.3 Maximal effects in width difference

We now explore the consequences of the bounds on the Wilson coefficients in Eq. (5.5.43) obtained in the previous section on the size of possible enhancements in $\Delta\Gamma_d$. Here we consider the new physics parameterization introduced in [52, 135]

$$\begin{aligned} M_{12}^q &= M_{12}^{q,\mathrm{SM}}\,\Delta_q\,, \qquad & \Delta_q &= |\Delta_q|\,e^{i\phi_q^\Delta}\,, \\ \Gamma_{12}^q &= \Gamma_{12}^{q,\mathrm{SM}}\,\tilde{\Delta}_q\,, \qquad & \tilde{\Delta}_q &= |\tilde{\Delta}_q|\,e^{-i\tilde{\phi}_q^\Delta}\,. \end{aligned} \tag{5.5.57}$$

Constraint	$\lvert C_{S,AB}(m_b)\rvert$	$\lvert C_{V,AB}(m_b)\rvert$	$\lvert C_{T,A}(m_b)\rvert$
direct			
$\mathcal{B}r\,(B_d \to \tau^+\tau^-)$	1.1	2.2	—
$\mathcal{B}r\,(B \to X_d\tau^+\tau^-)$	10.6	5.3	1.5
$\mathcal{B}r\,(B^+ \to \pi^+\tau^+\tau^-)$	5.9	6.2	2.9
indirect			
$\mathcal{B}r\,(B \to X_d\gamma)$	—	—	0.2 for $A = R$ 0.1 for $A = L$
$\mathcal{B}r\,(B^+ \to \pi^+\mu^+\mu^-)$	—	4.0	1.2

Table 5.3: Summary of direct and indirect bounds on the Wilson coefficients in Eq.(5.5.43) at the bottom-quark mass scale $m_b = \overline{m}_b(\overline{m}_b) \simeq 4.2$ GeV. The constraint from $B_d \to \tau^+\tau^-$ decay follows from the experimental 90% CL bound $\mathcal{B}r\,(B_d \to \tau^+\tau^-) < 4.1 \cdot 10^{-3}$, whereas those from $B \to X_d\tau^+\tau^-$ and $B^+ \to \pi^+\tau^+\tau^-$ refer to the 90% CL estimate from Eq.(5.5.51). Note that the bounds are independent of the chiral structure $A, B = L, R$ unless explicitly indicated.

The observables are then modified with respect to their SM predictions according to

$$\frac{\Delta M_q}{\Delta M_q^{\rm SM}} = |\Delta_q|\,, \qquad \frac{\Delta\Gamma_q}{\Delta\Gamma_q^{\rm SM}} = |\tilde{\Delta}_q|\,\frac{\cos\phi_q}{\cos\phi_q^{\rm SM}}\,, \qquad \frac{a_{sl}^q}{a_{sl}^{q,\,\rm SM}} = \frac{|\tilde{\Delta}_q|}{|\Delta_q|}\,\frac{\sin\phi_q}{\sin\phi_q^{\rm SM}}\,, \tag{5.5.58}$$

where the mixing phase is given by

$$\phi_q = \phi_q^{\rm SM} + \phi_q^{\Delta} + \tilde{\phi}_q^{\Delta}\,. \tag{5.5.59}$$

For the B_s-meson case expressions for this quantity as a function of the relevant Wilson coefficients were presented in [116], and we can make use of these results after a trivial substitution of CKM factors. Assuming single operator dominance,

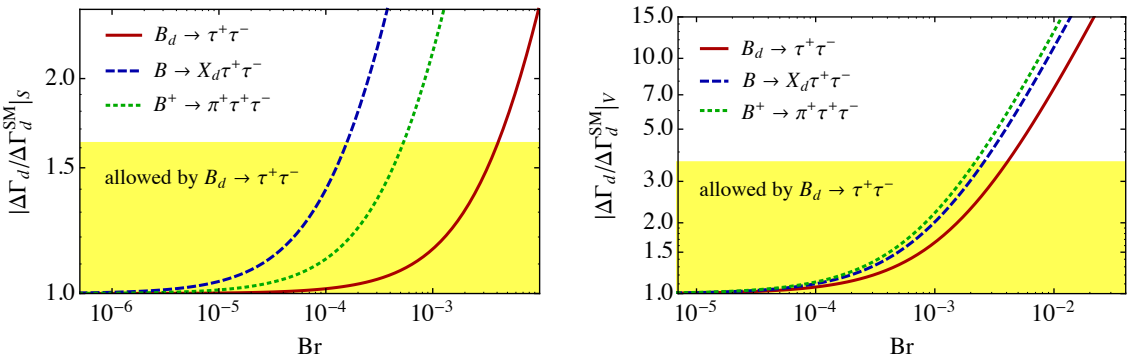

Figure 5.2: 90% CL bounds on possible enhancements of $\Delta\Gamma_d$ induced by the different $(\bar{d}b)(\bar{\tau}\tau)$ operators. The left panel shows the effect of scalar operators, while the right panel illustrates the case of vector operators. In both panels the yellow region indicates the maximal enhancements that are consistent with Eq.(5.5.47). The effect of an experimental improvement in the $B_d \to \tau^+\tau^-$, $B \to X_d\tau^+\tau^-$ and $B^+ \to \pi^+\tau^+\tau^-$ branching ratios is indicated by the solid red, the dashed blue and the dotted green curves, respectively.

we then find

$$\begin{aligned} |\tilde{\Delta}_d|_{S,AB} &< 1 + \left(0.41^{+0.13}_{-0.08}\right)\,|C_{S,AB}(m_b)|^2\,, \\ |\tilde{\Delta}_d|_{V,AB} &< 1 + \left(0.42^{+0.13}_{-0.08}\right)\,|C_{V,AB}(m_b)|^2\,, \\ |\tilde{\Delta}_d|_{T,A} &< 1 + \left(3.81^{+1.21}_{-0.74}\right)\,|C_{T,A}(m_b)|^2\,, \end{aligned} \tag{5.5.60}$$

where the quoted uncertainties are related to the theory error of $\Delta\Gamma_d^{\rm SM}$. The numerical input values of the bag parameters B_V, B_S and $\widetilde{B}_S$ are given in Tab.3 of [2]. Using the strongest bounds from Tab. 5.3, i.e. $|C_{S,AB}(m_b)| \lesssim 1.1$, $|C_{V,AB}(m_b)| \lesssim 2.2$, $|C_{T,L}(m_b)| \lesssim 0.1$ and $|C_{T,R}(m_b)| \lesssim 0.2$, results in

$$|\tilde{\Delta}_d|_{S,AB} \lesssim 1.6\,, \quad |\tilde{\Delta}_d|_{V,AB} \lesssim 3.7\,, \quad |\tilde{\Delta}_d|_{T,L} \lesssim 1.05\,, \quad |\tilde{\Delta}_d|_{T,R} \lesssim 1.2\ . \tag{5.5.61}$$

These numbers imply that the scalar operators can lead to an enhancement of about 60% over the SM prediction, whereas in the case of vector operators even deviations in excess of 270% are allowed. The possible deviations due to tensor operators can, on the other hand, amount to at most 20%. Such small effects are undetectable given that the hadronic uncertainty in $\Delta\Gamma_d$ is of similar size.

It is also interesting to study the impact future improved extractions of $\mathcal{B}r\,(B_d \to \tau^+\tau^-)$,

$\mathcal{B}r\,(B \to X_d\tau^+\tau^-)$ and $\mathcal{B}r\,(B^+ \to \pi^+\tau^+\tau^-)$ will have on the maximal enhancements in $\Delta\Gamma_d$. Such a comparison is provided in Fig.5.2 for the scalar operators (left panel) and the vector operators (right panel). The plots show that for both the scalar and the vector operators and fixed branching ratio the $B_d \to \tau^+\tau^-$ decay always provides the most stringent constraint on $|\Delta\Gamma_d/\Delta\Gamma_d^{\rm SM}|$. This implies that in order to restrict possible new-physics effects in $\Delta\Gamma_d$, future measurements of the $B \to X_d\tau^+\tau^-$ or $B^+ \to \pi^+\tau^+\tau^-$ branching ratio have to surpass the present bound in Eq.(5.5.47) on $\mathcal{B}r\,(B_d \to \tau^+\tau^-)$. Numerically, we find that limits of $\mathcal{B}r\,(B^+ \to \pi^+\tau^+\tau^-) \lesssim 5.3{\cdot}10^{-4}$ and $\mathcal{B}r\,(B \to X_d\tau^+\tau^-) \lesssim 2.6 \cdot 10^{-3}$ would be required in the case of the scalar and vector operators to reach the current sensitivity of the $B_d \to \tau^+\tau^-$ branching ratio.

Chapter 6

Constraints on the Hadron Quark duality from Mixing observables

6.1 Introduction

Despite having passed numerous tests, the SM of particle physics, leaves many fundamental questions unanswered, which might be resolved by extensions of this model. Flavour physics is an ideal candidate for general indirect new physics searches, as well as for dedicated CP-violating studies, for this purpose hadronic uncertainties on flavour observables have to be under control. Various flavour experiments have achieved a high precision in many observables, in many cases challenging the precision of theory calculations. LHCb in particular contributes to the currently impressive status of experimental precision. As we attempt to test the SM to the highest level of precision, the question of how sure we can be about any deviations from the current theoretical predictions being evidence of new physics comes to the fore. Such a question is the subject we tackle in this chapter in the context of mixing observables for the B_s^0, B_d^0 and the D meson sectors.

Many current theory predictions rely on the Heavy Quark Expansion (HQE), we will examine how the idea of quark-hadron duality – which is assumed by the HQE – can be tested. We will use current data from B-mixing, the dimuon asymmetry, and B-meson lifetimes to constrain violations of quark-hadron duality, and then see how this affects the predicted values of other observables. We also investigate how

the current trouble with inclusive predictions of mixing in the charm sector can be explained through quark-hadron duality violation.

We discuss what improvements could be made in both theory and experiment in order to further constrain duality violating effects, and what level of precision would be necessary to properly distinguish between genuine new physics and merely a non-perturbative contribution to the SM calculation. In this spirit, we also provide a first attempt at improving the theory prediction, using the latest results and aggressive error estimates to see how theory uncertainties could reduce in the near future.

6.2 Duality violation

In 1979 the notion of duality was introduced by Poggio, Quinn and Weinberg [136] for the process $e^+ + e^- \to \textit{hadrons}$, actually the concept of duality was already used in 1970 for electron proton scattering by Bloom and Gilman [137, 138]. The basic assumption is that this process can be well approximated by a quark level calculation of $e^+ + e^- \to q + \bar{q}$. Here we will investigate duality in the case of decays of heavy hadrons, which are described by the heavy quark expansion (see e.g. [139–146] for pioneering papers and [120] for a recent review). The HQE is a systematic expansion of the decay rates of b-hadrons in inverse powers of the heavy quark mass

$$\Gamma = \Gamma_0 + \frac{\Lambda}{m_b}\Gamma_1 + \frac{\Lambda^2}{m_b^2}\Gamma_2 + \frac{\Lambda^3}{m_b^3}\Gamma_3 + \frac{\Lambda^4}{m_b^4}\Gamma_4 + \dots , \tag{6.2.1}$$

with Λ being a scale of the order of the hadronic scale. Having a closer look one finds that there are no corrections of order $1/m_b$ and that corrections from the order $1/m_b^3$ onwards can be enhanced by an additional phase space factor of $16\pi^2$. The HQE assumes quark hadron duality, i.e. that the hadron decays can be described at the quark-level. A violation of duality could correspond to non-perturbative terms like $\exp[-m_b/\Lambda]$, which give vanishing contributions, when being Taylor expanded around $\Lambda/m_b = 0$ (see e.g. [147] and also [148] for a detailed discussion of duality, its violations and some possible models for duality violations). To estimate the possible size of these non-perturbative terms we note first that the actual expansion parameter of the HQE is the hadronic scale Λ normalised to the momentum release $\sqrt{M_i^2 - M_f^2}$. For the decay of a free b-quark we get the set of numerical values

Channel	Expansion parameter x	Numerical value	Exp[-1/x]
$b \to c\bar{c}s$	$\frac{\Lambda}{\sqrt{m_b^2-4m_c^2}} \approx \frac{\Lambda}{m_b}\left(1+2\frac{m_c^2}{m_b^2}\right)$	$0.054 - 0.58$	$9.4 \cdot 10^{-9} - 0.18$
$b \to c\bar{u}s$	$\frac{\Lambda}{\sqrt{m_b^2-m_c^2}} \approx \frac{\Lambda}{m_b}\left(1+\frac{1}{2}\frac{m_c^2}{m_b^2}\right)$	$0.045 - 0.49$	$1.9 \cdot 10^{-10} - 0.13$
$b \to u\bar{u}s$	$\frac{\Lambda}{\sqrt{m_b^2-4m_u^2}} = \frac{\Lambda}{m_b}$	$0.042 - 0.48$	$4.2 \cdot 10^{-11} - 0.12$

Table 6.1: Possible values for the HQE expansion parameter and non-perturbative term for different $b \to s$ transitions. Here 0.2 GeV $< \Lambda <$ 2.0 GeV, 4.18 GeV $< m_b <$ 4.78 GeV and 0.975 GeV $< m_c <$ 1.67 GeV.

for the expansion parameter and the non-perturbative term presented on Tab.6.1 (varying Λ within 0.2 and 2 GeV, m_b within 4.18 and 4.78 GeV and m_c within 0.975 and 1.67 GeV).

From this simple numerical exercise one finds that duality violating terms could easily be of a similar size as the expansion parameter of the HQE. Moreover, decay channels like $b \to c\bar{c}s$ might be more strongly affected by duality violations compared to e.g. $b \to u\bar{u}s$. This agrees with the naive expectation that decays with a smaller final state phase space might be more sensitive to duality violation.

Obviously duality cannot be proved directly, because this would require a complete solution of QCD and a sub-sequent comparison with the HQE expectations, which is clearly not possible. To make statements about duality violation in principle two strategies can be performed:

- Study simplified models for QCD, e.g. the t'Hooft model (a two-dimension model for QCD, see e.g. [147–152]) and develop models for duality violations, like instanton-based and resonance-based models (see e.g. [147, 148]).

- Use a pure phenomenological approach, by comparing experiment with HQE predictions.

Here we followed the second strategy and used a simple parameterisation for duality violation in mixing observables and lifetime ratios, which was most pronounced for the $b \to c\bar{c}s$ channel. At this stage it is interesting to note that for many years there

have been problems related to application of the HQE for inclusive b-hadron decays and most of them seemed to be related to the $b \to c\bar{c}s$ channel:

- The experimental Λ_b lifetime was considerably lower than the theory prediction, see e.g. the discussion in [153], where also a simple model for a modification of the HQE was suggested in order to explain experiment, see also [121] and [122]. The dominant contribution to the Λ_b lifetime is given by the $b \to c\bar{u}d$ and $b \to c\bar{c}s$ transitions. To a large extent the Λ_b-lifetime problem has now been solved experimentally, see the detailed discussion in [120], mostly by new measurements from LHCb [154–156]. However, there is still a remaining large theory uncertainty due to unknown non-perturbative matrix elements that could be calculated within lattice-QCD.

- For quite some time the values of the inclusive semi-leptonic branching ratio of B-mesons as well as the average number of charm quarks per b-decay (missing charm puzzle) disagreed between experiment and theory, see e.g. [157–160]. Modifications of the decay $b \to c\bar{c}s$ were considered as a potential candidate for solving this problem. This issue has been improved considerably by new data and and new calculations [108]. Again, there is still a considerable uncertainty remains due to unknown NNLO-QCD corrections. First estimates suggest, that these corrections could be large [161].

- Because of a cancellation of weak annihilation contributions it is theoretically expected (based on the HQE) that the B_s^0-lifetime is more or less equal to the B_d^0-lifetime, see e.g. [120]. For quite some time experiment found deviations of $\tau(B_s^0)/\tau(B_d^0)$ from one - we have plotted the experimental averages from HFAG [1] from 2003 on in Fig.6.1. Currently, there is still a small difference between data and the HQE prediction, which will be discussed further Section 6.2.3. Here again a modification of the $b \to c\bar{u}d$ and/or the $b \to c\bar{c}s$ transitions might solve the problem.

All of these problems are currently considerably softened and huge duality violations are now ruled out by experiment [162], in particular by the measurement of $\Delta\Gamma_s$,

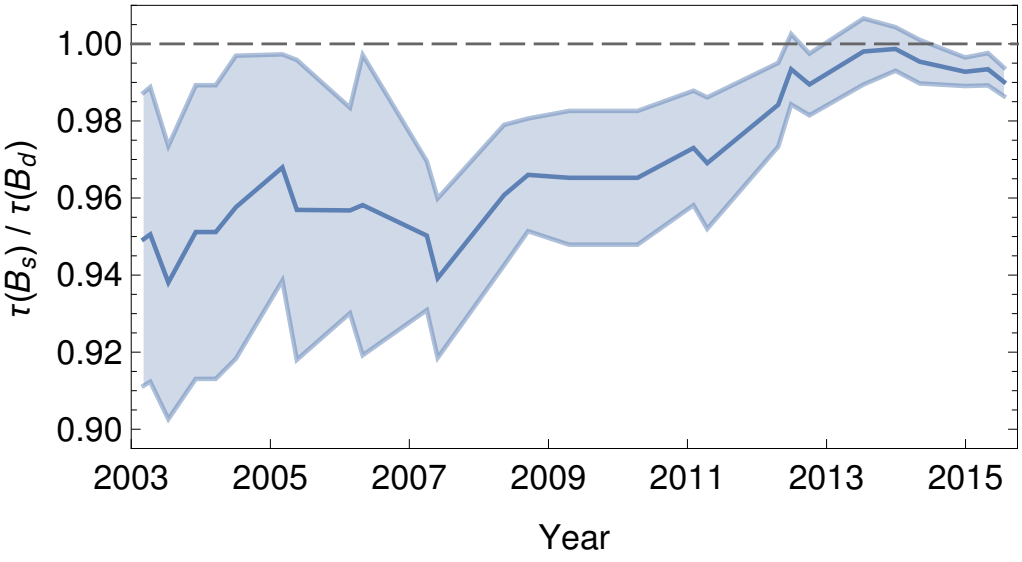

Figure 6.1: Historical values of the lifetime ratio $\tau(B_s)/\tau(B_d)$ as reported by HFAG [1] since 2003. The solid line shows the central value and the shaded line indicates the 1 sigma region, the dotted line corresponds to the theory prediction, which is essentially one, with a tiny uncertainty.

which is dominated by a $b \to c\bar{c}s$ transition. But there is still space for a small amount of duality violation - this amount will be quantified later in this Chapter.
We will thus investigate decay rate difference $\Delta\Gamma_s$ in more detail. According to the HQE we get the following expansion for $\Delta\Gamma_s = 2|\Gamma_{12}^s|\cos\phi_{12}^s$

$$\Gamma_{12}^s = \frac{\Lambda^3}{m_b^3}\left(\Gamma_3^{s,(0)} + \frac{\alpha_s}{4\pi}\Gamma_3^{s,(1)} + ...\right) + \frac{\Lambda^4}{m_b^4}\left(\Gamma_4^{s,(0)} + ...\right) + ... \,. \tag{6.2.2}$$

The leading term $\Gamma_3^{s,(0)}$ has been calculated quite some time ago in [163–168], NLO-QCD corrections $\Gamma_3^{s,(1)}$ have been determined in [48, 53, 169] and sub-leading mass corrections were done in [170–172]. Corresponding lattice values were determined in [173–176].
The most recent numerical update for the mixing quantities is given in [15] (superseding the numerical predictions in [52, 177]) and can be compared to the experimental values from e.g. HFAG [1]. The theory prediction uses conservative ranges for the input parameters - we will present a more aggressive estimate in Section 6.3 and in Appendix E.
Experiment and theory agree very well for the quantities ΔM_q and $\Delta\Gamma_s$. The semi-

Observable	SM	Experiment
ΔM_s	$(18.3 \pm 2.7)\,\text{ps}^{-1}$	$(17.757 \pm 0.021)\,\text{ps}^{-1}$
$\Delta\Gamma_s$	$(0.088 \pm 0.020)\,\text{ps}^{-1}$	$(0.082 \pm 0.006)\,\text{ps}^{-1}$
a_{sl}^s	$(2.22 \pm 0.27) \cdot 10^{-5}$	$(-750 \pm 410) \cdot 10^{-5}$
$\Delta\Gamma_s/\Delta M_s$	$48.1\,(1 \pm 0.173) \cdot 10^{-4}$	$46.2\,(1 \pm 0.073) \cdot 10^{-4}$
ΔM_d	$(0.528 \pm 0.078)\,\text{ps}^{-1}$	$(0.5055 \pm 0.0020)\,\text{ps}^{-1}$
$\Delta\Gamma_d$	$(2.61 \pm 0.59) \cdot 10^{-3}\,\text{ps}^{-1}$	$0.657895(1 \pm 10) \cdot 10^{-3}\,\text{ps}^{-1}$
a_{sl}^d	$(-4.7 \pm 0.6) \cdot 10^{-4}$	$(-15 \pm 17) \cdot 10^{-4}$
$\Delta\Gamma_d/\Delta M_d$	$49.4\,(1 \pm 0.172) \cdot 10^{-4}$	$13.0147\,(1 \pm 10) \cdot 10^{-4}$

Table 6.2: Numerical update for different mixing observables in the B_s^0 and the B_d^0 sectors as presented in [15].

leptonic asymmetries and the decay rate difference in the B_d^0-system have not been observed yet. More profound statements about the validity of the theory can be made by comparing the ratio of $\Delta\Gamma_s$ and ΔM_s, where many theoretical uncertainties cancel and we get

$$\frac{\left(\frac{\Delta\Gamma_s}{\Delta M_s}\right)^{\text{Exp}}}{\left(\frac{\Delta\Gamma_s}{\Delta M_s}\right)^{\text{SM}}} = 0.96 \pm 0.19\,. \tag{6.2.3}$$

The central value shows a perfect agreement of experiment and HQE predictions. The remaining uncertainty leaves some space for new physics effects or for violations of duality. Thus we can make statements like: in the most sensitive decay channel $b \to c\bar{c}s$ duality is violated by at most 19%. In the next section we try to investigate these questions a little more in detail.

Assuming no new physics in ΔM_s we can further reduce the theory error for $\Delta\Gamma_s$ by using

$$\Delta\Gamma_s^{2015,\text{SMb}} = \left(\frac{\Delta\Gamma_s}{\Delta M_s}\right)^{\text{SM}} \cdot \Delta M_s^{\text{Exp}} = 0.085 \pm 0.015\,\text{ps}^{-1}\,. \tag{6.2.4}$$

This is currently the most precise prediction for the decay rate difference; in Section 6.3 we will give a less conservative estimate of the SM prediction for $\Delta\Gamma_s$, with an even smaller uncertainty.

In the ratio $\Delta\Gamma_s/\Delta M_s$ theoretical uncertainties are cancelling and thus the corresponding theory error is smaller than for $\Delta\Gamma_s$ alone. We would re-introduce this uncertainty by multiplying with the theory value of ΔM_s. Using instead the experimental value of ΔM_s, which has in comparison a negligible error we get a more precise prediction of $\Delta\Gamma_s$, which, however, only holds under the assumption that ΔM_s^{Exp} is given by its SM value.

6.2.1 B-mixing

We introduce a simple model for duality violation in B-mixing. Such effects are typically expected to be larger, if the phase-space of a B_s^0 decay becomes smaller. Thus b-quark decays into two charm quarks are expected to be more strongly affected by duality violating effects compared to b-quark decays into two up quarks. Motivated by the observations in Section 6.2 we modify the on-shell terms of the mixing diagram Γ_{12}^s according to

$$\Gamma_{12}^{s,cc} \rightarrow \Gamma_{12}^{s,cc}(1+4\delta)\,, \tag{6.2.5}$$

$$\Gamma_{12}^{s,uc} \rightarrow \Gamma_{12}^{s,uc}(1+\delta)\,, \tag{6.2.6}$$

$$\Gamma_{12}^{s,uu} \rightarrow \Gamma_{12}^{s,uu}(1+0\delta)\,. \tag{6.2.7}$$

Similar models have been used in [178–180] for penguin insertions with a $c\bar{c}$-loop. The $c\bar{c}$ contribution is affected by a correction of 4δ, $c\bar{u}$ by δ and $u\bar{u}$ is not affected at all. Already at this stage ones sees that such a model is softening GIM cancellations in the ratio Γ_{12}^s/M_{12}^s; we get

$$\frac{\Gamma_{12}^s}{M_{12}^s} = 10^{-4}\left[c(1+4\delta) + \frac{\lambda_u}{\lambda_t}\left(a+\delta(6c+a)\right) + \frac{\lambda_u^2}{\lambda_t^2}(b+\delta(2c+a))\right]\,. \tag{6.2.8}$$

Studying this expression, we find that the decay rate difference is mostly given by the first term on the r.h.s., so we expect $\Delta\Gamma_s/\Delta M_s \approx -c(1+4\delta)\cdot 10^{-4}$, which is equivalent to our naive starting point of comparing experiment and theory prediction for $\Delta\Gamma_s$. The semi-leptonic CP asymmetries will be dominantly given by the second term on the r.h.s., $a_{sl}^s \approx \Im(\lambda_u/\lambda_t)\left[a+\delta(6c+a)\right]\cdot 10^{-4}$. Now the duality violating coefficient δ is GIM enhanced by $(6c+a)$ compared to the leading term a. Having an

Observable	B_s^0	B_d^0
$\frac{\Delta\Gamma_q}{\Delta M_q}$	$48.1(1+3.95\delta)\cdot 10^{-4}$	$49.5(1+3.76\delta)\cdot 10^{-4}$
$\Delta\Gamma_q$	$0.0880(1+3.95\delta)\,\mathrm{ps}^{-1}$	$2.61(1+3.759\delta)\cdot 10^{-3}\,\mathrm{ps}^{-1}$
a_{sl}^q	$2.225(1-22.3\delta)\cdot 10^{-5}$	$-4.74(1-24.5\delta)\cdot 10^{-4}$

Table 6.3: Duality violation dependency for different B-mixing observables in the B_s^0 and the B_d^0 sectors based on the model introduced by Eq. (6.2.5,6.2.6,6.2.7)

agreement of experiment and theory for semi-leptonic CP asymmetries could thus provide very strong constraints on duality violation. Using the values of a, b and c from Tab.2.2 and the CKM elements from Eq.(2.1) we get for the observables ΔM_q, $\Delta\Gamma_q$ and a_{sl}^q the following dependence on the duality violating parameter δ:
As expected we find that the duality violating parameter δ has a decent leverage on $\Delta\Gamma_q$ and a sizeable one on a_{sl}^q. The expressions for $\Delta\Gamma_q$ were obtained by simply multiplying the theory ratio $\Delta\Gamma_q/\Delta M_q$ with the theoretical values of the mass difference, as given on Tab.6.2.
Comparing experiment and theory for the ratio of the decay rate difference $\Delta\Gamma_s$ and the mass difference ΔM_s we found (see Eq.(6.2.3)) an agreement with a deviation of at most 19%. Thus the duality violation - i.e. the factor $1+3.95\delta$ in Tab.6.3 - has to be smaller than this uncertainty:

$$1+3.95\delta \leq 0.96 \pm 0.19 \Rightarrow \delta \in [-0.0583, 0.0380]\,. \tag{6.2.9}$$

Equivalently this bound tells us that the duality violation in the cc-channel is at most $+15.2\%$ or -23.3%, if the effect turns out to be negative. If there would also be an 19% agreement of experiment and theory for the semi-leptonic asymmetry a_{sl}^s, then we could shrink the bound to δ down to 0.00851. Unfortunately experiment is still far away from the SM prediction, see Tab.6.2. However, we can turn around the argument: i.e. having a duality violation that lifts GIM suppression - the theory prediction of a_{sl}^s can be enhanced/diminished at most to

$$a_{sl}^s \;=\; [0.336, 5.12]\cdot 10^{-5}\,. \tag{6.2.10}$$

In the B_d^0-system a comparison of experiment and theory for the ratio of decay

rate difference and mass difference turns out to be tricky, since $\Delta\Gamma_d$ is not yet measured, see Tab.6.2. If we would use the current experimental bound on the decay rate difference $\Delta\Gamma_d$, we would get artificially large bounds on δ. Looking at the structure of the loop contributions necessary to calculate Γ_{12}^d and Γ_{12}^s, one finds very similar $c\bar{c}$-, $u\bar{c}$-, $c\bar{u}$- and $u\bar{u}$-contributions. Our duality violation model is based on the phase space differences of decays like $B_s^0 \to D_s D_s$ (cc), $B_s^0 \to D_s K$ (uc) and $B_s^0 \to \pi K$ (uu), which are very pronounced. On the other hand we find that the phase space differences of B_s^0- and B_d^0-decays are not very pronounced, i.e. the difference between e.g. $B_s^0 \to D_s D_s$ vs. $B_d^0 \to D_s D$ is small - compared to the above differences due to different internal quarks. Hence, we conclude that the duality violation bounds from the B_s^0-system can also be applied to a good approximation to the B_d^0-system. With the B_s^0-bound we get that the theory prediction of a_{sl}^d and $\Delta\Gamma_d$ can be enhanced/diminished due to duality violations at most to

$$a_{sl}^d \in [-11.5, -0.326] \cdot 10^{-4} , \tag{6.2.11}$$

$$\Delta\Gamma_d \in [2.04, 2.98] \cdot 10^{-3} \text{ ps}^{-1} . \tag{6.2.12}$$

These numbers can be compared to the SM values obtained in [15], see Tab.6.2. In principle any measurement of these observables outside the ranges in Eq.(6.2.10), Eq.(6.2.11) and Eq.(6.2.12) would be a clear indication of new physics. New physics in $\Delta\Gamma_d$ could have the very interesting effect of reducing [102] the still existing discrepancy of the dimuon asymmetry measured at D0 [104–107]. Currently a sizeable enhancement of $\Delta\Gamma_d$ is not excluded by theoretical or experimental bounds [2]. Thus it clearly important to distinguish hypothetical duality violating effects in $\Delta\Gamma_d$ from new physics effects.

Considering that our conclusions (new physics or unknown hadronic effects) are quite far-reaching, we try to be as conservative as possible and we will firstly use a more profound statistical method, a likelihood ratio test. For our likelihood function we use a Gaussian function

$$\mathcal{L} = \exp\left(-\frac{(\text{theory} - \text{experiment})^2}{2\sigma^2}\right)$$

where, to take into account the uncertainty on both theory and experiment, we take

for our error the quadrature sum, i.e.

$$\sigma^2 = \sigma^2_{\text{exp}} + \sigma^2_{\text{theory}}$$

The test we apply is $-2\ln\mathcal{L}/\widehat{\mathcal{L}} \leq 2.71$, where our choice of 2.71 gives a 90% confidence limit on our parameters and in principle we normalise by the maximum likelihood $\widehat{\mathcal{L}}$. However, in our model the maximum likelihood of $\widehat{\mathcal{L}} = 1$ is always achievable, and so our test reduces to simply $-2\ln\mathcal{L} \leq 2.71$.

Our more conservative bound for δ is now supposed to be given by

$$-0.0879 \leq \delta \leq 0.0679\,, \tag{6.2.13}$$

with a 90% confidence level (1.6 standard deviations). This more conservative statistical method almost doubles the allowed region for δ. Inserting these values into the predictions for $a_{sl}^{d,s}$ and $\Delta\Gamma_d$ we see that duality violation can give at most the following ranges for the mixing observables:

$$a_{sl}^s \in [-1.15, 6.59]\cdot 10^{-5}\,, \tag{6.2.14}$$

$$a_{sl}^d \in [-14.9, 3.14]\cdot 10^{-4}\,, \tag{6.2.15}$$

$$\Delta\Gamma_d \in [1.75, 3.28]\cdot 10^{-3}\ \text{ps}^{-1}\,. \tag{6.2.16}$$

The second modification to ensure that our estimates are conservative concerns our ad-hoc ansatz in Eqs.(6.2.5), (6.2.6), (6.2.7), where we assumed that the cc-part is affected by duality violations four times as much as the cu-part and the uu-part is not affected at all; we can obtain more general results with the following modification

$$\Gamma_{12}^{s,cc} \to \Gamma_{12}^{s,cc}(1+\delta^{cc})\,, \tag{6.2.17}$$

$$\Gamma_{12}^{s,uc} \to \Gamma_{12}^{s,uc}(1+\delta^{uc})\,, \tag{6.2.18}$$

$$\Gamma_{12}^{s,uu} \to \Gamma_{12}^{s,uu}(1+\delta^{uu})\,, \tag{6.2.19}$$

with $\delta^{cc} \geq \delta^{uc} \geq \delta^{uu}$ and the requirement that all δs must have the same sign. Now we get for the observables

$$\frac{\Delta\Gamma_s}{\Delta M_s} = 48.1(1 + 0.982\delta^{cc} + 0.0187\delta^{uc} - 0.000326\delta^{uu})\cdot 10^{-4}\,, \tag{6.2.20}$$

$$\Delta\Gamma_d = 26.1(1 + 0.852\delta^{cc} + 0.350\delta^{uc} - 0.202\delta^{uu})\cdot 10^{-4}\text{ps}^{-1}\,, \tag{6.2.21}$$

$$a_{sl}^s = 2.225(1 - 7.75\delta^{cc} + 8.67\delta^{uc} + 0.0780\delta^{uu})\cdot 10^{-5}\,, \tag{6.2.22}$$

$$a_{sl}^d = -4.74(1 - 8.52\delta^{cc} + 9.60\delta^{uc} - 0.0787\delta^{uu})\cdot 10^{-4}\,. \tag{6.2.23}$$

In the case of $\Delta\Gamma_s$, which will be used to determine the size of the duality violating δs, the coefficients of the uu component are suppressed by more than three orders of magnitude compared to the rest and therefore neglected. For the semi-leptonic CP asymmetries the uu duality violating component is about two orders of magnitude lower than the rest, thus we neglect the uu component in the following. This might lead to an uncertainty of about 20% in the duality bounds for $\Delta\Gamma_d$, which we will keep in mind.

Considering only δ^{cc} and δ^{uc} we get with the likelihood ratio test the bounds depicted in Fig.6.2 at a 90% confidence level. Fig.6.2 shows that a duality violation of no

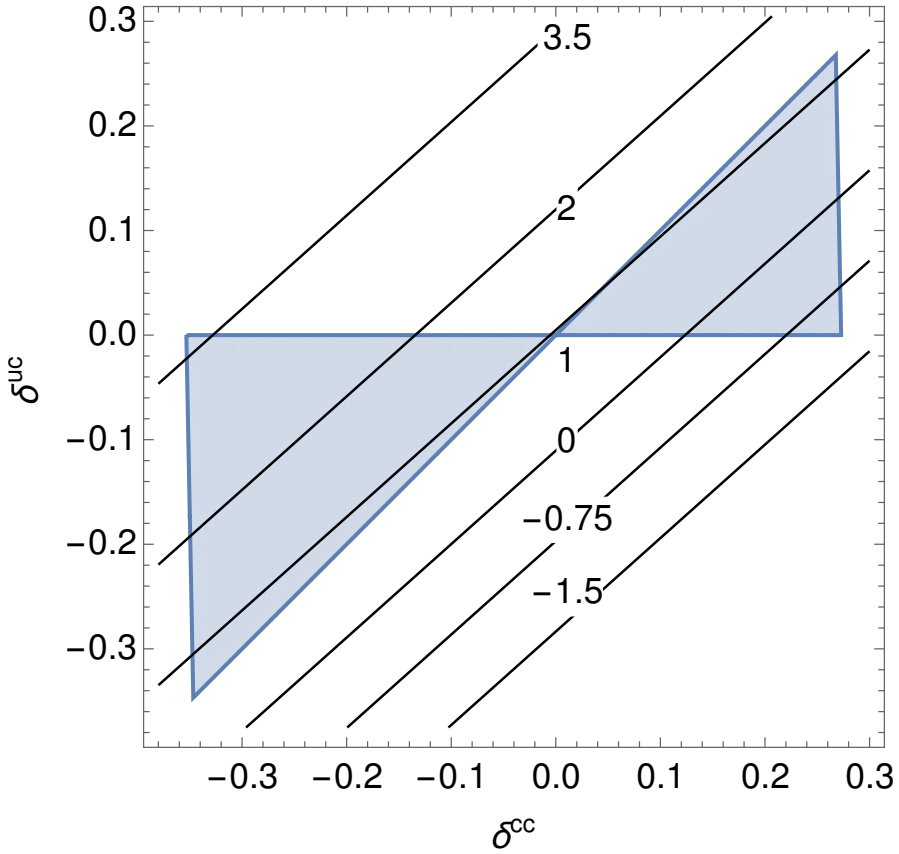

Figure 6.2: 90% confidence limits on δ^{cc} and δ^{uc} for the B_s^0-system from a comparison of the experimentally allowed region of $(\Delta\Gamma_s/\Delta M_s)$ with the theory expression in Eq.(6.2.20). The allowed regions for the δs are shaded blue(grey). A deviation of the δs from zero will also affect the theory prediction of a_{sl}^s in Eq. 6.2.23. The modification factors of $a_{sl}^s/a_{sl}^{s,\mathrm{SM}}$ are denoted by the black lines.

more than 35% is allowed in either Γ^s_{cc} or in Γ^s_{uc}. We also see that it is in principle possible to see duality violation in $\Delta\Gamma_s$ but not in a^s_{sl} and vice versa. Moreover, we find from the functional form of a^s_{sl}, that this quantity achieves a maximum (minimum) when $\delta_{uc} = 0$ and $\delta_{cc} < 0$ or (> 0). Our generalised parameterisation of duality violation gives now the most conservative bounds on the mixing observables

$$a^s_{sl} \in [-2.48, 8.32] \cdot 10^{-5}\,, \tag{6.2.24}$$

$$a^d_{sl} \in [-19.0, 6.28] \cdot 10^{-4}\,, \tag{6.2.25}$$

$$\Delta\Gamma_d \in [1.52, 3.45] \cdot 10^{-3}\,\mathrm{ps}^{-1}\,. \tag{6.2.26}$$

We are now in a position to make a strong statement: any measurement outside this range, cannot be due to duality violation and it will be an unambiguous signal for new physics.

Considering that the ranges in Eq.(6.2.24), Eq.(6.2.25) and Eq.(6.2.26) are considerably larger than the uncertainties of the corresponding SM prediction given on Tab.6.2 the question of how to further shrink the duality bounds is arising. Currently the bound on the duality violating parameters δ comes entirely from $\Delta\Gamma_s$, where the current experimental and theoretical uncertainty adds up to $\pm 19\%$.Any improvement on this uncertainty will shrink the allowed regions on δ. In Section 6.3 we will discuss a more aggressive estimate of the theory predictions for the mixing observable, indicating that a theory uncertainty of about $\pm 10\%$ or even $\pm 5\%$ in $\Delta\Gamma_s/\Delta M_s$ might come into sight. Including also possible improvements in experiment this would indicate a region for δ that is considerably smaller than the ones given in Eq.(6.2.24), Eq.(6.2.25) and Eq.(6.2.26). The current (and a possible future) situation are summarised in Fig.6.3. On the l.h.s. of Fig.6.3 $\Delta\Gamma_d$ is investigated. The current experimental bound is given by the blue region, which can be compared to the SM prediction (green). As we have seen above, because of still sizeable uncertainties in $\Delta\Gamma_s$ duality violation of up to 35% can currently not be excluded - this would lead to an extended region (brown) for the SM prediction including duality violation. If in future $\Delta\Gamma_s$ will be known with a precision of about 5% both in theory and experiment, than the brown region will shrink to the orange

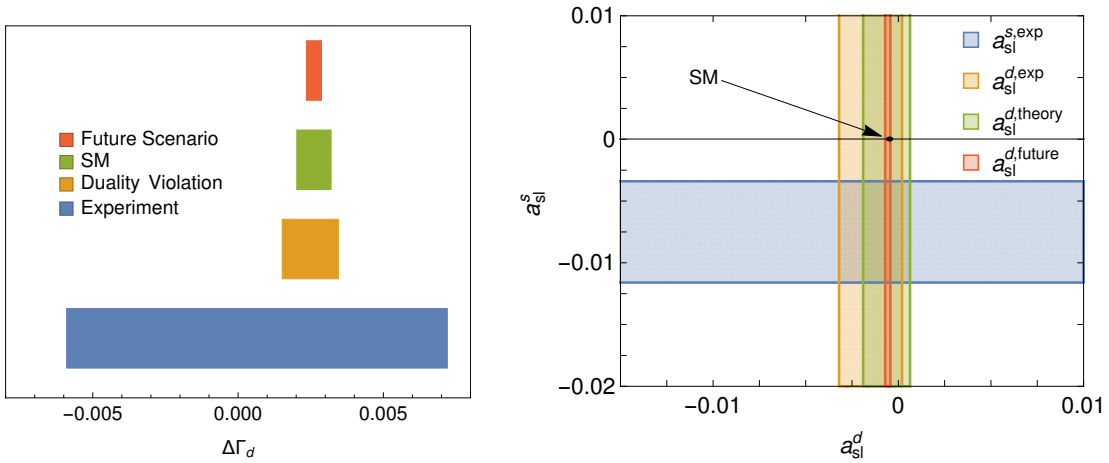

Figure 6.3: Comparison of SM prediction (green), SM + duality violation (brown), SM + duality violation in future (orange) and current experimental (blue) bound for $\Delta\Gamma_d$ (l.h.s.). One the r.h.s. the experimental bounds on a_{sl}^d (brown) and a_{sl}^s (blue) are shown in comparison to their theory values. Any measurement outside the allowed theory regions will be a clear indication for new physics. The theory uncertainties for a_{sl}^s are so small, that they cannot be resolved, they are depicted by the black line. For a_{sl}^d the duality allowed region (green) has quite some overlap with the experimental one, in future this region can be shrinked to the red region.

one - here also the intrinsic precision of the SM value will be reduced. In other words, currently any measurement of $\Delta\Gamma_d$ outside the brown region will be a clear signal of new physics; in future any measurement outside the orange region can be a signal of new physics. The same logic is applied for the r.h.s. of Fig.6.3, where a^d_{sl} and a^s_{sl} are investigated simultaneously. For a^s_{sl} still any measurement outside the bounds in Eq.(6.2.24) would be clear indication of new physics. This bound in Fig.6.3 is so small, compared to the current blue experimental region, that it can only be resolved as a single line (black). For a^d_{sl} the current experimental region is given by the orange region, which is only slightly larger, than the green region, which is indicating the theory prediction including duality violation. Future improvement in experiment and theory for $\Delta\Gamma_s$ will reduce the green region to the red one and then any measurement outside the red region will be a clear signal of new physics.
In addition we can ask if there are more observables that will be affected by the above discussed duality violations. An obvious candidate is the dimuon asymmetry, which depends on a^d_{sl}, a^s_{sl} and $\Delta\Gamma_d$. This will be discussed in Sec. 6.2.2. Another candidate is the the lifetime ratio $\tau(B^0_s)/\tau(B^0_d)$, where the dominant diagrams are very similar to the mixing ones, this observable will be studied further in Sec. 6.2.3.

6.2.2 Duality bounds from the dimuon asymmetry

In section 5.3 we introduced the like-sign dimuon asymmetry and we mentioned the discrepancies with respect to the SM found in the measurements performed by D0. Here we want to investigate the possibility of explaning the gap between theory and experiment as an effect of duality violation. Our starting point is Eq. (5.3.8), even though we have already identified problems on its derivation we will take into account the suggested factor of 0.5 in the coefficient of $\Delta\Gamma_d$ as a first correction to the interference contribution as pointed out by [115].
Using the information provided in [107] we determine the set of coefficients for mixing and interference shown on Tab.6.4
With the inputs on Tab.6.4 we obtain a SM estimate for A_{CP} of

$$A^{\rm SM}_{CP} \;=\; (-2.61 \pm 0.64)\cdot 10^{-4}\,. \tag{6.2.27}$$

Parameter	Value
C_{sl}^d	0.220 ± 0.018
C_{sl}^s	0.157 ± 0.013
C_{int}	-0.040 ± 0.013

Table 6.4: Mixing and Interference coefficients for the like-sign dimuon asymmetry formula in the Borissov-Honeisen interpretation.

Using our simple model for duality violation, see Tab.6.3, we get for the theory prediction of A_{CP} after including duality violating effects

$$A_{CP} = -2.61(1 - 7.17\delta) \cdot 10^{-4} \,. \tag{6.2.28}$$

This can be compared to the experimental result provided by D0 [107]

$$A_{CP} = (-2.35 \pm 0.84) \cdot 10^{-3} \,. \tag{6.2.29}$$

We find that there is an agreement of experiment and theory if δ lies in the following region (90 % confidence level)

$$-1.87 \leq \delta \leq -0.37 \,. \tag{6.2.30}$$

This is clearly out of the range found in Eq. (6.2.13) from the direct constraints of mixing observables. On the other hand we find with the allowed δ-regions given in Eq. (6.2.13), that A_{CP} can be at most enhanced to

$$-4.25 \cdot 10^{-4} \leq A_{CP} \leq -1.34 \cdot 10^{-4} \,, \tag{6.2.31}$$

which is considerably smaller thant the experimental result. This excludes the possibility of explaining the current value for A_{CP} as an effect of duality violation at the 2σ level.

6.2.3 Duality bounds from lifetime ratios

Very similar diagrams to the ones in Γ_{12}^q arise in the lifetime ratio $\tau(B_s^0)/\tau(B_d^0)$, see Fig.6.4. The obvious difference between the two diagrams is the trivial exchange of

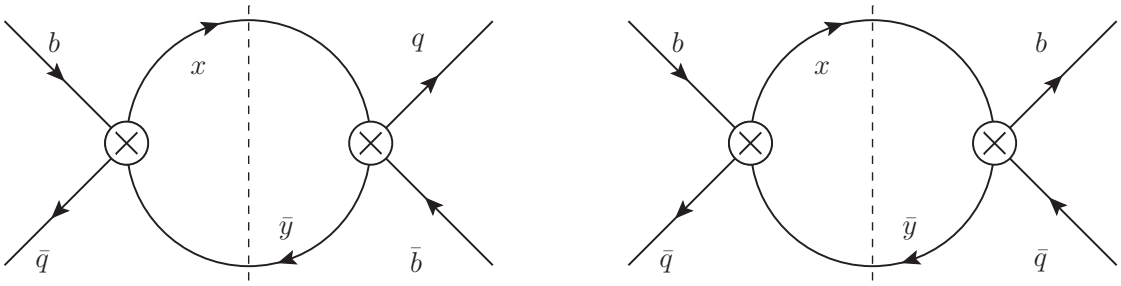

Figure 6.4: Diagrams contributing to the Γ_{12}^q (l.h.s.) and diagrams contributing to the lifetime of a B_q^0-meson (r.h.s.).

b- and q-lines at the right end of the diagrams. A more subtle and more important difference lies in the possible intermediate states, when cutting the diagrams in the middle. In the case of lifetimes all possible intermediate states that can originate from a $x\bar{y}$ quark pair, can arise. In the case of mixing, we have only the subset of all intermediate states into which both B_q^0 and $\bar{B}_q^0$ can decay. Independent of this observation, our initial argument that the phase space for intermediate $c\bar{c}$-states is smaller than the one for intermediate $u\bar{c}$-states, which is again smaller that the $u\bar{u}$-case, still holds. Hence we assume that the $x\bar{y}$-loop for the lifetime ratio, has the same duality violating factor δ^{xy} as the $x\bar{y}$-loop for Γ_{12}^q. It turns out that the largest weak annihilation contribution to the B_s^0-lifetime is given by a cc-loop, while for the B_d^0-lifetime a uc-loop is dominating. This observation tells us that duality will not not drop out in the lifetime ratio, because the dominating contributions for B_s^0 and B_d^0 are affected differently. Using our above model and modifying the cc-loop with a factor $1 + 4\delta$ and the uc-loop with a factor $1 + \delta$, we get with the expressions in [120–123]

$$\frac{\tau(B_s^0)}{\tau(B_d^0)} = 1.00050 \pm 0.00108 - 0.0225\,\delta\,. \tag{6.2.32}$$

A detailed estimate of the theoretical error is given in Appendix E. Unfortunately, the SM prediction relies strongly on lattice calculations that are already 15 years old [181] and no update has been performed since then. For a more detailed discussion of the status of lifetime predictions, see [120]. Nevertheless, one finds a big impact of the duality violating factor δ on the final result. A value of $\delta = 1$ would have huge effects, compared to the central value within the SM and its uncertainty.

Our theory prediction can be compared to the current experimental value for the lifetime ratio [1]

$$\frac{\tau(B_s^0)}{\tau(B_d^0)} = 0.990 \pm 0.004\,. \tag{6.2.33}$$

If the tiny deviation between theory and experiment is attributed to duality violation, then we get an allowed range for δ of

$$\delta \in [+0.243, +0.698] \text{ (naive)}\,, \tag{6.2.34}$$

$$\delta \in [+0.179, +0.743] \text{ (likelihood ratio 90\%)}\,. \tag{6.2.35}$$

There is currently a discrepancy of about 2.5σ between experiment (Eq.(6.2.33)) and theory (Eq.(6.2.32)) and this difference could stem from new physics or a sizeable duality violation of $\delta \approx 0.5$ in lifetimes. The allowed region of the duality violating parameter δ can be read off Fig.6.5, where the current experimental bound from Eq.(6.2.33) is given by the blue region and theory prediction including hypothetical duality violation by the red region. It goes without saying that 2.5 standard deviations is much too little to justify profound statements, thus we consider next future scenarios where the experimental uncertainty of the lifetime ratio will be reduced to ± 0.001.

- Scenario I: the central value will stay at the current slight deviation from one:

$$\frac{\tau(B_s^0)}{\tau(B_d^0)}^{\text{Scenario I}} = 0.990 \pm 0.001\,. \tag{6.2.36}$$

  This scenario corresponds to a clear sign of duality violation or new physics in the lifetime ratio. Assuming the first one, we get a range of δ of (see the violet region in Fig.6.5)

$$\delta \in [0.377, 0.563] \text{ naive}\,, \tag{6.2.37}$$

$$\delta \in [0.359, 0.575] \text{ likelihood ratio } 90\%\,. \tag{6.2.38}$$

  Thus the lifetime ratio requires large values of δ. Our final conclusions depend now on the future developments of $\Delta\Gamma_s$. Currently $\Delta\Gamma_s$ requires small values of δ, which is in contrast to scenario I. Thus we have to assume additional new physics effects - either in mixing or in lifetimes - that might solve the

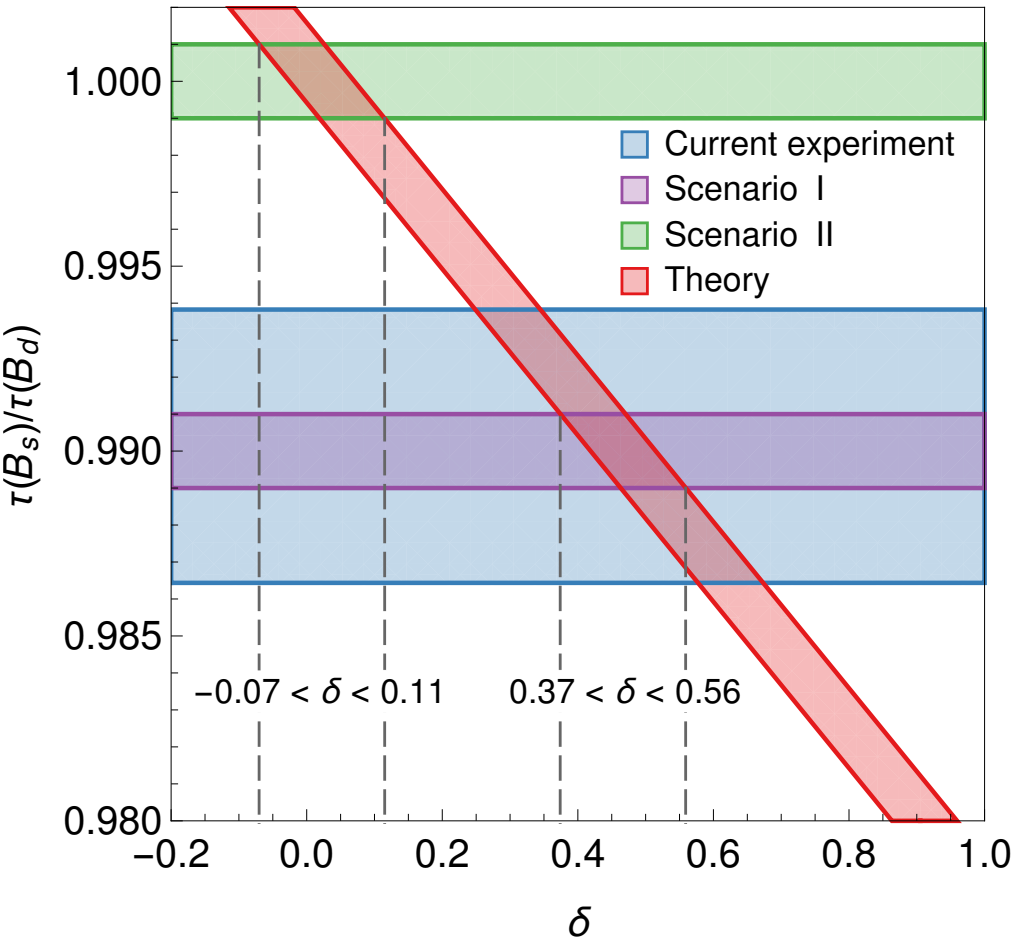

Figure 6.5: Duality bounds extracted from the lifetime ratio $\tau(B_s^0)/\tau(B_d^0)$. The red band shows the theoretical expected value, see Eq.(6.2.32) of the lifetime ratio in dependence of the δ. The current experimental bound is given by the blue region and the overlap of both gives the current allowed region δ, indicated in Eq.(6.2.35). The future scenarios are indicated by the violet band (Scenario I) and the green band (Scenario II). Again the overlap of the future scenarios with the theory prediction gives future allowed regions for δ.

discrepancy. If in future the theory value of $\Delta\Gamma_s$ will go up sizeable or the experimental value will go down considerably, then mixing might also require a big value of δ and we then would have duality violation as a simple solution for explaining discrepancies in both lifetimes and B_s^0-mixing.

- Scenario II: the central value will go up to the SM expectation:

$$\frac{\tau(B_s^0)}{\tau(B_d^0)}^{\text{Scenario II}} = 1.000 \pm 0.001\,, \tag{6.2.39}$$

In that case we will find only a small allowed region for δ around zero, see the green region in Fig.6.5

$$\delta \in [-0.0708, 0.116]\,\text{naive}\,, \tag{6.2.40}$$

$$\delta \in [-0.0853, 0.130]\,\text{likelihood ratio } 90\%\,. \tag{6.2.41}$$

The above region is, however, still larger than the one obtained from $\Delta\Gamma_s$. New lattice determinations of lifetime matrix elements might change this picture and in the end the lifetime ratio might also lead to slightly stronger duality violating bounds than $\Delta\Gamma_s$. Again our final conclusion depends on future developments related to $\Delta\Gamma_s$. If both experiment and theory for mixing stay at their current central values, we simply get very strong bounds on δ. If theory or experiment will change in future, this could be indications for deviations in mixing, which have to be compared to the agreement of experiment and theory for lifetimes in Scenario II.

In Section 6.3 we will discuss a possible future development of future theory predictions for mixing observables.

Before we proceed let us make a comment about our duality model. In principle we also could generalise our duality ansatz, and modify the cc-loop with a factor $1 + \delta^{cc}$ and the uc-loop with a factor $1 + \delta^{uc}$, as we did in the mixing case. We get the following expression

$$\frac{\tau(B_s^0)}{\tau(B_d^0)} = 1 + 0.0005(1 - 13.4\delta^{cc} + 8.92\delta^{uc}) \tag{6.2.42}$$

Here one sees a pronounced cancellation of the cc and the uc contribution, if one allows δ^{cc} to be of similar size as δ^{uc}. This is, however, not what we expect from our

phase space estimates for duality violation. Thus we use for the lifetime ratio only our model given in Eq.(6.2.32).

6.3 Numerical Updates of Standard Model Predictions

We have already pointed out that more precise values of $\Delta\Gamma_s$ are needed to derive more stringent bounds on duality violation in the B-system. Very recently the Fermilab MILC collaboration presented a comprehensive study of the non-perturbative parameters that enter B-mixing [79].[1]
A brief summary of their results reads:

- Improved numerical values for the non-perturbative matrix elements $\langle Q\rangle$, $\langle Q_S\rangle$, $\langle \tilde{Q}_S\rangle$, $\langle R_0\rangle$, $\langle R_1\rangle$ and $\langle \tilde{R}_1\rangle$ that are necessary for $\Delta\Gamma_q$ and ΔM_q. Hence we have numerical values for all operators that are arising up to dimension seven in the HQE, up to R_2 and R_3, which are still unknown and can only be estimated by using vacuum insertion approximation.

- The results provide a very strong confirmation of vacuum insertion approximation. All their bag parameters turn out to be in the range of 0.8 to 1.2. Sometimes in the literature different normalisations of the matrix elements are used, that lead to values of the bag parameters that differ from one in vacuum insertion approximation, see e.g. the discussion in [15]. The definitions in [79] are all consistent with $B = 1 \pm 0.2$ in vacuum insertion approximation.

- The numerical values of $f_{B_q}^2 B$ are larger than most previous lattice calculations.

Based on these new results we perform a more aggressive - compared to the recent study in [15] - numerical analysis of the SM predictions, where we try to push

[1] A first numerical analysis with this new inputs was already performed in [182]; but the authors put their emphasis on the implications for the correlation between $\Delta M_{s,d}$ and ϵ_K in models with constrained MFV and implications for $\Delta\Gamma_{s,d}$ have not been analized.

the current theory uncertainties to the limits. In particular we will modify the predictions in [15] by using

- Most recent values of the CKM parameter from CKMfitter [17] (similar values can be obtained from UTfit [54]).
- New Fermilab MILC results for the bag parameters of Q, $\tilde{Q}_S$, R_0, R_1 and $\tilde{R}_1$. We do not try to average with other lattice results, e.g. the values given by FLAG [183].
- Assume vacuum insertion approximation for R_2 and R_3 with a small uncertainty of $B = 1 \pm 0.2$. We note that this is not clearly justified yet and it has to be confirmed by independent determinations of the corresponding bag parameters.
- Use results derived from equations of motion $\tilde{B}_{R_3} = 7/5 B_{R_3} - 2/5 B_{R_2}$ and $\tilde{B}_{R_2} = -B_{R_2}$ [170].

All inputs are listed in Appendix E. We first note that the overall normalisation due to $f_{B_q}^2 B$ seems to be considerably enhanced now, so we expect enhancements in ΔM_q and $\Delta\Gamma_q$ that will cancel in the ratio. Moreover the uncertainty in the bag parameter ratio $\tilde{B}_S/B$ is larger than e.g. in [15]. On the other hand the dominant uncertainty due to R_2 and R_3 will now be dramatically be reduced.

Putting everything together we get with the new parameters, the predictions presented on Tab.6.3 for the two neutral B-systems, which are compared with the more conservative theory predictions [15] and the experimental values from HFAG [1], that were already given on Tab.6.2.

The new theory values for ΔM_q and $\Delta\Gamma_q$ are larger than the ones presented in [15] and they are further from experiment. For the ratios $\Delta\Gamma_q/\Delta M_q$ and a_{sl}^q the central values are only slightly enhanced. The overall error shrinks by about a factor of two for ΔM_s and also sizeably for ΔM_d, $\Delta\Gamma_q$ and the ratios $\Delta\Gamma_q/\Delta M_q$. For the semi-leptonic asymmetries the effect is less pronounced. In Appendix E a detailed analysis of the errors is given.

It is now interesting to consider the ratios of the new SM predictions normalised to

Observable	SM - conservative	SM - aggressive	Experiment
ΔM_s (ps^{-1})	(18.3 ± 2.7)	(20.31 ± 1.37)	(17.757 ± 0.021)
$\Delta\Gamma_s$ (ps^{-1})	(0.088 ± 0.02)	(0.098 ± 0.014)	(0.082 ± 0.006)
a_{sl}^s	$(2.22 \pm 0.27) \cdot 10^{-5}$	$(2.27 \pm 0.25) \cdot 10^{-5}$	$(-7.5 \pm 4.1) \cdot 10^{-3}$
$\frac{\Delta\Gamma_s}{\Delta M_s}$	$48.1\,(1 \pm 0.173) \cdot 10^{-4}$	$49.3\,(1 \pm 0.125)$	$46.2\,(1 \pm 0.073) \cdot 10^{-4}$
ΔM_d (ps^{-1})	(0.528 ± 0.078)	(0.606 ± 0.056)	(0.5055 ± 0.0020)
$\Delta\Gamma_d$ (ps^{-1})	$(2.61 \pm 0.59) \cdot 10^{-3}$	$(2.99 \pm 0.52) \cdot 10^{-3}$	$(0.658 \pm 6.579) \cdot 10^{-3}$
a_{sl}^d	$(-4.7 \pm 0.6) \cdot 10^{-4}$	$(-4.90 \pm 0.54) \cdot 10^{-4}$	$(-1.5 \pm 1.7) \cdot 10^{-3}$
$\frac{\Delta\Gamma_d}{\Delta M_d}$	$49.4\,(1 \pm 0.172) \cdot 10^{-4}$	$49.3\,(1 \pm 0.149)$	$13.0147\,(1 \pm 10) \cdot 10^{-3}$

Table 6.5: Comparison between the conservative and the aggressive estimates for B_s^0 and B_d^0 mixing observables

the experimental numbers.

$$\frac{\Delta M_s^{\mathrm{SMagr.}}}{\Delta M_s^{\mathrm{Exp}}} = 1.133(1 \pm 0.068)(1 \pm 0.0012) \tag{6.3.1}$$

$$= 1.133(1 \pm 0.068)\,, \tag{6.3.2}$$

$$\frac{\Delta\Gamma_s^{\mathrm{SMagr.}}}{\Delta\Gamma_s^{\mathrm{Exp}}} = 1.20(1 \pm 0.142)(1 \pm 0.073) \tag{6.3.3}$$

$$= 1.20(1 \pm 0.16)\,, \tag{6.3.4}$$

$$\frac{\left(\frac{\Delta\Gamma_s}{\Delta M_s}\right)^{\mathrm{Exp.}}}{\left(\frac{\Delta\Gamma_s}{\Delta M_s}\right)^{\mathrm{SMagr.}}} = 0.947(1 \pm 0.125)(1 \pm 0.073) \tag{6.3.5}$$

$$= 0.947(1 \pm 0.145)\,, \tag{6.3.6}$$

$$\frac{\Delta M_d^{\mathrm{SMagr.}}}{\Delta M_d^{\mathrm{Exp}}} = 1.201(1 \pm 0.093)(1 \pm 0.0040) \tag{6.3.7}$$

$$= 1.20(1 \pm 0.09)\,. \tag{6.3.8}$$

Here one clearly sees the enhancements of the mass differences, which are up to 20% or more than two standard deviations above the experimental value. The decay rate difference $\Delta\Gamma_s$ is also enhanced by about 20% above the measured value; due to larger uncertainties, this is statistically less significant. The dominant source for this enhancement is the new value of $\langle Q \rangle$. The ratio $\Delta\Gamma_s/\Delta M_s$ is slightly lower than before, but still consistent with the corresponding experimental number.

Taking the deviations above seriously, we can think about several possible interpretations:

1. Statistical fluctuations in the experimental results of the order of three standard deviations might explain the deviation in $\Delta\Gamma_s$, while the deviation in ΔM_s cannot be explained by a fluctuation in the experiment.

2. Duality violations alone cannot explain these deviations, because they have no visible effects on ΔM_q.

3. The lattice normalisation for $f_B^2 B$ is simply too high, future investigations will bring down the value and there is no NP in mixing. Currently there is no foundation for this possibility, but we try to leave no stone unturned. Since $f_B^2 B$ cancels in the ratio of mass and decay rate difference, we can use the new values to give the most precise SM prediction of $\Delta\Gamma_s$ via

$$\frac{\Delta\Gamma_s}{\Delta M_s} \cdot 17.757\,\text{ps}^{-1} (\equiv \Delta M_s^{\text{exp}}) \;=\; 0.087 \pm 0.010\,\text{ps}^{-1}\,. \tag{6.3.9}$$

   Now the theory error is very close to the experimental one and it would be desirable to have more precise values in theory and in experiment. In that case we also get an indication of the short-term perspectives for duality violating bounds. The above numbers indicate an uncertainty of ± 0.138 for the ratio $\Delta\Gamma_s/\Delta M_s$, which corresponds - in the case of a perfect agreement of experiment and theory - to a bound on δ of ± 0.035. This would already be a considerable improvement compared to the current situation.

4. Finally the slight deviation might be a first hint for NP effects.

   (a) To explain the deviation in the decay rate difference one needs new physics effects in tree level decays, while deviation in M_{12} might be solved by new physics effects in loop contributions.

   (b) In principle one can think of the possibility of new tree-level effects that modify both $\Delta\Gamma_s$ and ΔM_s, but which cancels in the ratio. ΔM_s is affected by a double insertion of the new tree-level operators. Following the strategy described in e.g. [2], we found, however, that the possible effects on the mass difference are much too small.

(c) Finally there is also the possibility of having a duality violation of about 20% in $\Delta\Gamma_s$, while the effect in ΔM_s is due to new physics in loops. This possibility can be tested in future by more precise investigations of the lifetime ratio $\tau(B_s^0)/\tau(B_d^0)$.

In order to draw any definite conclusions about these interesting possibilities, we need improvements in several sectors: from experiment we need more precise values for $\Delta\Gamma_s$ and $\tau(B_s^0)/\tau(B_d^0)$. A first measurement of $\Delta\Gamma_d$ will also be very helpful. A measurement of the semi-leptonic asymmetries outside the duality-allowed regions would already be a clear manifestation of new physics in the mixing system. From the theory side we need (in ranked order)

1. A first principle determination of the dimension 7 operators $B_{R_{2,3}}$ and the corresponding colour-rearranged ones.

2. Independent lattice determinations of the matrix elements of Q, Q_S, $\tilde{Q}_S$, R_0, R_1 and $\tilde{R}_1$.

3. NNLO QCD calculations for the perturbative part of Γ_{12}.

These improvements seem possible in the next few years and they might lead the path to a detection of new physics effects in meson mixing.

6.4 D-mixing

D-mixing is by now experimentally well established and the values of the mixing parameters are quite well measured [1]:

$$x = (0.37 \pm 0.16) \cdot 10^{-2}\,, \tag{6.4.1}$$

$$y = (0.66^{+0.07}_{-0.10}) \cdot 10^{-2}\,. \tag{6.4.2}$$

Using $\tau(D^0) = 0.4101$ ps [184], this can be translated into

$$\Delta M_D = \frac{x}{\tau(D^0)} = 0.00902\,\text{ps}^{-1}\,, \tag{6.4.3}$$

$$\Delta\Gamma_D = 2\frac{y}{\tau(D^0)} = 0.0322\,\text{ps}^{-1}\,. \tag{6.4.4}$$

When trying to compare these numbers with theory predictions, we face the problem that it is not obvious if our theory tools are also working in the D-system. Till now the mixing quantities have been estimated via exclusive and inclusive approaches. The exclusive approach is mostly based on phase space and $SU(3)_F$-symmetry arguments, see e.g. [185, 186]. Within this approach values for x and y of the order of 1% can be obtained. Thus, even if it is not a real first principle approach, this method seems to be our best currently available tool to describe D-mixing. Inclusive HQE calculations worked very well in the B-system, but their naive application to the D-system gives results that are several orders of magnitude lower than the experimental result [187, 188]. Hence it seems we are left with some of the following options:

- The HQE is not valid in the charm system. This obvious solution might however, be challenged by the fact that the tiny theoretical D-mixing result is solely triggered by an extremely effective GIM cancellation [55], see e.g. the discussion in [189], and not by the smallness of the first terms of the HQE expansion. A breakdown of the HQE in the charm system could best be tested by investigating the lifetime ratio of D-mesons. From the theory side, the NLO QCD corrections have been determined for the lifetime ratio in [190] and it seems that the experimental measured values can be reproduced. To draw a definite conclusion about the agreement of experiment and theory for lifetimes and thus about the convergence of the HQE in the charm system, lattice evaluations of the unknown charm lifetime matrix elements are urgently needed. So this issue is currently unsettled.

- Bigi and Uraltsev pointed out in 2000 [191] that the extreme GIM cancellation in D-mixing might be lifted by higher terms in HQE, i.e. the $1/m_c$-suppression of higher terms in the HQE is overcompensated by a lifting of the GIM cancellation in higher order terms. There are indications for such an effect, see [189, 192], but it is not clear whether the effect is large enough to explain the experimental mixing values. To make further progress in that direction we need the perturbative calculation of the dimension 9 and 12 terms of the OPE and an idea of how to estimate the matrix elements of the arising

D=9 and D=12 operators. Hence this possibility is not ruled out yet.

- The deviation of theory and experiment could of course also be due to new physics effects. Bounds on new physics models from determining their contributions to D-mixing, while more or less neglecting the SM contributions were studied e.g. in [193].

In this work we will investigate the related question, whether relatively small duality violating effects in inclusive charm decays could explain the deviation between experiment and the inclusive approach. We consider the decay rate difference $\Delta\Gamma_D$ for this task. According to the relation (see the derivation in Section 1.3.3)

$$\Delta\Gamma_D \leq 2|\Gamma_{12}|\,, \tag{6.4.5}$$

we will only study $|\Gamma_{12}|$ and test whether it can be enhanced close to the experimental value of the decay rate difference. This is of course only a necessary, but not a sufficient condition for an agreement of experiment and theory. A complete answer would also require a calculation of $|M_{12}|$, which is beyond the scope of this work.
Γ_{12} consists again of three CKM contributions

$$\Gamma_{12} = -\left(\lambda_s^2\Gamma_{12}^{ss} + 2\lambda_s\lambda_d\Gamma_{12}^{sd} + \lambda_d^2\Gamma_{12}^{dd}\right)\,, \tag{6.4.6}$$

with the CKM elements $\lambda_d = V_{cd}V_{ud}^*$ and $\lambda_s = V_{cs}V_{us}^*$. Using again the unitarity of the CKM matrix ($\lambda_d + \lambda_s + \lambda_b = 0$) we get

$$\Gamma_{12} = -\lambda_s^2\left(\Gamma_{12}^{ss} - 2\Gamma_{12}^{sd} + \Gamma_{12}^{dd}\right) + 2\lambda_s\lambda_b\left(\Gamma_{12}^{sd} - \Gamma_{12}^{dd}\right) - \lambda_b^2\Gamma_{12}^{dd}\,. \tag{6.4.7}$$

The CKM-factor have now a very pronounced hierarchy, they read

$$\lambda_s^2 = 4.81733\cdot 10^{-2} - 3.00433\cdot 10^{-6}i\,, \tag{6.4.8}$$

$$2\lambda_s\lambda_b = 2.49872\cdot 10^{-5} + 5.90908\cdot 10^{-5}i\,, \tag{6.4.9}$$

$$\lambda_b^2 = -1.48814\cdot 10^{-8} + 1.53241\cdot 10^{-8}i\,. \tag{6.4.10}$$

The numerical values of the Γ_{12}^{xy} can be expanded in powers of $\bar{z}_s = (\bar{m}_s(\bar{m}_c)/\bar{m}_c(\bar{m}_c))^2 \approx 0.0092$.

$$\Gamma_{12}^{ss} = 1.8696 - 5.5231\bar{z}_s - 13.8143\bar{z}^2 + ...\bar{z}^3 + ...\,, \tag{6.4.11}$$

$$\Gamma_{12}^{sd} = 1.8696 - 2.7616\bar{z}_s - 7.4906\bar{z}^3 + ...\bar{z}^3 + ...\,, \tag{6.4.12}$$

$$\Gamma_{12}^{dd} = 1.8696\,. \tag{6.4.13}$$

Looking at the expressions in Eq.(6.4.7) we see an extreme GIM cancellation in the CKM-leading term, while the last term without any GIM cancellation is strongly CKM suppressed. We get

$$\Gamma_{12}^{ss} - 2\Gamma_{12}^{sd} + \Gamma_{12}^{dd} = 1.17\bar{z}^2 - 59.5\bar{z}^3 + \dots , \tag{6.4.14}$$

$$\Gamma_{12}^{sd} - \Gamma_{12}^{dd} = -2.76\bar{z} + \dots . \tag{6.4.15}$$

Using our simplest duality violating model

$$\Gamma_{12}^{ss} \to \Gamma_{12}^{ss}(1+4\delta) , \tag{6.4.16}$$

$$\Gamma_{12}^{sd} \to \Gamma_{12}^{sd}(1+\delta) , \tag{6.4.17}$$

$$\Gamma_{12}^{dd} \to \Gamma_{12}^{dd}(1+0\delta) , \tag{6.4.18}$$

we find

$$\begin{aligned} \Gamma_{12}^{ss} - 2\Gamma_{12}^{sd} + \Gamma_{12}^{dd} &= 1.17\bar{z}^2 - 59.5\bar{z}^3 + \dots \\ &\quad +\delta\left(3.7392 - 16.5692z - 40.276z^2 + \dots\right) , \end{aligned} \tag{6.4.19}$$

$$\begin{aligned} \Gamma_{12}^{sd} - \Gamma_{12}^{dd} &= -2.76\bar{z} + \dots \\ &\quad +\delta\left(1.8696 - 2.7616z - 7.4906 + \dots\right) . \end{aligned} \tag{6.4.20}$$

Eq.(6.4.20) shows that our duality violating model completely lifts the GIM cancellation and that even tiny values of δ will lead to an overall result that is much bigger than the usual SM predictions within the inclusive approach. For our final conclusions we will use the generalised duality violating model

$$\Gamma_{12}^{ss} \to \Gamma_{12}^{ss}(1+\delta^{ss}) , \tag{6.4.21}$$

$$\Gamma_{12}^{sd} \to \Gamma_{12}^{sd}(1+\delta^{sd}) , \tag{6.4.22}$$

$$\Gamma_{12}^{dd} \to \Gamma_{12}^{dd}(1+\delta^{dd}) , \tag{6.4.23}$$

with $\delta^{ss} \geq \delta^{sd} \geq \delta^{dd}$. Next we test for what values of δ the inclusive approach can reproduce the experimental results for $\Delta\Gamma_D$. The corresponding allowed regions for $\delta^{ss,sd,dd}$ are given as shaded areas in Fig.6.6. As expected, very small values of δ cannot give an agreement between HQE and experiment, surprisingly, however, values as low as $\delta^{ss} \approx 0.18$ can explain the current difference. So a duality violation

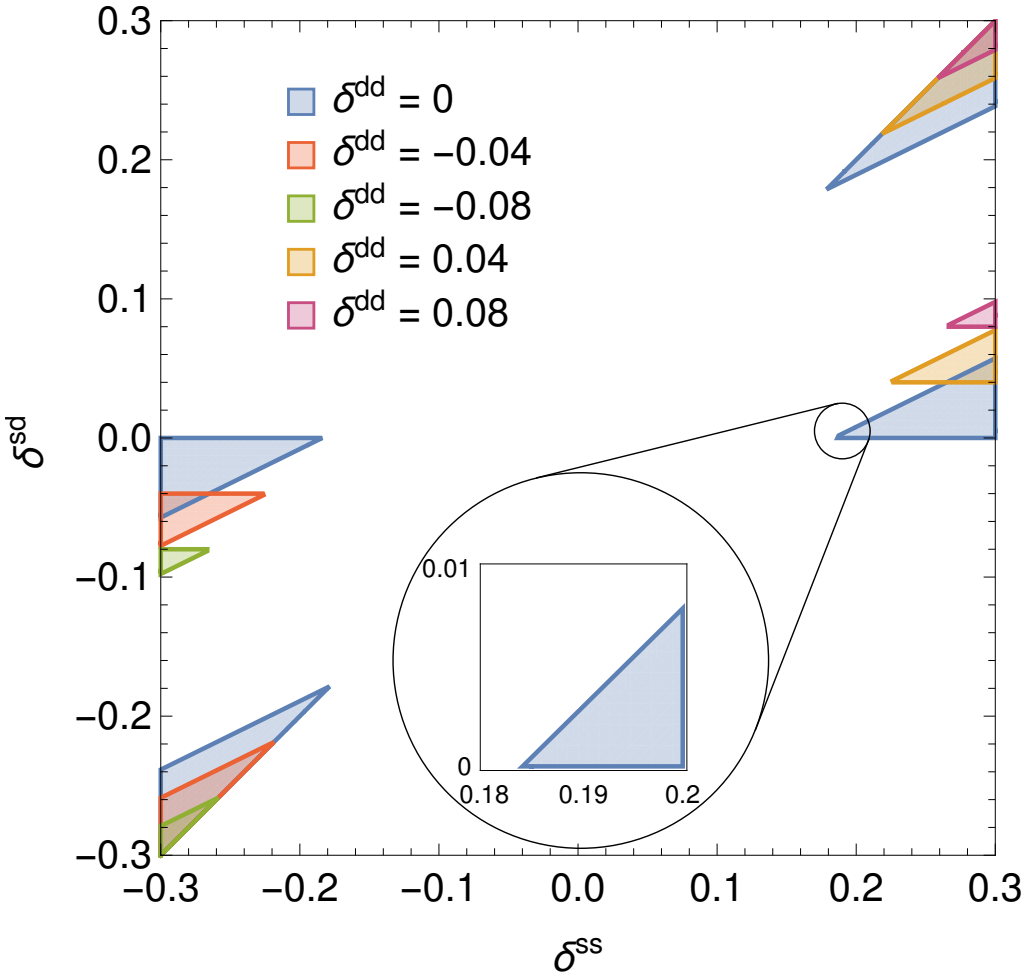

Figure 6.6: 90% confidence limits on δ^{ss}, δ^{sd} and δ^{dd} for the D-system from a comparison of the experimentally allowed region of $\Delta\Gamma_D$ with the theory prediction based on the HQE. The allowed regions for the δs are shaded. Depending on the values of δ^{dd}, different colours are used. As expected for small values of δ the experimental value of $\Delta\Gamma_D$ can not be reproduced. Thus the area in the centre is free. Starting from values of about 20% on duality violation can explain the difference between experiment and HQE. To see more precisely, where the smallest possible value of δ lies, we have zoomed into the overlap region.

of the order of 20% in the HQE for the charm system is sufficient to explain the huge discrepancy between a naive application of the HQE and the measured value for $\Delta\Gamma_D$.

Chapter 7

Conclusions

This thesis summarizes the investigation on different aspects of neutral B meson phenomenology. We started by questioning the well accepted assumption of having no new physics in tree level decays, in particular we explored for possible deviations with respect to the SM values in the dimension six current-current operators $\hat{Q}_1$ (colour suppressed) and $\hat{Q}_2$ (colour allowed) associated with the quark level transitions $b \to q\bar{q}'s$ and $b \to q\bar{q}'d$ $(q, q' = u, c)$. We evaluated the size of the new physics effects by modifying the corresponding Wilson coefficients according to $C_1 \to C_1 + \Delta C_1$, $C_2 \to C_2 + \Delta C_2$, for $\Delta C_{1,2} \in \mathcal{C}$; we found that sizeable deviations in $\Delta C_{1,2}$ are not ruled out by the recent experimental data. Our analysis was based on a statistical fit where we included different B-physics observables involving the decay processes: $\bar{B}^0_d \to \pi\pi$, $\bar{B}^0_d \to \pi\rho$, $\bar{B}^0_d \to \rho\rho$, $\bar{B}^0_d \to D^*\pi$, $\bar{B}^0_d \to D^*h^0$ (where h^0 stands for the mesons π^0, ω, η), $\bar{B}^0_d \to J/\psi K_S$, $B \to X_d\gamma$ and $B \to X_s\gamma$. We also considered neutral B mixing observables: the semileptonic asymmetries a^s_{sl} and a^d_{sl} as well as the decay width difference $\Delta\Gamma_s$ of B^0_s oscillations. For the amplitudes of the hadronic transitions $\bar{B}^0_d \to \pi\pi$, $\bar{B}^0_d \to \pi\rho$ and $\bar{B}^0_d \to \rho\rho$ we used the formulas calculated within the QCD factorization framework. We have identified a high sensitivity on $\Delta C_{1,2}$ with respect to the power corrections arising in the annihilation topologies and in some cases in those for the hard-spectator scattering as well. It is also important to mention that the uncertainty in the parameter λ_B used to describe the first moment of the light cone distribution for the neutral B mesons plays a crucial role in defining the size of ΔC_1 and ΔC_2. We made a channel by channel

study by combining different constraints for the decay chains $b \to u\bar{u}d$, $b \to c\bar{u}d$ and $b \to c\bar{c}d$; we also performed a universal fit where we included observables mediated by $b \to qq's$ decays as well. The universal fit provides the strongest bounds on the new physics deviations, we found that $|\mathrm{Re}(\Delta C_1)| \sim \mathcal{O}(30\%)$, $|\mathrm{Re}(\Delta C_2)| \sim \mathcal{O}(10\%)$, $|\mathrm{Im}(\Delta C_1)| \sim \mathcal{O}(10\%)$ and that $|\mathrm{Im}(\Delta C_2)| \sim \mathcal{O}(10\%)$ whereas for the independent channel analyses the corresponding deviations can be at least two times larger.

We analysed the implications of having new physics in tree level b quark transitions over the decay width difference of neutral B_d^0 mixing $\Delta\Gamma_d$, this makes sense considering that its most recent experimental average is still consistent with zero. We found that enhancements in $\Delta\Gamma_d$ with respect to its SM value in the interval $-3.9 < \Delta\Gamma_d/\Delta\Gamma_d^{SM} < 2.6$ are consistent with current the experimental data. Next we evaluated the effect of our regions for ΔC_1 and ΔC_2 over the theoretical determination of the CKM phase γ, where the absence of penguins leads in principle to an exceptional theoretical cleanness. We found that γ is highly sensitive to the imaginary components of ΔC_1 and ΔC_2. Here the observable $sin(2\beta_d)$ plays a central role in reducing the size of $\mathrm{Im}(\Delta C_1)$, where the amplitude for the process $B \to J/\psi K_S$ is an essential ingredient. Our current evaluation of the topological amplitudes determining the overall amplitude of the process $B \to J/\psi K_S$ gives an uncertainty of 60% and relays in relatively old expressions for the hard spectator functions, an update will be fundamental in order to reduce the possible value for ΔC_1 and hence to minimize the deviations $\delta\gamma$ due to new physics at tree level. Our regions for ΔC_1 and ΔC_2 lead to deviations $\delta\gamma$ that saturate the uncertainty reported in the latest experimental average $-6.30^\circ < \delta\gamma < 7.00^\circ$, this is a non negligible effect that deserves serious consideration in the theoretical estimation of the CKM angle γ. It should be stressed that during the computation of $\delta\gamma$ the ratios of the matrix elements $\langle \bar{D}^0 K^- | Q_1^{\bar{u}cs} | B^- \rangle / \langle \bar{D}^0 K^- | Q_2^{\bar{u}cs} | B^- \rangle$ and $\langle D^0 K^- | Q_1^{\bar{c}us} | B^- \rangle / \langle D^0 K^- | Q_2^{\bar{c}us} | B^- \rangle$ were required, unfortunately they have not been calculated elsewhere, so we made a naive estimation based on the colour structure of the initial and final states and the ratio of the decay constants and form factors of the hadronic processes involved. Then, in order to make solid statements on the possible size of $\delta\gamma$, it is important

to determine these ratios from more fundamental principles.

The possibility of having enhancements on $\Delta\Gamma_d$ due to operators of the form $\left(\bar{d}b\right)\left(\bar{\tau}\tau\right)$ with respect to the SM was also considered. Depending on the Lorentz structure (scalar, vector, tensor) these operators contribute at tree level to the decays $B_d^0 \to \tau^+\tau^-$, $B \to X_d\tau^+\tau^-$ and $B^+ \to \pi^+\tau^+\tau^-$. For the decay $B_d^0 \to \tau^+\tau^-$ there is a direct experimental bound available, on the other hand for the decays $B \to X_d\tau^+\tau^-$ and $B^+ \to \pi^+\tau^+\tau^-$ an indirect bound was derived using the life-time difference of the B_d^0 and B_s^0 mesons. Further bounds for the tensor version of the operators $\left(\bar{d}b\right)\left(\bar{\tau}\tau\right)$ can be obtained using the processes $B \to X_d\gamma$, $B^+ \to \pi^+\mu^+\mu^-$ and $B_d^0 \to \gamma\gamma$, where $\left(\bar{d}b\right)\left(\bar{\tau}\tau\right)$ enters indirectly when it mixes with the operators mediating the decay chains $b \to d\gamma$, $b \to dl^+l^-$ $(l = e, \mu)$. As in the case of our tree-level study we found that enhancements of several 100% are not excluded finding the largest enhancement factors from the operators with the vector Lorentz structure. It was argued that $\Delta\Gamma_d$ is proportional to the $\mathcal{CP}$ violation in interference contribution to the like sign dimuon asymmetry measured by the D0 collaboration -Borissov-Hoeneisen interpretation-, this is highly interesting considering that this measurement is anomalous with respect to the SM expectation and that $\Delta\Gamma_d$ as described above is rather unconstrained. However, a careful analysis has shown that this relationship faces conceptual problems that remain to be solved.

Finally in the last chapter, we quantified the size of possible violations to the Hadron Quark duality in the neutral $B_{s,d}^0$ and D^0 sectors. We introduced a simple parameterization of duality violating effects δ based on phase space arguments: the smaller the remaining phase space in a heavy hadron decay is, the larger the duality violation might be. Our strongest bound on the duality violation parameter δ was obtained from the ratio

$$\frac{\left(\frac{\Delta\Gamma_s}{\Delta M_s}\right)^{\text{Exp}}}{\left(\frac{\Delta\Gamma_s}{\Delta M_s}\right)^{\text{SM}}} = 0.96 \pm 0.19 \;\to\; |\delta| \lesssim 0.1. \tag{7.0.1}$$

Currently $a_{sl}^{s,d}$ and $\Delta\Gamma_d$ have not been observed yet. Consequently we use our bounds on δ from $\Delta\Gamma_s$ to determine the maximal possible size of $a_{sl}^{s,d}$ and $\Delta\Gamma_d$ as the result of duality violations; this allow us to identify ranges for the values of these observ-

ables that can be explained as the result of the SM plus duality violation effects. These regions are compared with current experimental ranges in Fig.6.3. Based in our analysis we made the following statement: any measurement outside the region allowed by duality violation is a clear signal for new physics. We explored future scenarios where duality violation is further constrained by more precise values of $\Delta\Gamma_s$ in both experiment and theory.

We also studied the possibility of explaining the anomalous measurement of the like-sign dimuon asymmetry reported by D0 as an effect of duality violation. To do so, we used the Borissov-Hoeneisen interpretation including the correction factor for $\Delta\Gamma_d$ indicated by [115]; nevertheless we found that an agreement between theory and experiment for the dimuon asymmetry will require values of $\delta \in (-1.9, -0.4)$, this is considerably outside the bounds established by $\Delta\Gamma_s$. Hence, duality violation cannot explain the value of the like-sign dimuon asymmetry in the Borissov-Hoeneisen theoretical interpretation.

We have shown that the duality violating parameter δ will also affect the lifetime ratio $\tau(B_s^0)/\tau(B_d^0)$, where there is currently a deviation of about 2.5 standard deviations between experiment and theory. The historical development of this ratio suggests that this effect could be a statistical fluctuation. If we take the current deviation seriously, then we can consider two alternatives, this is either a hint for new physics or a sizeable indication for duality violations of the order of $\delta \sim 0.5$, which is inconsistent with the bounds on δ derived from $\Delta\Gamma_s$. A future reduction of the experimental error of $\tau(B_s^0)/\tau(B_d^0)$ will give us valuable insight. We have considered two future scenarios where we investigated the effects of reducing the experimental uncertainty on this ratio plus keeping its central value, or reducing the uncertainty in the experiment and taking its central value equal to the SM one. The conclusions however depend on how the theoretical and the experimental values for $\Delta\Gamma_s$ develop in the future; for instance if $\Delta\Gamma_s$ remains unchanged then duality violation will not be able to explain the results of the lifetimes and mixing observables simultaneously leading to potential signals of new physics. It is very important to note that the theory prediction has a very strong dependence on almost unknown lattice parameters; from the error budget for the lifetime ratio in Tab.(E.14) (Appendix E) it

can be seen that any new calculation of the bag parameters $\epsilon_{1,2}$ would bring large improvements in the theory prediction for $\tau(B_s^0)/\tau(B_d^0)$.

The SM predictions for the mixing observables $\Delta\Gamma_{s,d}$, $\Delta M_{s,d}$, and $a_{sl}^{s,d}$ were updated based on the recent Fermilab-MILC lattice results [79] for non-perturbative matrix elements, the latest CKM parameters from CKMfitter [17], and an aggressive error estimate on the unknown bag parameters of dimension seven operators. With this set of inputs the central value in Eq. (7.0.1) remains relatively unchanged, whereas the uncertainty drops to ± 0.15. On the other hand the central values of the mixing observables are enhanced by 20% above the measurements with a significance of around 2 standard deviations. Before deriving any conclusions from these new results the following points should be addressed: 1) a first principle calculation of $\langle R_{2,3} \rangle$ - triggered by the results of [79] we simply assumed small deviations from vacuum insertion approximation; 2) an independent confirmation of the larger values of the matrix element $\langle Q \rangle$ found by [79].

In the case of neutral D^0 mixing we found that the current discrepancy of several orders of magnitude between the theoretical result estimated using the Heavy Quark Expansion and the experiment can be explained if we have duality violation effects as low as 20%, this is a remarkable and unexpected result. However, in order to derive solid conclusions a lattice calculation of the matrix elements arising in the ratio of charm lifetimes is mandatory.

Based on the results described above we can see that questioning well accepted assumptions in high energy physics is well motivated. Our first journey in this direction has proven to be particularly illuminating in the sector of B meson physics, for instance our knowledge on certain theoretical quantities such as tree level Wilson coefficients and duality violation effects seems to be poorer than previously expected. Thus, a careful consideration of all these deviations is an essential factor that should be taken into account when making comparisons between theory and experiment. As a matter of fact our actual uncertainty on quantities that are supposed to be under good theoretical control can compete against the current precision data of experiments such as LHCb. Our investigations highlight the importance of

improvements in the theoretical tools used to calculate hadronic transitions, for instance we have just unveiled once more the relevance of having a first principles determination of power corrections in QCD factorization. Moreover, increasing the experimental precision in $\mathcal{CP}$ asymmetries is crucial to reduce the uncertainty on possible BSM weak phases.

We would like to mention possible future directions for our studies. During the first stage of our phenomenological analysis we have followed a model independent approach; for the sake of completeness it would be interesting to construct a theoretical model able to reproduce the deviations on ΔC_1 and ΔC_2 obtained in Chapter 4. During our new physics at tree level analysis we have generated a set of python libraries containing different B-physics observables, our plan is to use them as the starting point for a flavour fit program available to the public. This will allow the user to perform global fits and to investigate possible new physics effects not only in current-current operators but also in QCD and electroweak penguins. Finally, we would like to remark the importance of improving the theoretical and the experimental status of mixing quantities of neutral B mesons, here one crucial ingredient is the calculation of the matrix elements of the dimension 7 operators arising during the calculation of Γ_{12}^q. Currently there are plans for the estimation of these contributions using lattice techniques and QCD sum-rules. In view of our conclusions we want to highlight once more the importance of revising old assumptions in the light of new data and not to underestimate potential sources of uncertainties based on well accepted prejudices.

Bibliography

[1] Y. Amhis *et al.* [Heavy Flavor Averaging Group (HFAG) Collaboration], [hep-ex/1412.7515] and update available at http://www.slac.stanford.edu/xorg/hfag/index.html.

[2] C. Bobeth, U. Haisch, A. Lenz, B. Pecjak and G. Tetlalmatzi-Xolocotzi, JHEP **1406** (2014) 040 [hep-ph/1404.2531].

[3] J. Brod, A. Lenz, G. Tetlalmatzi-Xolocotzi and M. Wiebusch, Phys. Rev. D **92** (2015) 033002 [hep-ph/1412.1446].

[4] S. Weinberg. Phys. Rev. Lett. **19** (1967) 1264-1266.

[5] A. D. Sakharov, Pisma Zh. Eksp. Teor. Fiz. **5** (1967) 32-35, JETP Lett. **5** (1967) 24-27, Sov. Phys. Usp. **34** (1991) 392-393, Usp. Fiz. Nauk **161** (1991) 61-64.

[6] N. Cabibbo, Phys. Rev. Lett. **10** (1963) 531.

[7] M. Kobayashi and T. Maskawa, Prog. Theor. Phys. **49**, (1973) 652.

[8] L. L. Chau and W. Y. Keung, Phys. Rev. Lett. **53** (1984) 1802.

[9] L. Wolfenstein, Phys. Rev. Lett. **51** (1983) 1945.

[10] A.J. Buras et al., Phys. Rev. D **50** (1994) 3433 [hep-ph/9403384].

[11] C. Jarlskog, Phys. Rev. Lett. **55** (1985) 1039.

[12] C. Jarlskog, Phys. Rev. D. **35** (1987) 1685.

[13] K.A. Olive et al. [Particle Data Group Collaboration], Chin. Phys. C **38** (2014) 090001 and 2015 update.

[14] C. Jarlskog [hep-ph/1102.2823].

[15] M. Artuso, G. Borissov and A. Lenz, [hep-ph/1511.09466].

[16] T. Jubb, M. Kirk, A. Lenz, G. Tetlalmatzi-Xolocotzi [hep-ph/1603.07770].

[17] J. Charles *et al.* [CKMfitter Group Collaboration], Eur. Phys. J. C **41** (2005) 1 [hep-ph/0406184]. For the CKM inputs we used the updated value from 2015.

[18] A. Bevan, Eur. Phys. J. C. **74** (2014) 3026.

[19] M. Gronau and D. London, Phys. Lett. B **253** (1991) 483.

[20] M. Gronau and D. Wyler, Phys. Lett. B **265** (1991) 172.

[21] D. Atwood, I. Dunietz and A. Soni, Phys. Rev. Lett. **78** (1997) 3257 [hep-ph/9612433].

[22] D. Atwood, I. Dunietz and A. Soni, Phys. Rev. D **63** (2001) 036005 [hep-ph/0008090].

[23] P. del Amo Sanchez et al. [BABAR Collab.], Phys. Rev. D **82** (2010) 072004 [hep-ex/1007.0504]; B. Aubert et al. [BABAR Collab.], Phys. Rev. D **78** (2008) 092002 [hep-ex/0807.2408]; Phys. Rev. D **80** (2009) 092001 [hep-ex/0909.3981]; P. del Amo Sanchez et al. Phys. Rev. D **82** (2010) 072006 [hep-ex/1006.4241]; J.P. Lees et al. Phys. Rev. D **84** (2011) 012002 [hep-ex/1104.4472]. K. Abe et al. [Belle Collab.], Phys. Rev. D **73** (2006) 051106 [hep-ex/0601032]; Y. Horii et al., Phys. Rev. Lett. **106** (2011) 231803 [hep-ex/1103.5951].

[24] T. Aaltonen et al. [CDF Collab.], Phys. Rev. D **81** (2010) 031105 [hep-ex/0911.0425].

[25] R. Aaij et al. [LHCb Collab.], Phys. Lett. B **712** (2012) 203 [Erratum ibid. 713, 351 (2012)] [hep-ex/1203.3662]; Phys. Lett. B **723** (2013) 44 [hep-ex/1303.4646].

[26] A. Giri, Y. Grossman, A. Soffer and J. Zupan, Phys. Rev. D 68 (2003) 054018 [hep-ph/0303187].

[27] A. Poluektov et al. [Belle Collab.], Phys. Rev. D **81** (2010) 112002 [hep-ex/1003.3360].

[28] B. Aubert et al. [BABAR Collab.], Phys. Rev. Lett. **105** (2010) 121801 [hep-ex/1005.1096].

[29] J. P. Lees et al. [BABAR Collab.], Phys. Rev. D **87** (2013) 052015 [hep-ex/1301.1029].

[30] K. Trabelsi et al. [Belle Collab.], C12-09-28 [hep-ex/1301.2033].

[31] The LHCb Collaboration, LHCb-CONF-2016-001.

[32] M. Gronau and D. London, Phys. Rev. Lett. **65** (1990) 3381.

[33] I. Adachi et al. [Belle Collab.], Phys.Rev. D **88** (2013) 092003 [hep-ex/1302.0551].

[34] J.P. Lees et al. [BABAR Collab.], Phys.Rev. D **87** (2013) 052009 [hep-ex/1206.3525].

[35] Bernard Aubert et al. [BABAR Collab.], Phys.Rev. D **76** (2007) 052007 [hep-ex/0705.2157].

[36] P. Vanhoefer et al. [Belle Collab.], Phys.Rev. D **93** (2016) 032010 [hep-ex/1510.01245].

[37] A. E. Snyder, H. R. Quinn, Phys. Rev. D **48** (1993) 2139-2144.

[38] H. R. Quinn, J. P. Silva, Phys. Rev. D **62** (2000) 054002 [hep-ph/0001290].

[39] A. Kusaka et al. [Belle Collab.], Phys. Rev. Lett. **98** (2007) 221602 [hep-ex/0701015].

[40] A. J. Buras, *Weak Hamiltonian, CP violation and rare decays, in Probing the standard model of particle interactions. Proceedings, Summer School*

in Theoretical Physics, NATO Advanced Study Institute, 68th session, Les Houches, France, July 28-September 5, 1997. Pt. 1, 2, pp. 281539, 1998. [hep-ph/9806471].

[41] K. G. Wilson, Phys. Rev. **179** (1969) 1499.

[42] K.G. Wilson and W. Zimmermann, Comm. Math. Phys. **24** (1972) 87.

[43] W. Zimmermann, Proc. 1970 Brandeis Summer Institute in Theor. Phys, (eds. S. Deser, M. Grisaru and H. Pendleton), MIT Press, 1971, p.396.

[44] W. Zimmermann, Ann. Phys. **77** (1973) 570.

[45] M. Beneke, G. Buchalla, M. Neubert and C.T. Sachrajda, Nucl.Phys.B **606** (2001) 245-321 [hep-ph/0104110].

[46] A. J. Buras, M. Jamin, M.E. Lautenbacher and P. H. Weisz. Nucl. Phys. B **370** (1992) 69.

[47] G. Buchalla, A. J. Buras and M. E. Lautenbacher, Rev. Mod. Phys. **68** (1996) 1125 [hep-ph/9512380].

[48] M. Beneke, G. Buchalla, C. Greub, A. Lenz and U. Nierste, Phys. Lett. B **459** (1999) 631 [hep-ph/9808385].

[49] T. Inami, and C.S. Lim, Prog. Theor. Phys. **65**, 297 [Erratum-ibid. 65 (1981) 1772].

[50] A. J. Buras, M. Jamin and P. H. Weisz, Nucl. Phys. B **347** (1990) 491.

[51] M. Beneke, G. Buchalla and I. Dunietz, Phys. Rev. D **54** (1996) 7 [hep-ph/9609357].

[52] A. Lenz and U. Nierste, JHEP **0706** (2007) 072 [hep-ph/0612167].

[53] M. Beneke, G. Buchalla, A. Lenz and U. Nierste, Phys. Lett. B **576** (2003) 173 [hep-ph/0307344].

[54] M. Ciuchini, G. D'Agostini, E. Franco, V. Lubicz, G. Martinelli, F. Parodi, P. Roudeau and A. Stocchi, JHEP **0107** (2001) 013 [hep-ph/0012308].

[55] S. L. Glashow, J. Iliopoulos and L. Maiani, Phys. Rev. D **2** (1970) 1285.

[56] M. Beneke, G. Buchalla, M. Neubert, C.T. Sachrajda Phys. Rev. Lett. **83** (1999) 1914 [hep-ph/9905312].

[57] M. Beneke, G. Buchalla, M. Neubert and C. T. Sachrajda, Nucl. Phys. B **591** (2000) 313 [hep-ph/0006124].

[58] G. P. Lepage and S. J. Brodsky, Phys. Rev. D **22** 2157 (1980).

[59] D. Fakirov and B. Stech, Nucl. Phys. B **133** (1978) 315.

[60] N. Cabibbo and L. Maiani, Phys. Lett. B **73** (1978) 418; ibid. **76** (1978) 663 (E).

[61] M. Beneke and M. Neubert, Nucl. Phys. B **675** (2003) 333 [hep-ph/0308039].

[62] C. Bobeth, M. Gorbahn, S. Vickers, Eur. Phys. J. C **75** (2015) no.7 340 [hep-ph/1409.3252].

[63] M. Wiebusch, Comput. Phys. Commun. **184** (2013) 2438-2445 [hep-ph/1207.1446], documenation online available at https://myfitter.hepforge.org/.

[64] G. Bell and V. Pilipp, Phys. Rev. D **80** (2009) 054024 [hep-ph/0907.1016].

[65] M. Beneke, J. Rohrwild , Eur.Phys.J. C **71** (2011) 1818 [hep-ph/1110.3228].

[66] A. Heller et al, Phys. Rev. D **91** (2015) 112009 (2015) [hep-ex/1504.05831].

[67] M. Beneke, T. Huber and X. -Q. Li, Nucl. Phys. B **832** (2010) 109 (2010) [hep-ph/0911.3655].

[68] V. M. Braun, D. Yu. Ivanov and G. P. Korchemsky, Phys. Rev. D **69** (2004) 034014 [hep-ph/0309330].

[69] S. J. Lee, M. Neubert, Phys.Rev. D **72** (2005) 094028 [hep-ph/0509350].

[70] M. Beneke and S. Jager, Nucl. Phys. B **751** (2006) 160-185 [hep-ph/0512351].

[71] G. Bell, Nucl. Phys. B **822** (2009) 172 [hep-ph/0902.1915].

[72] M. Beneke, J. Rohrer and D. Yang, Nucl. Phys. B **774** (2007) 64 [hep-ph/0612290].

[73] M. Bartsch, G. Buchalla and C. Kraus [hep-ph/0810.0249].

[74] J. D. Bjorken, Nucl. Phys. 11 (Proc. Suppl.) (1989) 325.

[75] T. Huber, S. Krankl and X. Q. Li [hep-ph/1606.02888]

[76] R. Fleischer, N. Serra and N. Tuning, Phys. Rev. D **83** (2011) 014017 [hep-ph/1012.2784]

[77] H. Boos, T. Mannel, J. Reuter, Phys. Rev. D **70** (2004) 036006 [hep-ph/0403085].

[78] A. J. Buras, W. Slominski, H. Steger, Nucl. Phys. B **245** (1984) 369.

[79] A. Bazavov *et al.* [Fermilab Lattice and MILC Collaborations], [hep-lat/1602.03560v2].

[80] A. Ali, H. Asatrian, C. Greub, Phys. Lett. B **429** (1998) 87-98 [hep-ex/9803314].

[81] A. Crivellin, L. Mercolli, Phys. Rev. D **84** (2011) 114005 [hep-ph/1106.5499].

[82] P. del Amo Sanchez et al. (BABAR), Phys. Rev. D **82** (2010) 051101 [hep-ex/1005.4087].

[83] W. Wang, *Proceeding of CKM2010, the 6th international Workshop on the CKM Unitarity Triangle, University of Warwick, UK, 6-10 September 2010* [hep-ex/1102.1925].

[84] T. Hurth, E. Lunghi and W. Porod, Nucl. Phys. B **704** (2005) 56 [hep-ph/0312260].

[85] M. Czakon, P. Fiedler, T. Huber, M. Misiak, T. Schutzmeier and M. Steinhauser, JHEP **1504** (2015) 168 [hep-ph/1503.01791].

[86] K.G. Chetyrkin, M. Misiak and M. Münz, Phys. Lett. B **400** (1997) 206, Phys. Lett. B **425** (1998) 414 (E) [hep-ph/9612313].

[87] M. Misiak and M. Steinhauser, Nucl. Phys. B **764** (2007) 62 [hep-ph/0609241].

[88] C. Greub, T. Hurth, D. Wyler, Phys. Rev. D **54** (1996) 3350 [hep-ph/9603404].

[89] A. J. Buras, A. Czarnecki, M. Misiak and J. Urban, Nucl. Phys. B **631** (2002) 219 [hep-ph/0203135].

[90] Hai-Yang Cheng, Kwei-Chou Yang, Phys. Rev. D **63** (2000) 074011 [hep-ph/0011179].

[91] Prof. Yang private communication.

[92] J. Brod, Phys. Lett. B **743** (2015) 56-60 [hep-ph/1412.3173]

[93] J. P. Silva and A. Soffer, Phys. Rev. D **61** (2000) 112001 [hep-ph/9912242].

[94] Y. Grossman, A. Soffer and J. Zupan, Phys. Rev. D **72** (2005) 031501 [hep-ph/0505270].

[95] A. Bondar, A. Poluektov and V. Vorobiev, Phys. Rev. D **82** (2010) 034033 [hep-ph/1004.2350].

[96] M. Rama, Phys. Rev. D **89** (2014) 014021 [hep-ex/1307.4384].

[97] M. Martone and J. Zupan, Phys. Rev. D **87** (2013) 034005 [hep-ph/1212.0165].

[98] Y. Grossman and M. Savastio, JHEP **1403** (2014) 008 [hep-ph/1311.3575].

[99] J. Brod and J. Zupan, JHEP **1401** (2014) 051 [hep-ph/1308.5663].

[100] Letter of Intent for the LHCb Upgrade, CERN-LHCC-2011-001; LHCC-I-018, 2011.

[101] T. Abe *et al.* [Belle-II Collaboration], [physics.ins-det/1011.0352].

[102] G. Borissov and B. Hoeneisen, Phys. Rev. D **87** (2013) 074020 [hep-ph/1303.0175].

[103] V. M. Abazov et al. (D0 Collaboration), Phys. Rev. D **74** (2006) 092001 [hep-ex/0609014v1].

[104] V. M. Abazov *et al.* [D0 Collaboration], Phys. Rev. D **82** (2010) 032001 [hep-ex/1005.2757].

[105] V. M. Abazov *et al.* [D0 Collaboration], Phys. Rev. Lett. **105** (2010) 081801 [hep-ex/1007.0395].

[106] V. M. Abazov *et al.* [D0 Collaboration], Phys. Rev. D **84** (2011) 052007 [hep-ex/1106.6308].

[107] V. M. Abazov *et al.* [D0 Collaboration], Phys. Rev. D **89** (2014) 012002 [hep-ex/1310.0447].

[108] F. Krinner, A. Lenz and T. Rauh, Nucl. Phys. B **876** (2013) 31 [hep-ph/1305.5390].

[109] F. del Aguila, M. Perez-Victoria and J. Santiago, JHEP **0009** 011 (2000) [hep-ph/0007316].

[110] S. Casagrande, F. Goertz, U. Haisch, M. Neubert and T. Pfoh, JHEP **0810** (2008) 094 [hep-ph/0807.4937].

[111] O. Eberhardt, A. Lenz and J. Rohrwild, Phys. Rev. D **82** (2010) 095006 [hep-ph/1005.3505].

[112] F. J. Botella, G. C. Branco, M. Nebot and A. Sánchez, Phys. Rev. D **91** (2015) 035013 [hep-ph/1402.1181].

[113] G. Borissov, Private communication.

[114] I. Dunietz, R. Fleischer and U. Nierste, Phys. Rev. D **63** (2001) 114015 [hep-ph/0012219]

[115] U. Nierste, talk at CKM2014 in Vienna.

[116] C. Bobeth and U. Haisch, Acta Phys. Polon. B **44** (2013) 127 [hep-ph/1109.1826].

[117] B. Aubert *et al.* [BaBar Collaboration], Phys. Rev. Lett. **96** (2006) 241802 [hep-ex/0511015].

[118] C. Bobeth, T. Ewerth, F. Krüger and J. Urban, Phys. Rev. D **66** (2002) 074021 [hep-ph/0204225].

[119] C. Bobeth, M. Gorbahn, T. Hermann, M. Misiak, E. Stamou and M. Steinhauser, Phys. Rev. Lett. **112** (2014) 101801 [hep-ph/1311.0903].

[120] A. Lenz, [hep-ph/1405.3601]. A. Lenz, Int. J. Mod. Phys. A **30** (2015) 10, 1543005.

[121] N. G. Uraltsev, Phys. Lett. B **376** (1996) 303 [hep-ph/9602324].

[122] M. Neubert and C. T. Sachrajda, Nucl. Phys. B **483** (1997) 339 [hep-ph/9603202].

[123] E. Franco, V. Lubicz, F. Mescia and C. Tarantino, Nucl. Phys. B **633** (2002) 212 [hep-ph/0203089].

[124] A. Khodjamirian, T. Mannel, N. Offen and Y. -M. Wang, Phys. Rev. D **83** (2011) 094031 [arXiv:1103.2655 [hep-ph]].

[125] D. Guetta and E. Nardi, Phys. Rev. D **58** (1998) 012001 [hep-ph/9707371].

[126] P. Ball and R. Zwicky, Phys. Rev. D **71** (2005) 014015 [hep-ph/0406232].

[127] P. Gambino and M. Misiak, Nucl. Phys. B **611** (2001) 338 [hep-ph/0104034].

[128] R. Aaij *et al.* [LHCb Collaboration], JHEP **1212** (2012) 125 [hep-ex/1210.2645].

[129] A. Ali, A. Y. Parkhomenko and A. V. Rusov, Phys. Rev. D **89** (2014) 094021 [hep-ph/1312.2523].

[130] M. Beneke, T. Feldmann and D. Seidel, Eur. Phys. J. C **41** (2005) 173 [hep-ph/0412400].

[131] M. Dimou, J. Lyon and R. Zwicky, Phys. Rev. D **87** (2013) 074008 [hep-ph/1212.2242].

[132] B. Grinstein and D. Pirjol, Phys. Rev. D **70** (2004) 114005 [hep-ph/0404250].

[133] M. Beylich, G. Buchalla and T. Feldmann, Eur. Phys. J. C **71** (2011) 1635 [hep-ph/1101.5118].

[134] C. Bobeth, T. Ewerth, F. Krüger and J. Urban, Phys. Rev. D **64** (2001) 074014 [hep-ph/0104284].

[135] A. J. Lenz, Phys. Rev. D **84** (2011) 031501 [hep-ph/1106.3200].

[136] E. C. Poggio, H. R. Quinn and S. Weinberg, Phys. Rev. D **13** (1976) 1958.

[137] E. D. Bloom and F. J. Gilman, Phys. Rev. Lett. **25** (1970) 1140.

[138] E. D. Bloom and F. J. Gilman, Phys. Rev. D **4** (1971) 2901.

[139] V. A. Khoze and M. A. Shifman, Sov. Phys. Usp. **26** (1983) 387.

[140] M. A. Shifman and M. B. Voloshin, Sov. J. Nucl. Phys. **41** (1985) 120 [Yad. Fiz. **41** (1985) 187].

[141] I. I. Y. Bigi and N. G. Uraltsev, Phys. Lett. B **280** (1992) 271.

[142] I. I. Y. Bigi, N. G. Uraltsev and A. I. Vainshtein, Phys. Lett. B **293** (1992) 430 [Phys. Lett. B **297** (1993) 477] [hep-ph/9207214].

[143] B. Blok and M. A. Shifman, Nucl. Phys. B **399** (1993) 441 [hep-ph/9207236].

[144] B. Blok and M. A. Shifman, Nucl. Phys. B **399** (1993) 459 [hep-ph/9209289].

[145] J. Chay, H. Georgi and B. Grinstein, Phys. Lett. B **247** (1990) 399.

[146] M. E. Luke, Phys. Lett. B **252** (1990) 447.

[147] M. A. Shifman, In *Shifman, M. (ed.): At the frontier of particle physics, vol. 3* 1447-1494 [hep-ph/0009131].

[148] I. I. Y. Bigi and N. Uraltsev, Int. J. Mod. Phys. A **16** (2001) 5201 [hep-ph/0106346].

[149] B. Grinstein, Phys. Rev. D **64** (2001) 094004 [hep-ph/0106205].

[150] B. Grinstein, PoS HEP **2001** (2001) 099.

[151] R. F. Lebed and N. G. Uraltsev, Phys. Rev. D **62** (2000) 094011 [hep-ph/0006346].

[152] I. I. Y. Bigi, M. A. Shifman, N. Uraltsev and A. I. Vainshtein, Phys. Rev. D **59** (1999) 054011 [hep-ph/9805241].

[153] G. Altarelli, G. Martinelli, S. Petrarca and F. Rapuano, Phys. Lett. B **382** (1996) 409 [hep-ph/9604202].

[154] R. Aaij *et al.* [LHCb Collaboration], Phys. Rev. Lett. **111** (2013) 102003 [hep-ex/1307.2476].

[155] R. Aaij *et al.* [LHCb Collaboration], Phys. Lett. B **734** (2014) 122 [hep-ex/1402.6242].

[156] R. Aaij *et al.* [LHCb Collaboration], JHEP **1404** (2014) 114 [hep-ex/1402.2554].

[157] I. I. Y. Bigi, B. Blok, M. A. Shifman and A. I. Vainshtein, Phys. Lett. B **323** (1994) 408 [hep-ph/9311339].

[158] A. F. Falk, M. B. Wise and I. Dunietz, Phys. Rev. D **51** (1995) 1183 [hep-ph/9405346].

[159] G. Buchalla, I. Dunietz and H. Yamamoto, Phys. Lett. B **364** (1995) 188 [hep-ph/9507437].

[160] A. Lenz [hep-ph/0011258].

[161] A. Czarnecki, M. Slusarczyk and F. V. Tkachov, Phys. Rev. Lett. **96** (2006) 171803 [hep-ph/0511004].

[162] A. Lenz, [hep-ph/1205.1444].

[163] J. R. Ellis, M. K. Gaillard, D. V. Nanopoulos and S. Rudaz, Nucl. Phys. B **131** (1977) 285 Erratum: [Nucl. Phys. B **132** (1978) 541].

[164] J. S. Hagelin, Nucl. Phys. B **193** (1981) 123.

[165] E. Franco, M. Lusignoli and A. Pugliese, Nucl. Phys. B **194** (1982) 403.

[166] L. L. Chau, Phys. Rept. **95** (1983) 1.

[167] A. J. Buras, W. Slominski and H. Steger, Nucl. Phys. B **245** (1984) 369.

[168] V. A. Khoze, M. A. Shifman, N. G. Uraltsev and M. B. Voloshin, Sov. J. Nucl. Phys. **46** (1987) 112 [Yad. Fiz. **46** (1987) 181].

[169] M. Ciuchini, E. Franco, V. Lubicz, F. Mescia and C. Tarantino, JHEP **0308** (2003) 031 [hep-ph/0308029].

[170] M. Beneke, G. Buchalla and I. Dunietz, Phys. Rev. D **54** (1996) 4419 [E. Phys. Rev. D **83** (2011) 119902] [hep-ph/9605259].

[171] A. S. Dighe, T. Hurth, C. S. Kim and T. Yoshikawa, Nucl. Phys. B **624** (2002) 377 [hep-ph/0109088].

[172] A. Badin, F. Gabbiani and A. A. Petrov, Phys. Lett. B **653** (2007) 230 [hep-ph/0707.0294].

[173] C. M. Bouchard, E. D. Freeland, C. Bernard, A. X. El-Khadra, E. Gamiz, A. S. Kronfeld, J. Laiho and R. S. Van de Water, PoS LATTICE **2011** (2011) 274 [hep-lat/1112.5642].

[174] N. Carrasco *et al.* [ETM Collaboration], JHEP **1403** (2014) 016 [hep-lat/1308.1851].

[175] R. J. Dowdall, C. T. H. Davies, R. R. Horgan, G. P. Lepage, C. J. Monahan and J. Shigemitsu, [hep-lat/1411.6989].

[176] D. Becirevic, V. Gimenez, G. Martinelli, M. Papinutto and J. Reyes, JHEP **0204** (2002) 025 [hep-lat/0110091].

[177] A. Lenz and U. Nierste [hep-ph/1102.4274].

[178] W. F. Palmer and B. Stech, Phys. Rev. D **48** (1993) 4174.

[179] I. Dunietz, J. Incandela, F. D. Snider and H. Yamamoto, Eur. Phys. J. C **1** (1998) 211 [hep-ph/9612421].

[180] A. Lenz, U. Nierste and G. Ostermaier, Phys. Rev. D **56** (1997) 7228 [hep-ph/9706501].

[181] D. Becirevic, PoS HEP **2001** (2001) 098 [hep-ph/0110124].

[182] M. Blanke and A. J. Buras, [hep-ph/1602.04020].

[183] S. Aoki, Y. Aoki, C. Bernard, T. Blum, G. Colangelo, M. Della Morte, S. Dürr and A. X. E. Khadra *et al.*, [hep-lat/1310.8555].

[184] K. A. Olive *et al.* [Particle Data Group Collaboration], Chin. Phys. C **38** (2014) 090001.

[185] A. F. Falk, Y. Grossman, Z. Ligeti and A. A. Petrov, Phys. Rev. D **65** (2002) 054034 [hep-ph/0110317].

[186] A. F. Falk, Y. Grossman, Z. Ligeti, Y. Nir and A. A. Petrov, Phys. Rev. D **69** (2004) 114021 [hep-ph/0402204].

[187] H. Georgi, Phys. Lett. B **297** (1992) 353 [hep-ph/9209291].

[188] T. Ohl, G. Ricciardi and E. H. Simmons, Nucl. Phys. B **403** (1993) 605 [hep-ph/9301212].

[189] M. Bobrowski, A. Lenz, J. Riedl and J. Rohrwild, JHEP **1003** (2010) 009 [hep-ph/1002.4794]. M. Bobrowski, A. Lenz, J. Riedl and J. Rohrwild, [hep-ph/0904.3971].

[190] A. Lenz and T. Rauh, Phys. Rev. D **88** (2013) 034004 [hep-ph/1305.3588].

[191] I. I. Y. Bigi and N. G. Uraltsev, Nucl. Phys. B **592** (2001) 92 [hep-ph/0005089].

[192] M. Bobrowski, A. Lenz and T. Rauh, [hep-ph/1208.6438].

[193] E. Golowich, S. Pakvasa and A. A. Petrov, Phys. Rev. Lett. **98** (2007) 181801 [hep-ph/0610039].

[194] P. Ball, G. W. Jones and R. Zwicky, Phys. Rev. D **75** (2007) 054004 [hep-ph/0612081].

[195] P. Ball and R. Zwicky, Phys. Lett. B **633** (2006) 289 [hep-ph/0510338].

[196] P. Ball, V. M. Braun, A. Lenz, JHEP **0605** (2006) 004 [hep-ph/0603063].

[197] P. Ball, V. M. Braun, A. Lenz, JHEP **0708** (2007) 090 [hep-ph/0707.1201].

[198] A. J. Buras, P. Gambino and U. A. Haisch, Nucl. Phys. B **570** (2000) 117 [hep-ph/9911250].

[199] S. S. Wilks, Ann. Math. Statist. **9**, (1938) 60.

Appendix A

Numerical inputs (Chapters 4 & 5)

Parameter	Value	Unit	Ref.	Parameter	Value	Unit	Ref.
Lepton masses, gauge boson masses and couplings							
m_μ	0.105	GeV	[13]	G_F	$1.16638 \cdot 10^{-5}$	GeV^{-2}	[13]
m_τ	1.777	GeV	[13]	$\alpha_s(M_Z)$	0.1185		[13]
M_Z	91.1876	GeV	[13]	α	$7.29735 \cdot 10^{-3}$		[13]
M_W	80.385	GeV	[13]	$\Lambda_{\overline{MS}}$	0.233	GeV	[13]
CKM							
$\lvert V_{us}\rvert$	$0.22548^{+0.00068}_{-0.00034}$		[17]	γ	$(67.08^{+0.97}_{-2.17})^\circ$		[17]
$\lvert V_{cb}\rvert$	$0.04117^{+0.00090}_{-0.00114}$		[17]	$\sin(2\beta)_{dir.}$	0.710 ± 0.011		[17]
$\lvert V_{ub}/V_{cb}\rvert$	0.0862 ± 0.0044		[17]	$\sin(2\beta)_{indir.}$	$0.748^{+0.030}_{-0.032}$		[17]

Table A.1: Collection of input parameters for the analysis of new physics in tree level b-quark effective operators and possible BSM enhancements in the observable $\Delta\Gamma_d$ (Chapters 4 and 5 respectively). The observable $\sin(2\beta)$ is the result of a combined fit, two versions are presented including ($\sin(2\beta)_{dir}$) and excluding ($\sin(2\beta)_{indir.}$) the direct measurement.

Parameter	Value	Unit	Ref.	Parameter	Value	Unit	Ref.
Quark masses							
m_d	0	GeV		m_b^{1S}	4.66 ± 0.03	GeV	[13]
$m_s(2\text{ GeV})$	0.0935 ± 0.0025	GeV	[13]	$m_{t;dir.}$	173.21 ± 0.87	GeV	[13]
$\bar{m}_c(\bar{m}_c)$	1.275 ± 0.025	GeV	[13]	$m_t^{\overline{MS}}$	160^{+5}_{-4}	GeV	[13]
$\bar{m}_c(\bar{m}_b)$	0.975 ± 0.019	GeV		m_t^{pole}	$176.7^{+4.0}_{-3.4}$	GeV	[13]
$\bar{m}_b(\bar{m}_b)$	4.18 ± 0.03	GeV	[13]	$m_t(m_t)$	165.696 ± 0.726	GeV	
m_b^{pole}	4.78 ± 0.06	GeV	[13]	$m_t(m_W)$	175.9 ± 0.771	GeV	
B- and light meson properties							
m_{B_u}	5279.25 ± 0.26	MeV	[13]	f_ρ	216 ± 3	MeV	[64, 194]
m_{B_d}	5279.55 ± 0.26	MeV	[13]	$f_\rho^\perp$	145 ± 4	MeV	[197]
m_{B_s}	5366.7 ± 0.4	MeV	[13]	$F^{B\to\pi}$	0.28 ± 0.05		[64]
m_{π^+}	139.57	MeV	[13]	$A_0^{B\to\rho}$	0.37 ± 0.06		[64]
m_{π^0}	134.98	MeV	[13]	λ_B	400 ± 150	MeV	[64]
m_ρ	775.26 ± 0.25	MeV	[13]	$a_{1\pi}$	0.0		[195, 196]
m_ω	0.783	MeV	[13]	$a_{2\pi}$	0.17 ± 0.10		[196]
m_{K^0}	497.614 ± 0.024	MeV	[13]	$a_{1\rho}$	0.0		[197]
$f_{B_{u,d}}$	190.5 ± 4.2	MeV	[183]	$a_{1\rho}^\perp$	0.0		[197]
$f_{B_d}\sqrt{B}$	175 ± 12	MeV	[183]	$a_{2\rho}$	0.1 ± 0.05		[197]
$f_{B_s}\sqrt{B}$	216 ± 15	MeV	[183]	$a_{2\rho}^\perp$	0.11 ± 0.05		[197]
f_π	130.41 ± 0.20	MeV	[13]	Λ_h	500	MeV	[61]

Table A.2: Collection (continuation) of input parameters for the analysis of new physics in tree level b-quark effective operators and possible BSM enhancements in the observable $\Delta\Gamma_d$ (Chapters 4 and 5 respectively).

Parameter	Value	Unit	Ref.	Parameter	Value	Unit	Ref.
B- and light meson properties (continuation)							
$\tilde{B}_S/B(B_s^0)$	1.07 ± 0.06		[15]	$\tilde{B}_{R_1}/B(B_d^0)$	1.04 ± 0.12		[15]
$\tilde{B}_{R_0}$	$1.0/0.8 \pm 0.3$			$\tilde{B}_{\tilde{R}_1}/B(B_{d,s}^0)$	1.27 ± 0.16		[15]
$B_{R_1}/B(B_{d,s}^0)$	1.71 ± 0.26		[15]	$\tilde{B}_{R_3}/B(B_{d,s}^0)$	1.14 ± 0.5		
$B_{R_2}/B(B_{d,s}^0)$	1.14 ± 0.5			$\tau(B_s^0)$	1.505 ± 0.004	ps	[1]
$B_{R_3}/B(B_{d,s}^0)$	1.14 ± 0.5			$\tau(B_d^0)$	1.520 ± 0.004	ps	[1]

Table A.3: Collection (continuation) of input parameters for the analysis of new physics in tree level b-quark effective operators and possible BSM enhancements in the observable $\Delta\Gamma_d$ (Chapters 4 and 5 respectively).

Appendix B

Statistical Inference

In Chapter 4 we described a global fit to evaluate possible new physics regions for the Wilson coefficients C_1 and C_2 of the tree level b quark operators $\hat{Q}_1$ and $\hat{Q}_2$. In this section we summarize the statistical theory behind our analysis. The main source of the information presented here is the documentation of the software MyFitter [63] used to automate the study.

To begin with let us introduce some definitions, we will denote by $\vec{x} = (x_1, ..., x_n)$ a set of physical observables depending on the input parameters $\vec{\omega}$. For example in our analysis in Chapter 4, $\vec{x}$ includes $\mathcal{CP}$ asymmetries, branching ratios for B meson processes, etc. The components of our vector $\vec{\omega}$ are masses of different mesons, decay constants, hadronic form factors and so on. The vector $\vec{\omega}$ should also contain the parameters we want to "fit", in our case these are the new physics contributions ΔC_1 and ΔC_2.

To denote the full parameter space we will use the symbol Ω, then $\vec{\omega} \in \Omega$. Our aim is to identify the subregions $\Omega_0 \subset \Omega$ ruled out at a given confidence level in view of the experimental results $\vec{x_0}$ available.

To solve this problem we use frequentist statistics through a "hypothesis test" T, this requires the introduction of the probability density function f corresponding to the joint distribution of observables in $\vec{x}$. Then, under the assumption of a particular set of values for the inputs $\vec{\omega_0}$, our null hypothesis, we calculate the probability of obtaining the experimental results $\vec{x_0}$ at a given confidence level. This is done using

a statistical test T, here we consider a likelihood ratio test defined by[1]

$$T(\vec{x}) \;:=\; -2\ln\frac{\max_{\vec{\omega}_0\in\Omega_0} f(\vec{x},\vec{\omega}_0)}{\max_{\vec{\omega}'\in\Omega} f(\vec{x},\vec{\omega}')}. \tag{B.0.1}$$

In Eq. (B.0.1) the probability density function f is maximized twice, firstly under the assumption of the null hypothesis $\vec{\omega}_0$ (numerator) and then under the assumption of an alternative hypothesis $\vec{\omega}'$ (denominator), in the literature $\vec{\omega}'$ is also called "alternative model". Then the numerator and the denominator in Eq. (B.0.1) are the maximum likelihood estimators for our null hypothesis $\vec{\omega}_0$ and for the alternative model $\vec{\omega}'$ respectively. If we use the analysis of Chapter 4 as an example then $\vec{\omega}_0$ includes the set of values for the physical parameters that minimize f if we assume a particular null hypothesis for the real and imaginary components of ΔC_1 and ΔC_2. Alternatively $\vec{\omega}'$ contains the combination of inputs that maximize f globally (this determines the entries $\vec{\omega}'$ maximally compatibility with data).
Under the definition

$$\chi^2 := -2\ \ln f(\vec{x},\vec{\omega}'), \tag{B.0.2}$$

we can express Eq. (B.0.1) as

$$T(\vec{x}) = \min_{\vec{\omega}_0\in\Omega_0}\chi^2(\vec{x},\vec{\omega}_0) - \min_{\vec{\omega}'\in\Omega}\chi^2(\vec{x},\vec{\omega}') := \Delta\chi^2(\vec{x}). \tag{B.0.3}$$

Qualitatively we can judge how probable is our null hypothesis by looking at the magnitude of $\Delta\chi^2(\vec{x})$. Large values for $\Delta\chi^2$ suggest that the null hypothesis is very unlikely. In our example $\vec{\omega}'$ includes values for ΔC_1 and ΔC_2 close to 0, then assuming huge new physics contributions ΔC_1 and ΔC_2 will produce sizeable deviations between $\min_{\vec{\omega}_0\in\Omega_0}\chi^2(\vec{x},\vec{\omega}_0)$ and the alternative model outcome $\min_{\vec{\omega}'\in\Omega}\chi^2(\vec{x},\vec{\omega}')$.

In order to make quantitative statements we evaluate the p value associated with our null hypothesis $\vec{\omega}_0$. The p-value measures the probability of getting a result for the observables $\vec{y}$ equal or more extreme than the one obtained in the experiment $\vec{x}_0$, if we assume that the null hypothesis is true. We compare $\vec{y}$ with $\vec{x}_0$ through

[1]Notice also that we have written the argument of the statistical test T in a generic way so that it can be applied to any set of values for the observables $\vec{x}$. Then if we want to calculate T for the experimental results we should evaluate $T(\vec{x}_0)$.

their corresponding $\Delta\chi^2$ functions and evaluate the p-value associated with $\vec{\omega}_0$ using the following expression

$$p(\Omega_0, \vec{x}_0) = \max_{\vec{\omega_0}\in\Omega_0} \int d^n\vec{y} f(\vec{y}, \vec{\omega_0}) \theta\Big(\Delta\chi^2(\vec{y}) - \Delta\chi^2(\vec{x}_0)\Big). \tag{B.0.4}$$

We can simplify Eq.(B.0.4) in the case of "Linear regression models". In a linear regression model the parameter space $\Omega = \mathbb{R}^k$ is a k-dimensional real vector space and f is a normal distribution given by

$$\begin{aligned} f(\vec{x}, \vec{\omega}) &\propto \exp\Big[-\frac{1}{2}\Big(\vec{x} - \vec{\mu}(\vec{\omega})\Big)^T \Sigma^{-1}\Big(\vec{x} - \vec{\mu}(\vec{\omega})\Big)\Big], \\ \vec{\mu}(\vec{\omega}) &= A\vec{\omega} + \vec{b}. \end{aligned} \tag{B.0.5}$$

Where Σ is a fixed symmetric matrix containing all the information about the experimental uncertainties and possible correlations (covariance matrix). The vector $\vec{\mu}(\vec{\omega})$ is a linear function of the parameters $\vec{\omega}$, A is a non-singular $\Big(n \times k\Big)$ matrix and $\vec{b}$ is an n dimensional real vector. If Ω_0 is a linear k_0-dimensional subspace of Ω then the analytical solution of Eq. (B.0.4) can be written in terms of the upper incomplete Gamma function Q as

$$p(\Omega_0, \vec{x}_0) = Q_{(k-k_0)/2}\Big(\Delta\chi^2(\vec{x}_0)/2\Big). \tag{B.0.6}$$

According to Wilks theorem [199] we still can use Eq. (B.0.6) as an asymptotic limit when the number of independent observations goes to infinity even if the models we deal with are non linear regression models. The application of Wilks theorem requires the following implicit assumptions: the argument in the exponential of Eq. (B.0.6) depends only on the difference $\vec{x} - \vec{\mu}(\vec{\omega})$ and has at most a quadratic dependence on it.

In the case of our analysis in Chapter 4, $\vec{\mu}$ in Eq. (B.0.5) corresponds to the theoretical expressions for our observables. Based on the equations for the hadronic amplitudes shown in Chapter 4, it is evident that our statistical model is non-linear; however, we rely on the applicability of Wilks theorem in order to estimate our p-values according to Eq.(B.0.6). Then we accept a particular combination for ΔC_1 and ΔC_2 if the corresponding p value is above a given threshold p_0 predefined within the analysis; normally we make reference to the confidence level CL rather than the p value, the connection between both is

$$p = 1 - CL. \tag{B.0.7}$$

Usually the confidence level of a likelihood ratio test is quoted in terms of the number of standard deviations Z, the relationship with the p value is then given by

$$Z = \sqrt{2}\mathrm{Erf}^{-1}\Big(1 - p\Big) \tag{B.0.8}$$

where Erf is the error function.

Appendix C

Initial conditions for the ΔB=1 Wilson coefficients

The LO contributions are given by

$$C_{s,2}^{(0)}(M_W) = 1\,, \qquad C_{s,i}^{(0)}(M_W) = 0 \quad \text{for} \quad i = 1,3,...,10\,.$$
$$C_{7\gamma}^{(0)} = -\frac{1}{2}D_0'(x_t) \qquad C_{8g}^{(0)}(M_W) = -\frac{1}{2}E_0'(x_t), \tag{C.0.1}$$

with the functions

$$\begin{aligned} D_0'(x_t) &= \frac{3x_t^3 - 2x_t^2}{4(x_t-1)^4}\ln x_t + \frac{-8x_t^3 - 5x_t^2 + 7x_t}{24(x_t-1)^3}, \\ E_0'(x_t) &= \frac{-3x_t^2}{4(x_t-1)^4}\ln x_t + \frac{-x_t^3 + 5x_t^2 + 2x_t}{8(x_t-1)^3}. \end{aligned} \tag{C.0.2}$$

The QCD NLO corrections read

$$C_{s,1}^{(1)} = \frac{11}{2}\,, \qquad C_{s,2}^{(1)} = -\frac{11}{6}\,, \tag{C.0.3}$$
$$C_{s,3}^{(1)} = -\frac{1}{6}\tilde{E}_0(x_t)\,, \qquad C_{s,4}^{(1)} = \frac{1}{2}\tilde{E}_0(x_t)\,, \tag{C.0.4}$$
$$C_{s,5}^{(1)} = -\frac{1}{6}\tilde{E}_0(x_t)\,, \qquad C_{s,6}^{(1)} = \frac{1}{2}\tilde{E}_0(x_t)\,, \tag{C.0.5}$$
$$C_{s,i}^{(1)} = 0 \quad \text{for} \quad i = 7,8,9,10\,, \tag{C.0.6}$$

with the loop functions

$$\begin{aligned} E_0(x_t) &= -\frac{2}{3}\ln x_t + \frac{x_t(18 - 11x_t - x_t^2)}{12(1-x_t)^3} + \frac{x_t^2(15 - 16x_t + 4x_t^2)}{6(1-x_t)^4}\ln x_t\,, \\ \tilde{E}_0(x_t) &= E_0(x_t) - \frac{2}{3}\,, \end{aligned} \tag{C.0.7}$$

where $x_t = m_t^2/M_W^2$.

The leading electro-weak terms are given by

$$\begin{aligned}
C_{e,i}^{(0)}(M_W) &= 0 \quad \text{for} \quad i = 1,4,5,6,8,10\,, && \text{(C.0.8)}\\
C_{e,2}^{(0)}(M_W) &= -\frac{35}{18}\,, && \text{(C.0.9)}\\
C_{e,3}^{(0)}(M_W) &= \frac{2}{3}\frac{1}{sin^2(\theta_W)}\Big(2B_0(x_t) + C_0(x_t)\Big)\,, && \text{(C.0.10)}\\
C_{e,7}^{(0)}(M_W) &= \frac{x_t}{3}\,, && \text{(C.0.11)}\\
C_{e,9}^{(0)}(M_W) &= \frac{x_t}{3} + \frac{2}{3sin^2(\theta_W)}\Big(10B_0(x_t) - 4C_0(x_t)\Big)\,, && \text{(C.0.12)}
\end{aligned}$$

with the loop functions

$$\begin{aligned}
B_0(x_t) &= \frac{1}{4}\Big[\frac{x_t}{1-x_t} + \frac{x_t \ln x_t}{(1-x_t)^2}\Big]\,, && \text{(C.0.13)}\\
C_0(x_t) &= \frac{x_t}{8}\Big[\frac{x_t-6}{x_t-1} + \frac{3x_t+2}{(x_t-1)^2 \ln x_t}\Big]\,. && \text{(C.0.14)}
\end{aligned}$$

We use the following approximations [45] based on the results obtained in [198]

$$\begin{aligned}
C_{e,7}^{(1)}(M_W) &\approx -29.6 x_t^{1.142} + 28.52 x_t^{1.148}\\
C_{e,8}^{(1)}(M_W) &\approx 0.94 x_t^{0.661}\\
C_{e,8}^{(1)}(M_W) &\approx -571.62 x_t^{0.580} + 566.40 x_t^{0.590}\\
C_{e,10}^{(1)}(M_W) &\approx -5.51 x_t^{1.107}. && \text{(C.0.15)}
\end{aligned}$$

The initial conditions for the remainder functions are

$$R_{e,7}^{(0)} = R_{e,9}^{(0)} = \frac{8}{3}C_0(x_t) + \frac{2}{3}\tilde{D}(x_t) - \frac{x_t}{3}, \qquad \text{(C.0.16)}$$

with

$$\begin{aligned}
\tilde{D}_0(x_t) &= D_0(x_t) - \frac{4}{9},\\
D_0(x_t) &= -\frac{4}{9}\ln x_t + \frac{-19x_t^3 + 25x_t^2}{36(x_t-1)^3} + \frac{x_t^2(5x_t^2 - 2x_t - 6)}{18(x_t-1)^4}\ln x_t\,. && \text{(C.0.17)}
\end{aligned}$$

To reproduce the $\mathcal{O}(\alpha)$ conditions for $C_{e,7}(M_W)$ and $C_{e,9}(M_W)$ given in [46] we should consider $C_{e,7}^{(0)}(M_W) + R_{e,7}^{(0)}$ and $C_{e,9}^{(0)}(M_W) + R_{e,9}^{(0)}$ respectively. As indicated in section 2.3.1 we are following a different treatment of the QCD and the electroweak corrections in comparison with [46]. In our case we are taking into account x_t and $\sin^2\theta_W$ enhancements to the different α suppressed terms as suggested by [45].

Appendix D

QCD factorization formulas

D.1 Overall amplitude factors

$$\begin{aligned}
A_{\pi\pi} &= i\frac{G_F}{\sqrt{2}}m_B^2 F_0^{B\to\pi}(0)f_\pi,\\
A_{\pi\rho} &= -i\frac{G_F}{\sqrt{2}}m_B^2 F_0^{B\to\pi}(0)f_\rho,\\
A_{\rho\pi} &= -i\frac{G_F}{\sqrt{2}}m_B^2 A_0^{B\to\rho}(0)f_\pi,\\
A_{\rho\rho} &= i\frac{G_F}{\sqrt{2}}m_B^2 A_0^{B\to\rho}(0)f_\rho,\\
B_{\pi\pi} &= i\frac{G_F}{\sqrt{2}}f_B f_\pi f_\pi,\\
B_{\pi\rho} &= B_{\rho\pi} = -i\frac{G_F}{\sqrt{2}}f_B f_\pi f_\rho,\\
B_{\rho\rho} &= i\frac{G_F}{\sqrt{2}}f_B f_\rho f_\rho.
\end{aligned} \tag{D.1.1}$$

D.2 r_χ factors

$$\begin{aligned}
r_\chi^\pi &= \frac{2m_\pi^2}{m_b(\mu)2m_q},\\
r_\perp^\rho(\mu) &= \frac{2m_\rho}{m_b(\mu)}\frac{f_\rho^\perp(\mu)}{f_\rho}.
\end{aligned} \tag{D.2.2}$$

Where

$$f_\rho^\perp(\mu) = f_\rho^\perp(\mu_0)\Big(\frac{\alpha_s(\mu)}{\alpha_s(\mu_0)}\Big)^{\frac{C_F}{\beta_0}}, \tag{D.2.3}$$

with $C_F = 4/3$ and $\beta_0 = 23/3$ for $N = 3$ and $f = 5$; m_q denotes an average of the up and down quark masses.

D.3 Extra topological amplitudes

$$\begin{aligned}
\tilde{\alpha}_4^{p,\pi\pi/\pi\rho} &= \alpha_4^{p,\pi\pi/\pi\rho} + r_\chi^{\pi/\rho}\alpha_6^{p,\pi\pi/\pi\rho}, \\
\tilde{\alpha}_4^{p,\rho\pi} &= \alpha_4^{p,\rho\pi} - r_\chi^{\pi}\alpha_6^{p,\rho\pi}, \\
\tilde{\alpha}_{4,EW}^{\pi\pi/\pi\rho} &= \alpha_{10}^{p,\pi\pi/\pi\rho} + r_\chi^{\pi/\rho}\alpha_8^{p,\pi\pi/\pi\rho}, \\
\tilde{\alpha}_{4,EW}^{\rho\pi} &= \alpha_{10}^{p,\rho\pi} - r_\chi^{\pi}\alpha_8^{p,\rho\pi}.
\end{aligned} \tag{D.3.4}$$

D.4 Vertices

$$\begin{aligned}
V_{1,2,4,10}^{\pi} &= 12\ln\frac{m_b}{\mu} - 18 + \Big[-\frac{1}{2} - 3i\pi + \Big(\frac{11}{2} - 3i\pi\Big)a_1^{\pi} - \frac{21}{20}a_2^{\pi}\Big], \\
V_{6,8}^{\pi} &= -6, \\
V_{1,2,3,4,9,10}^{\rho} &= V^{\rho} = 12\ln\frac{m_b}{\mu} - 18 + \Big[-\frac{1}{2} - 3i\pi + \Big(\frac{11}{2} - 3i\pi\Big)a_1^{\rho} - \frac{21}{20}a_2^{\rho}\Big], \\
V_{\perp}^{\rho} &= 9 - 6i\pi + \Big(\frac{19}{6} - i\pi\Big)a_{2,\perp}^{\rho}, \\
V_4^{\rho} &= \begin{cases} V^{\rho} & \text{for } \bar{B}_d^0 \to \pi^+\rho^-, \\ V^{\rho} - \frac{C_5}{C_3}r_\perp^{\rho}V_\perp^{\rho} & \text{for } \bar{B}_d^0 \to \rho\rho, \end{cases} \\
V_7^{\rho} &= -\Big(12\ln\frac{m_b}{\mu} - 6 + \Big[-\frac{1}{2} - 3i\pi - \Big(11/2 - 3i\pi\Big)a_1^{\rho} - \frac{21}{20}a_2^{\rho}\Big]\Big), \\
V_{6,8}^{\rho} &= 9 - 6i\pi + \Big(\frac{19}{6} - i\pi\Big)a_{2,\perp}^{\rho}, \\
V_{10}^{\rho} &= V^{\rho} - \frac{C_7}{C_9}r_\perp^{\rho}V_\rho^{\perp}.
\end{aligned} \tag{D.4.5}$$

D.5 Penguins

$$P_{1,2,3}^{p,M} = P_{1,2,3}^{M} = 0,$$

$$\begin{aligned} P_4^{p,\pi} = \frac{C_F\alpha_s}{4\pi N_c}\Big\{ & C_2\Big[\frac{4}{3}\ln\frac{m_b}{\mu} + \frac{2}{3} - G_\pi(s_p)\Big] + C_3\Big[\frac{8}{3}\ln\frac{m_b}{\mu} + \frac{4}{3} - G_\pi(0) - G_\pi(1)\Big] \\ & + \Big(C_4 + C_6\Big)\Big[\frac{20}{3}\ln\frac{m_b}{\mu} - 3G_\pi(0) - G_\pi(s_c) - G_\pi(1)\Big] - 6C_{8g}^{eff}\Big(1 + \alpha_1^\pi + \alpha_2^\pi\Big)\Big\}, \end{aligned}$$

$$\begin{aligned} P_6^{p,\pi} = \frac{C_F\alpha_s}{4\pi N_c}\Big\{ & C_2\Big[\frac{4}{3}\ln\frac{m_b}{\mu} + \frac{2}{3} - \hat{G}_\pi(s_p)\Big] + C_3\Big[\frac{8}{3}\ln\frac{m_b}{\mu} + \frac{4}{3} - \hat{G}_\pi(0) - \hat{G}_\pi(1)\Big] \\ & + \Big(C_4 + C_6\Big)\Big[\frac{20}{3}\ln\frac{m_b}{\mu} - 3\hat{G}_\pi(0) - \hat{G}_\pi(s_c) - \hat{G}_\pi(1)\Big] - 2C_{8g}^{eff}\Big\}, \end{aligned}$$

$$P_8^{p,\pi} = \frac{\alpha}{9\pi N_c}\Big\{\Big(N_cC_1 + C_2\Big)\Big[\frac{4}{3}\ln\frac{m_b}{\mu} + \frac{2}{3} - \hat{G}_\pi(s_p)\Big] - 3C_7^{eff}\Big\},$$

$$P_{10}^{p,M} = \frac{\alpha}{9\pi N_c}\Big\{\Big(N_cC_1 + C_2\Big)\Big[\frac{4}{3}\ln\frac{m_b}{\mu} + \frac{2}{3} - G_M(s_p)\Big] - 9C_7^{eff}\Big(1 + \alpha_1^M + \alpha_2^M\Big)\Big\},$$

$$P_4^{p,\rho} = \begin{cases} P_4^{\prime p,\rho} & \text{for } \bar{B}_d^0 \to \pi^+\rho^-, \\ P_4^{\prime p,\rho} - r_\perp^\rho P_4^{\prime\prime p,\rho} & \text{for } \bar{B}_d^0 \to \rho^+\rho^-, \end{cases}$$

$$\begin{aligned} P_4^{p,\rho} = \frac{C_F\alpha_s}{4\pi N_c}\Big\{ & C_2\Big[\frac{4}{3}\ln\frac{m_b}{\mu} + \frac{2}{3} - G_\rho(s_p)\Big] + C_3\Big[\frac{8}{3}\ln\frac{m_b}{\mu} + \frac{4}{3} - G_\rho(0) - G_\rho(1)\Big] \\ & + \Big(C_4 + C_6\Big)\Big[\frac{20}{3}\ln\frac{m_b}{\mu} - 3G_\rho(0) - G_\rho(s_c) - G_\rho(1)\Big] - 6C_{8g}^{eff}\Big(1 + \alpha_1^\rho + \alpha_2^\rho\Big)\Big\}, \end{aligned}$$

$$\begin{aligned} P_6^{p,\rho} = \frac{C_F\alpha_s}{4\pi N_c}\Big\{ & -\Big[C_2\hat{G}_\rho(s_p) + C_3\Big(\hat{G}_\rho(0) + \hat{G}_\rho(1)\Big) \\ & + \Big(C_4 + C_6\Big)\Big(3\hat{G}_\rho(0) + \hat{G}_\rho(s_p) + \hat{G}_\rho(1)\Big)\Big]\Big\}, \end{aligned}$$

$$\begin{aligned} P_4^{\prime\prime p,\rho} = & -\Big[C_2\hat{G}_\rho(s_p) + C_3\Big(\hat{G}_\rho(0) + \hat{G}_\rho(1)\Big) \\ & + \Big(C_4 + C_6\Big)\Big(3\hat{G}_\rho(0) + \hat{G}_\rho(s_p) + \hat{G}_\rho(1)\Big)\Big], \end{aligned}$$

$$\begin{aligned} P_{7,9}^{u,\rho} = \frac{\alpha}{9\pi}\Big\{ & \Big(N_cC_1 + C_2\Big)\Big[\frac{4}{3}\frac{m_b}{\mu} - \frac{10}{9} + \frac{4\pi^2}{3}\sum_{r=\rho,\omega}\frac{f_r^2}{m_\rho^2 - m_r^2 + im_r\Gamma_r} \\ & - \frac{2\pi}{3}\frac{m_\rho^2}{t_c}i + \frac{2}{3}\ln\frac{m_\rho^2}{m_b^2} + \frac{2}{3}\frac{t_c - m_\rho^2}{t_c}\ln\frac{t_c - m_\rho^2}{m_\rho^2}\Big] - 3C_{7,\gamma}^{eff}\Big\}, \end{aligned}$$

i	1	2	3	4	5	6	7	8
a_i	14/23	16/23	6/23	−12/23	0.4086	−0.4230	−0.89994	0.1456
h_i	2.2996	−1.0880	−3.0/7.0	−1.0/14.0	−0.6494	−0.0380	−0.0185	−0.0057
$\bar{h}_i$	0.8623	0.0	0.0	0.0	−0.9135	0.0873	−0.0571	0.0209

Table D.1: Coefficients used in the determination of $C_{7\gamma}^{eff}$ and C_{8g}^{eff}.

$$
\begin{aligned}
P_{7,9}^{c,\rho} &= \frac{\alpha}{9\pi}\Big\{\Big(N_cC_1+C_2\Big)\Big[\frac{4}{3}\ln\frac{m_b}{\mu}+\frac{2}{3}+\frac{4}{3}\ln\frac{m_c}{m_b}\Big]-3C_\gamma^{eff}\Big\},\\
P_8^{p,\rho} &= -\frac{\alpha}{9\pi N_c}\Big(N_cC_1+C_2\Big)\hat{G}_\rho(s_p),\\
P_{10}^{p} &= \frac{C_F\alpha_s}{4\pi}\Big(P_{10}^{\prime p,\rho}-r_\perp^\rho P_{10}^{\prime\prime p,\rho}\Big),\\
P_{10}^{\prime p,\rho} &= \Big(N_cC_1+C_2\Big)\Big[\frac{4}{3}\ln\frac{m_b}{\mu}+\frac{2}{3}-G_\rho(s_c)\Big]-9C_{7,\gamma}^{eff}\Big(1+\alpha_1^\rho+\alpha_2^\rho\Big),\\
P_{10}^{\prime\prime p,\rho} &= -\Big(N_cC_1+C_2\Big)\hat{G}_\rho(s_p).
\end{aligned}
\tag{D.5.6}
$$

In $P_{1,2,3}^M$ and $P_{10}^{p,M}$ the superindex stands for $M=\pi,\rho$. In $P_{7,9}^{u,\rho}$ the symbol t_c is given by

$$
t_c \;=\; 4\pi^2(f_\rho^2+f_\omega^2). \tag{D.5.7}
$$

For the index p in the expressions in Eq. (D.5.6) we have $p=u,c$ and the argument of the G and $\hat{G}$ functions is $s_p=(m_p/m_b)^2$. In the case of m_u we take $s_u=0$.
All the Wilson coefficients should be evaluated at the scale $\mu\sim m_b$ according to the theory presented in Chapter 2. For the effective coefficients we have [47]

$$
\begin{aligned}
C_{7\gamma}^{(0)eff}(\mu) &= \eta^{-16/23}C_{7\gamma}^{(0)}(M_W)+\frac{8}{3}(\eta^{-14/23}-\eta^{-16/23})C_{8G}^{(0)}(M_W)+C_2^{(0)}(M_W)\sum_{i=1}^{8}h_i\eta^{-a_i},\\
C_{8G}^{(0)eff}(\mu) &= \eta^{-14/23}C_{8G}^{(0)}(M_W)+C_2^{(0)}(M_W)\sum_{i=1}^{8}\bar{h}_i\eta^{-a_i},
\end{aligned}
\tag{D.5.8}
$$

with $\eta=\alpha_s(\mu)/\alpha_s(M_W)$. The set of numbers $h_i,\bar{h}_i$ and a_i are presented in Tab. D.1.
The expression for $P_4^{\prime\rho}$ can be calculated from $P_4^{p,\pi}$ under the replacements $\alpha^\pi\to\alpha^\rho$ and $G_\pi(x)\to G_\rho(x)$. We present next the functions G_M for $M=\pi,\rho$.

$$
\begin{aligned}
G_M(s_c) &= \frac{5}{3}-\frac{2}{3}\ln(s_c)+\frac{\alpha_1^{iM}}{2}+\frac{\alpha_2^M}{5}+\frac{4}{3}\Big(8+9\alpha_1^M+9\alpha_2^M\Big)s_c+2\Big(8+63\alpha_1^M\\
&\quad +214\alpha_2^M\Big)s_c^2-24\Big(9\alpha_1^M+80\alpha_2^M\Big)s_c^3+2880\alpha_2^M s_c^4-\frac{2}{3}\sqrt{1-4s_c}\Big(\\
&\quad 2\text{arctanh}\sqrt{1-4s_c}-i\pi\Big)\Big[1+2s_c+6\Big(4+27\alpha_1^M+78\alpha_2^M\Big)s_c^2\\
&\quad -36\Big(9\alpha_1^M+70\alpha_2^M\Big)s_c^3+4320\alpha_2^M s_c^4\Big]+12s_c^2\Big(2\text{arctanh}\sqrt{1-4s_c}-i\pi\Big)^2\Big[\\
&\quad 1+3\alpha_1^M+6\alpha_2^M-\frac{4}{3}\Big(1+9\alpha_1^\rho+36\alpha_2^M\Big)s_c+18\Big(\alpha_1^M+10\alpha_2^M\Big)s_c^2-240\alpha_2^M s_c^3\Big],\\
G_M(0) &= \frac{5}{3}+\frac{2i\pi}{3}+\frac{\alpha_1^M}{2}+\frac{\alpha_2^M}{5},\\
G_M(1) &= \frac{85}{3}-6\sqrt{3}\pi+\frac{4\pi^2}{9}-\Big(\frac{155}{2}-36\sqrt{3}\pi+12\pi^2\Big)\alpha_1^M\\
&\quad +\Big(\frac{7001}{5}-504\sqrt{3}\pi+136\pi^2\Big)\alpha_2^M,\\
\hat{G}_\pi^p(s_c) &= \frac{16}{9}\Big(1-3s_c\Big)-\frac{2}{3}\Big(\ln(s_c)+\Big(1-4s_c\Big)^{3/2}\Big(2\text{arctan}\sqrt{1-4s_c}-i\pi\Big)\Big),\\
\hat{G}_\pi^p(0) &= \frac{16}{9}+\frac{2\pi i}{3},\\
\hat{G}_\pi^p(1) &= \frac{2\pi}{\sqrt{3}}-\frac{32}{9},\\
\hat{G}_\rho(s_c) &= 1+\frac{\alpha_{1,\perp}^\rho}{3}+\frac{\alpha_{2,\perp}^\rho}{6}-4s_c\Big(9+12\alpha_{1,\perp}^\rho+14\alpha_{2,\perp}^\rho\Big)-6s_c^2\Big(8\alpha_{1,\perp}^\rho+35\alpha_{2,\perp}^\rho\Big)\\
&\quad +360s_c^3\alpha_{2,\perp}^\rho+12s_c\sqrt{1-4s_c}\Big(1+\Big[1+4s_c\Big]\alpha_{1,\perp}^\rho+\Big[1+15s_c\\
&\quad -30s_c^2\Big]\alpha_{2,\perp}^\rho\Big)\Big(2\text{arctanh}\sqrt{1-4s_c}-i\pi\Big)-12s_c^2\Big(1+\Big[3-4s_c\Big]\alpha_{1,\perp}^\rho\\
&\quad +2\Big[3-10s_c+15s_c^2\Big]\alpha_{2,\perp}^\rho\Big)\Big(2\text{arctanh}\sqrt{1-4s_c}-i\pi\Big)^2,\\
\hat{G}_\rho(0) &= 1+\frac{1}{3}\alpha_{1,\perp}^\rho+\frac{1}{6}\alpha_{2,\perp}^\rho,\\
\hat{G}_\rho(1) &= -35+4\sqrt{3}\pi+\frac{4\pi^2}{3}+\Big(-\frac{287}{3}+20\sqrt{3}\pi-\frac{4\pi^2}{3}\Big)\alpha_{1,\perp}^\rho\\
&\quad +\Big(\frac{565}{6}-56\sqrt{3}\pi+\frac{64\pi^2}{3}\Big)\alpha_{2,\perp}^\rho.
\end{aligned}
\tag{D.5.9}
$$

D.6 Hard Scattering functions

D.6.1 Hard Scattering functions for $B \to \pi\pi$ and $B \to \rho\rho$

$$
\begin{aligned}
H^{\pi\pi}_{1,2,4,10}(\mu) &= \frac{B_{\pi\pi}}{A_{\pi\pi}}\frac{m_B}{\lambda_B}\Big[9\Big((1+a_1^\pi+a_2^\pi\Big)^2+3r_\chi^\pi(\mu)\Big(1-a_1^\pi+a_2^\pi\Big)X_H\Big],\\
H^{\pi\pi}_{6,8}(\mu) &= 0,\\
H^{\pi\rho}_{2,4,10}(\mu) &= \frac{B_{\pi\rho}}{A_{\pi\rho}}\frac{m_B}{\lambda_B}\Big(9(1+a_1^\pi+a_2^\pi)(1+a_1^\rho+a_2^\rho)+3r_\chi^\pi(\mu)(1-a_1^\rho+a_2^\rho)X_H\Big),\\
H^{\pi\rho}_{6,8}(\mu) &= 0,\\
H^{\rho\pi}_{2,4,10} &= \frac{B_{\rho\pi}}{A_{\rho\pi}}\frac{m_B}{\lambda_B}\Big(9(1+a_1^\pi+a_2^\pi)(1+a_1^\rho+a_2^\rho)+3r_\chi^\rho(\mu)(1-a_1^\pi+a_2^\pi)\Big[\\
&\quad 3(1+a_{1,\perp}^\rho+a_{2,\perp}^\rho)X_H-(6+9a_{1,\perp}^\rho+11a_{2,\perp}^\rho+...)\Big]\Big),\\
H^{\rho\pi}_{6,8}(\mu) &= 0,\\
H^{\rho\rho}_{1,2,4,9,10}(\mu) &= \frac{B_{\rho\rho}}{A_{\rho\rho}}\Big[\frac{m_{B_d}}{\lambda_B}\Big]\Big[9\Big(1+a_1^\rho+a_2^\rho\Big)^2+9r_\perp^\rho(\mu)\Big(1-a_1^\rho+a_2^\rho\Big)\Big(X_H-2\Big)\Big],\\
H^{\rho\rho}_{7}(\mu) &= -\frac{B_{\rho\rho}}{A_{\rho\rho}}\Big[\frac{m_{B_d}}{\lambda_B}\Big]\Big[9\Big(1+a_1^\rho+a_2^\rho\Big)\Big(1-a_1^\rho+a_2^\rho\Big)+9r_\perp^\rho(\mu)\Big(1+a_1^\rho\\
&\quad +a_2^\rho\Big)\Big(X_H-2\Big)\Big].
\end{aligned}
\tag{D.6.10}
$$

D.6.2 Hard Scattering functions for $B \to J/\psi K$

$$
\begin{aligned}
f_I &= \int_0^1 d\xi\phi^{J/\psi}(\xi)\Big\{\frac{2z\xi}{1-z(1-\xi)}+(3-2\xi-8\xi^2)\frac{\ln\xi}{1-\xi}\\
&\quad +\Big(-\frac{3}{1-z\xi}+\frac{1+8\xi}{1-z(1-\xi)}-\frac{2z\xi}{[1-z(1-\xi)]^2}\Big)z\xi\ \ln z\xi\\
&\quad +\Big(3(1-z)+2z\xi-8z\xi^2+\frac{2z^2\xi^2}{1-z(1-\xi)}\Big)\times\frac{\ln(1-z)-i\pi}{1-z(1-\xi)}\Big\},\\
g_I &= \int_0^1 d\xi\phi^{J/\psi}(\xi)\Big\{\frac{4\xi(2\xi-1)}{(1-z)(1-\xi)}\ \ln\xi+\frac{z\xi}{[1-z(1-\xi)]^2}\times\ \ln(1-z)\\
&\quad +\Big(\frac{1}{(1-z\xi)^2}-\frac{1}{[1-z(1-\xi)]^2}-\frac{8\xi}{(1-z)(1-z\xi)}\\
&\quad +\frac{2(1+z-2z\xi)}{(1-z)(1-x\xi)^2}\Big)z\xi-i\pi\frac{z\xi}{[1-z(1-\xi)]^2}\Big\}.
\end{aligned}
\tag{D.6.11}
$$

D.6.3 Annihilation coefficients

$$
\begin{aligned}
\beta_i^{p,M_1M_2} &= \frac{B_{M_1M_2}}{A_{M_1M_2}} b_i^{p,M_1M_2},\\
b_1^{M_1M_2} &= \frac{C_F}{N_c^2} C_1 A_1^{i,M_1M_2},\\
b_2^{M_1M_2} &= \frac{C_F}{N_c^2} C_2 A_1^{i,M_1M_2},\\
b_3^{p,M_1M_2} &= \frac{C_F}{N_c^2}\Big[C_3 A_1^{i,M_1M_2} + C_5\Big(A_3^{i,M_1M_2} + A_3^{f,M_1M_2}\Big) + N_c C_6 A_3^{f,M_1M_2}\Big],\\
b_4^{p,M_1M_2} &= \frac{C_F}{N_c^2}\Big[C_4 A_1^{i,M_1M_2} + C_6 A_2^{i,M_1M_2}\Big],\\
b_{3,EW}^{p,M_1M_2} &= \frac{C_F}{N_c^2}\Big[C_9 A_1^{i,M_1M_2} + C_7\Big(A_3^{i,M_1M_2} + A_3^{f,M_1M_2}\Big) + N_c C_8 A_3^{f,M_1M_2}\Big],\\
b_{4,EW}^{p,M_1M_2} &= \frac{C_F}{N_c^2}\Big[C_{10} A_1^{i,M_1M_2} + C_8 A_2^{i,M_1M_2}\Big].
\end{aligned}
\tag{D.6.12}
$$

D.6.4 Annihilation kernels

$$
\begin{aligned}
A_1^{i,\pi\pi} &\approx A_2^{i,\pi\pi} \approx 2\pi\alpha_s(\mu_h)\Big[9\Big(X_A - 4 + \frac{\pi^2}{3}\Big) + r_\chi^\pi r_\chi^\pi X_A^2\Big]\\
A_1^{i,\pi\rho} &= A_1^{i,\rho\pi} \approx 6\pi\alpha_s\Big[3\Big(X_A - 4 + \frac{\pi^2}{3}\Big) + r_\chi^\rho r_\chi^\pi\Big(X_A^2 - X_A\Big)\Big]\\
A_2^{i,\pi\rho} &= A_2^{i,\rho\pi} \approx -A_1^{i,\pi\rho}\\
A_3^{i,\pi\pi} &\approx 0\\
A_3^{i,\pi\rho} &= A_3^{i,\rho\pi} \approx 6\pi\alpha_s\Big[-3r_\chi^\rho\Big(X_A^2 - 2X_A - \frac{\pi^2}{3} + 4\Big) + r_\chi^\pi\Big(X_A^2 - 2X_A + \frac{\pi^2}{3}\Big)\Big]\\
A_1^{f,\pi\rho} &= A_2^{f,\pi\rho} = A_1^{f,\rho\pi} = A_2^{f,\rho\pi} = 0\\
A_3^{f,\pi\pi} &\approx 12\pi\alpha_s r_\chi^\pi\Big(2X_A^2 - X_A\Big)\\
A_3^{f,\pi\rho} &= -A_3^{f,\rho\pi} \approx 6\pi\alpha_s\Big[3r_\chi^\rho\Big(2X_A - 1\Big)\Big(X_A - 2\Big) + r_\chi^\pi\Big(2X_A^2 - X_A\Big)\Big]\\
A_1^{i,\rho\rho} &= A_2^{i,\rho\rho} \approx 18\pi\alpha_s\Big[\Big(X_A - 4 + \frac{\pi^2}{3}\Big) + (r_\perp^\rho)^2(X_A - 2)^2\Big]\\
A_3^{i,\rho\rho} &= 0\\
A_3^{f,\rho\rho} &\approx -36\pi\alpha_s r_\perp^\rho\Big(2X_A^2 - 5X_A + 2\Big).
\end{aligned}
\tag{D.6.13}
$$

Appendix E

Inputs & errors for Chapter 6

Parameter	Update	ABL review 2015 [15]
$f_{B_s}\sqrt{B}$	$0.223 \pm 0.007\,\text{GeV}$	$0.215 \pm 0.015\,\text{GeV}$
$f_{B_d}\sqrt{B}$	$0.185 \pm 0.008\,\text{GeV}$	$0175 \pm 0.012\,\text{GeV}$
$\tilde{B}_S/B(B_s^0)$	1.15 ± 0.16	1.07 ± 0.06
$\tilde{B}_S/B(B_d^0)$	1.17 ± 0.24	1.04 ± 0.12
$\tilde{B}_{R_0}/B(B_s^0)$	0.54 ± 0.55	1.00 ± 0.3
$\tilde{B}_{R_0}/B(B_d^0)$	0.35 ± 0.80	1.00 ± 0.3
$\tilde{B}_{R_1}/B(B_s^0)$	1.61 ± 0.10	1.71 ± 0.26
$\tilde{B}_{R_1}/B(B_d^0)$	1.72 ± 0.15	1.71 ± 0.26
$\tilde{B}_{\tilde{R}_1}/B(B_s^0)$	1.223 ± 0.093	1.27 ± 0.16
$\tilde{B}_{\tilde{R}_1}/B(B_d^0)$	1.31 ± 0.14	1.27 ± 0.16
$\lvert V_{cb}\rvert$	$0.04180^{+0.00033}_{-0.00068}$	$0.04117^{+0.00090}_{-0.00114}$

Table E.1: Inputs used in the evaluation of mixing observables. The update (left column) is based on the lattice updates presented in [79]. For comparison the inputs used in the previous determination (right column) are also shown.

Parameter	Update	ABL review 2015 [15]
$\lvert V_{ub}/V_{cb}\rvert$	0.0889 ± 0.0019	0.0862 ± 0.0044
γ	$1.170^{+0.015}_{-0.035}$	$1.171^{+0.017}_{-0.038}$
$\lvert V_{us}\rvert$	$0.22542^{+0.00042}_{-0.00031}$	$0.22548^{+0.00068}_{-0.00034}$

Table E.2: Inputs used in the evaluation of mixing observables (cont.). The update (left column) is based on the lattice updates presented in [79]. For comparison the inputs used in the previous determination (right column) are also shown.

	Update for mixing quantities
M_{12}^s	$10.5 - 0.377 \cdot i$
M_{12}^d	$0.214 + 0.215 \cdot i$
$\arg(M_{12}^s)$	-0.0375
$\arg(M_{12}^d)$	0.788
Γ_{12}^s	$-0.0490 + 0.00207 \cdot i$
Γ_{12}^d	$-0.000950 - 0.00116 \cdot i$
$\arg(\Gamma_{12}^s)$	-0.0422
$\arg(\Gamma_{12}^d)$	0.886
Γ_{12}^s/M_{12}^s	$-0.00488 + 0.0000227 \cdot i$
Γ_{12}^d/M_{12}^d	$-0.00493 - 0.000490 \cdot i$

Table E.3: Predictions for $M_{12}^{d,s}$ and $\Gamma_{12}^{d,s}$ using the updated inputs in Tab. E.1.

Observable	Update for mixing observables
ΔM_s	$20.11 \pm 1.37\,\mathrm{ps}^{-1}$.
ΔM_d	$0.606 \pm 0.056\,\mathrm{ps}^{-1}$.
$\Delta\Gamma_s$	$0.098 \pm 0.014\,\mathrm{ps}^{-1}$.
$\Delta\Gamma_d$	$0.00299 \pm 0.00052\,\mathrm{ps}^{-1}$.
$\mathcal{I}m\left(\Gamma_{12}^s/M_{12}^s\right)$	-0.00488 ± 0.00061 ,
$\mathcal{R}e\left(\Gamma_{12}^d/M_{12}^d\right)$	-0.00493 ± 0.00061 ,
$\mathcal{I}m\left(\Gamma_{12}^s/M_{12}^s\right)$	$0.0000227 \pm 2.50 \cdot 10^{-6}$,
$\mathcal{I}m\left(\Gamma_{12}^d/M_{12}^d\right)$	-0.000490 ± 0.000054 ,
$\pi - \arg\left(\Gamma_{12}^s/M_{12}^s\right)$	0.00466 ± 0.00105 $= (0.267 \pm 0.060)^\circ$,
$\pi - \arg\left(\Gamma_{12}^d/M_{12}^d\right)$	0.0989 ± 0.0233 $= (5.67 \pm 1.34)^\circ$

Table E.4: Mixing observables for $B_{s,d}^0$ using the updated inputs in Tab. E.1.

	B_s^0	B_d^0
c	-48.65 ± 6.10	-49.32 ± 7.33
a	$+12.22 \pm 1.31$	11.73 ± 1.27
b	$+0.77 \pm 0.10$	0.23 ± 0.04

Table E.5: Mixing parameters a, b, c (see Eq.(2.4.114)) calculated with the updated inputs in Tab. E.1.

Parameter	Update	ABL review 2015 [15]
$\delta(f_{B_s}\sqrt{B})$	0.0635	0.139
$\delta(\lvert V_{cb}\rvert)$	0.0240	0.049
$\delta(m_t)$	0.0066	0.007
$\delta(\Lambda_{QCD})$	0.0013	0.001
$\delta(\gamma)$	0.0009	0.001
$\delta(m_b)$	0.0005	< 0.001
$\delta(\lvert V_{ub}/V_{cb}\rvert)$	0.0004	0.001
$\sum \delta$	0.0682	0.148

Table E.6: Error budget for ΔM_s using the updated inputs in Tab. E.1.

Parameter	Update	ABL review 2015 [15]
$\delta(f_{B_d}\sqrt{B})$	0.0872	0.137
$\delta(\lvert V_{cb}\rvert)$	0.0240	0.049
$\delta(m_t)$	0.00656	0.001
$\delta(\Lambda_{QCD})$	0.00129	0.0
$\delta(\gamma)$	0.0208	0.002
$\delta(m_b)$	0.000515	0.0
$\delta(\lvert V_{ub}/V_{cb}\rvert)$	0.000133	0.0
$\sum \delta$	0.0931	0.148

Table E.7: Error budget for ΔM_d using the updated inputs in Tab. E.1.

Parameter	Update	ABL review 2015 [15]
$\delta(\mu)$	0.0889	0.084
$\delta(f_{B_s})$	0.0635	0.139
$\delta(B_{R_2})$	0.0604	0.148
$\delta(B_S)$	0.0539	0.021
$\delta(\lvert V_{cb}\rvert)$	0.0240	0.049
$\delta(B_{R_0})$	0.0310	0.021
$\delta(\bar{z})$	0.0109	0.011
$\delta(m_b)$	0.0080	0.008
$\delta(B_{\tilde{R}_1})$	0.0038	0.007
$\delta(m_s)$	0.0024	0.001
$\delta(B_{R_3})$	0.0023	0.002
$\delta(B_{R_1})$	0.0018	0.005
$\delta(\gamma)$	0.0010	0.001
$\delta(\Lambda_{QCD})$	0.0010	0.001
$\delta(\lvert V_{ub}/V_{cb}\rvert)$	0.0004	0.001
$\delta(m_t)$	0	< 0.001
$\sum \delta$	0.1421	0.228

Table E.8: Error budget for $\Delta\Gamma_s$ using the updated inputs in Tab. E.1.

Parameter	Update	ABL review 2015 [15]
$\delta(\mu)$	0.0929	0.079
$\delta(f_{B_d})$	0.0872	0.137
$\delta(B_{R_2})$	0.0623	0.144
$\delta(\tilde{B}_S)$	0.0809	0.04
$\delta(\lvert V_{cb}\rvert)$	0.0240	0.049
$\delta(B_{R_0})$	0.0533	0.025
$\delta(\bar{z})$	0.0109	0.011
$\delta(m_b)$	0.0076	0.008
$\delta(B_{\tilde{R}_1})$	0.0	0.0
$\delta(m_d)$	$--$	$--$
$\delta(B_{R_3})$	0.0023	0.005
$\delta(B_{R_1})$	0.0	0.0
$\delta(\gamma)$	0.0232	0.002
$\delta(\Lambda_{QCD})$	0.0009	0.001
$\delta(\lvert V_{ub}/V_{cb}\rvert)$	0.0008	0.001
$\sum \delta$	0.175	0.227

Table E.9: Error budget for $\Delta\Gamma_d$ using the updated inputs in Tab. E.1.

Parameter	Update
$\delta(\mu)$	0.0889
$\delta(B_{R_2})$	0.0604
$\delta(B_S)$	0.0539
$\delta(B_{R_0})$	0.0301
$\delta(\bar{z})$	0.0109
$\delta(m_b)$	0.0080
$\delta(m_t)$	0.0066
$\delta(\tilde{B}_{R_1})$	0.0038
$\delta(\Lambda_{QCD})$	0.0024
$\delta(m_s)$	0.0023
$\delta(B_{R_3})$	0.0023
$\delta(B_{R_1})$	0.0018
$\delta(\gamma)$	0.0001
$\delta(V_{ub}/V_{cb})$	0.0
$\delta(V_{cb})$	0.0
$\sum \delta$	0.125

Table E.10: Error budget for $\mathcal{R}e(\Gamma^s_{12}/M^s_{12})$ using the updated inputs in Tab. E.1.

Parameter	Update
$\delta(\mu)$	0.0929
$\delta(B_{R_2})$	0.0623
$\delta(B_S)$	0.0809
$\delta(B_{R_0})$	0.0533
$\delta(\bar{z})$	0.0109
$\delta(m_b)$	0.0076
$\delta(m_t)$	0.0066
$\delta(\tilde{B}_{R_1})$	0.0
$\delta(\Lambda_{QCD})$	0.0022
$\delta(m_d)$	0.0
$\delta(B_{R_3})$	0.0023
$\delta(B_{R_1})$	0.0
$\delta(\gamma)$	0.0025
$\delta(\lvert V_{ub}/V_{cb}\rvert)$	0.000887
$\delta(\lvert V_{cb}\rvert)$	0.0
$\sum \delta$	0.149

Table E.11: Error budget for $\mathcal{R}e(\Gamma_{12}^d/M_{12}^d)$ using the updated inputs in Tab. E.1.

Parameter	Update
$\delta(\mu)$	0.0946
$\delta(\bar{z})$	0.0462
$\delta(V_{ub}/V_{cb})$	0.0211
$\delta(\gamma)$	0.0118
$\delta(B_{R3})$	0.0106
$\delta(m_b)$	0.0101
$\delta(m_t)$	0.0066
$\delta(B_S)$	0.0078
$\delta(\Lambda_{QCD})$	0.0053
$\delta(B_{R2})$	0.0039
$\delta(\tilde{B}_{R1})$	0.0030
$\delta(B_{R0})$	0.0026
$\delta(m_s)$	0.0021
$\delta(B_{R1})$	0.0001
$\delta(V_{cb})$	0.0
$\sum \delta$	0.1098

Table E.12: Error budget for $\mathcal{I}m(\Gamma^s_{12}/M^s_{12})$ using the updated inputs in Tab. E.1.

Parameter	Update
$\delta(\mu)$	0.0937
$\delta(\bar{z})$	0.0487
$\delta(\lvert V_{ub}/V_{cb}\rvert)$	0.0215
$\delta(\gamma)$	0.0105
$\delta(B_{R3})$	0.0115
$\delta(m_b)$	0.0129
$\delta(m_t)$	0.0066
$\delta(B_S)$	0.0123
$\delta(\Lambda_{QCD})$	0.0054
$\delta(B_{R2})$	0.0042
$\delta(\tilde{B}_{R1})$	0.0
$\delta(B_{R0})$	0.0049
$\delta(m_d)$	0.0
$\delta(B_{R1})$	0.0
$\delta(\lvert V_{cb}\rvert)$	0.0
$\sum \delta$	0.111

Table E.13: Error budget for $\mathcal{I}m(\Gamma_{12}^d/M_{12}^d)$ using the updated inputs in Tab. E.1.

	$\tau(B_s^0)/\tau(B_d^0)$
Central value	1.000503791
$\delta(\epsilon_1)$	0.00071
$\delta(\epsilon_2)$	0.00051
$\delta(f_{B_s})$	0.00029
$\delta(\mu_G^2(B_s)/\mu_G^2(B_d))$	0.00028
$\mu_\pi^2(B_s) - \mu_\pi^2(B_d))$	0.00023
$\delta(f_{B_d})$	0.00023
$\delta(c_3)$	0.00023
$\delta(\mu)$	0.00016
$\delta(B_1)$	0.00014
$\delta(\mu_G^2(B_d))$	0.00013
$\delta(B_2)$	0.00010
$\delta(c_G)$	0.000068
$\delta(m_b)$	0.000040
$\delta(\lvert V_{cb}\rvert)$	0.000025
$\delta(m_c)$	0.0000072
$\delta(\tau_{B_s})$	0.0000013
$\delta(M_{B_s})$	0.00000055
$\delta(M_{B_d})$	0.00000025
$\delta(\lvert V_{us}\rvert)$	0.000000027
$\delta(\gamma)$	0.000000020
$\delta(\lvert V_{ub}/V_{cb}\rvert)$	0.000000010
$\sum \delta$	0.00108

Table E.14: Error budget for the life-time ratio in Eq. (6.2.32).